

THE PROBLEM OF FREQUENCY DEPENDENCE
IN TRANSMISSION LINE MODELLING

by

JOSE R. MARTI

Elec. Engr., Central University of Venezuela, 1971
M.E.E.P.E., Rensselaer Polytechnic Institute, 1974

A THESIS SUBMITTED IN PARTIAL FULFILLMENT OF
THE REQUIREMENTS FOR THE DEGREE OF

DOCTOR OF PHILOSOPHY

in

THE FACULTY OF GRADUATE STUDIES

Department of Electrical Engineering

We accept this thesis as conforming
to the required standard

c

THE UNIVERSITY OF BRITISH COLUMBIA
April 1981

© José R. Martí, 1981

In presenting this thesis in partial fulfilment of the requirements for an advanced degree at the University of British Columbia, I agree that the Library shall make it freely available for reference and study. I further agree that permission for extensive copying of this thesis for scholarly purposes may be granted by the head of my department or by his or her representatives. It is understood that copying or publication of this thesis for financial gain shall not be allowed without my written permission.

Department of Electrical Engineering

The University of British Columbia
2075 Wesbrook Place
Vancouver, Canada
V6T 1W5

Date June 3, 1981

ABSTRACT

In this work, the accurate representation of transmission lines for the digital simulation of electromagnetic transients in power systems has been examined. A model has been developed that accounts for the frequency dependence and distributed nature of the line parameters over the entire frequency range. This model can easily be incorporated into a time-domain network solution of the complete power system.

The model consists simply of a constant resistance in parallel with a current source evaluated at each time step of the solution. The equivalent resistance results from a finite-step-width discretization of the differential equations of a resistance-capacitance (R-C) network that simulates the line characteristic impedance. The equivalent current source accounts for the time delays and attenuations of the different frequency components of the travelling waves and for the discretization of the time-domain equations.

Rational-function approximations are used to synthesize the R-C network and the line propagation ("weighting") function in the frequency domain. These rational approximations allow the corresponding time-domain functions to be obtained directly in a closed-form, thus circumventing the need for numerical inverse Fourier transformations.

The numerical technique used to obtain the rational functions yields very accurate, high-order approximations. This technique is based on a direct, step-by-step allocation (and reallocation) of poles and zeros and avoids the instability problems which can be encountered with optimization techniques based on search methods.

A series of analytical evaluations and simulation tests were performed in order to assess the validity of the model. The results of these tests show that the model is accurate, fast, and reliable.

The model was incorporated into the code of the University of British Columbia's version of Dr. H.W. Dommel's Electromagnetic Transients Program (EMTP).

TABLE OF CONTENTS

	<u>Page</u>
ABSTRACT	ii
ACKNOWLEDGEMENT	vii
INTRODUCTION	1
General Perspective on the Problem of Transient Studies, 1	
Purposes and Objectives of the Present Work, 5	
CHAPTER 1: Wave Propagation in Transmission Lines	6
1.1 General Line Equations, 6	
1.2 Solution of the Line Equations in the Frequency Domain, 11	
1.3 Solution of the Line Equations in the Time Domain, 13	
CHAPTER 2: Simulation of Electromagnetic Transients	19
2.1 Complete Network Solution: Time Domain vs. Frequency Domain, 19	
2.2 Network Solution in the Time Domain, 20	
CHAPTER 3: The Problem of Frequency Dependence	24
3.1 General Considerations, 24	
3.2 Admittances Formulation: Budner, 25	
3.3 Travelling Functions Approach: Snelson; Meyer and Dommel, 30	
3.4 New Formulation, 37	
CHAPTER 4: Synthesis of the Characteristic Impedance and Weighting Function	50
4.1 General Considerations, 50	
4.2 Synthesis of Equivalent Network to Represent the Characteristic Impedance, 52	

4.2.1	General Considerations,	52
4.2.2	Rational Approximation of $Z_c(\omega)$,	56
4.2.3	Equivalent R-C Network,	57
4.3	Weighting Function and History Convolution,	59
4.3.1	General Considerations,	59
4.3.2	Recursive Convolution,	61
4.3.3	Rational Approximation of $A_1(\omega)$,	65
4.4	Numerical Synthesis of Rational Approximations for $Z_c(\omega)$ and $A_1(\omega)$,	66
4.4.1	General Considerations,	66
4.4.2	Approximation Techniques by Other Authors,	69
4.4.3	Rational Approximation Technique in the New Formulation,	70

CHAPTER 5: Implementation of the Solution 75

5.1	Recapitulation,	75
5.2	Evaluation of the Weighted History Source,	76
5.3	Equivalent Impedance,	78
5.4	Some General Comments on Numerical Integration,	82
5.5	Reduced Equivalent Circuit,	83
5.6	Algorithm of Solution,	85
5.7	Initial Conditions,	86
5.8	Interface with the EMTP,	89

CHAPTER 6: Numerical Results 93

6.1	Introduction,	93
6.2	Frequency-Dependent Line Parameters,	93
6.3	Simulation of the Characteristic Impedance,	95
6.4	Approximation of the Weighting Function,	98

6.5 Analytical Tests: Frequency Domain, 103	
6.6 Analytical Tests: Time Domain, 109	
6.7 Examples of Transient Simulations, 114	
6.8 Field Test Simulation, 119	
List of Graphs, 122	
CONCLUSIONS	187
APPENDICES	
APPENDIX I: Some Matrix Relations	189
I.1 Diagonalization of the Propagation Equations, 189	
I.2 Diagonalization of the Drop Equations, 190	
APPENDIX II: Integration Coefficients	194
II.1 Recursive Convolution Property, 194	
II.2 Dommel's Model for R-C Network, 196	
BIBLIOGRAPHY	198

ACKNOWLEDGEMENT

For the completion of this work, I would like to say thanks,

To Gail, who worked at it as hard as (or harder than) the author.

To Mae, who tried to teach me the idiosyncrasies and beauty of the English language, but who is not to blame for the pupil's limitations.

To my brother, Luis, who shares a dream with me.

To Dr. Dommel, whom I admire.

To Dr. Moore and "his girls", for making me feel not a stranger in the Department.

To the people responsible for the computing facilities at the University of British Columbia, who make computers a "bit" less mysterious.

To Central University of Venezuela who financed my leave of absence at U.B.C., for their support.

To my parents.

INTRODUCTION

GENERAL PERSPECTIVE ON THE PROBLEM OF TRANSIENT STUDIES

The size and cost of the equipment in a power system is largely dependent on the stresses that occur during transient periods. The equipment must have enough insulation to withstand the overvoltages, enough thermic capacity to withstand the overcurrents, and enough mechanical strength to withstand the increased mechanical forces.

Transients occur in a power system when the normal steady-state operation is disturbed. The state of the system can be disturbed by necessary internal switching operations, such as those needed for connecting or disconnecting the various system components, or by undesirable extrinsic perturbations, such as atmospheric discharges, faulty insulation, and mechanical breakdowns.

Due to the inertia of its components, the system cannot, after a perturbation, instantly adapt itself to the new conditions. Depending on the nature of the disturbance and the parameters of the system, the transient processes involved can be very fast, with the currents and voltages reaching very high magnitude peaks and having "arbitrary" waveforms.

A series of protective devices, such as lightning arresters and fault-detection relays, are normally employed to limit the magnitude and duration of transient conditions produced by undesirable perturbations. These devices can be quite effective in protecting the system, but at the same time, their location and adjustment can be quite critical. A premature or untimely action on their part can cause interference with switching operations and thus jeopardize the normal functioning of the system. The overvoltages produced

during switching operations can also, to a certain degree, be controlled. A common practice for this purpose is the pre-insertion of resistors before connecting or disconnecting a given part of the system.

The effectiveness of protective strategies in moderating transient conditions and the ability of the equipment to sustain the "remaining" transients can only be properly assessed if the behaviour of the system during these periods is accurately described and predicted. Tolerances in view of uncertainties can represent considerable increases in equipment costs with no guarantee of optimum operation. This becomes even more important for very high voltage systems where the dimensions of the equipment and their associated financial and environmental costs are very critical.

Electromagnetic transients in power systems can be very fast and peak values may occur within microseconds. When the periods of the signals are comparable to or smaller than the travelling times of the electromagnetic waves, as it is usually the case in transmission lines, lumped-parameter representations are no longer adequate and the mathematical description of the phenomena must be formulated in terms of partial differential equations in time and space. In transmission lines the conductors are coupled to each other and, therefore, the formulation results in a system of mutually coupled partial differential equations.

For purposes of analysis, each component of an n-phase system is normally represented by an equivalent mathematical model of order n. For transmission lines with ground return, the parameters of these models may be very sensitive to variations in the frequency. Since during transient conditions the signals usually contain a wide range of frequencies, the

accurate description of the phenomena involves a system of coupled partial differential equations with non-constant coefficients.

Due to the complexity of the problem, early studies of transients in power system (before the advent of digital computers) had to be restricted to very small systems, and involved a large number of simplifications. (Despite these limitations, some of these early works (e.g. [1] to [5]) are of great merit, and many of their practical results are still being used in industry today.) The need for more general and accurate solutions led to the development of analogical representations in the form of Transient Network Analyzers (TNA) (Peterson, 1939, [6]). In these representations the system components are simulated by bench-size physical models.

TNA's represented a large step forward from manual computations and made possible the study of more complex problems with less simplifications. As systems grew in complexity and size, however, TNA's became more elaborate and cumbersome. As a result, its use became more restricted to specialized centers which could provide the required physical facilities and trained personnel. (Some of these centers are still in operation today (e.g. [7], p.3).)

In addition to the size and cost factors, TNA's are also limited in their ability to simulate real physical systems. One of these limitations is that distributed-parameter elements, such as transmission lines, are represented by lumped-parameter models. To diminish the error, the line is represented as segmented into smaller sections, but a very large number of sections would be necessary for an accurate representation of the high frequency components. Another main limitation of TNA's is the modelling of frequency dependence.

The most important advances in solving the transient simulation problem are probably the ones made in the last two decades. The development of digital computers, numerical methods of analysis, and efficient processing algorithms have made possible the study of larger and more complex systems with less simplifications. Probably the most important contributions in this new period have been the works by Wedepohl (1963, [8]), Hedman (1965, [9]), and Dommel (1969, [10]).

Wedepohl and Hedman (independently from each other) applied the mathematical theories of matrix manipulation and modal decoupling to the analysis of multiphase systems. These methods allow the reduction of coupled multiconductor systems into equivalent single-phase units.

Dommel developed a general computer program capable of simulating a large variety of transient conditions for systems of any size and complexity. In this program the differential equations describing the transient behaviour of the system components are transformed into discrete models at finite time increments. A complete network solution is then formulated to solve for the system conditions at each time step.

The problem of frequency dependence has been the subject of much study in the last decade. Some of the most important contributions to the solution of this problem are listed in references [11] to [17]. Despite the progress made in this area, the formulations implemented at the present time still present a series of numerical problems, and their use requires many particular considerations. These factors have limited the usefulness of these methods for a general class of transient simulations.

PURPOSES AND OBJECTIVES OF THE PRESENT WORK

It has been the purpose of the work presented in this Dissertation to try to develop a formulation for the problem of frequency dependence of transmission systems that is accurate, reliable, and easy to apply for a general class of transient simulations. In the development of this work the previous contributions to the solution of the problem have been studied, and their advantages and disadvantages taken into consideration.

To achieve the mentioned objectives, the following general philosophical precepts have been observed:

- i) The mathematical complexity of the problem should not obscure the physical concepts involved.
- ii) Within the boundaries of the problem studied, the formulation should be of a general nature; that is, it should not be restricted to particular cases or conditions.
- iii) The numerical methods of solution and computer routines should have the following characteristics:
 - a) The computer routines should be easy to implement and interface with existing general transient programs (namely, those based on Dommel's formulation).
 - b) The numerical methods should be fast and accurate, but, increased accuracy should be limited to the extent where the additional time, cost, and effort involved are justified by corresponding improvements in the final results.
 - c) The general nature of the computer routines should be easy to understand, and their external characteristics easy to manipulate by the users of the transient programs.

CHAPTER 1

WAVE PROPAGATION IN TRANSMISSION LINES

1.1 General Line Equations

A transmission line in an n-phase power system may have a certain number of conductors per phase, ground wires, and ground return (fig. 1.1(a)). However, if the line equations are formulated in the frequency domain, the

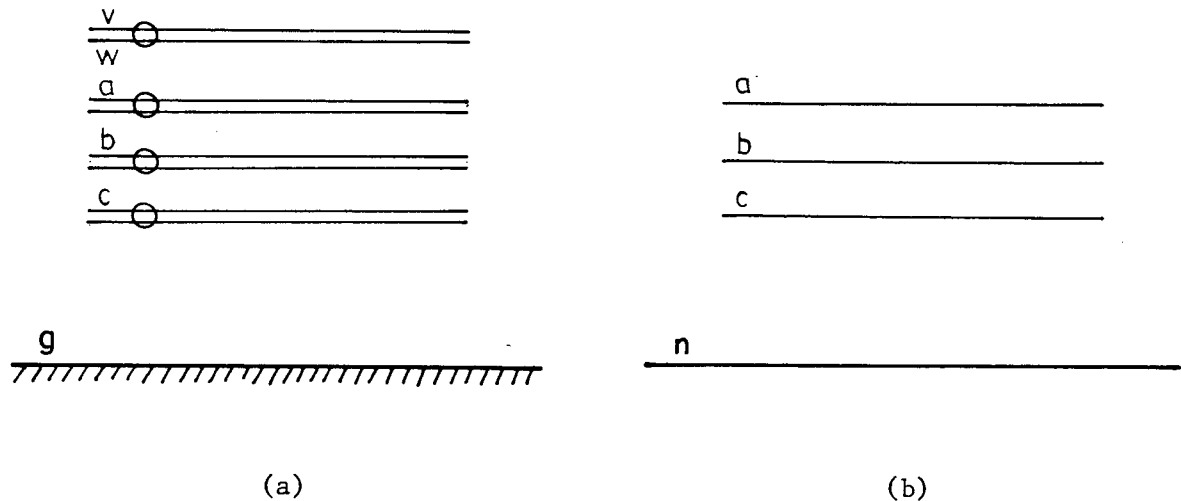


Fig. 1.1: Transmission line. (a) Original system. (b) Equivalent system.

original system can be reduced by matrix manipulation techniques to a system with only one equivalent conductor per phase and a neutral return (fig. 1.1(b)). The effects of the bundling of phase conductors, the presence of ground wires, and the behaviour of the ground return path are all included in the equivalent impedances and admittances of the reduced system.

The line equations, in terms of the reduced equivalent system, are reviewed next. To simplify the notation, capital letters are used to represent

matrices in the frequency domain; for example,

$$Z_{ph} = \begin{bmatrix} Z_{aa}(\omega) & Z_{ab}(\omega) & Z_{ac}(\omega) \\ Z_{ba}(\omega) & Z_{bb}(\omega) & Z_{bc}(\omega) \\ Z_{ca}(\omega) & Z_{cb}(\omega) & Z_{cc}(\omega) \end{bmatrix},$$

$$V_{ph} = \begin{bmatrix} V_a(\omega) \\ V_b(\omega) \\ V_c(\omega) \end{bmatrix}, \quad \text{and} \quad I_{ph} = \begin{bmatrix} I_a(\omega) \\ I_b(\omega) \\ I_c(\omega) \end{bmatrix}.$$

Voltages are measured from phase to neutral, and impedances and admittances are expressed in per unit length.

The relation between voltage and current along the line is given by

$$-\frac{dV_{ph}}{dx} = Z_{ph} I_{ph} \quad (\text{series voltage drop equation}), \quad (1.1)$$

and

$$-\frac{dI_{ph}}{dx} = Y_{ph} V_{ph} \quad (\text{shunt current drop equation}). \quad (1.2)$$

Differentiating with respect to x , the wave propagation equations in the frequency domain are obtained:

$$\frac{d^2 V_{ph}}{dx^2} = (Z_{ph} Y_{ph}) V_{ph} \quad (\text{voltage propagation equation}), \quad (1.3)$$

and

$$\frac{d^2 I_{ph}}{dx^2} = (Y_{ph} Z_{ph}) I_{ph} \quad (\text{current propagation equation}). \quad (1.4)$$

Since all the quantities are matrices, these equations constitute systems of coupled differential equations. The equations can be decoupled, however, through matrix transformations (e.g. Wedepohl [8] and Hedman [9]). Some of the

properties of these transformations are reviewed next.

From matrix theory, a square matrix A can be diagonalized (under certain conditions) by a transformation of the form

$$T^{-1} A T , \quad (1.5)$$

where T is obtained from the eigenvectors of A.

Although the strict mathematical conditions under which the diagonalization is possible can be elaborate, the product $(Z_{ph} Y_{ph})$ in equation 1.3 is usually diagonalizable. Assuming this is the case, it is shown in Appendix I.1 that the inverse product $(Y_{ph} Z_{ph})$ in equation 1.4 is also diagonalizable. That is, if

$$P = \text{diagonalizing matrix for } (Z_{ph} Y_{ph}) , \quad (1.6)$$

then

$$Q = \text{diagonalizing matrix for } (Y_{ph} Z_{ph}) \quad (1.7)$$

exists.

A general relationship between P and Q (App. I.1) is given by

$$Q = (P^t)^{-1} D_c , \quad (1.8)$$

where $(P^t)^{-1}$ is the inverse of P transposed, and D_c is an arbitrary, constant, diagonal matrix.

To introduce the diagonalized forms into the propagation equations (1.3 and 1.4), a new set of variables (modal quantities) are defined by similarity (modal) transformations:

$$V_{ph} = P V_m \quad (1.9)$$

and

$$I_{ph} = Q I_m . \quad (1.10)$$

Substitution of these transformations into the propagation equations gives

$$\frac{d^2V_m}{dx^2} = [P^{-1}(Z_{ph} Y_{ph}) P] V_m = D_{zy} V_m \quad (1.11)$$

and

$$\frac{d^2I_m}{dx^2} = [Q^{-1}(Y_{ph} Z_{ph}) Q] I_m = D_{yz} I_m, \quad (1.12)$$

where, as shown in Appendix I.1,

$$D_{zy} = D_{yz}. \quad (1.13)$$

With the change of variables indicated in 1.9 and 1.10, the drop equations (1.1 and 1.2) become

$$-\frac{dV_m}{dx} = (P^{-1} Z_{ph} Q) I_m \quad (1.14)$$

and

$$-\frac{dI_m}{dx} = (Q^{-1} Y_{ph} P) V_m. \quad (1.15)$$

It is shown in Appendix I.2 that the coefficient matrices in these equations are diagonal, that is

$$P^{-1} Z_{ph} Q = D_z \quad (\text{diagonal}) \quad (1.16)$$

and

$$Q^{-1} Y_{ph} P = D_y \quad (\text{diagonal}). \quad (1.17)$$

Matrices D_z and D_y represent the equivalent series impedances and shunt admittances of the decoupled modal system:

$$D_z = Z_m \quad (\text{modal series impedances}) \quad (1.18)$$

$$D_y = Y_m \quad (\text{modal shunt admittances}) \quad (1.19)$$

Matrix 1.13 gives the propagation constant for the different line modes:

$$D_{zy} = D_{yz} = \gamma^2 \quad (\text{propagation constant squared}) \quad (1.20)$$

With the indicated properties of the modal transformations, the line equations in the mode-frequency domain can be written as:

$$-\frac{dV_m}{dx} = Z_m I_m \quad (\text{voltage drop equation}), \quad (1.21)$$

$$-\frac{dI_m}{dx} = Y_m V_m \quad (\text{current drop equation}), \quad (1.22)$$

$$\frac{d^2V_m}{dx^2} = \gamma^2 V_m \quad (\text{voltage propagation equation}), \quad (1.23)$$

$$\frac{d^2I_m}{dx^2} = \gamma^2 I_m \quad (\text{current propagation equation}). \quad (1.24)$$

All these equations are decoupled.

Differentiating equations 1.21 and 1.22 and comparing with equations 1.23 and 1.24, the propagation constant γ can be obtained directly as

$$\gamma = \sqrt{Z_m Y_m} . \quad (1.25)$$

To recapitulate: As described by equations 1.21 to 1.24 the original coupled system of figure 1.1 has been converted by the modal transformations 1.9 and 1.10 into a new decoupled system. Each one of the component modes of this decoupled system can be studied individually as a single-phase system.

Accordingly, in what follows in this work, the line solutions are formulated for single-phase lines, with the understanding that these solutions apply to any of the decoupled modes.

1.2 Solution of the Line Equations in the Frequency Domain

With a single-phase line as the reference unit (fig. 1.2), the solution to the line equations in the frequency domain is next formulated. (Lower case letters are used to denote quantities in the time domain whereas capital letters are used to denote quantities in the frequency domain.)

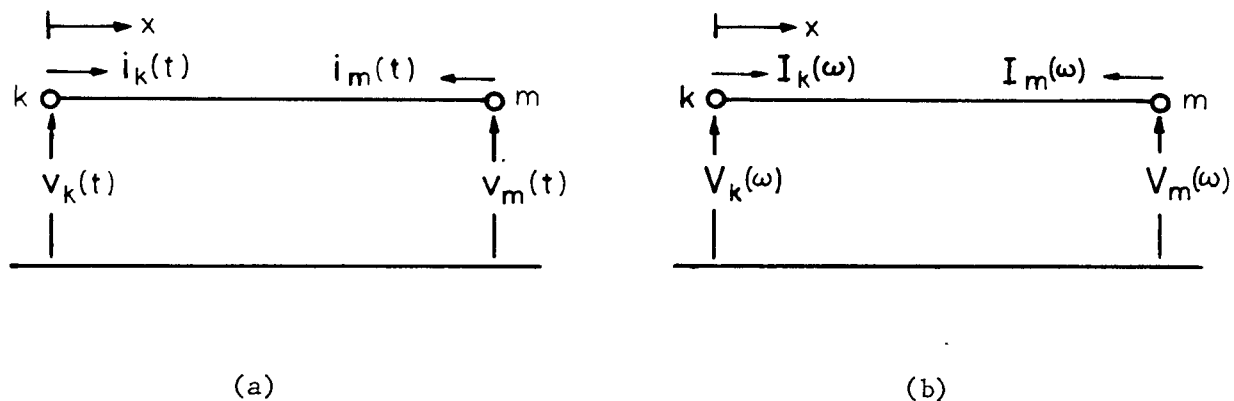


Fig. 1.2: Single-phase line (or component mode).
 (a) Time domain. (b) Frequency domain.

In figure 1.2(b) the voltage and current drop equations are given by

$$-\frac{dV}{dx} = Z' I \quad (1.26)$$

and

$$-\frac{dI}{dx} = Y' V, \quad (1.27)$$

where

$Z' = R'(\omega) + j\omega L'(\omega)$ (R' , L' = series resistance and inductance per unit length),

$Y' = G'(\omega) + j\omega C'(\omega)$ (G' , C' = shunt conductance and capacitance per unit length),

$V = V(\omega, x)$ (line to neutral voltage),

and

$I = I(\omega, x)$ (series current).

(It is emphasized that in the most general case all the parameters are frequency dependent and the variables are functions of frequency and space.)

Differentiating equations 1.26 and 1.27,

$$\frac{d^2V}{dx^2} = (Z'Y') V \quad (1.28)$$

and

$$\frac{d^2I}{dx^2} = (Y'Z') I. \quad (1.29)$$

From these equations, and with 1.26 and 1.27, the general solutions for voltage and current are given by

$$V(\omega, x) = A e^{-\gamma(\omega)x} + B e^{\gamma(\omega)x} \quad (1.30)$$

and

$$I(\omega, x) = \frac{A}{Z_c(\omega)} e^{-\gamma(\omega)x} - \frac{B}{Z_c(\omega)} e^{\gamma(\omega)x}, \quad (1.31)$$

where

$$\gamma(\omega) = \sqrt{Z'(\omega) Y'(\omega)} = \alpha(\omega) + j\beta(\omega) = \text{propagation constant}, \quad (1.32)$$

$\alpha(\beta)$ = attenuation,

$\beta(\omega)$ = phase displacement ,

and

$$Z_c(\omega) = \sqrt{\frac{Z'(\omega)}{Y'(\omega)}} = \text{characteristic impedance}. \quad (1.33)$$

The constants A and B in equations 1.30 and 1.31 are defined by the boundary conditions at any point of the line. At the receiving end ($x = \ell$),

$$V_m = A e^{-\gamma \ell} + B e^{\gamma \ell}$$

and

$$-I_m = \frac{A}{Z_c} e^{-\gamma \ell} - \frac{B}{Z_c} e^{\gamma \ell},$$

from where,

$$A = \left(\frac{V_m - Z_c I_m}{2} \right) e^{\gamma \ell}$$

and

$$B = \left(\frac{V_m + Z_c I_m}{2} \right) e^{-\gamma \ell}.$$

As a function of the conditions at node m , the voltage and current at node k are then given by

$$V_k = V_m \left(\frac{e^{\gamma \ell} + e^{-\gamma \ell}}{2} \right) - Z_c I_m \left(\frac{e^{\gamma \ell} - e^{-\gamma \ell}}{2} \right)$$

and

$$I_k = \frac{V_m}{Z_c} \left(\frac{e^{\gamma \ell} - e^{-\gamma \ell}}{2} \right) - I_m \left(\frac{e^{\gamma \ell} + e^{-\gamma \ell}}{2} \right),$$

or in terms of hyperbolic functions (and emphasizing the dependence on ω),

$$V_k(\omega) = \cosh[\gamma(\omega)\ell] V_m(\omega) - Z_c(\omega) \sinh[\gamma(\omega)\ell] I_m(\omega) \quad (1.34)$$

and

$$I_k(\omega) = \frac{1}{Z_c(\omega)} \sinh[\gamma(\omega)\ell] V_m(\omega) - \cosh[\gamma(\omega)\ell] I_m(\omega). \quad (1.35)$$

These equations represent the "classical" solution to the line equations in the frequency domain (e.g. Woodruff [18], pp. 93-120).

1.3 Solution of the Line Equations in the Time Domain

The difficulty in obtaining a complete solution to the line equations in the time domain can be illustrated from their frequency domain form. Considering, for instance, equation 1.28

$$\begin{aligned}\frac{d^2V}{dx^2} &= (R' + j\omega L')(G' + j\omega C')V \\ &= [(R'G' - \omega^2 L'C') + j\omega(R'C' + G'L')]V, \quad (1.36)\end{aligned}$$

and noting that in general the parameters are a certain function of frequency, it can readily be seen that obtaining the corresponding time-domain form is not straightforward. Before proceeding with this point, it may be useful to briefly examine the nature of the frequency dependence of the parameters in a real system.

In the most elementary case of a conductor carrying an electrical current, the distribution of this current across the conductor is not uniform, but depends on the rate of change (frequency) of the current. The higher the frequency the more the current is displaced towards the outside of the conductor, thus changing the resistance and internal inductance (skin effect). The analytical solutions describing the variation of these parameters with frequency are fairly complicated and involve Bessel functions (e.g. Woodruff [18], pp. 53-710). Nevertheless, in this elementary case the most important component of the total impedance is the external inductance (which is not affected by the frequency) and studies that neglect frequency dependence can still give acceptable results.

A more critical case in power transmission systems is that of a phase conductor with ground return. In the case of the ground, which can be imagined as a huge conductor, the resistance and internal inductance constitute a large portion of the total impedance, and the effect of the frequency is thus very important. The expressions for the variation of these parameters with frequency are again rather complicated and involve Bessel functions. (The solution for this case was first given by Carson, 1926 [19], and, independently, by Pollaczek, 1926 [20].).

Going back to equation 1.36, the complicated form of the functions $R'(\omega)$ and $L'(\omega)$ makes direct transformation of this equation into the time domain very difficult, if not practically impossible. (The parameters G' and C' can be considered for practical purposes as independent of the frequency.) Despite not being able to obtain a closed-form solution, it is still interesting for the purpose of understanding the phenomenon, to consider the form of the line equations in the time domain under simplifying conditions. To inverse transform the frequency-domain equations, the following property is first recalled:

$$\frac{d^n f(t)}{dt^n} \xleftrightarrow{\mathcal{F}} (j\omega)^n F(\omega) .$$

The following conditions are next considered:

a) With R' , G' , L' and C' independent of ω , the inverse transform of equation 1.36 is given by

$$\frac{\partial^2 v}{\partial x^2} = (R'G')v + L'C' \frac{\partial^2 v}{\partial t^2} + (R'C' + G'L') \frac{\partial v}{\partial t} . \quad (1.37)$$

A similar expression is obtained from equation 1.29 for the current. From equation 1.37 it can be seen that even with the simplifying assumption of frequency-independent parameters, the resulting time domain form is still complicated.

b) Neglecting the losses (that is, $R' = G' = 0$), the inverse transform of equations 1.28 and 1.29 is now given by

$$\frac{\partial^2 v}{\partial x^2} = L'C' \frac{\partial^2 v}{\partial t^2} \quad (1.38)$$

and

$$\frac{\partial^2 i}{\partial x^2} = C'L' \frac{\partial^2 i}{\partial t^2} . \quad (1.39)$$

In a similar way, for the drop equations (1.26 and 1.27),

$$-\frac{\partial v}{\partial x} = L' \frac{\partial i}{\partial t} \quad (1.40)$$

and

$$-\frac{\partial i}{\partial x} = C' \frac{\partial v}{\partial t} . \quad (1.41)$$

Equations 1.38 to 1.41 are the "classical" equations for wave propagation in a lossless line. They could have been formulated directly in the time domain, but were instead derived from the frequency domain in order to emphasize the limitations under which they apply. A general solution to these equations was first given by d'Alembert in 1747 in the form

$$v = f_1(x - at) + f_2(x + at) \quad (1.42)$$

and

$$i = \frac{1}{R_c} f_1(x - at) - \frac{1}{R_c} f_2(x + at) , \quad (1.43)$$

where

$$R_c = \sqrt{\frac{L'}{C'}} = \text{surge impedance (resistance)}$$

and

$$a = \sqrt{\frac{1}{L'C'}} = \text{velocity of propagation} .$$

The functions f_1 and f_2 are defined from boundary and initial conditions. Combining equations 1.42 and 1.43 the following relationship is obtained:

$$v + R_c i = 2f_1(x - at) . \quad (1.44)$$

From this relation, it can be seen that for $(x - at)$ constant the quantity $(v + R_c i)$ is also constant. The quantity $(v + R_c i)$ at point 1 on the line will "appear" at point 2 (at a distance Δx from point 1) after a time

$$\Delta t = \frac{\Delta x}{a} .$$

This can be interpreted by saying that the quantity $(v + R_c i)$ "travels" along the line with a velocity "a". The time needed by this "wave" to travel from one extreme of the line to the other is given by

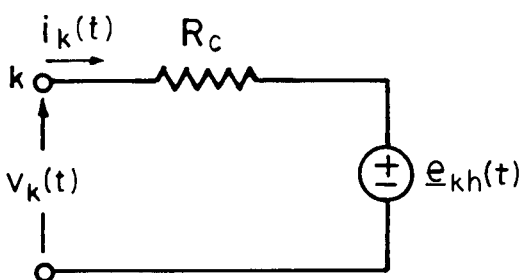
$$\tau = \text{line travelling time} = \frac{\text{line length}}{a} . \quad (1.45)$$

Relation 1.44 is the basis for Bergeron's "Method of Characteristics", which is a graphical approach to relate currents and voltages at different points on the line.

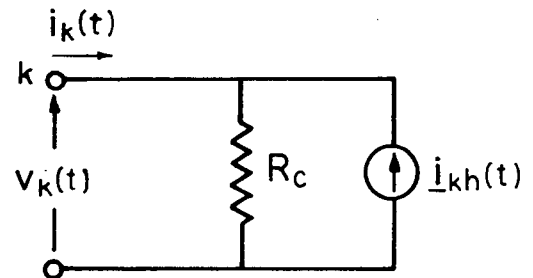
From the above interpretation of equation 1.44, Dommel [10] observed that the present value of the quantities at node k (fig. 1.2(a)) is related to the past value of the quantities at node m by

$$v_k(t) + R_c (-i_k(t)) = v_m(t - \tau) + R_c i_m(t - \tau) . \quad (1.46)$$

That is, the relation between current and voltage at node k at a given time t is known if the past values of the corresponding quantities at node m at τ units of time earlier have been recorded. With this relation, the equivalent circuits shown in fig. 1.3 are obtained. (Similar representations are obtained for node m.) To take the losses into account Dommel represents them as



(a)



(b)

Fig. 1.3: Dommel's representation of a transmission line as seen from node k at time t . (a) Series form. (b) Shunt form. (No frequency dependence or distributed losses are considered.)

concentrated at the ends and middle of the line. No frequency dependence is considered in this basic representation.

In the formulation developed in the research work presented in this Dissertation, the line models have exactly the same form as the circuits in fig. 1.3. However, the resistance and equivalent current source are derived in such a way that the frequency dependence of the parameters and the distributed nature of the losses are taken into account. The development of this model is introduced in Chapter 3. In Chapter 2, presented next, some characteristics of time-domain transient simulations are considered.

CHAPTER 2

SIMULATION OF ELECTROMAGNETIC TRANSIENTS

2.1 Complete Network Solution: Time Domain vs. Frequency Domain

As indicated in Chapter 1, the solution to the line equations can easily be found in the frequency domain, whereas its formulation in the time domain requires many simplifications in order to obtain practical results. However, despite the advantages of modelling transmission lines in the frequency domain, the solution of a complete system, in which a large variety of conditions and operations are simulated, is more easily formulated in the time domain.

As a principle, time-domain formulations have the advantage of dealing directly with real physical phenomena instead of with mathematical (sometimes "obscure") equations. This philosophical advantage manifests itself in practice in many forms. For example, one of the major inconveniences in frequency-domain methods is the simulation of sequential operations (time as a variable does not appear explicitly in the frequency domain). An important example of sequential operations is the opening or closing of circuit breakers at specific times, or as a function of the value of certain variables (e.g. when the current first passes through zero). Another example is the closing or opening of gaps as a function of the magnitude of the voltage. Simulation of switching operations in frequency domain solutions requires going back and forth between frequency and time domains for each change of switch position, thus making the process quite lengthy and cumbersome. On the other hand, simulation of switching operations in the time domain is straightforward. Time domain formulations also greatly facilitate the modelling

of other non-linear elements, such as surge arresters and saturable reactors and transformers. In these cases, piece-wise linear or non-linear models can easily be implemented.

Because of the mentioned factors, most general-purpose programs solve the transients problem directly in the time domain. It is in connection with these programs that the present work has been developed. Dommel's general approach [10] has been used as the basic reference work for time-domain formulations.

2.2 Network Solution in the Time Domain

In Dommel's formulation [10], each element in the system is represented at each time step t by a resistance in parallel with a current source. The resistances are constant and the values of the current sources are updated according to the conditions at previous time steps. The general form of the network equations at time t is

$$[G][v(t)] = [i(t)] + [\underline{i}_h(t)] , \quad (2.1)$$

where

- [G] = constant nodal conductance matrix
- [v(t)] = vector with (unknown) node voltages at time t
- [i(t)] = vector with (known) values of external current sources at time t
- [\underline{i}_h(t)] = vector with (known from history) values of internal equivalent current sources at time t.

The quantities in equation 2.1 are phase quantities. However, as indicated in the preceding chapter, the line models are much simpler if first derived in terms of decoupled modes. To incorporate the mode models into equation 2.1, the time-mode quantities must be transformed into time-phase quantities. These

transformations are considered next.

The relationship between phase and mode quantities is defined in the frequency domain by transformations 1.9 and 1.10:

$$V_{ph} = PV_m \quad (2.2)$$

and

$$I_{ph} = QI_m. \quad (2.3)$$

The time-domain form of these relations is obtained by applying the inverse Fourier transform :

$$v_{ph} = \mathcal{F}^{-1}\{P \cdot V_m\} \quad (2.4)$$

and

$$i_{ph} = \mathcal{F}^{-1}\{Q \cdot I_m\}. \quad (2.5)$$

In the case of completely balanced lines, the line equations can be exactly decoupled by means of real, constant matrices that are independent of the particular line. Examples of these matrices are the Clark Transformation (α , β , 0 components) [3] and the Karrenbauer Transformation [21]. The Karrenbauer Transformation has the advantage that it can be applied to any number of phases. (This transformation is the one used by Dommel in the "Electromagnetic Transients Program" (EMTP) ([24], [38])). The traditional symmetrical components transformation has the computational disadvantage of having complex elements.

For transposed lines the above mentioned matrices can decouple the line to a very good degree of accuracy which depends on the type of transposition scheme.

In the general case of unbalanced, untransposed lines the modal transformation matrices are a function of the frequency and depend on the

particular line configuration. However, it has been found in studies of this problem (e.g. [22] and [23]) that, especially in the case of single-circuit lines, reasonably accurate results can still be obtained assuming constant transformation matrices evaluated at some "mid-range" frequency.

Assuming that the transformation matrices P and Q are constant, equations 2.4 and 2.5 give

$$v_{ph}(t) = Pv_m(t) \quad (2.6)$$

and

$$i_{ph}(t) = Qi_m(t) . \quad (2.7)$$

These equations establish a direct relationship between the time domain quantities of the different line modes and the corresponding phase quantities in the "physical system".

A constant diagonal matrix in the time-mode domain (a resistance in the individual mode equivalent circuits) can be transformed into the time-phase domain as follows. With

$$V_m = R_m I_m ,$$

from equations 2.2 and 2.3,

$$V_{ph} = (PR_m Q^{-1}) I_{ph} ,$$

and assuming P and Q constant,

$$v_{ph}(t) = (PR_m Q^{-1}) i_{ph}(t) , \quad (2.8)$$

thus giving,

$$R_{ph} = PR_m Q^{-1} . \quad (2.9)$$

From this relation, in equation 2.1

$$G_{ph} = R_{ph}^{-1} = QR_m^{-1} P^{-1} . \quad (2.10)$$

The vector with the history current sources from the modal equivalent circuits is transformed directly into phase quantities by relation 2.7:

$$\underline{i}_{hph} = Q \underline{i}_{hm} . \quad (2.11)$$

CHAPTER 3

THE PROBLEM OF FREQUENCY DEPENDENCE

3.1 General Considerations

Two major conclusions can be derived from the general observations made in the preceding chapters:

- a) The complete line equations, including the frequency variation of the parameters and the distributed nature of the losses, are much more easily formulated in the frequency domain.
- b) A general transient solution for a complete system is much more conveniently formulated in the time domain.

To reconcile both premises, the analytical problem can be stated in terms of developing a formulation, such that, starting from the complete line equations in the frequency domain leads to a time-domain form that can be incorporated into a general time-domain solution. Due to the complexity of the frequency functions involved, the conversion of the line equations from frequency to time domain has to be done numerically. As a result, a series of factors, such as computer time, numerical stability, and accuracy, become major considerations.

As mentioned in the Introduction, the formulations that have been suggested in the past to solve this problem have not yet provided a satisfactory general solution. One of the difficulties with some of these formulations is that the elaborate mathematical manipulations required in the process of solution tend to obscure the physical concepts involved in the problem, thus making it difficult to localize the sources of "unexpected" problems.

The present work is based on the strong conviction that a formulation that facilitates the physical visualization of the concepts involved, such as one based on the concept of an equivalent circuit, is easier to understand, and thus the possible sources of error easier to assess, than in the case of other "more mathematical" formulations. In this chapter, the evolution of ideas associated with equivalent circuit formulations, from the works of Budner (1970, [11]), Snelson (1972, [12]), Meyer and Dommel (1974, [13]), to the new models developed in this work, are presented. In addition to the mentioned works, very useful concepts have been derived from other formulations. These formulations will be referred to when these concepts are considered.

3.2 Admittances Formulation: Budner

Budner (1974, [11]) presents a very direct circuit-approach to obtain a frequency-dependence line model. From the line solution in the frequency domain (equations 1.34 and 1.35),

$$V_k = \cosh(\gamma\ell) V_m - Z_c \sinh(\gamma\ell) I_m \quad (3.1)$$

and

$$I_k = \frac{1}{Z_c} \sinh(\gamma\ell) V_m - \cosh(\gamma\ell) I_m , \quad (3.2)$$

Budner looks at the line as a two-port network (fig. 3.1). By nodal analysis the equations of this network are

$$I_k = Y_{kk} V_k + Y_{km} V_m \quad (3.3)$$

and

$$I_m = Y_{mk} V_k + Y_{mm} V_m . \quad (3.4)$$

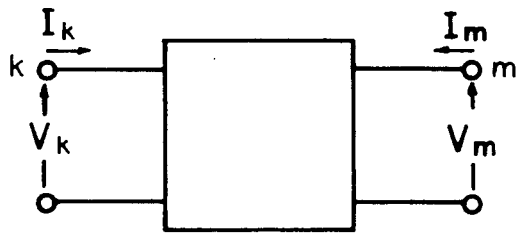


Fig. 3.1: Single-phase transmission line as a two-port network.

From equations 3.1 and 3.2 the admittances are given by

$$Y_{kk} = Y_{mm} = \frac{1}{Z_c} \coth(\gamma\ell) \quad (3.5)$$

and

$$Y_{km} = Y_{mk} = -\frac{1}{Z_c} \operatorname{csch}(\gamma\ell) . \quad (3.6)$$

Taking the inverse Fourier transform of equations 3.3 and 3.4, the following time domain relations are obtained:

$$i_k(t) = y_{kk}(t) * v_k(t) + y_{km}(t) * v_m(t) \quad (3.7)$$

and

$$i_m(t) = y_{km}(t) * v_k(t) + y_{kk}(t) * v_m(t) . \quad (3.8)$$

In these equations the symbol "*" indicates convolution of the functions involved. (In general, for any two functions f and g ,

$$f(t) * g(t) = \int_{-\infty}^{\infty} f(u).g(t-u)du = \int_{-\infty}^{\infty} f(t-u).g(u)du . \quad (3.9)$$

Due to the form of the convolution integrals, the y -functions in equations 3.7 and 3.8 can be referred to as "weighting functions".

After evaluating the convolution integrals in equations 3.7 and 3.8, $i_k(t)$ and $i_m(t)$ can be expressed as a function of their corresponding voltages

and of values known from previous time steps:

$$i_k(t) = y_s v_k(t) + i_{kh}(t) \quad (3.10)$$

and

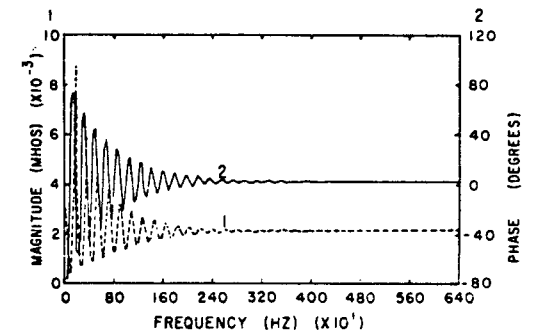
$$i_m(t) = y_s v_m(t) + i_{mh}(t), \quad (3.11)$$

where y_s is a constant, and i_{kh} and i_{mh} are functions of past values. From these relations, an equivalent circuit having the form of the circuit in fig. 1.3(b) can be directly obtained. One major difficulty in arriving at these equations, however, is the evaluation of the convolution integrals.

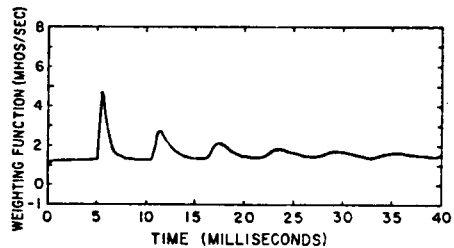
To calculate the time-domain form of the admittances (weighting functions in the convolution integrals) Budner uses a fast Fourier transform program. The frequency and time domain forms of these admittance functions (for the zero sequence mode of the line studied by Budner) are shown in fig. 3.2 (reproduced from reference [11]). A number of numerical complications are encountered when inverse-transforming the $Y(\omega)$ functions. These problems are due in part to the nature of the discrete Fourier transform and, in part, to the form of the $Y(\omega)$ functions.

One of the restrictions of inverse Fourier transform methods is that the frequency functions must be band-limited. In order to cope with this problem, Budner limits the upper frequency to a certain value, at the expense of possible loss of detail in the corresponding time domain forms. Apart from this problem, the cyclic nature and the sharp peaks of the $Y(\omega)$ functions make accurate numerical evaluation of the corresponding $y(t)$ functions fairly difficult. Improved accuracy requires very small $\Delta\omega$'s and, hence, long computer times.

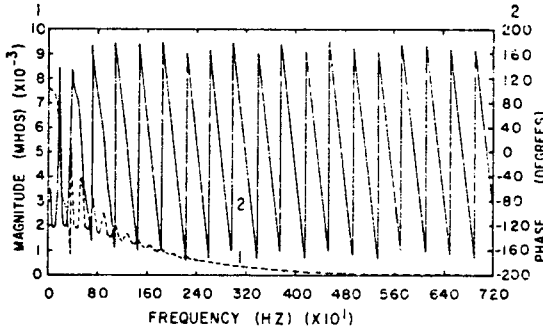
Even assuming that the $y(t)$ functions could be accurately evaluated, the subsequent steps of this formulation still present other numerical problems.



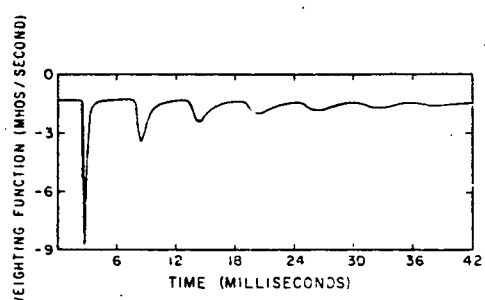
(a)



(b)



(c)



(d)

Fig. 3.2: Budner's admittance functions. Zero sequence mode. (a) $Y_{kk}(\omega)$. (b) $y_{kk}(t)$. (c) $Y_{km}(\omega)$. (d) $y_{km}(t)$.

As can be seen from figs. 3.2(b) and (d), the $y(t)$ functions are made up of series of spikes, at first very sharp and then becoming very flat and extending towards infinite time (these characteristics are even more pronounced for the positive sequence mode, see reference [11]). Because of this form, evaluation of the convolution integrals in equations 3.7 and 3.8 presents two important numerical problems: first, the signals have to be cut-off after some finite time, and second, a large amount of information can be lost in the convolutions with the very sharp spikes and the very flat ones. In general, the convolution process, which has to be performed at each step of the complete network solution, tends to become very time consuming and inaccurate.

It is interesting, for the purpose of understanding the physical significance of this formulation, to consider the following particular

conditions. Let in equations 3.3 and 3.4

$$v_m(\omega) = 0 \rightarrow v_m(t) = 0 \quad (\text{end } m \text{ short-circuited})$$

and

$$v_k(\omega) = 1 \rightarrow v_k(t) = \delta(t) \quad (\text{impulse applied at end } k).$$

This results in:

$$I_k(\omega) = Y_{kk}(\omega) \rightarrow i_k(t) = y_{kk}(t)$$

and

$$I_m(\omega) = Y_{km}(\omega) \rightarrow i_m(t) = y_{km}(t);$$

y_{kk} and y_{km} thus represent currents i_k and i_m in the system shown in fig. 3.3.

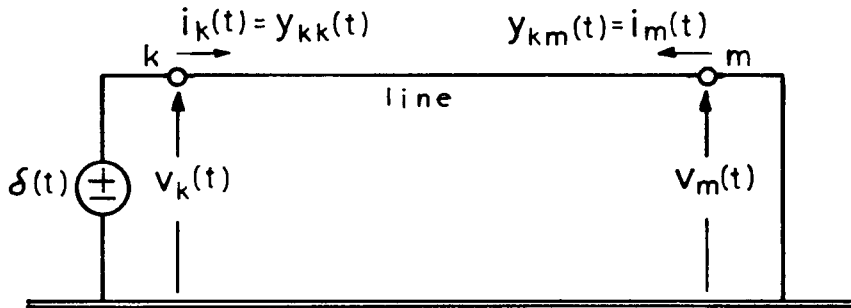


Fig. 3.3: Physical interpretation of Budner's weighting functions.

The form of the y -weighting-functions (figs. 3.2(b) and (d)) can be visualized from the conditions in the system in fig. 3.3. The current impulse originated at node k needs a certain travelling time to reach node m . Since a time impulse has a uniform frequency distribution, and since different frequencies have different travelling times and attenuations, when the perturbation reaches node m the impulse has become a spike. This is the first peak of y_{km} (fig. 3.2(d)) (the negative sign is due to the assumed direction for

i_m). The wave reflected at m travels back to k and, after the corresponding travelling times and attenuations, it reaches this node, making up the first spike in the function y_{kk} (fig. 3.2 (b)). After travelling twice over the line, the spike looks now much flatter: smaller magnitudes and more spread out. The wave is reflected again and the same process continues indefinitely.

Another important observation that can be derived from the system of fig. 3.3 is that the $y(t)$ functions have to be zero for $t < 0$, that is, they are "causal" time functions. This follows from the fact that these functions are associated with real physical variables, $i_k(t)$ and $i_k(m)$, and as such cannot exist before the impulse is applied. This consideration is very important because it sets a boundary in the evaluation of the convolution integrals. This is illustrated next for one of these integrals:

$$y_{kk}(t) * v_k(t) = \int_{-\infty}^{\infty} v_k(t-u) y_{kk}(u) du = \int_0^{\infty} v_k(t-u) y_{kk}(u) du . \quad (3.12)$$

If the lower limit of this integral was less than zero, this would imply that values of v_k for times larger than t would have to be known, and it would not be possible to find the relation 3.10 between $v_k(t)$ and $i_k(t)$.

3.3 Travelling Functions Approach: Snelson; Meyer and Dommel

By analogy with Bergeron's interpretation of the lossless, constant-parameter transmission line, Snelson (1972, [12]) defines a new set of variables to relate currents and voltages at the ends of the line. This new set of variables leads to simpler weighting functions than those encountered in Budner's formulation. Snelson's idea is further developed by Meyer and Dommel (1974, [13]) and implemented into the "Electromagnetic Transients Program" (EMTP) of the Bonneville Power Administration (BPA).

The new variables are defined as follows:

forward travelling functions:

$$f_k(t) = v_k(t) + R_1 i_k(t), \quad (3.13)$$

$$f_m(t) = v_m(t) + R_1 i_m(t), \quad (3.14)$$

and backward travelling functions:

$$b_k(t) = v_k(t) - R_1 i_k(t), \quad (3.15)$$

$$b_m(t) = v_m(t) - R_1 i_m(t). \quad (3.16)$$

For the subsequent development of these equations, R_1 could be chosen as any real constant. However, Snelson makes a particular choice and defines R_1 as $R_1 = \lim_{\omega \rightarrow \infty} Z_c(\omega)$, where $Z_c(\omega)$ is the line characteristic impedance (equation 1.33). It is interesting to observe that for a line with constant parameters and no losses, the forward and backward travelling functions in equations 3.13 to 3.14 are the same as the functions f_1 and f_2 in d'Alembert's solution (equations 1.42 and 1.43).

Relations 3.13 and 3.14 defining the functions f_k and f_m can be visualized physically from the system in fig. 3.4, where

$$v_k(t) = f_k(t) - R_1 i_k(t)$$

and

$$v_m(t) = f_m(t) - R_1 i_m(t).$$

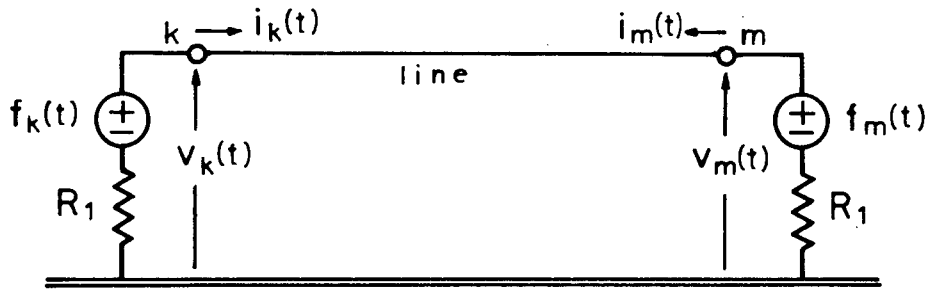


Fig. 3.4: Equivalent circuit interpretation of the functions f_k and f_m .

The functions b_k and b_m can be interpreted as containing the rest of the information defining "the internal behaviour of the line".

To relate the time-domain functions f and b to the exact line solution in the frequency domain, equations 3.13 to 3.16 are transformed into the frequency domain:

forward travelling functions:

$$F_k(\omega) = V_k(\omega) + R_1 I_k(\omega) , \quad (3.17)$$

$$F_m(\omega) = V_m(\omega) + R_1 I_m(\omega) . \quad (3.18)$$

and backward travelling functions:

$$B_k(\omega) = V_k(\omega) - R_1 I_k(\omega) , \quad (3.19)$$

$$B_m(\omega) = V_m(\omega) - R_1 I_m(\omega) . \quad (3.20)$$

Comparing equations 3.17 to 3.20 with the exact line solution (equations 1.34 and 1.35), it follows that

$$B_k(\omega) = A_1(\omega) F_m(\omega) + A_2(\omega) F_k(\omega) \quad (3.21)$$

and

$$B_m(\omega) = A_1(\omega) F_k(\omega) + A_2(\omega) F_m(\omega), \quad (3.22)$$

where

$$A_1(\omega) = \frac{1}{\cosh(\gamma\ell) + \frac{1}{2} \left(\frac{Z_c}{R_1} + \frac{R_1}{Z_c} \right) \sinh(\gamma\ell)} \quad (3.23)$$

and

$$A_2(\omega) = \frac{1}{2} \left(\frac{Z_c}{R_1} - \frac{R_1}{Z_c} \right) \sinh(\gamma\ell) \cdot A_1(\omega). \quad (3.24)$$

In equations 3.21 and 3.22 the information regarding the frequency dependence of Z_c and of γ is carried by the functions A_1 and A_2 . This information is transferred into the time domain by transforming equations 3.21 and 3.22 into this domain, thus giving

$$b_k(t) = a_1(t) * f_m(t) + a_2(t) * f_k(t) \quad (3.25)$$

and

$$b_m(t) = a_1(t) * f_k(t) + a_2(t) * f_m(t), \quad (3.26)$$

where $a_1(t)$ and $a_2(t)$ are the weighting functions for the time domain convolutions.

After evaluating the convolutions in equations 3.25 and 3.26, equations 3.15 and 3.16 (representing the "internal behaviour of the line") give at each time step of the solution the following equivalent representations for the line as seen from nodes k and m:

$$i_k(t) = \frac{1}{R_1} v_k(t) + \underline{i}_{kh}(t) \quad (3.27)$$

and

$$i_m(t) = \frac{1}{R_1} v_m(t) + \underline{i}_{mh}(t); \quad (3.28)$$

\underline{i}_{kh} and \underline{i}_{mh} are defined from the past values of the variables. This equivalent

circuit has the same form as the one in fig. 1.3(b), and therefore it can be directly incorporated into Dommel's general transients program. Equations 3.27 and 3.28 are similar to the ones obtained by Budner (equations 3.10 and 3.11). They differ, however, in the procedure for obtaining the representation: in the present case, through the weighting functions $a_1(t)$ and $a_2(t)$.

As in Budner's case, the form of the weighting functions can be visualized physically by considering some particular conditions. For this purpose, let

$$F_k(\omega) = 1 \text{ and } F_m(\omega) = 0 . \quad (3.29)$$

Substitution of these conditions into equations 3.21 and 3.22 gives

$$B_k(\omega) = A_2(\omega) \text{ and } B_m(\omega) = A_1(\omega) . \quad (3.30)$$

Transforming relations 3.29 and 3.30 into the time domain,

$$f_k(t) = \delta(t) , \quad f_m(t) = 0 , \quad (3.31)$$

$$b_k(t) = a_2(t) \text{ and } b_m(t) = a_1(t) . \quad (3.32)$$

With conditions 3.31, the system in fig. 3.4 results in the system shown in

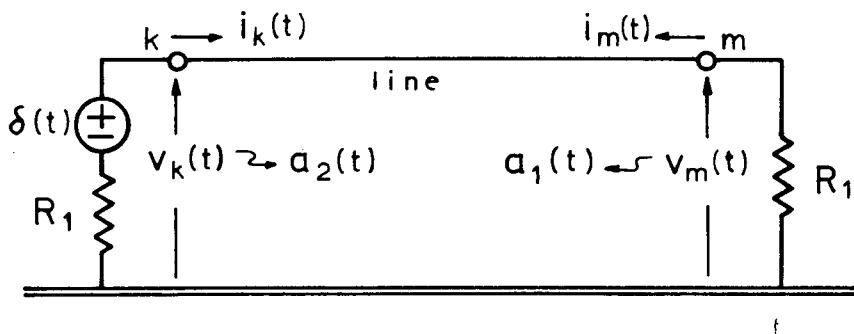


Fig. 3.5: Physical meaning of the weighting functions $a_1(t)$, $a_2(t)$.

fig. 3.5. Substitution of relations 3.32 into relations 3.15 and 3.16 gives

$$a_2(t) = v_k(t) - R_1 i_k(t) \quad (3.33)$$

and

$$a_1(t) = v_m(t) - R_1 i_m(t), \quad (3.34)$$

which express $a_1(t)$ and $a_2(t)$ in terms of the variables in the circuit of fig. 3.5. It then follows from this circuit that

$$a_2(t) = 2v_k(t) - \delta(t) \quad (3.35)$$

and

$$a_1(t) = 2v_m(t). \quad (3.36)$$

In the system of fig. 3.5, the weighting functions $a_1(t)$ and $a_2(t)$ are generated by the voltage impulse $\delta(t)$ travelling along the line. The resulting form of these functions is illustrated in fig. 3.6. (In this figure, the magnitude of the second and subsequent reflexions in $a_1(t)$ and $a_2(t)$ has been exaggerated for the purpose of illustration. In reality, these secondary spikes are very small.)

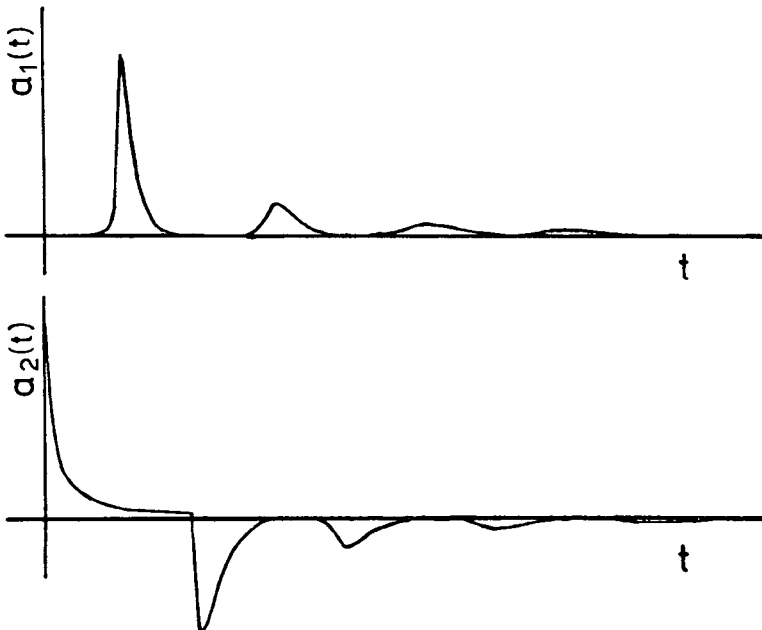


Fig. 3.6: Weighting functions in Snelson, Meyer, and Dommel's formulation.

The numerical differences between Budner's and Snelson's weighting functions can be understood from the physical interpretations in figs. 3.3 and 3.5. In Budner's case, the voltage impulse applied at the beginning of the line undergoes full reflection when it reaches the short-circuited receiving end, and similarly when it comes back to the sending end. In Snelson's case, the line is terminated at both ends by the impedance R_1 defined as $R_1 = \lim_{\omega \rightarrow \infty} Z_c(\omega)$. Therefore, for each frequency component of the applied impulse, the line termination is much closer to the line characteristic impedance $Z_c(\omega)$ than a short circuit is (the higher the frequency the more this is true). As a result, the reflections are much smaller and the spikes in the weighting functions attenuate much faster in Snelson's than in Budner's case. Since the a -functions decay much faster than the y -functions, the corresponding time-domain convolutions at each step of the network solution require much less computer time. Also, the frequency domain form of these functions is less oscillatory in Snelson's than in Budner's case, thus facilitating the numerical evaluation of the corresponding time domain forms.

Snelson's formulation of the line equations, as implemented by Meyer and Dommel in the EMTP at BPA, has given satisfactory results in many cases of production experience in the use of this program. Nevertheless, some problems have been encountered. The main source of problems has been the behaviour of the routines at low frequencies (including 60 Hz). In some cases, after a correct simulation of the initial transient period, the routines have had troubles in simulating the subsequent stationary conditions. Experience in trying to correct these problems seems to indicate that they are associated with the difficulty in evaluating with accuracy the "tail" portion of the $a_1(t)$ and $a_2(t)$ functions (the portion of these functions after the main spikes). Accurate evaluation of these tail portions is important because despite their

small magnitudes the spikes extend over a long period of time, and therefore their total contribution to the convolution integrals can be significant.

In Meyer and Dommel's implementation, the time domain form of the weighting functions is calculated from their corresponding frequency domain definitions (equations 3.23 and 3.24) through inverse Fourier transforms. Comparisons in which the time domain functions are brought back into the frequency domain by the direct Fourier transform have given smaller magnitudes than the original values in the low frequency region. These results seem to corroborate the erratic behaviour of the routines at low frequencies. Also, in these studies, the function $a_2(t)$ has presented more error than the function $a_1(t)$.

3.4 New Formulation

Several considerations lead to the belief that, as mentioned at the end of the preceding section, the difficulties in evaluating with accuracy the tail portions of the a-weighting-functions in Meyer and Dommel's formulation are responsible for the problems encountered with this method at low frequencies. The resistance of the line (especially for the zero sequence mode) increases considerably with frequency. This means that the higher frequency components of the signals are attenuated much faster than the lower frequency components. Therefore, in the tail portions of $a_1(t)$ and $a_2(t)$ there is much less contribution of high frequencies than of low frequencies. In addition to this factor, the resistance R_1 in fig. 3.5 is much closer to the line characteristic impedance at high frequencies than it is at low frequencies. This means that the more reflections the applied voltage impulse undergoes, the higher the ratio of low frequency components with respect to high frequency components.

According to the preceding considerations, one way of improving the low frequency response would be to choose for R_1 a value that is closer to the characteristic impedance for low frequencies. But, this would probably worsen the high frequency response and, consequently, the simulation of the very fast initial period of the transient phenomenon. A compromise would be to make R_1 close to $Z_c(\omega)$ for some mid-range frequency.

Following the above line of reasoning, a much more definitive solution to the problem would be to have at the ends of the line in fig. 3.5, instead of a simple resistance R_1 , a certain network whose frequency response matches the line characteristic impedance, $Z_c(\omega)$, over the entire frequency range. This is shown in fig. 3.7. In this case the voltage impulse generated

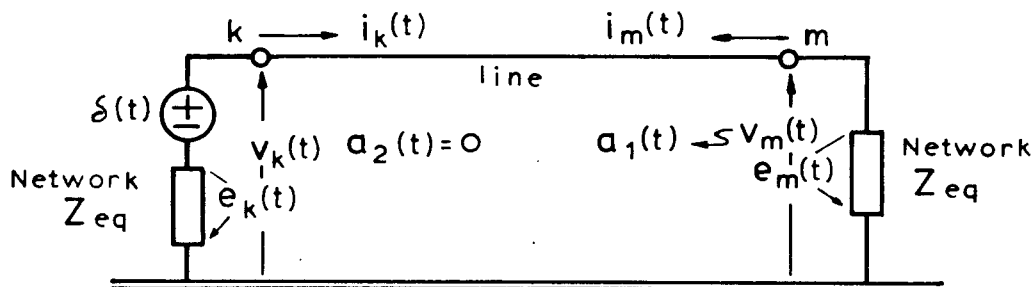


Fig. 3.7: Physical interpretation of the new weighting functions.

at node k would not be reflected back from node m , and $a_1(t)$ would consist of only one spike; $a_2(t)$ would be completely eliminated, that is, $a_2(t) = 0$. The resulting new weighting functions would thus have the form shown in fig. 3.8. How to formulate the line equations in order to arrive at the weighting functions generated by the system in fig. 3.7 is considered next.

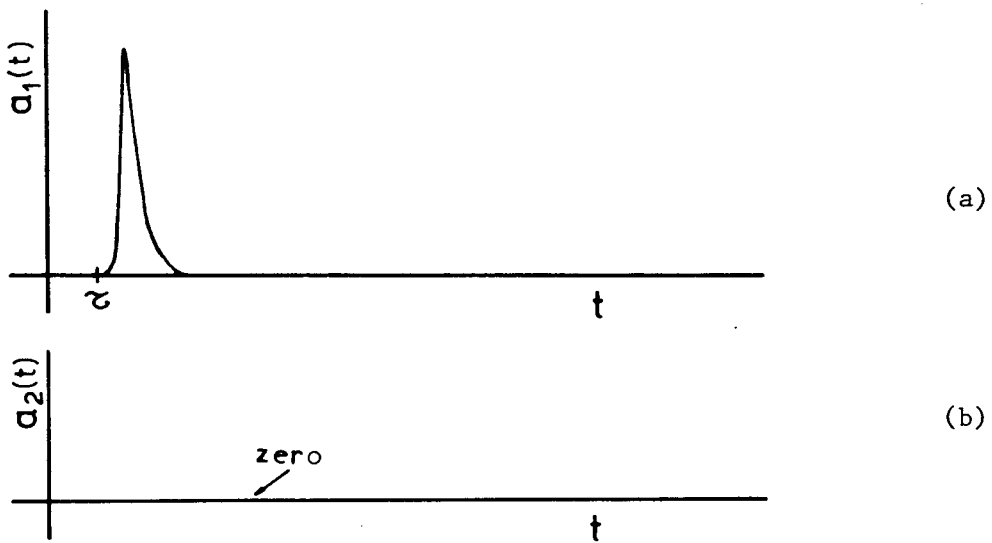


Fig. 3.8: Weighting functions in the new formulation.
 (a) $a_1(t)$. (b) $a_2(t)$ (equal to zero).

General equations:

For the new formulation, Snelson's travelling functions are redefined as follows:

forward travelling functions:

$$f_k(t) = v_k(t) + e_k(t) , \quad (3.37)$$

$$f_m(t) = v_m(t) + e_m(t) , \quad (3.38)$$

and backward travelling functions:

$$b_k(t) = v_k(t) - e_k(t) , \quad (3.39)$$

$$b_m(t) = v_m(t) - e_m(t) , \quad (3.40)$$

where

$e_k(t)$ = voltage across equivalent network Z_{eq} due to $i_k(t)$

and

$e_m(t)$ = voltage across equivalent network Z_{eq} due to $i_m(t)$.

Equations 3.37 and 3.38 are represented in the system shown in fig. 3.9.

Equations 3.39 and 3.40 contain the information leading to the new weighting functions.

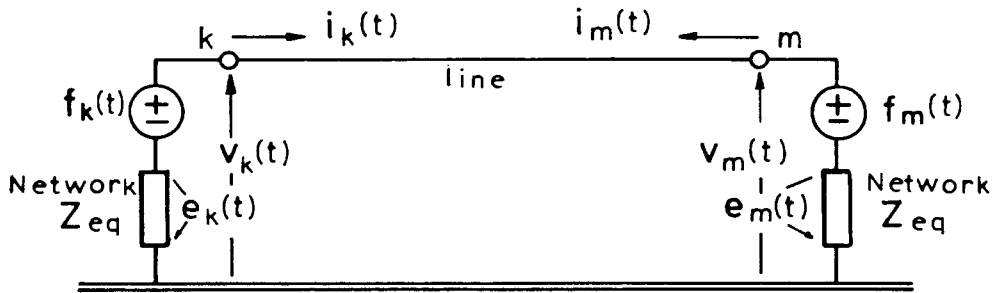


Fig. 3.9: Equivalent circuit interpretation of the new f_k and f_m functions.

Assuming that the network Z_{eq} is linear, equations 3.37 to 3.40 can be transformed into the frequency domain as follows:

forward travelling functions:

$$F_k(\omega) = V_k(\omega) + Z_{eq}(\omega) I_k(\omega) , \quad (3.41)$$

$$F_m(\omega) = V_m(\omega) + Z_{eq}(\omega) I_m(\omega) , \quad (3.42)$$

and backward travelling functions:

$$B_k(\omega) = V_k(\omega) - Z_{eq}(\omega) I_k(\omega) , \quad (3.43)$$

$$B_m(\omega) = V_m(\omega) - Z_{eq}(\omega) I_m(\omega) . \quad (3.44)$$

These equations correspond to Snelson's 3.17 to 3.20 substituting R_1 by $Z_{eq}(\omega)$. The voltages across Z_{eq} in the time domain are related to the corresponding voltages in the frequency domain by

$$e_k(t) \xleftrightarrow{\mathcal{F}} E_k(\omega) = Z_{eq}(\omega) I_k(\omega) \quad (3.45)$$

and

$$e_m(t) \xleftrightarrow{\mathcal{F}} E_m(\omega) = Z_{eq}(\omega) I_m(\omega), \quad (3.46)$$

where

$$Z_{eq}(\omega) = Z_c(\omega) \quad (3.47)$$

(within the limits of the approximation).

Comparing equations 3.41 to 3.44 with the general solution for the line equations in the frequency domain, equations 1.34 and 1.35, and with 3.47, it follows that

$$B_k(\omega) = A_1(\omega) F_m(\omega) \quad (3.48)$$

and

$$B_m(\omega) = A_1(\omega) F_k(\omega), \quad (3.49)$$

where

$$A_1(\omega) = e^{-\gamma(\omega) \cdot \ell} = \frac{1}{\cosh(\gamma\ell) + \sinh(\gamma\ell)}. \quad (3.50)$$

Referring back to Meyer and Dommel's $A_1(\omega)$ and $A_2(\omega)$ functions (equations 3.23 and 3.24), it can be seen that by replacing in these equations R_1 by $Z_c(\omega)$, equation 3.50 is obtained for $A_1(\omega)$ and $A_2(\omega) = 0$, thus corresponding to the results of the present derivation.

The time domain form of equations 3.48 and 3.49 is given by

$$b_k(t) = a_1(t) * f_m(t) \quad (3.51)$$

and

$$b_m(t) = a_1(t) * f_k(t), \quad (3.52)$$

which correspond to equations 3.25 and 3.26 in Meyer and Dommel's formulation.

The convolution integrals in equations 3.51 and 3.52 are given by

$$b_k(t) = \int_{-\infty}^{\infty} f_m(t-u) a_1(u) du = \int_{\tau}^{\infty} f_m(t-u) a_1(u) du \quad (3.53)$$

and

$$b_m(t) = \int_{-\infty}^{\infty} f_k(t-u) a_1(u) du = \int_{\tau}^{\infty} f_k(t-u) a_1(u) du. \quad (3.54)$$

The lower limit in the above integrals is τ , since $a_1(t) = 0$ for $t < \tau$ (fig. 3.8). With reference to fig. 3.7, τ represents the time needed by the fastest frequency component of the applied voltage impulse to reach the receiving end of the line. (This time is given by $\tau = \text{line length} \cdot \sqrt{LC}$ for $\omega \rightarrow \infty$.) In a discrete numerical solution of the system network, if the time step Δt is chosen to be smaller than τ , then the values for f_k and f_m in the convolution integrals 3.53 and 3.54 are known (at discrete points) from the previous time steps and these integrals can be evaluated.

Since the new weighting function $a_1(t)$ consists of only one spike, the upper limit in the "history integrals", equations 3.53 and 3.54, does not extend beyond τ for very long, and the time interval during which these integrals have to be evaluated is much shorter than in the case of Meyer and Dommel's formulation.

From the preceding considerations, the following advantages of the new formulation compared to Meyer and Dommel's can be noted:

- a) The problem of accurate evaluation of the tail portions of the weighting functions has been eliminated.

b) The interval of integration to evaluate the history functions is much shorter, thus considerably reducing computer time in numerical evaluations of these integrals.

c) The problem of accurate evaluation of the weighting function $a_2(t)$ has been eliminated.

Physical interpretation of $a_1(t)$ in the new formulation:

The original objective in establishing the new formulation was to arrive at the physical interpretation in fig. 3.7. That this objective has been accomplished is verified next. Let in equations 3.48 and 3.49

$$F_m(\omega) = 0 \quad \text{and} \quad F_k(\omega) = 1 . \quad (3.55)$$

Then

$$B_k(\omega) = 0 \quad \text{and} \quad B_m(\omega) = A_1(\omega) , \quad (3.56)$$

which in the time domain gives

$$f_m(t) = 0 , \quad f_k(t) = \delta(t) , \quad (3.57)$$

$$b_k(t) = 0 \quad \text{and} \quad b_m(t) = a_1(t) . \quad (3.58)$$

With conditions 3.57 in the original definition of the new forward travelling functions (equations 3.37 and 3.38), it follows that

$$v_k(t) = \delta(t) - e_k(t) \quad (3.59)$$

and

$$v_m(t) = -e_m(t) . \quad (3.60)$$

With relations 3.57, 3.59, and 3.60, the system of fig. 3.9 becomes the originally desired system of fig. 3.7. Substitution of conditions 3.58 in

the new backward travelling functions (equations 3.39 and 3.40) gives

$$v_k(t) = e_k(t) \quad (3.61)$$

and

$$v_m(t) = a_1(t) + e_m(t) . \quad (3.62)$$

From equations 3.60 and 3.62 it then follows that

$$a_1(t) = 2v_m(t) , \quad (3.63)$$

thus verifying the original assumption regarding the form of the new $a_1(t)$ weighting function. The function $a_2(t)$ does not appear in this new formulation.

Line equivalent circuit:

At a given time step t of the network solution, the values of the functions $b_k(t)$ and $b_m(t)$ are defined from the history of the line variables (equations 3.53 and 3.54). Substitution of these values in the original definition of the functions b_k and b_m (equations 3.39 and 3.40) gives the line equivalent circuits at nodes k and m . That is, let, from equations 3.53 and 3.54,

$$b_k(t) = \underline{e}_{kh} \quad (\text{from history}) \quad (3.64)$$

and

$$b_m(t) = \underline{e}_{mh} \quad (\text{from history}) . \quad (3.65)$$

Then, from equations 3.39 and 3.40,

$$v_k(t) = e_k(t) + \underline{e}_{kh}(t) \quad (3.66)$$

and

$$v_m(t) = e_m(t) + \underline{e}_{mh}(t) , \quad (3.67)$$

where e_k and e_m represent the voltages across the network Z_{eq} . Equations 3.66 and 3.67 can be represented by the equivalent circuits shown in fig. 3.10.

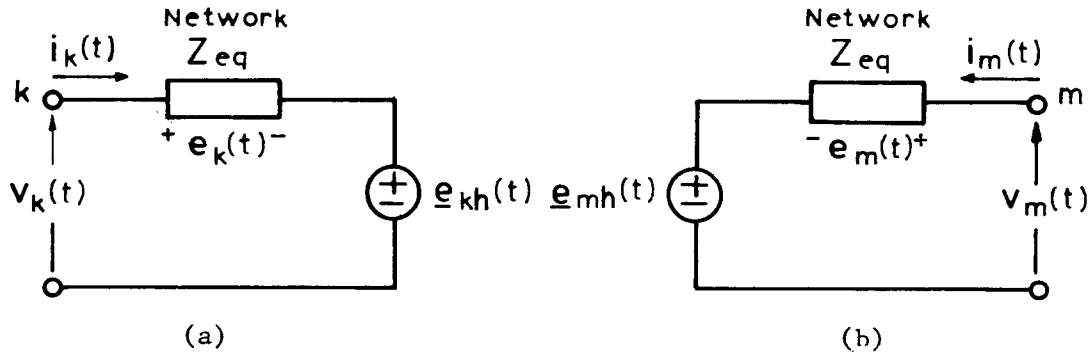


Fig. 3.10: New line models at time step t . (a) Node k . (b) Node m . (e_{kh} and e_{mh} known from past values .)

The circuits in fig. 3.10 have the same form as the circuit in fig. 1.3(a) of Dommel's representation for the simplified line. The only difference in the circuits is that the simple resistance R_c , representing the characteristic impedance of the simplified line, has now been replaced by the network Z_{eq} , which represents the frequency-dependent characteristic impedance of the real line.

As will be discussed in detail later in this work, the network Z_{eq} in the models in fig. 3.10 can be simulated, to a high degree of accuracy, by a combination of Resistance-Capacitance (R-C) building blocks. As in Dommel's general transient program [10], these R-C blocks can in turn be simulated by pure resistances in combination with corresponding history current sources. The line models in fig. 3.10 can then be further reduced to an equivalent resistance in parallel with a total equivalent history current source, and thus to the same simple form of the circuit in fig. 1.3(b).

The idea of using R-C combinations to model the line characteristic impedance is considered in the work by Groschupf [25], who uses a simple

R-C model to approximate $Z_c(\omega)$ over the low- and mid-frequency ranges. Yet, Groschupf concludes that the effect of the frequency dependence of the characteristic impedance is not very significant. The results presented later in this Dissertation, however, show that Groschupf's conclusions are correct only for some simple cases of open-circuited lines. For a general class of transient studies, and particularly when short circuits are involved, the correct simulation of $Z_c(\omega)$ can become very important.

Some additional physical considerations:

In order to explore further the physical meaning of the weighting function $a_1(t)$, it is interesting to consider the simplified case when the system has no losses and the parameters do not depend on the frequency. Under these conditions there will be no distortion or attenuation, and in the system in fig. 3.7 the impulse injected at node k will arrive unmodified at node m after a time τ . The comparison between the form of $a_1(t)$ for this ideal case and the form of $a_1(t)$ for the general case is shown in fig. 3.11.

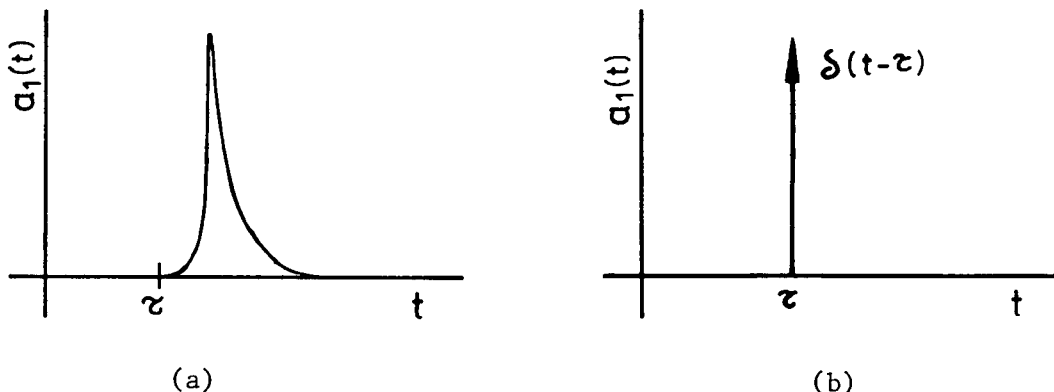


Fig. 3.11. Weighting function $a_1(t)$: (a) general case; (b) ideal case.

For the ideal $a_1(t)$ in fig. 3.11(b), the history function $b_m(t)$ in equation 3.54 becomes

$$b_m(t) = \int_{-\infty}^{\infty} f_k(t-u) a_1(u) du = \int_{-\infty}^{\infty} f_k(t-u) \delta(u-\tau) du = f_k(t-\tau), \quad (3.68)$$

and with equations 3.40 and 3.37,

$$v_m(t) - e_m(t) = v_k(t-\tau) + e_k(t-\tau). \quad (3.69)$$

But, for constant parameters and no losses

$$Z_c(\omega) = R_c = \text{constant},$$

and then

$$e_m(t) = R_c i_m(t) \quad (3.70)$$

and

$$e_k(t-\tau) = R_c i_k(t-\tau), \quad (3.71)$$

finally giving,

$$v_m(t) - R_c i_m(t) = v_k(t-\tau) + R_c i_k(t-\tau). \quad (3.72)$$

This equation is exactly the same as equation 1.46 of Dommel's formulation for the simplified line representation.

Comparing the forms of $a_1(t)$ for the general and simplified cases (fig. 3.11), it is interesting to note that in the general case the relationship between current and voltage at one of the nodes at time t depends not only on the past conditions at the other node τ units of time earlier (as in the ideal case), but on the "weighted" effect of past conditions from τ to the time at which $a_1(t)$ becomes negligible. This is a consequence of different frequency components having different travelling times and attenuations.

The preceding observations illustrate the effect of a "non-ideal" weighting function. The effect of a "non-ideal" characteristic impedance (that is, of a frequency-dependent Z_c) can be seen from equation 3.69, where $a_1(t)$ has been assumed to be ideal, but the voltages across the equivalent

impedance, e_m and e_k , are still general. For the equivalent history voltage source, equation 3.69 gives the same model as Dommel's simplified representation in fig. 1.3(a). The only difference is that now the simple resistance R_c is replaced by the equivalent characteristic impedance network Z_{eq} .

Size of the integration step:

For the evaluation of the history convolution integrals in equations 3.53 and 3.54, it was assumed that the integration step Δt in the complete network solution was smaller than the line travelling time τ . However, in some studies combining relatively long and relatively short lines, it might seem convenient, in order to save computer time, to choose a Δt that is larger than the travelling time of some of the shorter lines. A possible solution to this problem would be to represent the shorter lines by models that include the effect of $\tau < \Delta t$. This case is mentioned in Meyer and Dommel's work of reference [13] and leads to mutual coupling between the equivalent circuits at nodes k and m. This coupling complicates the solution of the complete system network.

Another alternative to the modelling of "relatively short" lines would be to represent these lines by frequency-dependent lumped-parameter sections. The modelling of frequency dependence in lumped-parameter elements is briefly discussed next.

Frequency dependence of lumped-parameter elements:

In transient studies many of the system components are represented by lumped-parameter models. For many of these components (e.g. power transformers, reactors, generators, and loads) a more accurate representation could be obtained by taking into account the frequency dependence of their parameters.

With the techniques developed in this work for the modelling of frequency-dependent transmission lines, the modelling of frequency-dependent lumped-parameter elements can be considered as a particular, simplified case.

In the equivalent circuits of fig. 3.10 there are two phenomena to be modelled: the network Z_{eq} representing the frequency-dependent characteristic impedance, and the history voltage sources representing the voltages and currents travelling along the line from the opposite end. In the case of lumped parameters there are no travelling times involved, and the problem is reduced to the modelling of a frequency-dependent impedance. The techniques described later in this work for the modelling of the line characteristic impedance can be directly applied, as well, to the modelling of the frequency-dependent impedance of a lumped element. The application of these concepts for specific cases of frequency-dependent lumped-parameter elements is beyond the scope of this Dissertation and is left as an area of future research.

CHAPTER 4

SYNTHESIS OF THE CHARACTERISTIC IMPEDANCE AND WEIGHTING FUNCTION

4.1 General Considerations

The procedures for obtaining the parameters of the new frequency-dependence line model are discussed in this chapter. Since the equivalent circuits at both line ends are analogous to each other, in order to simplify the description, only one of the ends is considered.

Equations 3.43 and 3.39 give the basic relationships for the line equivalent circuit at node k in the frequency and time domains:

$$B_k(\omega) = V_k(\omega) - Z_{eq}(\omega) I_k(\omega) \quad (4.1)$$

and

$$b_k(t) = v_k(t) - e_k(t) . \quad (4.2)$$

The corresponding equivalent circuits are shown in fig. 4.1.

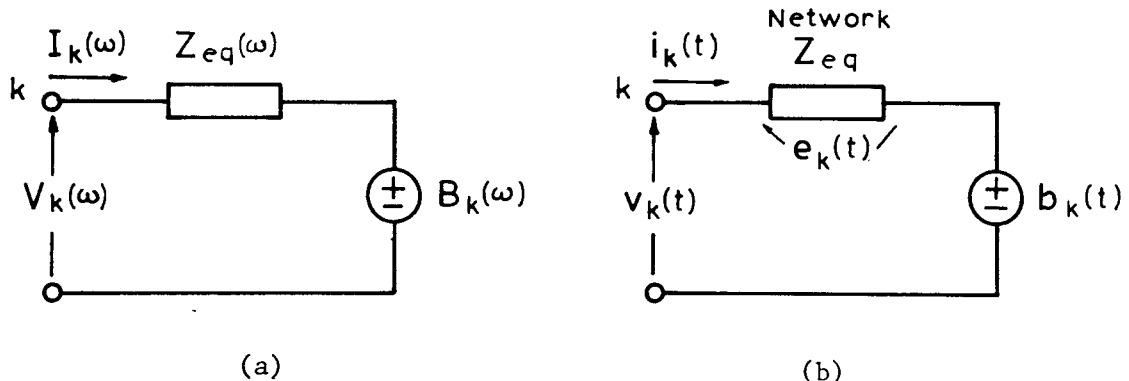


Fig. 4.1: Line equivalent circuit at node k.
 (a) Frequency domain.
 (b) Time domain.

In fig. 4.1(b) the network Z_{eq} is a constant-parameter linear network whose frequency response $Z_{eq}(\omega)$ simulates the line characteristic impedance, that is, ideally, $Z_{eq}(\omega) = Z_c(\omega)$. The history voltage source $b_k(t)$ is given by equation 3.53 as

$$b_k(t) = \int_{\tau}^{\infty} f_m(t-u) a_1(u) du. \quad (4.3)$$

In this integral, $a_1(u)$ is the history weighting function and is given by the time domain form of equation 3.50. The form of $a_1(t)$ was illustrated in fig. 3.8(a). The function $f_m(t-u)$ represents the past values of the voltage and current at the other end of the line (node m in this case) and is given, from its definition in equation 3.38, by

$$f_m(t-u) = v_m(t-u) + e_m(t-u). \quad (4.4)$$

In integral 4.3 the most recent value of f_m corresponds to $u = \tau$, that is, $f_m(t-\tau)$. As u increases, and for as long as $a_1(u) \neq 0$, the values of f_m go further back in time. For $u > t$, the values of f_m correspond to times before the transient process was started, that is, to initial conditions.

In equation 4.4 the values of v_m are the actual voltages at node m , and are thus known from the solution of the network at previous time steps and from initial conditions. The values of e_m can be obtained from the past values of v_m and from the past values of relation 3.40:

$$e_m(t-u) = v_m(t-u) - b_m(t-u). \quad (4.5)$$

Actually, $e_m(t-u)$ from this relation can be substituted in equation 4.4, giving a more direct relation for $f_m(t-u)$:

$$f_m(t-u) = 2v_m(t-u) - b_m(t-u). \quad (4.6)$$

The evaluation of the parameters of the circuit in fig. 4.1(b) presents, thus, two basic aspects:

- a) Synthesis of a linear network to simulate the line characteristic impedance.
- b) Calculation of the weighting function $a_1(t)$ and evaluation of the history voltage source $b_k(t)$.

These problems are discussed next.

4.2 Synthesis of Equivalent Network to Represent the Characteristic Impedance

4.2.1 General Considerations

From equation 1.33 the characteristic impedance for a given line mode is given by

$$Z_c(\omega) = \sqrt{\frac{Z'(\omega)}{Y'(\omega)}} , \quad (4.7)$$

where, in general,

$$Z'(\omega) = R'(\omega) + j\omega L'(\omega) \quad (4.8)$$

and

$$Y'(\omega) = G'(\omega) + j\omega C'(\omega) . \quad (4.9)$$

The variation of the series resistance (R') and inductance (L') with frequency is illustrated in fig. 4.2. The curves in this figure correspond to the zero and positive sequence modes of a typical 100-mi, 500kV, 3-phase transmission line, and were calculated using the UBC Line Constants Program [26]. This program uses Carson's formulae [19] to evaluate the frequency dependence of the line parameters.

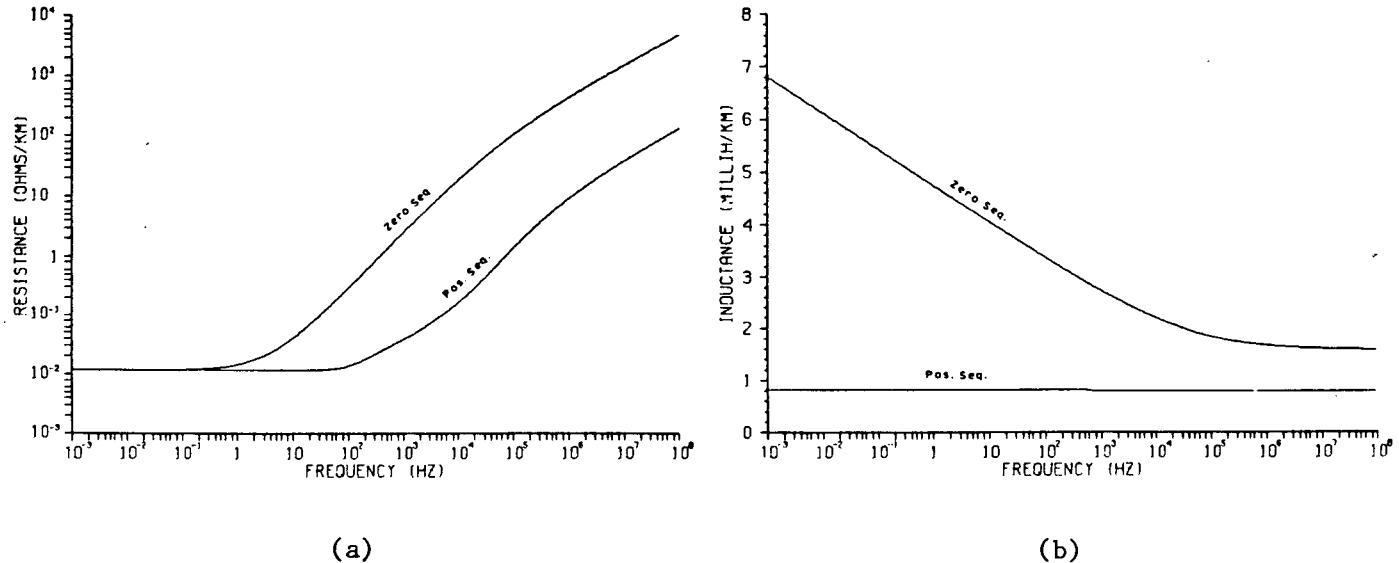


Fig. 4.2: Line parameters R' and L' as a function of frequency
 (a) R' zero and positive sequence.
 (b) L' zero and positive sequence.

In actual transmission lines the capacitance C' is not very sensitive to variations in frequency, and for frequencies up to about 1 MHz (e.g. Hedman [9]) it is usually assumed to be constant.

The shunt conductance G' is associated mainly with leakage at the insulators, and its value is affected by a series of external factors, such as humidity, pollution, and maintenance. The correct value of G' is therefore difficult to assess with accuracy. Fortunately, this value is normally small compared to the other system parameters (e.g. in the order of $.3 \times 10^{-7} \Omega^{-1}/\text{km}$, Dommel [27] p. 57), and its effect upon the system transient conditions is normally not very significant. However, as explained next, it is convenient for numerical reasons to consider a finite value of G' in the development of the line transient equivalent circuits.

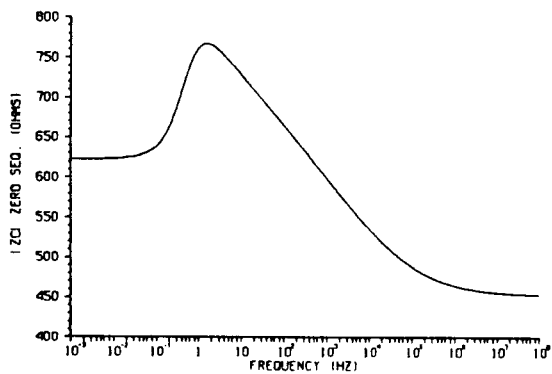
From equation 4.7,

$$Z_c(\omega) = \sqrt{\frac{R'(\omega) + j\omega L'(\omega)}{G' + j\omega C'}} . \quad (4.10)$$

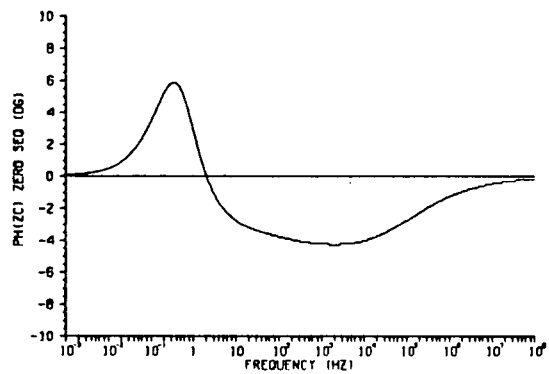
For $\omega = 0$ (dc conditions), since $R'(0)$ and $L'(0)$ are finite,

$$Z_c(\text{dc}) = \sqrt{\frac{R'(\text{dc})}{G'(\text{dc})}} . \quad (4.11)$$

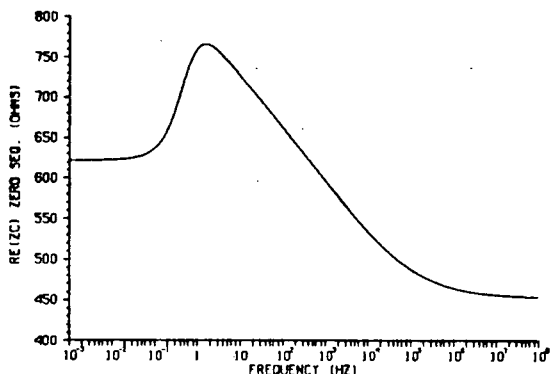
If $G'(\text{dc})$ is assumed to be zero, then $Z_c(\text{dc}) \rightarrow \infty$. Since $Z_c(\omega)$ appears as a factor (multiplying or dividing) in the formulation of the line equations,



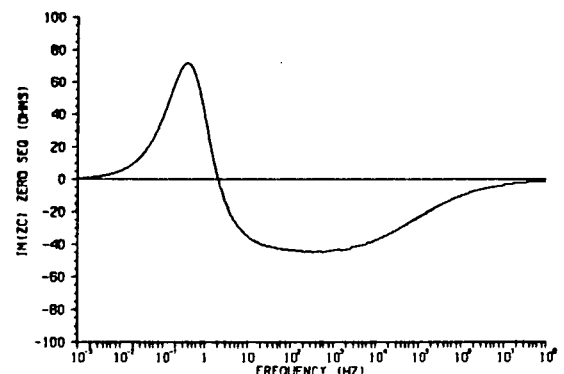
(a)



(b)



(c)

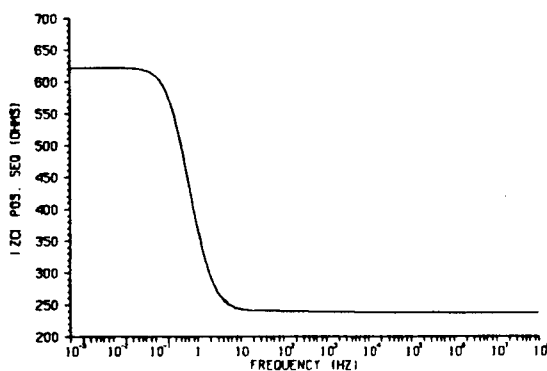


(d)

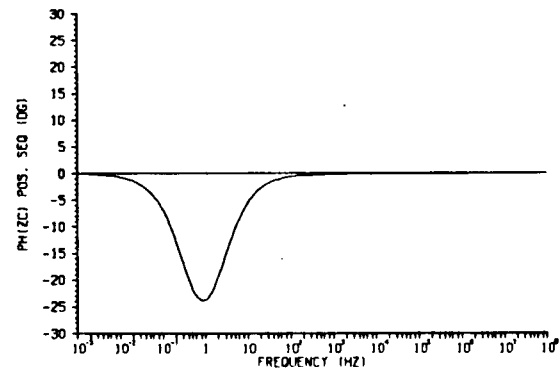
Fig. 4.3: Characteristic impedance $Z_c(\omega)$. Zero sequence mode.
a) Magnitude. b) Phase angle. c) Real part. d) Imaginary part.

having $Z_c(\omega) \rightarrow \infty$ for small or zero frequencies can cause numerical instability problems in transient studies involving d.c. or very low frequency components.

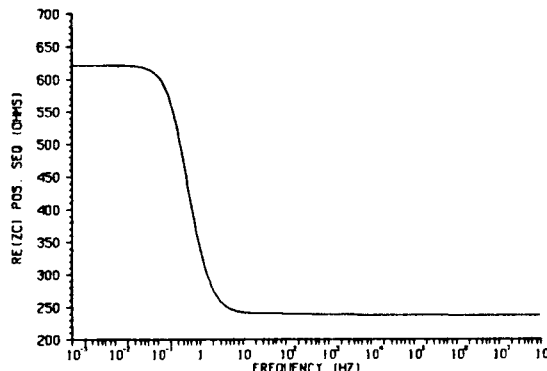
The form of the functions $Z_c(\omega)$ for the zero and positive modes of the reference line mentioned before are shown in figs. 4.3 and 4.4. These functions were evaluated from equation 4.10, where R' , L' , and C' were obtained from the UBC Line Constants Program and G' was assumed to be equal to $.3 \times 10^{-7} \Omega^{-1}/\text{km}$.



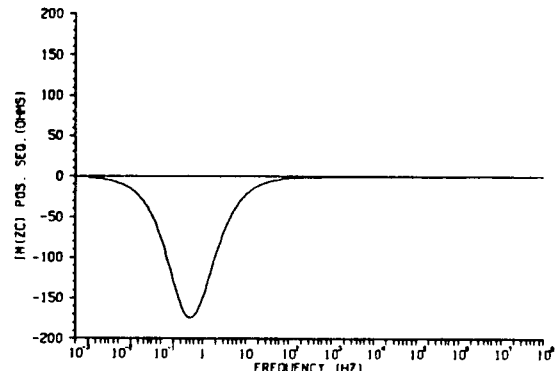
(a)



(b)



(c)



(d)

Fig. 4.4: Characteristic impedance $Z_c(\omega)$. Positive sequence mode.
a) Magnitude. b) Phase angle. c) Real part. d) Imaginary part.

4.2.2 Rational Approximation of $Z_c(\omega)$

The problem of finding a linear network whose frequency response approximates $Z_c(\omega)$ is a problem of network synthesis theory. A series of classical methods exist in network synthesis theory (e.g. Guillemin [28]) for the realization, using R, L, and C constant elements, of a given rational impedance function (a function expressed as a fraction of polynomials in the complex variable s , $s = \sigma + j\omega$). In the present case, however, the function $Z_c(\omega)$ is not known as a rational function, but only as a point by point (tabular) function of frequency. Therefore, the first step in order to simulate $Z_c(\omega)$ by an equivalent linear network is to find a rational approximation for this function.

Because of physical and numerical considerations that will be explained later, the rational function to simulate $Z_c(\omega)$ is chosen to have the following general form:

$$Z_{eq}(s) = H \frac{(s + z_1)(s + z_2) \dots (s + z_n)}{(s + p_1)(s + p_2) \dots (s + p_n)} , \quad (4.12)$$

with the following characteristics:

- (a) The constant H is real and positive.
- (b) The number of poles is equal to the number of zeros.
- (c) The poles and zeros are real, negative, and simple.

It can directly be seen that with this definition of Z_{eq} the boundary conditions of $Z_c(\omega)$ (figs. 4.3 and 4.4) can be satisfied. With $s = j\omega$ and

- i) $\omega \rightarrow 0$

$$Z_{eq}(s) \rightarrow H \frac{z_1 z_2 \dots z_n}{p_1 p_2 \dots p_n} = \text{real positive constant},$$

which should correspond to $Z_c(dc)$ in equation 4.3.

ii) $\omega \rightarrow \infty$

$$Z_{eq}(s) \rightarrow H = \text{real positive constant}$$

which should correspond to $Z_c(\omega)$ in equation 4.10 for $\omega \rightarrow \infty$.

4.2.3 Equivalent R-C Network

A rational function with real, negative, and simple poles and zeros and with the number of poles and zeros not differing by more than one can be realized by an R-C (resistance-capacitance) equivalent network. The function $Z_{eq}(s)$ in equation 4.12 satisfies these conditions. Since the line equivalent model in fig. 4.1(b) is first formulated in series form, it is convenient for the further reduction of this circuit to synthesize Z_{eq} by a series network.

Foster I realization:

The Foster I, R-C synthesis (e.g. Karni [29], p. 154) is based on a simple partial fraction expansion of the network function. In the case of equation 4.12, $Z_{eq}(s)$ can be expressed as

$$Z_{eq}(s) = k_0 + \frac{k_1}{s + p_1} + \frac{k_2}{s + p_2} + \dots + \frac{k_n}{s + p_n} , \quad (4.13)$$

where

$$k_0 = \lim_{s \rightarrow \infty} Z_{eq}(s) = H , \quad (4.14)$$

and

$$k_i = (s + p_i) Z_{eq}(s) \Big|_{s = -p_i} . \quad (4.15)$$

($i = 1, 2, \dots, n$)

(In this last relation, multiplication by the factor $(s + p_i)$ is to be understood as a cancelling out of the corresponding factor in the denominator

of $Z_{eq}(s)$, or as the limit of the product when $s \rightarrow -p_i$.)

In equation 4.13 the first term of $Z_{eq}(s)$ corresponds directly to a resistance R , and the other terms correspond to R-C parallel combinations:

$$R // \frac{1}{sC} = \frac{1/C}{s + 1/RC} . \quad (4.16)$$

The network corresponding to equation 4.13 is, therefore, as shown in fig.

4.5. The parameters of this network are given by:

$$R_0 = k_0 \quad (4.17)$$

and

$$R_i = k_i / p_i \quad (4.18)$$

$$C_i = 1/k_i \quad (4.19)$$

for $i = 1, 2, \dots, n$.

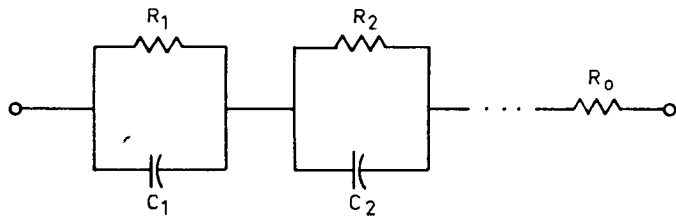


Fig. 4.5: Foster I realization of Z_{eq} .

It can readily be seen that the equivalent network in fig. 4.5 can follow the behaviour of the line characteristic impedance (figs. 4.3 and 4.4) at the boundary conditions. For very low frequencies the capacitances tend to open circuits, and at the limit ($\omega = 0$ (dc condition))

$$Z_{eq}(\omega = 0) = Z_c(\text{dc}) = R_0 + R_1 + R_2 + \dots + R_n . \quad (4.20)$$

For high frequencies the capacitances tend to short circuits, and for $\omega \rightarrow \infty$

$$Z_{eq}(\omega \rightarrow \infty) = Z_c(\omega \rightarrow \infty) = R_0 . \quad (4.21)$$

4.3 Weighting Function and History Convolution

4.3.1 General Considerations

After finding an equivalent network to simulate the characteristic impedance, the next step in completing the line equivalent circuit of fig. 4.1(b) is to find the history voltage source, $b_k(t)$. This function is given by

$$b_k(t) = \int_{\tau}^{\infty} f_m(t-u) a_1(u) du . \quad (4.22)$$

To evaluate this integral, the weighting function $a_1(t)$ has first to be determined. The frequency domain form of this function, $A_1(\omega)$, is known from its definition in terms of the system parameters. From equation 3.50,

$$A_1(\omega) = e^{-\gamma(\omega) \cdot \ell} , \quad (4.23)$$

where ℓ is the line length, and $\gamma(\omega)$ is given from equation 1.32 by

$$\gamma(\omega) = \sqrt{Z'(\omega) Y'(\omega)} , \quad (4.24)$$

which, with the considerations made earlier in connection with the frequency dependence of the parameters, can be expressed as

$$\gamma(\omega) = \sqrt{[R'(\omega) + j\omega L'(\omega)][G' + j\omega C']} . \quad (4.25)$$

The form of $A_1(\omega)$ for the zero and positive sequence modes of the reference 100-mi line is shown in figs. 4.6 and 4.7.

With $A_1(\omega)$ evaluated from the system parameters, the function $a_1(t)$ can be determined by means of an inverse Fourier transform numerical technique. Once $a_1(t)$ has been determined for a particular line mode, the history function in equation 4.22 can also be evaluated at each time step of the network solution by a numerical integration technique. There is an

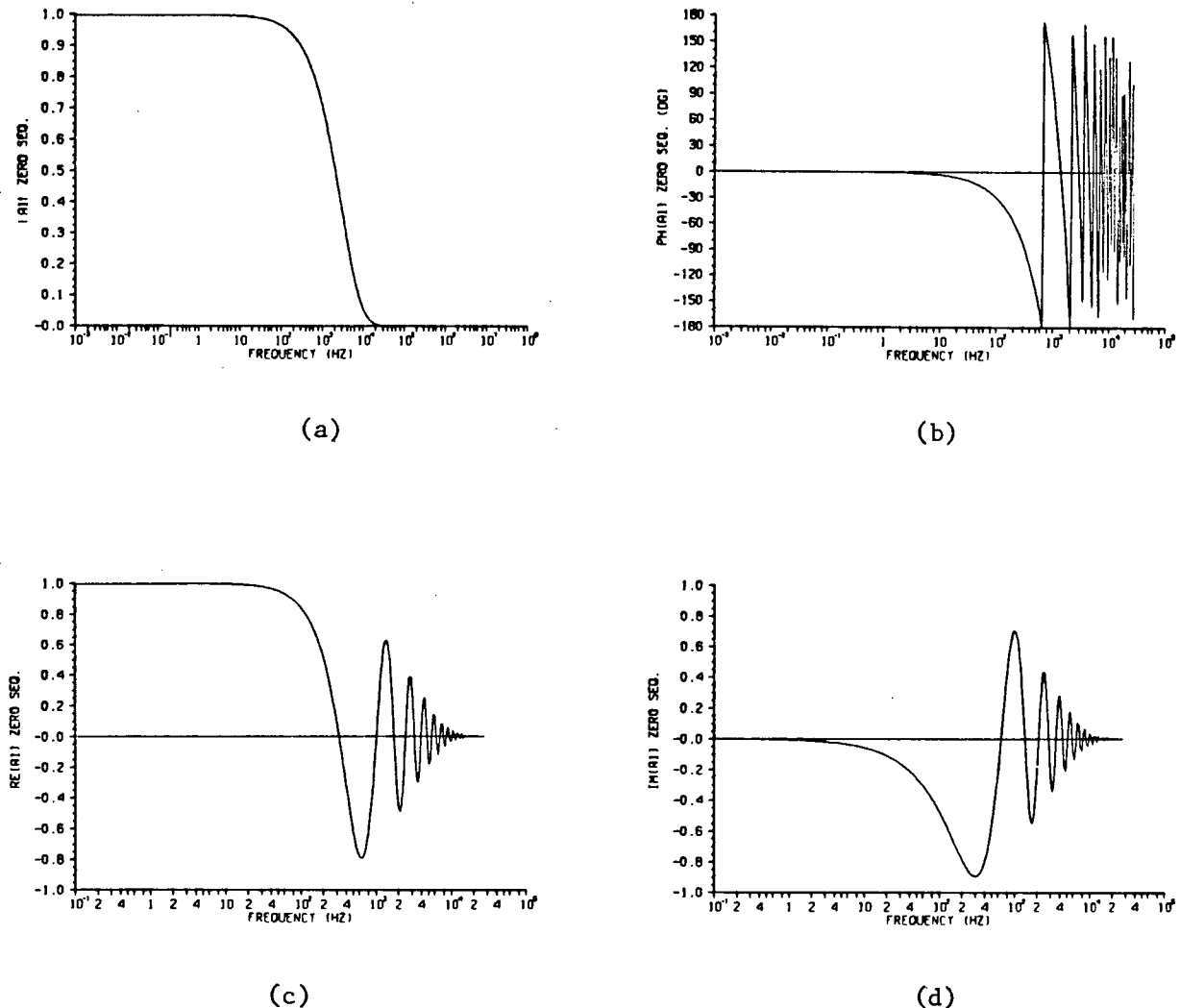


Fig. 4.6: Weighting function $A_1(\omega)$. Zero sequence mode.
 a) Magnitude. b) Phase angle. c) Real part
 d) Imaginary part.

alternative, however, to having to perform numerical integrations in order to evaluate the function $a_1(t)$ and the convolution integrals. This alternative is based on a property of the convolution of an arbitrary function with an exponential function, as discussed next.

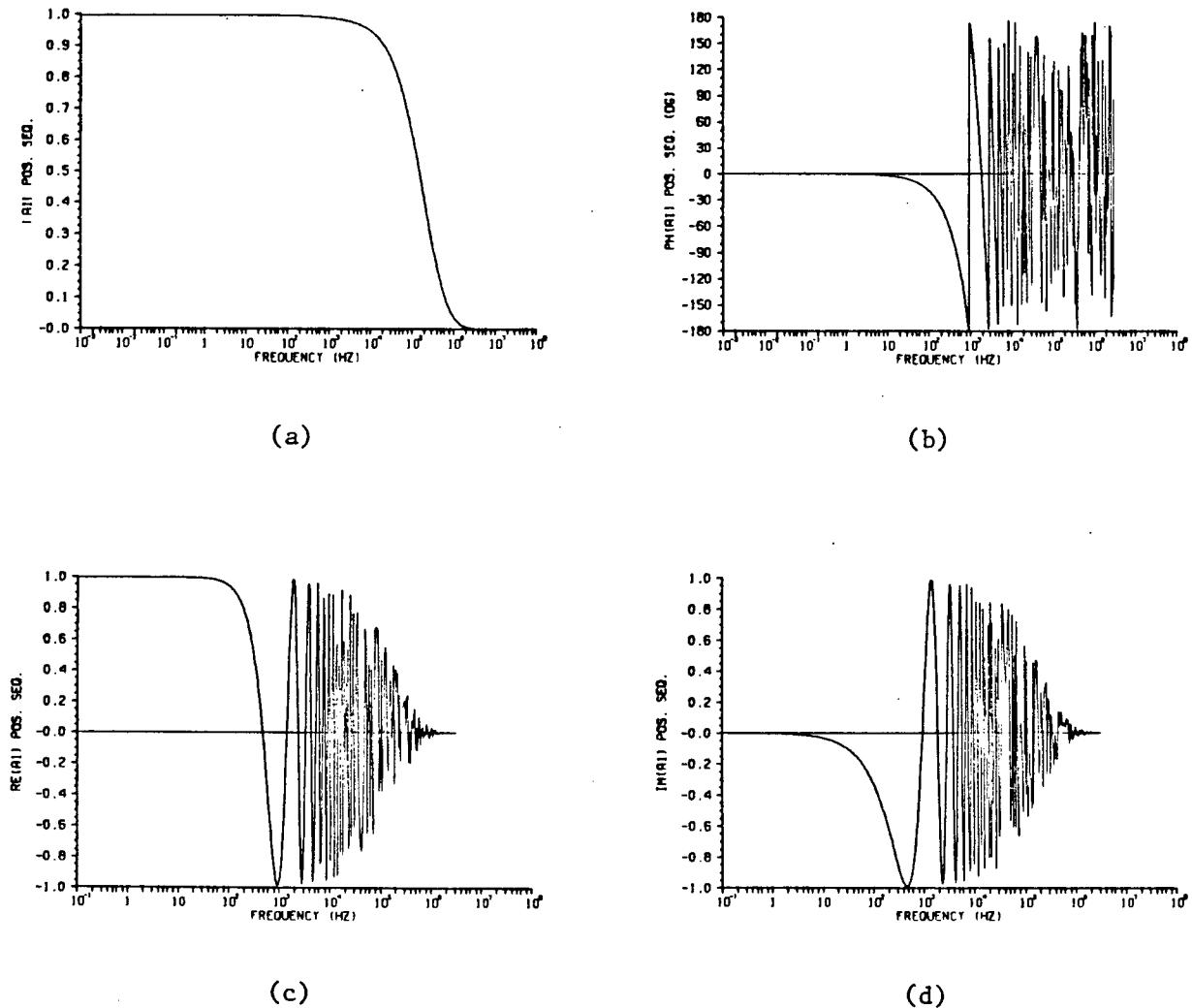


Fig. 4.7: Weighting function $A_1(\omega)$. Positive sequence mode.
 a) Magnitude. b) Phase angle. c) Real part.
 d) Imaginary part.

4.3.2 Recursive Convolution

If at each time step of a discrete process of solution the following convolution integral has to be evaluated:

$$s(t) = \int_T^\infty f(t-u) K e^{-\alpha(u-T)} du , \quad (4.26)$$

then $s(t)$ can be directly obtained from the known value of this function at the previous time step, $s(t - \Delta t)$, and the known history of the function f at T and $(T + \Delta t)$ units of time earlier, as follows:

$$s(t) = ms(t - \Delta t) + pf(t - T) + qf(t - T - \Delta t) . \quad (4.27)$$

In this relation, m , p , and q are constants that depend on k , α , the integration step Δt , and the numerical interpolation technique used to approximate the function f in an interval between $(t - T - \Delta t)$ and $(t - T)$. (This convolution property is derived in App. II.1.). The evaluation of $s(t)$ from relation 4.27 instead of evaluating the complete integral 4.26 (at each time step of the solution process) can save a considerable amount of computer time.

The recursive convolution property in the modelling of frequency dependence is used by Umoto and Hara [39], by Meyer and Dommel [13] (to evaluate the tail portions of the convolutions in equations 3.25 and 3.26), and has been strongly advocated by Semlyen in his contributions to the solution of this problem (e.g. [14], [16], and [30]).

In order to apply the property of recursive convolution to evaluate the history integral in equation 4.22, the function $a_1(t)$ has first to be approximated as a sum of exponential terms. However, a sum of exponentials in the time domain corresponds to a rational function in the frequency domain and, therefore, the approximation can be performed directly on the known function $A_1(\omega)$, thus sparing the need for a numerical inverse transformation to obtain $a_1(t)$. Besides the advantage of avoiding this numerical inverse transformation, and due to the forms of $A_1(\omega)$ and $a_1(t)$, the approximation of $A_1(\omega)$ by a rational function is much easier to perform with accuracy than the approximation of $a_1(t)$ by a sum of exponential terms.

Rational approximation vs. numerical integration:

In addition to the savings in computer time, the technique of rational approximation of $A_1(\omega)$ and recursive evaluation of the convolution integrals can also yield more accurate results than the direct numerical evaluation of these integrals. In this respect two aspects must be considered. First, in a direct evaluation of the convolution integrals, the function $a_1(t)$ has to be obtained by numerical inverse transformation of $A_1(\omega)$. But, even though in the overall the real and imaginary parts of $A_1(\omega)$ in the present formulation are less oscillatory than the corresponding functions in Budner's or Snelson's formulations, the upper part of the frequency range of these functions is still very oscillatory (e.g. figs. 4.6 and 4.7). This oscillatory behaviour becomes more pronounced when the damping becomes smaller. This is the case of aerial modes (fig. 4.7 as compared to fig. 4.6) and of short lines. Accurate numerical evaluation of the inverse Fourier transform in the very oscillatory regions can be fairly difficult, requiring a large number of frequency points. On the other hand, the magnitude of $A_1(\omega)$ (e.g. figs. 4.6(a) and 4.7(a)) is very smooth over the entire frequency range, regardless of the line mode or length. The numerical technique (described in detail later) employed in this work to find a rational approximation for the function $A_1(\omega)$ works directly with the magnitude function, whereas the phase function becomes automatically defined from the magnitude function. Since the magnitude function is evenly smooth, the entire frequency range of $A_1(\omega)$ can be evenly approximated and a very accurate closed-form series of exponentials can be obtained for $a_1(t)$.

The second aspect of the procedure to determine the history functions (equation 4.22) is the numerical evaluation of the convolution integrals at each time step of the network solution. In this respect, even assuming that $a_1(t)$ had been accurately determined from numerical inverse transformation of $A_1(\omega)$, $a_1(t)$ would only be available at discrete time points. Because of the sharp spike form of this function (fig. 3.8(a)), the fact of having its values at only discrete points may introduce significant additional errors in the evaluation of the convolution integrals. As before, this consideration becomes more important in the case of aerial modes and short lines, where the spike form of $a_1(t)$ becomes very high and narrow, tending, in the limit case of no losses, to an impulse. The technique of rational approximation of $A_1(\omega)$ permits $a_1(t)$ to be directly obtained in a closed-form; as a consequence, no additional interpolation errors are introduced in the evaluation of the history functions.

Before leaving this point, it is interesting to mention a possible improvement to the method of direct evaluation of $a_1(t)$ by numerical inverse transformation of $A_1(\omega)$. From fig. 3.8(a), $a_1(t)$ can be expressed as

$$a_1(t) = p(t - \tau), \quad (4.28)$$

where $p(t)$ has the same form as $a_1(t)$, but is displaced τ units of time towards the origin. From the time shifting property of the Fourier transform, the frequency domain form of relation 4.28 is given by

$$A_1(\omega) = P(\omega)e^{-j\omega\tau}. \quad (4.29)$$

The function $P(\omega)$ is then given by

$$P(\omega) = A_1(\omega)e^{j\omega\tau}. \quad (4.30)$$

The real and imaginary parts of $P(\omega)$ are much smoother than those of $A_1(\omega)$ over the entire frequency range. Numerical inverse transformation of $P(\omega)$ would then be much easier to perform with accuracy than that of $A_1(\omega)$. Once $p(t)$ had been determined, the function $a_1(t)$ would simply be given by relation 4.28. Further research would be necessary in order to assess the possibilities of this method.

The method of rational approximation of $A_1(\omega)$ and recursive evaluation of the convolution integrals is the one that has been adopted in this work. In the following section the form of the approximating function is considered. The corresponding numerical techniques for obtaining the approximation are discussed in the subsequent section.

4.3.3 Rational Approximation of $A_1(\omega)$

As introduced at the end of the preceding section, the function $a_1(t)$ can be expressed as

$$a_1(t) = p(t - \tau), \quad (4.31)$$

from where,

$$A_1(\omega) = P(\omega)e^{-j\omega\tau}. \quad (4.32)$$

In order to express $a_1(t)$ as a sum of exponentials, it is first assumed that the function $P(s)$, corresponding to $P(\omega)$ in the complex plane, can be approximated by a rational function of the form

$$P_a(s) = H \frac{(s + z_1)(s + z_2) \dots (s + z_n)}{(s + p_1)(s + p_2) \dots (s + p_m)}. \quad (4.33)$$

(The subscript "a" is used to indicate "approximating function.")

Since, as shown by equation 3.63 and the circuit in fig. 3.9, the function $A_1(\omega)$ corresponds to the response of a passive, physical system, the function $P_a(s)$ in equation 4.33 must be such that $n < m$, and the real part of the poles must lie in the left-hand side of the complex plane. Because of numerical considerations (to be explained later), the poles and zeros are further restricted to be negative, real, and simple.

Expanding $P_a(s)$ into partial fractions:

$$P_a(s) = \frac{k_1}{s + p_1} + \frac{k_2}{s + p_2} + \dots + \frac{k_m}{s + p_m}. \quad (4.34)$$

The corresponding time-domain form of this equation, assuming that the causality condition is satisfied ($p_a(t) = 0$ for $t < 0$), is given by

$$p_a(t) = [k_1 e^{-p_1 t} + k_2 e^{-p_2 t} + \dots + k_m e^{-p_m t}]U(t), \quad (4.35)$$

where $U(t)$ is the unit step function.

From equations 4.31 and 4.35, and with $a_{1a}(t)$ as the function approximating $a_1(t)$, it then follows that

$$a_{1a}(t) = [k_1 e^{-p_1(t-\tau)} + k_2 e^{-p_2(t-\tau)} + \dots + k_m e^{-p_m(t-\tau)}]U(t-\tau). \quad (4.36)$$

This function has the form required by equation 4.26 to allow recursive evaluation of the history convolution integral (equation 4.22).

4.4 Numerical Synthesis of Rational Approximations for $Z_C(\omega)$ and $A_1(\omega)$

4.4.1 General Considerations

A rational function in the complex plane has the general form

$$F(s) = \frac{P(s)}{Q(s)}, \quad (4.37)$$

where $P(s)$ and $Q(s)$ are polynomials in the complex variable $s = \sigma + j\omega$. If $F(s)$ corresponds to the response of a physical system, for instance, an immittance or transfer function, some restrictions are imposed on the relation between the degrees of $P(s)$ and $Q(s)$ and on the location of the roots (zero and poles) of these polynomials.

The problem of approximating a given function of frequency by the general rational function 4.37 is that of finding the polynomials $P(s)$ and $Q(s)$. This problem is not straightforward because, even with the restrictions imposed by the physical system, there is still an infinite number of possible solutions for $P(s)$ and $Q(s)$. As a result, the range of possible methods of solution is also very large. In general, as in other approximation problems, the question as to which method of solution should be preferred ought to be formulated in terms of obtaining accurate enough results by means of a formulation that can be implemented in a practical, "engineering" way with reasonable resources (e.g. costs, man-power, and facilities).

Different techniques are mentioned in the classical literature on network synthesis (e.g. Guillemin [28]) for the solution of the rational approximation problem. Examples of these traditional methods are approximations based on the concepts of Butterworth, Chebyshev, Fourier, Taylor, Padé, and "potential analogies". These methods were developed when limited computational resources were available (before digital computers) and were mainly applied to the particular problem of the ideal filter response. The function $F(s)$ in 4.37 was restricted, for example, to $P(s) = 1$ and to $Q(s)$ being a low order polynomial.

Of more recent development (with the development of digital computers) are very general optimization techniques [31], such as, the method of steepest descent, the conjugate gradient method, and the method

of Fletcher and Powell. These techniques are based on the optimization of the parameters of a pre-defined $F(s)$ function. Because of the capacity of digital computers much freedom and generality is allowed to the form of $F(s)$. However, this has created a new problem: too much freedom begets anarchy, and these methods often present convergence problems. The user actually has to supply, somehow, a starting form which is "close enough" to the solution so that the optimization process converges to a "better" final solution. In many approximation problems, this task is not easy and requires experience and familiarity with both the form of the function being approximated and the internal characteristics of the numerical algorithms. Quoting Szentirmai [32]: "Except for simple cases, the author has been able to coax reasonable results out of iterative optimization programs only by trial-and-error methods of parameter selection." Though this skeptical comment was made by Szentirmai in 1971, it still reflects the basic limitation of optimization methods: in many problems, a good guess of the final form has to be supplied beforehand.

In the modelling of frequency dependence in transmission lines, the form of the functions to be approximated depends on the particular line, its length, and the particular mode. A pre-selected form of approximating function, or one developed for a particular case, will not in general represent the best form for other cases, and unless adjustments are made by the user, optimization algorithms may give very poor results or not converge at all.

Before presenting the technique employed in this work for the rational approximation of the $Z_c(\omega)$ and $A_1(\omega)$ functions, reference will be made to approximation techniques employed by other authors in connection with frequency dependence formulations.

4.4.2 Approximation Techniques by Other Authors

Semlyen makes extensive use of the concept of recursive evaluation of the convolution integrals in his formulations of the frequency-dependence problem. These formulation are in terms of incident and reflected waves and involve the "system propagation function" and the "characteristic admittance function". The approximations used by Semlyen to model these functions have been restricted, however, to a low number of exponential terms (low order $Q(s)$) in equation 4.37), thus limiting the accuracy to specific frequency regions. In reference [14], the exponentials are obtained from response functions in the time domain; the propagation function is approximated by two exponentials and the characteristic admittance by a constant plus one exponential term (an additional exponential for the characteristic admittance is mentioned in the Closure to reference [14]). Later, in references [16] and [17], the propagation function is approximated directly in the frequency domain by means of a rational function with a $Q(s)$ of order three; the characteristic admittance, however, is assumed to be constant [17]. In Semlyen's most recent publication [30], the need for using higher order approximations for the propagation function (up to six exponentials) is recognized as desirable. The method mentioned in this reference to obtain the rational approximations is a modified Gram-Schmidt algorithm (orthogonal polynomials) for a least-square optimization. Problems of ill-conditioning and accuracy in determining the most adequate form of the approximation are also reported in this reference.

In another contribution to the modelling of frequency dependence, Ametani [15] suggests a piece-wise straight-line approximation of the system propagation and characteristic impedance functions in the time domain. Difficulties in the use of this method, however, have been indicated by the Bonneville Power Administration; one of the major difficulties has been the

transition between initial sinusoidal steady states and transient states.

4.4.3 Rational Approximation Technique in the New Formulation

The method implemented in this work for the synthesis of the equivalent characteristic impedance and for the rational approximation of the history weighting function is a very flexible and straightforward technique. It is not limited to low-order approximations, as the classical techniques, and does not require the user to supply the adequate parameters and functions, as in modern general optimization techniques. The order and parameters of the approximation are automatically determined by the routine as the approximating function "freely" adapts itself to the form of the approximated function. Since the form of the approximant is not determined beforehand, numerical instability and accuracy problems due to wrong choices are avoided. Also the entire frequency range of the function can be evenly considered.

The technique is based on an adaptation of the very simple concept of asymptotic approximation of the magnitude function, introduced by Bode in 1945 [33]. The basic principles for the implementation of this method for the synthesis of $Z_c(\omega)$ and the rational approximation of $A_1(\omega)$ are discussed next.

Approximation of the magnitude function:

Bode's procedure for approximating the magnitude of a rational function is illustrated in fig. 4.8 for the characteristic impedance. The magnitude (in decibels) is plotted as a function of the logarithm of the frequency. The basic principle of the procedure is to "trace" the approximated curve by straight-line segments. These segments may be either horizontal or have a slope that is a multiple of 20 decibels/decade. The

points of change of slope (corners or breaking points) define the poles and zeros of the rational approximating function.

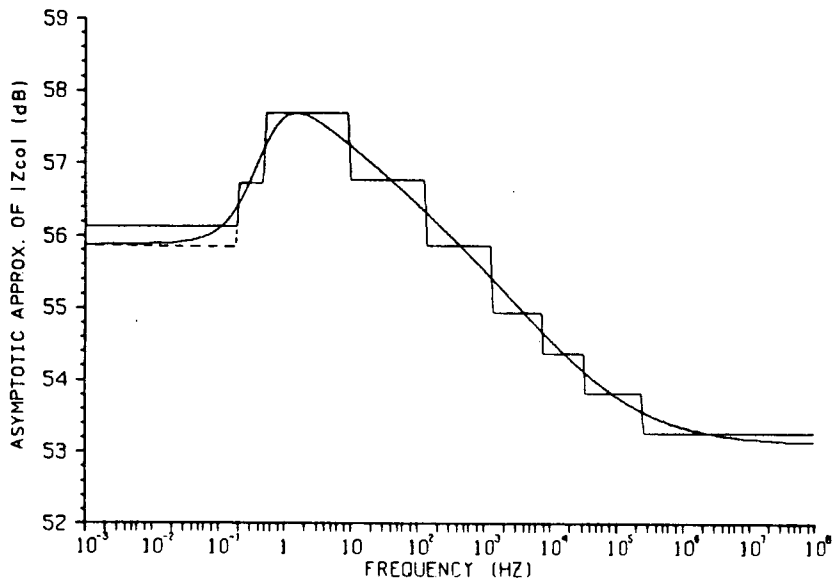


Fig. 4.8: Asymptotic approximation of the magnitude of $Z_c(\omega)$, zero seq.

The desired form of $Z_{eq}(s)$ is (from equation 4.12)

$$Z_{eq}(s) = H \frac{(s + z_1)(s + z_2) \dots (s + z_n)}{(s + p_1)(s + p_2) \dots (s + p_n)}. \quad (4.38)$$

Taking the logarithm of the magnitude of this function and multiplying by 20 (to follow the convention of considering the magnitude as gain or attenuation in decibels), it is obtained that

$$\begin{aligned} 20 \log|Z_{eq}(s)| &= 20 \log H + 20 \log|s + z_1| + \dots + 20 \log|s + z_n| \\ &\quad - 20 \log|s + p_1| - 20 \log|s + p_2| - \dots - 20 \log|s + p_n|. \end{aligned} \quad (4.39)$$

For $s = j\omega$, each one of the terms in this expression has a straight-line asymptotic behaviour with respect to ω . Considering, for instance, the term

$$20 \log|j\omega + z_1|,$$

it follows that

$$\lim \text{ for } \omega \ll z_1 = 20 \log z_1,$$

that is, a constant. And,

$$\lim \text{ for } \omega \gg z_1 = 20 \log \omega,$$

which, as a function of $(\log \omega)$, is a straight line having an increment of 20 decibels for each $\omega_2/\omega_1 = 10$, that is, a slope of 20 dB/dec. The combined asymptotic behaviour of all the terms in equation 4.39 can be visualized as follows. Imagining equation 4.38 (or equation 4.39) as constructed step by step, each time a zero corner (at $\omega = z_i$) is added, the slope of the asymptotic curve is increased by 20 dB. Each time a pole corner (at $\omega = p_i$) is added, the slope is decreased by 20 dB.

The foregoing description is a brief synthesis of the well-known fundamentals of Bode's asymptotic approximation. In fig. 4.8 it must be noted that the straight-line segments do not represent the actual form of the approximating function (equation 4.38) but only an asymptotic tracing of this curve. The actual approximating function is a smooth curve, with no sharp corners, and much closer to the approximated function.

Since the entire curve is traced during the approximation process, from $\omega \rightarrow 0$ (the dc condition can easily be exactly matched) to the highest frequency at which the approximated function becomes practically constant, there are no "left out" regions and a uniformly accurate approximation is obtained over the entire frequency range.

In the numerical procedure implemented in this work, the accuracy of the fitting is further improved by an algorithm that shifts the location of poles and zeros about their first asymptotic positions. In this process

the actual approximating function (equation 4.38) is compared to the approximated function. The entire process of solution is computationally very fast.

The same basic procedure described for the simulation of $Z_c(\omega)$ is applied for the simulation of $A_1(\omega)$.

Some additional considerations:

Since the curves to be approximated ($|Z_c(\omega)|$ and $|A_1(\omega)|$, e.g. figs. 4.3(a), 4.4(a), 4.6(a), and 4.7(a)) are smooth, only real poles and zeros are allowed in the corresponding rational functions (equation 4.12 for $Z_c(\omega)$ and equation 4.33 for $P_a(\omega)$). Complex poles or zeros can produce local ripples. The problem of local ripples is mentioned by Semlyen [30], who allows complex exponentials in the approximating functions. Also, in order to obtain an R-C network for the simulation of $Z_c(\omega)$ and simple exponentials in the time domain form of the weighting function, only simple (multiplicity one) poles are permitted.

Phase functions:

The rational functions 4.12 and 4.33, as determined by the method of asymptotic approximation, have no zeros in the right-hand side of the complex plane. Under these conditions, it is shown in Fourier transform theory (e.g. Papoulis [34], p. 204) that the corresponding phase functions are uniquely determined from the magnitude functions, and the rational functions belong to the class of minimum phase shift. The agreement between the phases of $Z_c(\omega)$ and $P(\omega)$, and the phases of the corresponding rational approximations obtained in this work confirms the validity of using minimum-phase-shift approximations.

The phase angle of the function approximating $A_1(\omega)$ is obtained from relation 4.32 by subtracting $-\omega\tau$ from the phase angle of $P_a(\omega)$:

$$\phi_{A1a} = \phi_{Pa} - \omega\tau . \quad (4.40)$$

The time delay τ in this relation is directly obtained by comparing the phase angle of $P_a(\omega)$ and the phase angle of $A_1(\omega)$:

$$\tau = \frac{\phi_{Pa} - \phi_{A1}}{\omega} . \quad (4.41)$$

If the approximation were exact, that is, $P_a(\omega) = P(\omega)$ for all ω , the value of τ obtained from relation 4.41 would be the same for all frequencies ω . In order to minimize the phase error in the approximation, the value of τ as given by 4.41 is averaged over the frequency range.

Causality condition:

The rational approximations $Z_{eq}(s)$ in equation 4.12 and $P_a(s)$ in equation 4.33 tend to a constant for $s = j\omega$ when $\omega \rightarrow \infty$, and have no poles in the right-hand side of the complex plane. These conditions are enough (e.g. Papoulis [34], pp. 213-214) to assure that the corresponding time domain functions are causal (that is, the function is equal to zero for $t < 0$) and thus correspond to the response of a passive physical system.

CHAPTER 5

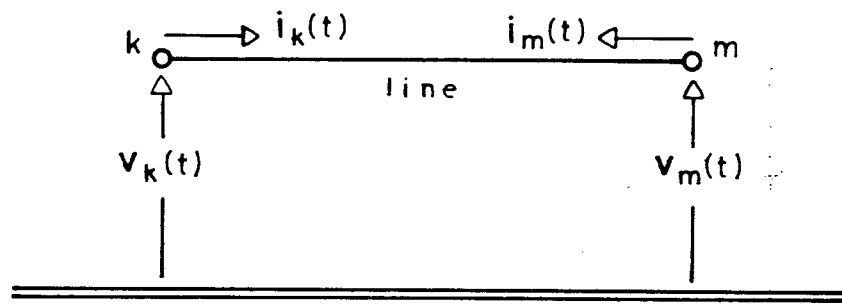
IMPLEMENTATION OF THE SOLUTION

5.1 Recapitulation

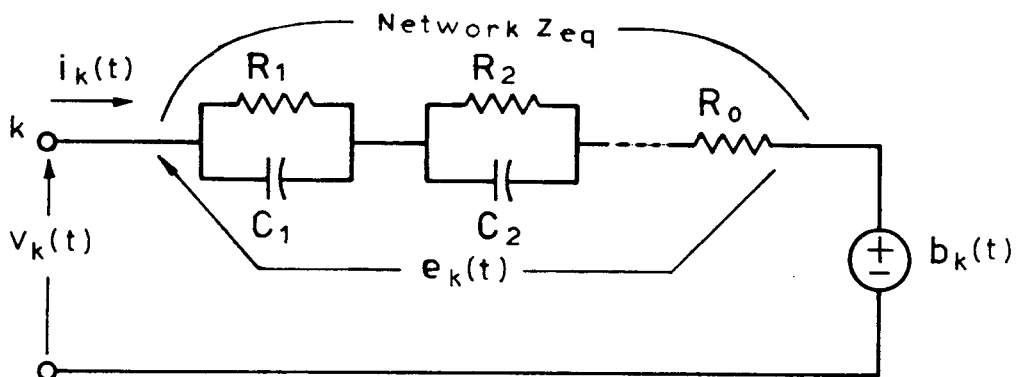
In the preceding chapters, the synthesis of a new model for the accurate and efficient representation of transmission lines in time-domain transient solutions has been discussed. In the present chapter, the final form of this model and the algorithms for its incorporation into Dommel's Electromagnetic Transients Program (EMTP) are considered.

In the new model, each line mode (fig. 5.1(a)) is represented by a lumped-parameter equivalent circuit (fig. 5.1(b)) that takes into account the frequency dependence of the line parameters and the distributed nature of the losses. This circuit consists of a constant R-C network that simulates the line characteristic impedance and a voltage source (evaluated at each time step of the system solution) that represents the weighted history of the current and voltage waves travelling along the line. The "weighting" of the travelling signals accounts for the different travelling times and attenuations of the different frequency components.

Before proceeding to reduce the line model in fig. 5.1(b) into its final form, it is interesting to emphasize the comparison between this circuit and Dommel's simplified one in fig. 1.3(a). With no losses or frequency dependence, the characteristic impedance is a simple resistance, that is, instead of the R-C network in fig. 5.1(b) the simple resistance R_c in fig. 1.3(a) is obtained. As for the voltage history source, it becomes in the simplified case (equation 3.68) a function of the voltage and current at the other end of the line at only τ units of time earlier ("ideal travelling time"); no weighting integrals are thus necessary.



(a)



(b)

Fig. 5.1: (a) Component mode of a transmission line.
 (b) Equivalent circuit for node k at time step t.

After the considerations presented next in this chapter, the line model in fig. 5.1(b) is further reduced to a single resistance in series with a history voltage source and therefore to exactly the same form as Dommel's simplified model. The new equivalent resistance and history source are, however, different from those of Dommel's model and such that the effect of the frequency dependence of the parameters and the distributed nature of the losses is automatically taken into account.

5.2 Evaluation of the Weighted History Source

From equation 3.53 ,

$$b_k(t) = \int_{\tau}^{\infty} f_m(t-u) a_1(u) du . \quad (5.1)$$

But, with $a_1(t)$ approximated as a sum of exponentials (from equation 4.36, changing the notation),

$$a_1(t) = [k_1' e^{-\beta_1(t-\tau)} + k_2' e^{-\beta_2(t-\tau)} + \dots + k_m' e^{-\beta_m(t-\tau)}] u(t-\tau) . \quad (5.2)$$

Integral 5.1 can then be expressed as

$$b_k(t) = b_{k_1}(t) + b_{k_2}(t) + \dots + b_{k_m}(t) , \quad (5.3)$$

where

$$b_{k_i}(t) = \int_{\tau}^{\infty} f_m(t-u) k_i' e^{-\beta_i(u-\tau)} du \quad (5.4)$$

for $i = 1, \dots, m$.

Writing the corresponding expression for b_{k_i} at the preceding time step $(t - \Delta t)$ of the complete network solution, it follows from the properties of recursive convolution (App. II.1) that

$$b_{k_i}(t) = e^{-\beta_i \Delta t} b_{k_i}(t - \Delta t) + k_i \int_{\tau}^{t + \Delta t} f_m(t-u) e^{-\beta_i(u-\tau)} du . \quad (5.5)$$

The original semi-infinite integral (equation 5.4) is then reduced to a constant times the value of the function at the previous time step plus a definite integral over the time step Δt .

The definite integral in equation 5.5 can be evaluated as follows.

The function f_m is known from history values only at discrete points of time, multiples of Δt . Substituting f_m in equation 5.5 by the equation of a straight line passing through the known values of f_m at $[t - \tau]$ and $[t - (\tau + \Delta t)]$ and evaluating the resulting closed-form integral (App. II.1), $b_{k_i}(t)$ can be expressed as

$$b_{k_i}(t) = g_i b_{k_i}(t - \Delta t) + c_i f_m(t - \tau) + d_i f_m(t - \tau - \Delta t) , \quad (5.6)$$

where

$$g_i = e^{-\beta_i \Delta t} , \quad (5.7)$$

and with $h_i' = \frac{1 - g_i}{\beta_i \Delta t} ,$

$$c_i = \frac{k_i'}{\beta_i} (1 - h_i') \quad (5.8)$$

and

$$d_i = -\frac{k_i'}{\beta_i} (g_i - h_i') . \quad (5.9)$$

Each one of the partial history sources in equation 5.3 can, therefore, be expressed as a function of their corresponding value at the previous time step and the history value of the variables at the other end of the line at (τ) and ($\tau + \Delta t$) units of time earlier. It is interesting to note that the values of f_m needed to evaluate the different b_{k_i} 's are the same: those at ($t - \tau$) and at ($t - \tau - \Delta t$). The numerical procedure has included the effect of different travelling times and attenuations in the different coefficients of the partial b_{k_i} sources.

5.3 Equivalent Impedance

The equivalent R-C network in fig. 5.1(b) could be directly incorporated in the EMTP, which can directly represent (using the trapezoidal rule of integration) lumped, constant parameters [10]. However, the interfacing can be simplified by further reducing the R-C network before it is interconnected with the rest of the system. Two forms of reduction are presented next. The first one follows directly from the particular nature of the R-C network and leads to an expression that has the same form as the one obtained for the weighted history source. The second reduction is

obtained from Dommel's representation of lumped-parameter elements.

Direct reduction of the R-C equivalent network:

From fig. 5.1(b), in the frequency domain

$$E_k(\omega) = I_k(\omega) Z_{eq}(\omega) , \quad (5.10)$$

where $Z_{eq}(\omega)$ is given by equation 4.12 with $s = j\omega$. The time-domain form of equation 5.10 is

$$e_k(t) = i_k(t) * z_{eq}(t) , \quad (5.11)$$

or,

$$e_k(t) = \int_{-\infty}^{\infty} i_k(t-u) z_{eq}(u) du , \quad (5.12)$$

where $z_{eq}(t)$ is the inverse Fourier transform of $Z_{eq}(\omega)$. From equation 4.13 (changing the notation), and with the causality condition,

$$z_{eq}(t) = [k_0 \delta(t) + k_1 e^{-\alpha_1 t} + k_2 e^{-\alpha_2 t} + \dots + k_n e^{-\alpha_n t}] U(t) . \quad (5.13)$$

With this form for z_{eq} , equation 5.12 can be expressed as

$$e_k(t) = e_{k_0}(t) + e_{k_1}(t) + e_{k_2}(t) + \dots + e_{k_n}(t) , \quad (5.14)$$

where

$$e_{k_0}(t) = k_0 i_k(t) = R_0 i_k(t) \quad (5.15)$$

and

$$e_{k_i}(t) = \int_0^{\infty} i_k(t-u) k_i e^{-\alpha_i u} du \quad (5.16)$$

for $i = 1, 2, \dots, n$.

Equation 5.16 has the same form as equation 5.4 with $\tau = 0$. The partial voltages in equation 5.14 can thus be expressed as

$$e_{k_0} = R_0 i_k(t) \quad (5.17)$$

and

$$e_{k_i}(t) = m_i e_{k_i}(t - \Delta t) + p_i i_k(t) + q_i i_k(t - \Delta t) \quad (5.18)$$

for $i = 1, 2, \dots, n$. As in equations 5.7 to 5.9 the "integration coefficients" are given by

$$m_i = e^{-\alpha_i \Delta t} \quad (5.19)$$

and with $h_i = \frac{1 - m_i}{\alpha_i \Delta t}$,

$$p_i = \frac{k_i}{\alpha_i} (1 - h_i) \quad (5.20)$$

and

$$q_i = - \frac{k_i}{\alpha_1} (m_i - h_i) . \quad (5.21)$$

Dommel's R-C representation:

Using Dommel's [10] representation for resistances and capacitances, each one of the R-C blocks in fig. 5.1(b) can be modelled as shown in fig. 5.2. From this model, the relation between $e(t)$ and $i(t)$ can be derived.

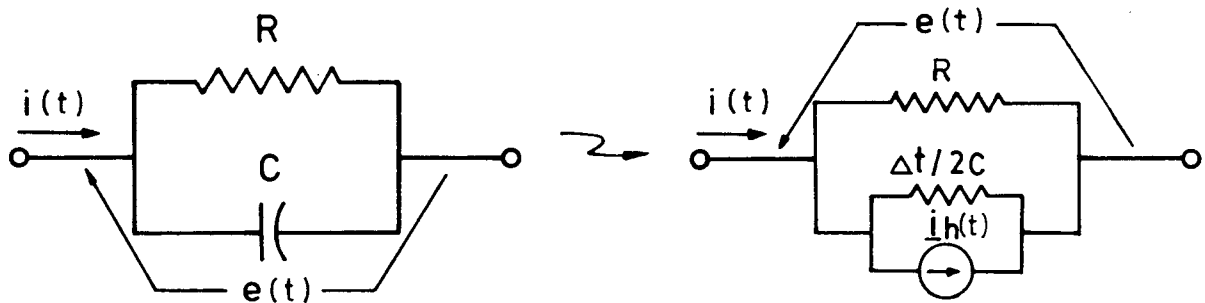


Fig. 5.2: Dommel's model for R-C combination.

This derivation is given in App. II.2. The resulting expression has the same form as equation 5.18, but now the integration coefficients are given by

$$m_i = \frac{1 - \frac{1}{2} (\alpha_i \Delta t)}{1 + \frac{1}{2} (\alpha_i \Delta t)} \quad (5.22)$$

and

$$p_i = q_i = k_i \left(\frac{\Delta t / 2}{1 + \frac{1}{2} (\alpha_i \Delta t)} \right) . \quad (5.23)$$

Actually, by analogy of the corresponding expressions, the same form of integration coefficients can also be used for the computation of the partial history sources b_{k_i} in equation 5.6. That is,

$$g_i = \frac{1 - \frac{1}{2} (\beta_i \Delta t)}{1 + \frac{1}{2} (\beta_i \Delta t)} \quad (5.24)$$

and

$$c_i = d_i = k_i' \left(\frac{\Delta t / 2}{1 + \frac{1}{2} (\beta_i \Delta t)} \right) . \quad (5.25)$$

Both sets of coefficients, the ones obtained from direct integration and the ones derived from Dommel's R-C combination, have been tested in this work. Even though in principle, the direct integration coefficients would be expected to give more accurate results, no significant differences were found

in the test cases studied.

5.4 Some General Comments on Numerical Integration

The recursive integration coefficients for the evaluation of the history source $b_k(t)$ (equations 5.7 to 5.9) and for the evaluation of the voltage across Z_{eq} (equations 5.19 to 5.21) were obtained from linear interpolation between the known values (at discrete time steps) of the variable functions $f_m(t)$ and $i_k(t)$, and exact evaluation of the corresponding integrations with the exponential functions (e.g. equation 5.5). Semlyen [30] suggests that a second order interpolation of the variable functions should lead to more accurate results.

However, it seems to be a paradox of numerical computations (COSERS [35], p. 54) that in many problems the more "refined" the differentials approximating the derivatives are, the more likely it is to encounter numerical instability problems. This - sometimes difficult to explain - phenomenon has been encountered many times in the analysis of power systems. As mentioned by Hornbeck ([36], p. 165): "One particularly difficult class of functions to integrate numerically is those which are [sic] highly oscillatory... it should be noted that the trapezoidal rule has certain highly desirable properties for periodic functions...". These observations have been corroborated in practice by the success of the simple trapezoidal rule in proving numerically stable and accurate for transient studies in power systems (e.g. Dommel, EMTP; Dommel and Sato, transient stability [37]). The advantage of simplicity in numerical approximations has also been found in the present work in connection with the simulation of the characteristic impedance and weighting function through asymptotic approximations.

For the point under consideration at this moment, that is, the coefficients in the recursive evaluation of the convolution integrals, reported experience in the use of second order interpolation coefficients seems to indicate that numerical instability problems have been encountered in some types of studies. On the other hand, in all the cases studied in this work, using linear interpolation coefficients or Dommel's R-C coefficients, no problems of numerical instability have occurred and the results obtained have been very accurate. In connection with the choice between these last two sets of coefficients, further work is needed in order to establish more definitely the advantages or disadvantages of one form as compared to the other.

5.5 Reduced Equivalent Circuit

With $b_k(t)$ expressed by relations 5.3 with 5.6, and $e_k(t)$ expressed by relations 5.14 with 5.17 and 5.18, the line equivalent circuit in fig. 5.1(b) can be simplified as follows. For the voltage across Z_{eq} :

$$\begin{aligned} e_k(t) &= e_{k_0}(t) + \sum e_{k_i}(t) \\ &= R_0 i_k(t) + (\sum p_i) i_k(t) + (\sum q_i) i_k(t - \Delta t) \\ &\quad + \{\sum m_i e_{k_i}(t - \Delta t)\}, \end{aligned} \tag{5.26}$$

where the summations are from $i = 1$ to $i = n$. Combining coefficients and separating present from history quantities,

$$e_k(t) = R_k i_k(t) + e_{khc}(t) + e_{khv}(t), \tag{5.27}$$

where

$$R_k = R_0 + \sum p_i + p \quad (5.28)$$

= equivalent constant resistance,

$$\underline{e}_{khc}(t) = (\sum q_i) i_k(t - \Delta t) = q_i i_k(t - \Delta t), \quad (5.29)$$

= history of current in Z_{eq}

and

$$\begin{aligned} \underline{e}_{khv}(t) &= \sum_{i=1}^m e_{ki}(t - \Delta t) \\ &= \text{history of partial voltages in } Z_{eq}. \end{aligned} \quad (5.30)$$

(Underscoring is used to emphasize that the quantities are completely defined from past values, that is, their value at time step t is known.)

For the weighted history source $b_k(t)$:

$$\begin{aligned} b_k(t) &= \sum b_{ki}(t) \\ &= f_m(t - \tau)(\sum c_i) + f_m(t - \tau - \Delta t)(\sum d_i) + \{\sum g_i b_{ki}(t - \Delta t)\}, \end{aligned} \quad (5.31)$$

where the summations are from $i = 1$ to $i = m$. Combining coefficients,

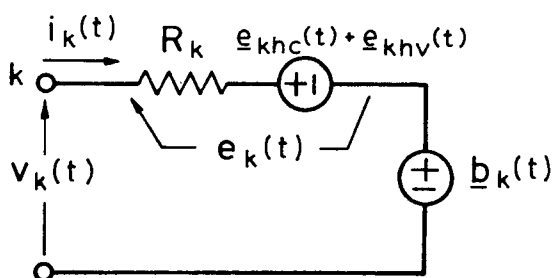
$$b_k(t) = cf_m(t - \tau) + df_m(t - \tau - \Delta t) + \sum g_i b_{ki}(t - \Delta t), \quad (5.32)$$

where

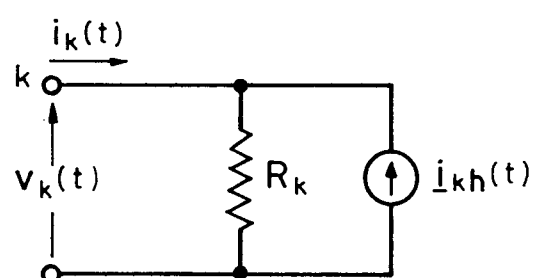
$$f_m(t - \tau) = 2v_m(t - \tau) - b_m(t - \tau) \quad (5.33)$$

and similarly for $f_m(t - \tau - \Delta t)$.

From relations 5.27 and 5.32 the circuit in fig. 5.1(b) yields the circuit in fig. 5.3(a) which can be reduced to the simple shunt form shown in fig. 5.3(b). This reduced shunt model has exactly the same form as



(a)



(b)

Fig. 5.3: New model reduced equivalent circuit.
(a) Series form. (b) Shunt form.

Dommel's representation for the simplified line (fig. 1.3(b)), and therefore it can directly be substituted for the simplified model in the Electromagnetic Transients Program. The parameters of the new line model are:

R_k = equivalent constant resistance (equation 5.28).

and

$\underline{i}_{kh}(t)$ = total history source

$$= [\underline{e}_{khc}(t) + \underline{e}_{khv}(t) + \underline{b}_k(t)]/R_k \quad (5.34)$$

($\underline{e}_{khc}(t)$ from equation 5.28, $\underline{e}_{khv}(t)$ from equation 5.30, and $\underline{b}_k(t)$ from equation 5.32).

5.6 Algorithm of Solution

The processing of frequency-dependent lines within the time-step loop of the general network solution can be summarized as follows:

a) Before solving the system network, evaluate from the recorded values at the previous time steps:

$$\underline{e}_{khc}(t) = q \underline{i}_k(t - \Delta t), \quad (5.35)$$

$$\underline{e}_{khv}(t) = \sum_1^n m_i \underline{e}_{k_i}(t - \Delta t), \quad (5.36)$$

$$\underline{b}_{kh}(t) = \sum_1^m g_i \underline{b}_{k_i}(t - \Delta t), \quad (5.37)$$

and

$$\underline{b}_k(t) = cf_m(t - \tau) + df_m(t - \tau - \Delta t) + \underline{b}_{kh}(t), \quad (5.38)$$

from which, the history current source is given by

$$\underline{i}_{kh}(t) = [\underline{e}_{khc}(t) + \underline{e}_{khv}(t) + \underline{b}_k(t)]/R_k. \quad (5.39)$$

b) Solve the system with the line being represented by the circuit in fig. 5.3(b).

c) After solving the system, update the history values needed for the subsequent time steps:

$$e_{ki}(t) = m_i e_{ki}(t - \Delta t) + p_i i_k(t) + q_i i_k(t - \Delta t) \quad (5.40)$$

$$b_{ki}(t) = g_i b_{ki}(t - \Delta t) + c_i f_m(t - \tau) + d_i f_m(t - \tau - \Delta t) \quad (5.41)$$

$$f_m(t) = 2v_m(t) - b_m(t) \quad (5.42)$$

The same process is performed for node m.

5.7 Initial Conditions

In the first steps of the transient study, evaluation of the history current source (fig. 5.3(b)) requires the value of the system variables to be known at times before the process is started, that is, the initial conditions at $t \leq 0$. The EMTP has a supporting routine to solve the system for initial sinusoidal steady-state conditions. Non-sinusoidal conditions have to be supplied by the user.

Initial sinusoidal steady-state conditions for the new line models are evaluated as follows. From the equivalent circuit in the frequency domain in fig. 4.1(a), the corresponding phasor circuit for sinusoidal steady-state conditions, shown in fig. 5.4, is directly obtained (upper-scored quantities are phasors). In this circuit \bar{V}_k and \bar{I}_k are known from the initial

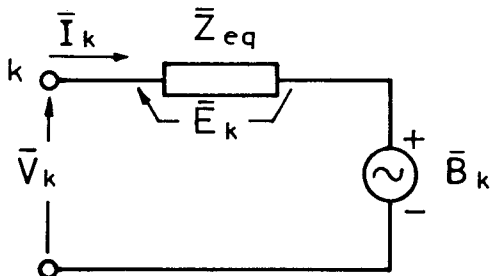


Fig. 5.4: Equivalent circuit for sinusoidal steady-state conditions at node k.

steady-state solution of the system given by the EMTP.

For the evaluation of the history current source (equation 5.34) in the transient circuit (fig. 5.3(b)), the following additional quantities are needed (in the time and phasor domains):

$$e_{k_i}(t) \longleftrightarrow \bar{E}_{k_i}$$

$$b_{k_i}(t) \longleftrightarrow \bar{B}_{k_i}$$

$$f_m(t) \longleftrightarrow \bar{F}_m$$

In the circuit in fig. 5.4

$$\bar{E}_k = \bar{Z}_{eq} \cdot \bar{I}_k , \quad (5.43)$$

but from equation 4.13,

$$\bar{Z}_{eq} = \bar{z}_0 + \bar{z}_1 + \bar{z}_2 + \dots + \bar{z}_n , \quad (5.44)$$

where

$$\bar{z}_0 = k_0 = R_0 \quad (5.45)$$

and

$$\bar{z}_1 = \frac{k_i}{j\omega + p_i} . \quad (5.46)$$

Equation 5.43 can thus be written as

$$\begin{aligned} \bar{E}_k &= (\bar{z}_0 + \bar{z}_1 + \bar{z}_2 + \dots + \bar{z}_n) \bar{I}_k \\ &= \bar{z}_0 \bar{I}_k + \bar{z}_1 \bar{I}_k + \dots + \bar{z}_n \bar{I}_k , \end{aligned} \quad (5.47)$$

and from the definition of the partial voltages in Z_{eq} (equation 5.14),

$$\bar{E}_{k_i} = \bar{z}_i \bar{I}_k \quad (5.48)$$

for $i = 1, \dots, n$.

The partial history sources \bar{B}_{k_i} are obtained as follows.

From equation 3.48

$$\bar{B}_k = \bar{A}_1 \bar{F}_m, \quad (5.49)$$

but from equations 4.32 and 4.34, \bar{A}_1 can be expressed as

$$\bar{A}_1 = \bar{A}_{1(1)} + \bar{A}_{1(2)} + \dots + \bar{A}_{1(m)}, \quad (5.50)$$

where

$$\bar{A}_{1(i)} = \frac{k_i}{j\omega + p_i} e^{-j\omega\tau}. \quad (5.51)$$

Equation 5.49 can then be written as

$$\begin{aligned} \bar{B}_k &= (\bar{A}_{1(1)} + \bar{A}_{1(2)} + \dots + \bar{A}_{1(m)}) \bar{F}_m \\ &= \bar{A}_{1(1)} \bar{F}_m + \bar{A}_{1(2)} \bar{F}_m + \dots + \bar{A}_{1(m)} \bar{F}_m, \end{aligned} \quad (5.52)$$

and from the definition of the partial history sources, equation 5.3,

$$\bar{B}_{k_i} = \bar{A}_{1(i)} \bar{F}_m \quad (5.53)$$

for $i = 1, \dots, m$.

\bar{F}_m can be found from relation 3.42:

$$\bar{F}_m = \bar{V}_m + \bar{Z}_{eq} \bar{I}_m. \quad (5.54)$$

From the phasor values obtained in equations 5.48, 5.53, and 5.54, the time domain values for steady-state conditions at $t \leq 0$ are given by

$$e_{k_i}(t) = |\bar{E}_{k_i}| \cos(\omega t + \phi_{\bar{E}_{k_i}}), \quad (5.55)$$

$$b_{k_i}(t) = |\bar{B}_{k_i}| \cos(\omega t + \phi_{\bar{B}_{k_i}}), \quad (5.56)$$

and

$$f_m(t) = |\bar{F}_m| \cos(\omega t + \phi_{\bar{F}_m}) . \quad (5.57)$$

Analogous relations are obtained for the corresponding equivalent circuit at node m.

5.8 Interface with the EMTP

The models described in this chapter have been incorporated into the UBC version of Dommel's electromagnetic transients program (EMTP) [38]. This implementation includes three aspects:

- a) Generation of the line parameters.
- b) Generation of the model parameters.
- c) Modification of the existing EMTP code for the processing of frequency-dependent lines.

Generation of the line and model parameters:

The steps required to obtain the line and model parameters are as follows:

- a) The parameters R, L, and C for the decoupled line modes as a function of frequency are obtained from the UBC version of the Line Constants Program [26]. The input data for this program are the characteristics of the conductors and the tower configuration of the line.
- b) The data obtained in (a) are processed by FDLINE to obtain the functions $Z_c(\omega)$ and $A_1(\omega)$.

c) From the data obtained in (b), the characteristic impedance function $Z_c(\omega)$ is simulated by TRAN.ZC. The parameters obtained from this simulation: R_0 , k_i , and α_i (see equations 5.17 to 5.21) are stored in the data file DA.TRAN.

d) From the data obtained in (b), the weighting function $A_1(\omega)$ is simulated by TRAN.A1. The parameters obtained from this simulation, k'_i and β_i (see equations 516 to 519) are stored in the data file DA.TRAN.

The parameters in the data file DA.TRAN are read in and processed by the new EMTP when the line mode is identified as frequency dependent.

Processing of frequency-dependent lines by the EMTP:

The existing form of data input for the EMTP has been maintained. A line mode to be simulated according to the frequency-dependence models is identified by specifying MODEL = - 1 in the corresponding branch card (fig. 5.5). The rest of the parameters in this card correspond, as in the

Model
53 54
- 1

Fig. 5.5: Frequency-dependent line mode.

existing version, to 60 Hz conditions. For frequency-dependent lines, these parameters are only used for initial steady-state conditions. When MODEL = - 1 is detected in a branch card, the parameters for the frequency-dependence model are read in from the data file DA.TRAN.

The main additions to the existing EMTP code for the simulation of frequency-dependent lines using the models developed in this work are the following:

- a) Evaluation of the coefficients and equivalent resistance.
- b) Initialization of the history vectors from initial conditions.
- c) Determination of the equivalent current sources.
- d) Incorporation of the new model parameters into the system network.
- e) Updating of the history vectors.

Some computational aspects:

The computer facilities used in the development of the programs are those of the University of British Columbia. The central unit in the U.B.C. Computing System is an Amdahl 470 V/6 Model II that is run under the MTS operating system. The programs were written in Fortran IV. An approximation of the number of Fortran lines and average running costs required by the frequency dependence routines is given next. The running costs are based on the University rates of \$1120 per hour of CPU time under Terminals use, and correspond to the modelling of the zero sequence mode of a typical 100-mi transmission line. For the frequency domain functions 50 points per decade are considered in a range from 10^{-3} to 10^8 Hz.

- a) Frequency-dependent line parameters.

Routine name: HWDO:DLINE:0 (UBC Line Constants Program)

Running cost: \$2.50

- b) Computation of $Z_c(\omega)$ and $A_1(\omega)$.

Routine name: FLIN

Fortran lines: 80

Running cost: \$.50

c) Simulation of $Z_c(\omega)$.

Routine name: TRAN.ZC

Fortran lines: 400

Running cost: \$1.00

d) Simulation of $A_1(\omega)$.

Routine name: TRAN.A1

Fortran lines: 500

Running cost: \$1.50

e) Additions to EMTP code.

Fortran lines: 300

Running cost: 10 to 40% more than with existing code.

CHAPTER 6

NUMERICAL RESULTS

6.1 Introduction

The results of a series of comparisons and tests for assessing the behaviour of the new line model are presented in this chapter. The results shown in graphical form have been grouped at the end of the chapter and are identified as P.N1.N2 (e.g. P.3.2 refers to plot 2 in Section 3 of this chapter). An index to these graphs is given in pages 122 to 126.

6.2 Frequency-Dependent Line Parameters

The transmission line studied in the cases presented in this chapter (with the exception of the field test comparisons) is a typical 500 kV, 3-phase, single-circuit, transposed, overhead transmission line.

The frequency-dependent line parameters are determined by the UBC Line Constants Program. The line input data for this program are:

- a) Tower configuration: fig. 6.1
- b) Phase conductors:

dc resistance = 0.0348 Ω/km

thickness/diameter = 0.3636

diameter = 40.69 mm

- c) Ground wires:

dc resistance = 1.62 Ω/km

thickness/diameter = 0.500

diameter = 9.80 mm

- d) Ground resistivity = 100 Ω-m
- e) Ground wires are segmented.

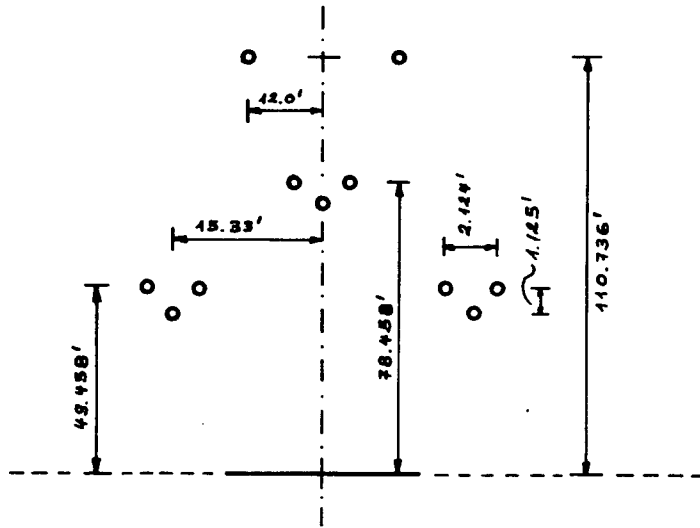


Fig. 6.1: Tower configuration of reference line.

The line constants program uses Carson's formulae [19] to obtain the variation of the phase parameters as a function of frequency and the standard symmetric component transformation to obtain the zero and positive sequence equivalent parameters.

The zero and positive sequence series resistance and inductance as a function of frequency were obtained for a range of frequencies between 10^{-3} Hz and 10^8 Hz, with 50 frequency points per decade. The variation of these parameters as a function of frequency is shown in graphs P.2.1 and P.2.2. The shunt capacitances and conductances are assumed constant at the following values:

zero sequence:

$$C = 7.730 \times 10^{-3} \mu\text{F}/\text{km}$$

$$G = 0.3 \times 10^{-7} \Omega^{-1}/\text{km}$$

positive sequence:

$$C = 14.15 \times 10^{-3} \mu\text{F}/\text{km}$$

$$G = 0.3 \times 10^{-7} \Omega^{-1}/\text{km}$$

6.3 Simulation of the Characteristic Impedance

Zero Sequence:

The form of the zero sequence characteristic impedance $Z_c(\omega)$ is shown in the following graphs:

- i) $|Z_c(\omega)| \rightarrow P.3.1$
- ii) $\phi\{Z_c(\omega)\} \rightarrow P.3.2$
- iii) $\text{Re}\{Z_c(\omega)\} \rightarrow P.3.3$
- iv) $\text{Im}\{Z_c(\omega)\} \rightarrow P.3.4$

The location of poles and zeros and the reference level of the approximating function $Z_{eq}(s)$ (eqn. 4.12) are shown in table 6.1. The parameters of the equivalent R-C network (fig. 4.5) are shown in table 6.2.

NUMBER OF ZEROS = 15
ZERO(1) = 0.157828E+00
ZERO(2) = 0.308852E+00
ZERO(3) = 0.388782E+00
ZERO(4) = 0.403171E+00
ZERO(5) = 0.404515E+01
ZERO(6) = 0.223324E+02
ZERO(7) = 0.130467E+03
ZERO(8) = 0.541386E+03
ZERO(9) = 0.207733E+04
ZERO(10) = 0.580248E+04
ZERO(11) = 0.124017E+05
ZERO(12) = 0.259181E+05
ZERO(13) = 0.607560E+05
ZERO(14) = 0.178462E+06
ZERO(15) = 0.119841E+07

NUMBER OF POLES = 15
POLE(1) = 0.165843E+00
POLE(2) = 0.318982E+00
POLE(3) = 0.416563E+00
POLE(4) = 0.436288E+00
POLE(5) = 0.375523E+01
POLE(6) = 0.209394E+02
POLE(7) = 0.122280E+03
POLE(8) = 0.507520E+03
POLE(9) = 0.194768E+04
POLE(10) = 0.553996E+04
POLE(11) = 0.120087E+05
POLE(12) = 0.250950E+05
POLE(13) = 0.588310E+05
POLE(14) = 0.172837E+06
POLE(15) = 0.115860E+07

$$MK = 0.455365E+03$$

Table 6.1: Parameters of $Z_{eq}(s)$. Zero sequence. (Location of corners in Hz, reference level MK in ohms.)

ELEMENTS OF FOSTER I EQUIVALENT NETWORK
R IN OHMS, C IN MICROFARADS

R(0) = 0.455365E+03	C(0) = ZERO
R(1) = -.276676E+02	C(1) = -.346858E+05
R(2) = -.135294E+02	C(2) = -.368786E+05
R(3) = 0.407864E+02	C(3) = 0.936750E+04
R(4) = -.161784E+03	C(4) = -.225481E+04
R(5) = 0.583433E+02	C(5) = 0.726428E+03
R(6) = 0.454623E+02	C(6) = 0.167188E+03
R(7) = 0.431615E+02	C(7) = 0.301557E+02
R(8) = 0.400909E+02	C(8) = 0.782206E+01
R(9) = 0.375514E+02	C(9) = 0.217608E+01
R(10) = 0.252554E+02	C(10) = 0.113752E+01
R(11) = 0.166585E+02	C(11) = 0.795585E+00
R(12) = 0.161149E+02	C(12) = 0.393555E+00
R(13) = 0.155492E+02	C(13) = 0.173983E+00
R(14) = 0.149980E+02	C(14) = 0.613974E-01
R(15) = 0.155056E+02	C(15) = 0.885923E-02

Table 6.2: Parameters of R-C equivalent network. Zero sequence.

The functions $Z_c(\omega)$ and $Z_{eq}(\omega)$ are compared in the following graphs:

- i) Magnitudes → P.3.5
- ii) Phase angles → P.3.6
- iii) Real parts → P.3.7
- iv) Imaginary parts → P.3.8

The magnitude error (in %) is shown in graph P.3.9 and the phase error (in degrees) in graph P.3.10. The maximum magnitude error in most of the curve is 0.2 to 0.3%, with a peak value of about 0.5% in the region of maximum vertical slope. The phase error is also very small, with a peak value of about 0.3° in the region of maximum vertical slope.

Positive Sequence:

The positive sequence characteristic impedance is shown in the following graphs:

- i) $|Z_c(\omega)| \rightarrow P.3.11$
- ii) $\phi\{Z_c(\omega)\} \rightarrow P.3.12$
- iii) $\text{Re}\{Z_c(\omega)\} \rightarrow P.3.13$
- iv) $\text{Im}\{Z_c(\omega)\} \rightarrow P.3.14$

The location of poles and zeros and the reference level of the approximating function are shown in table 6.3. The parameters R-C of the equivalent network are shown in table 6.4.

NUMBER OF ZEROS = 16	NUMBER OF POLES = 16
ZERO(1) = 0.452926E+00	POLE(1) = 0.341987E+00
ZERO(2) = 0.875163E+00	POLE(2) = 0.813008E+00
ZERO(3) = 0.128852E+01	POLE(3) = 0.118584E+01
ZERO(4) = 0.902754E+00	POLE(4) = 0.823318E+00
ZERO(5) = 0.120104E+01	POLE(5) = 0.109041E+01
ZERO(6) = 0.156883E+01	POLE(6) = 0.142411E+01
ZERO(7) = 0.203965E+01	POLE(7) = 0.185150E+01
ZERO(8) = 0.167770E+01	POLE(8) = 0.159506E+01
ZERO(9) = 0.194472E+01	POLE(9) = 0.185761E+01
ZERO(10) = 0.225354E+01	POLE(10) = 0.215220E+01
ZERO(11) = 0.264754E+01	POLE(11) = 0.253961E+01
ZERO(12) = 0.315367E+01	POLE(12) = 0.302588E+01
ZERO(13) = 0.389754E+01	POLE(13) = 0.373961E+01
ZERO(14) = 0.422686E+01	POLE(14) = 0.499851E+01
ZERO(15) = 0.654650E+01	POLE(15) = 0.633909E+01
ZERO(16) = 0.242515E+03	POLE(16) = 0.239900E+03

$$MK = 0.237623E+03$$

Table 6.3: Parameters of $Z_{eq}(s)$. Positive sequence. (Location of corners in Hz, reference level MK in ohms.)

ELEMENTS OF FOSTER I EQUIVALENT NETWORK
R IN OHMS, C IN MICROFARADS

R(0) = 0.237623E+03	C(0) = ZERO
R(1) = 0.199350E+03	C(1) = 0.233450E+04
R(2) = 0.411401E+03	C(2) = 0.475839E+03
R(3) = - .589326E+01	C(3) = - .227740E+05
R(4) = - .309485E+03	C(4) = - .624616E+03
R(5) = 0.603876E+02	C(5) = 0.241704E+04
R(6) = 0.196317E+02	C(6) = 0.569269E+04
R(7) = 0.142292E+03	C(7) = 0.604113E+03
R(8) = 0.241295E+01	C(8) = 0.413518E+05
R(9) = - .131995E+03	C(9) = - .649096E+03
R(10) = 0.169021E+01	C(10) = 0.437518E+05
R(11) = 0.292379E+01	C(11) = 0.214342E+05
R(12) = 0.293638E+01	C(12) = 0.179125E+05
R(13) = 0.194440E+01	C(13) = 0.218881E+05
R(14) = - .246582E+02	C(14) = - .129127E+04
R(15) = 0.871910E+01	C(15) = 0.287953E+04
R(16) = 0.258068E+01	C(16) = 0.257072E+03

Table 6.4: Parameters of R-C equivalent network. Positive sequence.

The functions $Z_c(\omega)$ and $Z_{eq}(\omega)$ are compared in the following graphs:

- i) Magnitudes → P.3.15
- ii) Phase angles → P.3.16
- iii) Real parts → P.3.17
- iv) Imaginary parts → P.3.18

The order of the approximation is 16. The magnitude error is shown in graph P.3.19 and the phase error in graph P.3.20. Even though the same tolerance, when assigning the asymptotes, was allowed in this case as in the case of the zero sequence, the resulting peak magnitude error is larger (about 2.5%). This error, however, occurs in the very high slope region, with the rest of the curve being more closely approximated. A larger error in the high slope region is probably not very significant because of the following considerations. Imagining the limit case in which the slope of the function is a vertical line, even a very small frequency displacement in the approximating function would give an infinite error. In practice, however, the frequency spectrum of the signals is continuous and a relatively small frequency displacement in the approximating function will probably have a very small effect in the final results.

6.4 Approximation of the Weighting Function

The weighting function $A_1(\omega)$ (eqn. 3.50) depends on the length of the line. For this reason, different lengths were considered for the testing of the fitting routines. The resulting approximations for the zero and positive sequence modes of these line lengths are shown in the following graphs:

Zero Sequence:

- i) 5-mi → P.4.1
- ii) 30-mi → P.4.3
- iii) 100-mi → P.4.5
- iv) 500-mi → P.4.7
- v) 1000-mi → P.4.9

Positive Sequence:

- i) 5-mi → P.4.2
- ii) 30-mi → P.4.4
- iii) 100-mi → P.4.6
- iv) 500-mi → P.4.8
- v) 1000-mi → P.4.10

As shown by these graphs, the approximation is very close to the function in all the cases.

The approximations were performed so as to allow a maximum magnitude error of 0.5% in the region of the curves between 0 Hz and the frequency at which the magnitude reaches 0.7. This error region was defined so as not to include the high-slope zone in the maximum error criteria (even though the resulting error in the high-slope zone is also very small). The number of poles and zeros of the approximating rational functions (eqn. 4.33) is shown in table 6.5.

length	5 mi		30 mi		100 mi		500 mi		1000 mi	
Seq.	zero	pos.	zero	pos.	zero	pos.	zero	pos.	zero	pos.
zeros	12	13	11	11	12	13	15	20	17	23
poles	16	14	15	14	20	17	21	25	23	29

Table 6.5: Rational approximations for different line lengths.

A more detailed study comparing the function and the approximation for a line length of 100 miles is presented next.

Zero Sequence (100 mi)

The form of $A_1(\omega)$ for the zero sequence mode and a length of 100 miles is shown in the following graphs:

- i) $|A_1(\omega)| \rightarrow P.4.11$
- ii) $\phi\{A_1(\omega)\} \rightarrow P.4.12$
- iii) $\text{Re}\{A_1(\omega)\} \rightarrow P.4.13$
- iv) $\text{Im}\{A_1(\omega)\} \rightarrow P.4.14$

The parameters of the rational approximating function $P_a(s)$ (eqn. 4.33) and the phase displacement τ (eqns. 4.31 and 4.32) are shown in table 6.6.

NUMBER OF ZEROS = 15

```

ZERO( 1) = 0.367679E+02
ZERO( 2) = 0.155040E+03
ZERO( 3) = 0.269450E+03
ZERO( 4) = 0.385017E+03
ZERO( 5) = 0.495961E+03
ZERO( 6) = 0.610179E+03
ZERO( 7) = 0.733576E+03
ZERO( 8) = 0.842268E+03
ZERO( 9) = 0.966982E+03
ZERO(10) = 0.108511E+04
ZERO(11) = 0.134982E+04
ZERO(12) = 0.184181E+04
ZERO(13) = 0.239982E+04
ZERO(14) = 0.213423E+04
ZERO(15) = 0.251200E+04

MK = 0.487557E+20
TAUO = 0.5976E-03

```

NUMBER OF POLES = 20

```

POLE( 1) = 0.359264E+02
POLE( 2) = 0.151515E+03
POLE( 3) = 0.263346E+03
POLE( 4) = 0.376262E+03
POLE( 5) = 0.484659E+03
POLE( 6) = 0.596240E+03
POLE( 7) = 0.716917E+03
POLE( 8) = 0.823059E+03
POLE( 9) = 0.944968E+03
POLE(10) = 0.106042E+04
POLE(11) = 0.124524E+04
POLE(12) = 0.167985E+04
POLE(13) = 0.216360E+04
POLE(14) = 0.183774E+04
POLE(15) = 0.239400E+04
POLE(16) = 0.326695E+04
POLE(17) = 0.119650E+05
POLE(18) = 0.712960E+04
POLE(19) = 0.156694E+05
POLE(20) = 0.226480E+05

```

Table 6.6: Parameters of the rational approximation of $A_1(\omega)$. Zero sequence mode, 100 miles. (Location of corners in Hz, reference level MK in p.u., τ in sec.)

In connection with the form of $A_1(\omega)$, the observation made at the end of Section 4.3.2 in the sense that the oscillatory behaviour of the phase of this function could be circumvented by considering the function $P(\omega)$ (eqn.

4.30) instead of $A_1(\omega)$ is corroborated by graph P.4.15 which shows the smooth phase variation of $P_a(\omega)$.

The function $A_1(\omega)$ and its rational approximation are compared in the following graphs:

- i) Magnitudes → P.4.16
- ii) Phase angles → P.4.17
- iii) Real parts → P.4.18
- iv) Imaginary parts → P.4.19

The magnitude error is shown in graph P.4.20 and the phase error in graph P.4.21. As mentioned before, the magnitude error is less than 0.5% in most of the curve. The highest peak error is about 2% in a region of very high vertical slope. For the reasons explained before, however, the higher error in this zone is not very significant, and as can be seen from graph P.4.16, the two curves are practically identical. The phase error along the curve is also very small, of about 0.3° . In the region where the magnitude is practically zero, the magnitude and phase errors lose their significance.

Positive Sequence (100 mi):

The function $A_1(\omega)$ for the positive sequence mode and a length of 100 miles is shown in the following graphs:

- i) $|A_1(\omega)| \rightarrow P.4.22$
- ii) $\phi\{A_1(\omega)\} \rightarrow P.4.23$
- iii) $\text{Re}\{A_1(\omega)\} \rightarrow P.4.24$
- iv) $\text{Im}\{A_1(\omega)\} \rightarrow P.4.25$

The phase angle of the function $P_a(\omega)$ ($= A_{1a}(\omega) e^{j\omega\tau}$) is shown in graph P.4.26.

The parameters of the corresponding rational approximation are shown in table 6.7.

NUMBER OF ZEROS = 13	NUMBER OF POLES = 17
ZERO(1) = 0.923471E+03	POLE(1) = 0.902475E+03
ZERO(2) = 0.852040E+04	POLE(2) = 0.832608E+04
ZERO(3) = 0.173949E+05	POLE(3) = 0.170000E+05
ZERO(4) = 0.260346E+05	POLE(4) = 0.254396E+05
ZERO(5) = 0.347048E+05	POLE(5) = 0.339150E+05
ZERO(6) = 0.431969E+05	POLE(6) = 0.422154E+05
ZERO(7) = 0.519331E+05	POLE(7) = 0.507520E+05
ZERO(8) = 0.603169E+05	POLE(8) = 0.589390E+05
ZERO(9) = 0.684622E+05	POLE(9) = 0.669031E+05
ZERO(10) = 0.768163E+05	POLE(10) = 0.750654E+05
ZERO(11) = 0.879200E+05	POLE(11) = 0.783631E+05
ZERO(12) = 0.136188E+06	POLE(12) = 0.117248E+06
ZERO(13) = 0.312719E+06	POLE(13) = 0.169485E+06
MK = 0.149967E+24	POLE(14) = 0.367547E+06
TAU0 = 0.5394E-03	POLE(15) = 0.512864E+06
	POLE(16) = 0.104240E+07
	POLE(17) = 0.231754E+07

Table 6.7: Parameters of the rational approximation of $A_1(\omega)$. Positive sequence mode, 100 miles. (Location of corners in Hz, reference level MK in p.u., τ in sec.)

The comparisons between the function and its approximations are shown in the following graphs:

- i) Magnitudes → P.4.27
- ii) Phase angles → P.4.28
- iii) Real parts → P.4.29
- iv) Imaginary parts → P.4.30

The magnitude error is shown in graph P.4.31 and the phase error in graph P.4.32. The apparent increase in the phase error in the upper range of graph P.4.32 is probably due to the lack of enough frequency points to follow the very fast variations of the phase function in this region of the curve.

Time domain form of the weighting functions:

The time domain form of the zero and positive sequence weighting functions, as obtained from eqn. 4.36 from inverse transformation of the

corresponding rational approximations, is shown in graphs P.4.33 and P.4.34. The phase displacement τ is 0.5976 msec for the zero sequence mode and 0.5394 msec for the positive sequence mode.

Some interesting conclusions can be derived by comparing the zero and positive sequence forms of $a_1(t)$. When the functions are compared on the time scale of graphs P.4.33 and P.4.34(a), a_1 -pos. looks almost like an impulse, $\delta(t-\tau)$, whereas the spike form of a_1 -zero is clearly apparent. This means that taking, for instance, a time step Δt for the transient process of about 1/10 of τ , say 0.05 msec, the "weighting" effect of a_1 -zero will be well taken into account, whereas a_1 -pos. will be almost an impulse. This is equivalent to having $A_1(\omega)$ -pos. constant in the frequency domain, which means that the larger damping of the higher frequency components is not taken into account. Actually, a period of 0.05 msec corresponds to a frequency of 20 kHz, at which point $A_1(\omega)$ -pos. (graph P.4.22) is just beginning to decay while $A_1(\omega)$ -zero (graph P.4.11) has decayed almost completely. The expanded time-axis plot of $a_1(t)$ -pos. in graph P.4.34(b) shows that taking, for instance, a Δt of about 0.001 msec the weighting effect of this function will be clearly represented. This Δt corresponds to a frequency of 10^6 Hz; at this frequency, $A_1(\omega)$ -pos. (graph P.4.22) has decayed almost completely.

6.5 Analytical Tests: Frequency Domain

Short circuit and open circuit terminations constitute extreme loading conditions in a transmission line. These limit conditions provide a simple and yet demanding way of assessing the effect of the approximations for the characteristic impedance and weighting function in simulating the line response in the frequency domain.

From the general solution of the line equations in the frequency domain (eqns. 1.34 and 1.35), with a purely sinusoidal (single frequency) voltage source (E_s) connected at the sending end of the line, and the receiving end short-circuited ($V_m = 0$), the current at the sending end in terms of $A_1(\omega)$ (eqn. 3.50) and $Z_c(\omega)$ is given by (in phasorial form):

$$\bar{I}_k(\omega) = \frac{\bar{E}_s(\omega)}{\bar{Z}_c(\omega)} \frac{1 + \bar{A}_1^2(\omega)}{1 - \bar{A}_1^2(\omega)}. \quad (6.1)$$

Similarly, with the receiving end of the line open-circuited, the voltage at this end is given by:

$$\bar{V}_m(\omega) = \bar{E}_s(\omega) \frac{2 \bar{A}_1(\omega)}{1 + \bar{A}_1^2(\omega)}. \quad (6.2)$$

It is interesting to observe from eqns. 6.1 and 6.2 that the open-circuit voltage is independent of the characteristic impedance, whereas the short-circuit response is directly proportional to $1/Z_c(\omega)$. This would explain why some frequency dependence models that assume a constant characteristic impedance can give acceptable results when tested only for open-circuit or close-to-open-circuit conditions. On the other hand, the correct modelling of the frequency dependence of $Z_c(\omega)$ is very important for short-circuit or near-to-short-circuit conditions.

From eqns. 6.1 and 6.2, the short-circuit and open-circuit responses of the line using the exact values of $Z_c(\omega)$ and $Z_1(\omega)$ can be compared with the responses obtained by using the values of the corresponding approximating functions. These comparisons can be made over the entire frequency range. Also, in order to illustrate the importance of taking into account the frequency dependence of the parameters, the short-circuit and open-circuit responses can be calculated assuming constant line parameters.

In the results presented next, the following responses were compared:

- a) Response with exact parameters (C) vs. response with approximated parameters (P).
- b) Response with exact parameters (C) vs. response with 60 Hz constant parameters (P60).
- c) Response with exact parameters (C) vs. response with 750 Hz constant parameters (P750).

In most transient simulations using constant parameters, these parameters are taken at 60 Hz in order to correctly reproduce the fundamental, 60-Hz signal injected by the generators. In an attempt to more closely simulate the higher harmonics, sometimes the constant parameters are taken at a higher frequency (e.g. 500 to 1000 Hz). As it will be shown in the comparisons with 750 Hz parameters, however, taking the parameters at these higher frequencies can represent a considerable detriment of the 60-Hz component, without major improvement in the frequency range outside the vicinity of the frequency at which the parameters are taken.

Zero Sequence Responses:

A) Short-circuit responses:

Assuming a source voltage of 100 kV, the magnitudes of the short-circuit currents (in amperes) at node k are compared in the following graphs:

- i) Exact vs. approximation → P.5.1
- ii) Exact vs. 60-Hz → P.5.2
- iii) Exact vs. 750-Hz → P.5.3

As can be seen from these plots, the agreement between the exact and approximated responses is very good. Sixty-hertz constant parameters give

a good agreement only from about 10 to 500 Hz, whereas the 750-Hz parameters cover (less well) a range from about 100 to 1000 Hz and give an error of about 40% at the fundamental 60-Hz frequency.

The magnitude errors are shown in the following plots:

- i) Exact vs. approximation → P.5.4
- ii) Exact vs. 60-Hz → P.5.5
- iii) Exact vs. 750-Hz → P.5.6

As shown in graphs P.5.4 the maximum error obtained with the approximating functions is less than about 1% in most of the frequency range. The error is relatively larger at about 300 Hz, where, however, it does not have much significance since the magnitude of the current is relatively close to zero. Another point where the error is slightly larger than 1% is at about 600 Hz which corresponds to a relatively narrow peak of the response. The errors at very narrow peaks have less significance than in the flatter regions since these points are almost singularities of the response function.

The error is also relatively larger in the range from about 0.1 to 5 Hz. This error in the short-circuit response at relatively low frequencies is very difficult to control. This is due to the numerical sensitivity of the factor $(1 + \bar{A}_1^2)/(1 - \bar{A}_1^2)$ in eqn. 6.1 when $A_1(\omega)$ is very close to 1. For instance, for A_1 exact = 0.9998 and A_1 approx. = 0.9999, that is, a difference of only + 0.01% in A_1 , the error in the factor is + 100%. (Actually, as can be seen in graph P.5.1(a), the "exact" response itself presents a slightly erratic behaviour in this region.) To mitigate this problem in the simulation of the low frequency region, the function $A_1(\omega)$ -approx. is matched with $A_1(\omega)$ -exact at $\omega = 0$ (dc condition) with an error of less than $10^{-14}\%$. This results in a practically exact matching of the dc short-circuit current and

helps in controlling the error over the low frequency range. This exact matching of the dc condition is very important because it assures the correct simulation of a dc level in the signals.

In the case of the constant-parameter approximations (graphs P.5.5(a) and P.5.6(a)) the error at low frequencies is very large and dc levels cannot be simulated.

It can also be seen from the error graphs that in the case of the approximation the response at 60 Hz is also exactly matched, thus assuring the correct simulation of the sources frequency.

B) Open-circuit responses:

Assuming a source voltage of 1.0 (per unit), the open-circuit voltage responses at the receiving end of the line are compared in the following graphs:

- i) Exact vs. approximation → P.5.7
- ii) Exact vs. 60-Hz → P.5.8
- iii) Exact vs. 750-Hz → P.5.9

As shown in these plots, the approximation response correctly matches the exact response over the entire frequency range. The constant-parameter representations, on the other hand, give a good approximation only for the range between 0 and about 200 Hz.

The magnitude errors are shown in the following graphs:

- i) Exact vs. approximation → P.5.10
- ii) Exact vs. 60-Hz → P.5.11
- iii) Exact vs. 750-Hz → P.5.12

The error for the approximation is less than about 1.5% over the entire frequency range, with slight increases in the regions of very high

vertical slope. The response at the fundamental 60 Hz frequency is exactly matched.

Positive Sequence Responses:

A) Short-circuit responses:

For a source voltage of 100 kV, the magnitudes of the short-circuit currents using the exact, approximating, and constant-parameter $Z_c(\omega)$ and $A_1(\omega)$ functions are shown in the following graphs:

- i) Exact vs. approximation → P.5.13
- ii) Exact vs. 60-Hz → P.5.14
- iii) Exact vs. 750-Hz → P.5.15

Considering first the frequency region of graphs (a) (10 to 10^6 Hz) it can be seen that the approximation follows the exact response very closely despite the very narrow resonance spikes. The constant-parameter responses, in contrast with the zero sequence case, also give a relatively fair approximation (with the exception of the very narrow spike regions) up to about 10^4 Hz.

Comparing now the low frequency responses (graphs (b)), it can be seen that with the exception of the range from about 0.1 to 5 Hz, the approximation follows the exact response very closely. As in the case of the zero sequence, however, the range between 0.1 and 5 Hz presents a larger error. For the positive sequence the relatively low frequency range is even more sensitive to very small differences in $A_1(\omega)$ than for the zero sequence because the values of $A_1(\omega)$ are closer to 1.0.

It is interesting to observe that for this line length the 60 Hz constant-parameter representation gives a very good simulation of the low-frequency range. This is not so, however, for the 750 Hz simulation.

The comparison between the magnitude errors are shown in the following graphs:

- i) Exact vs. approximation → P.5.16
- ii) Exact vs. 60-Hz → P.5.17
- iii) Exact vs. 750-Hz → P.5.18

B) Open-circuit responses:

Then open-circuit responses for a source voltage of 1.0 p.u. are compared in the following graphs:

- i) Exact vs. approximation → P.5.19
- ii) Exact vs. 60-Hz → P.5.20
- iii) Exact vs. 750-Hz → P.5.21

The corresponding magnitude errors are shown in graphs:

- i) Exact vs. approximation → P.5.22
- ii) Exact vs. 60-Hz → P.5.23
- iii) Exact vs. 750-Hz → P.5.24

As it can be seen from these graphs the approximation response is very good over the entire frequency range, whereas the constant-parameter responses give fair results only up to about 10^4 Hz.

6.6 Analytical Tests: Time Domain

The accuracy of the frequency domain approximations of the characteristic impedance and weighting function in simulating the response of the system was verified in the previous section for short-circuit and open-circuit frequency-response tests. Short-circuit and open-circuit single-frequency conditions also provide a simple way of verifying the numerical

behaviour of the time-domain line models.

For this purpose, the line, represented by its frequency-dependence transient model was energized by a purely sinusoidal voltage source. Starting from sinusoidal steady-state conditions, transient simulations (without disturbances), with the receiving end of the line short- and open-circuited, were run with the EMTP. Since no disturbances were introduced, the time-domain solutions obtained with the EMTP should be (ideally) perfectly sinusoidal waves. The magnitude and phase of these waves should agree with the values obtained analytically from eqns. 6.1 and 6.2.

In order to assess the accuracy of the numerical discretizations involved in the time-domain models, the results of the transient simulations were compared not with the analytical results using exact parameters, but with the analytical results using the values of $Z_c(\omega)$ and $A_1(\omega)$ given by the approximating functions. (The differences between the analytical values obtained from the exact and approximate parameters were presented in the previous section.)

These time-domain tests were performed for the zero and positive sequence modes of 100 miles of the reference line for different frequencies of the applied voltage source. In all the cases studied, the time-domain functions had the correct sinusoidal wave-form, and the magnitude peaks were in very good agreement with the analytical values.

Some of the results of these simulations (for the short circuit case) are presented next. In these cases, the simulations were also performed using the EMTP code with no frequency dependence (constant-parameter model). In order to compare the results of the constant-parameter model with the same reference value as in the case of the frequency-dependence model, the line parameters at the source frequency for the constant-parameter model were

calculated from the approximated $Z_c(\omega)$ and $A_1(\omega)$ functions. Since only one frequency is involved in these simulations, and the parameters at this frequency are used for the constant-parameter model, the results obtained with this model would also be expected to coincide with the analytical values. That this was not exactly the case, however, will be seen from the obtained results.

Zero Sequence Comparisons:

i) $f = 60.26$ Hz. The peak magnitudes of the simulations are shown in table 6.8. In this table,

I_{fd} = simulation with frequency-dependence model.

I_{cp} = simulation with constant-parameter model.

I_{ex} = analytical value from eqn. 6.1.

ΔI_{fd} and ΔI_{cp} = % variation with respect to I_{ex} .

Δt = time step in the transient simulation.

t (msec)	I_{fd} (A)	ΔI_{fd} (%)	I_{cp} (A)	ΔI_{cp} (%)
3.80	446.8	-0.04	447.3	0.07
12.1	-447.0	0.00	-447.6	0.13
20.4	446.8	-0.04	447.4	0.09
28.6	-447.0	0.00	-447.5	0.11
36.9	446.8	-0.04	447.5	0.11
45.2	-447.0	0.00	-447.5	0.11

Table 6.8: Short circuit, zero seq., $f=60.26$ Hz, $I_{ex}=447.0$ A, $\Delta t=0.1$ msec.

As shown in table 6.8 the results of the time domain simulations agree very well with the expected analytical value.

ii) $f = 2089$ Hz. The results for this case are shown in table 6.9.

$t(\text{msec})$	$I_{fd}(\text{A})$	$\Delta I_{fd}(\%)$	$I_{cp}(\text{A})$	$\Delta I_{cp}(\%)$
.23	-281.0	-0.35	-382.5	36
.47	281.0	-0.35	382.5	36
.71	-281.1	-0.32	-382.5	36
.95	281.1	-0.32	382.5	36
1.19	-281.1	-0.32	-382.5	36
1.42	281.4	-0.21	382.5	36

Table 6.9: Short circuit, zero seq., $f=2089 \text{ Hz}$, $I_{ex}=282.0$, $\Delta t=0.005 \text{ msec.}$

The large error in the case of the constant-parameter representation at this frequency is probably due to the fact that this model does not take into account the distributed nature of the system losses.

iii) $f = 1 \text{ Hz}$. The results for this case are shown in table 6.10.

$t(\text{msec})$	$I_{fd}(\text{A})$	$\Delta I_{fd}(\%)$	$I_{cp}(\text{A})$	$\Delta I_{cp}(\%)$
175	21 058	4.14	21 823	7.93
675	-19 996	-1.11	-21 823	7.93
1175	20 287	0.33	21 823	7.93

Table 6.10: Short circuit, zero seq., $f=1 \text{ Hz}$, $I_{ex}=20 220 \text{ A}$, $\Delta t=0.1 \text{ msec.}$

The initial offset in the case of the frequency-dependence simulation is probably due to the limited number of digits (four) that can be entered as input parameters for the pre-transient steady-state calculations in the EMTP. This is probably also the reason for the error in the constant-parameter simulation. No initial offset occurs for this model, however, since the parameters used for the steady-state and transient simulations are the same. The limitation in the number of digits for the steady-state parameters can be avoided in the frequency dependence version of the EMTP by calculating these

parameters internally from the transient parameters. This feature will be implemented in a future version of the program.

Positive Sequence Comparisons:

i) $f = 60.26$ Hz. The results of these simulations are shown in table 6.11.

t (msec)	I_{fd} (A)	ΔI_{fd} (%)	I_{cp} (A)	ΔI_{cp} (%)
4.1	1982	-0.10	1974	-0.50
12.4	-1985	0.05	-1977	-0.35
20.7	1982	-0.10	1974	-0.50
29.0	-1985	0.05	-1976	-0.40
37.3	1983	-0.05	1974	-0.50
45.5	-1985	0.05	-1976	-0.40

Table 6.11: Short circuit, pos. seq., $f=60.26$ Hz, $I_{ex}=1984$, $\Delta t=0.1$ msec.

ii) $f = 10\ 000$ Hz. The results for this case are shown in table 6.12.

t (msec)	I_{fd} (A)	ΔI_{fd} (%)	I_{cp} (A)	ΔI_{cp} (%)
.027	-771.6	-0.48	-774.4	-0.12
.077	771.6	-0.48	774.3	-0.13
.127	-771.6	-0.48	-774.3	-0.13
.177	771.6	-0.48	774.4	-0.12
.227	-771.6	-0.48	-774.5	-0.10
.277	771.6	-0.48	774.6	-0.09

Table 6.12: Short circuit, pos. seq., $f=10\ 000$ Hz, $I_{ex}=775.3$, $\Delta t=0.001$ msec.

The constant-parameter, lumped-resistance model gives much better results at high frequencies for the case of the positive sequence mode than it does for the zero sequence mode. This is probably due to the fact that

at these frequencies the resistance as compared to the reactance is much smaller for the positive sequence mode than it is for the zero sequence mode. As a consequence, the effect of the resistance being represented as concentrated instead of distributed has much less effect in the simulation.

iii) $f = 1$ Hz. The results for this case are shown in table 6.13.

$t(\text{msec})$	$I_{fd}(\text{A})$	$\Delta I_{fd}(\%)$	$I_{cp}(\text{A})$	$\Delta I_{cp}(\%)$
70	57 860	-0.50	57 600	-0.95
570	-58 130	-0.03	-57 600	-0.95
1070	58 160	0.02	57 600	-0.95

Table 6.13: Short circuit, pos. seq., $f=1$ Hz, $I_{ex} = 58 150$ A, $\Delta t=0.1$ msec.

6.7 Examples of Transient Simulations

The importance of correctly simulating the entire frequency range of the signals (from dc (0 Hz) to the very high frequencies) is illustrated in this section with some comparisons of transient simulations using the frequency-dependence models and using constant-parameter representations at 60 and 750 Hz.

In these examples, the zero sequence mode of 100 miles of the reference line was directly energized with an ideal voltage source at the sending end and various conditions were considered at the receiving end.

Short circuit simulations:

With zero initial conditions, a 60-Hz, 100 kV peak, sinusoidal voltage source was applied to the sending end of the line with the receiving end short-circuited. The applied voltage passes through zero at $t = 0$. The resulting short circuit currents at the receiving end are shown in the

following graphs:

- i) Frequency-dependence model → P.7.1
- ii) Constant 60-Hz-parameter model → P.7.2
- iii) Constant 750-Hz-parameter model → P.7.3

Due to the extended time range of these simulations, a relatively large time step, $\Delta t = 0.4$ msec was used. (The travelling time is $\tau = 0.5976$ msec.)

A most interesting element in these graphs is the simulations of the exponentially decaying dc component of the short-circuit current. This component dies very fast in the 60-Hz model and almost does not appear at all in the 750-Hz model. These results corroborate the predicted behaviour of the models from the short circuit frequency responses (graphs P5.1(a), P.5.2(a), and P.5.3(a)). They also show the importance of the line model to be capable of correctly simulating dc conditions.

A closer view of the first cycles of this simulation is shown in the graphs:

- i) Frequency dependence (P) vs. 60 Hz (P60) → P.7.4
- ii) Frequency dependence (P) vs. 750 Hz (P750) → P.7.5

These simulations were run with $\Delta t = 0.1$ msec.

The peak value of the short-circuit current given by the different simulations was, approximately:

- i) Frequency dependence: 860 A
- ii) 60 Hz parameters: 765 A (-11%)
- iii) 750 Hz parameters: 280 A (-67%)

Another important value is the first zero crossing (for fast circuit breakers). This value was approximately:

- i) Frequency dependence: 14.6 msec
- ii) 60-Hz parameters: 13.5 msec
- iii) 750-Hz parameters: 9.8 msec

A short circuit simulation for the case when the voltage is at its peak value at $t = 0$ is shown in the graphs:

- i) Frequency dependence vs. 60 Hz → P.7.6
- ii) Frequency dependence vs. 750 Hz → P.7.7

A Δt of 0.01 msec was used for these simulations. The difference in the harmonic content of the signals for the different models is quite noticeable. Since very little dc offset is present in this case, the 60-Hz simulation follows the general shape of the frequency-dependence simulation; the 750-Hz simulation, however, gives very inaccurate results in both magnitude and phase angle.

As a third example of short circuit modelling, the line was energized with a step voltage of 100 kV. The corresponding receiving end currents are shown in the following graphs:

- i) Frequency dependence vs. 60 Hz → P.7.8
- ii) Frequency dependence vs. 750 Hz → P.7.9

($\Delta t = 0.01$ msec).

The step response simulation for the frequency-dependence model was extended over a longer time (graph P.7.10; $\Delta t = 0.4$ msec) in order to verify that the model correctly reproduces the dc response. Neglecting the very small shunt current, the final asymptotic value of the step response should coincide with the value obtained in the frequency response curves (graph P.5.1(a)) and with the value calculated analytically. Reading the approximated values from the graphs,

from graph P.7.10, $I_{dc} = 53\ 500\ A$

from graph P.5.1, $I_{dc} = 53\ 600\ A$

and, analytically,

$$I_{dc} = \frac{100\ kV}{R_{dc}} = \frac{100\ kV}{1.867\Omega} = 53\ 562\ A.$$

Open circuit simulations:

With the receiving end of the line open and initial conditions equal to zero, a 60-Hz, 1-p.u.-peak, sinusoidal voltage source was applied to the sending end of the line (peak voltage at $t = 0$). The resulting voltages at the receiving end are shown in the following graphs:

- i) Frequency dependence vs. 60 Hz → P.7.11
- ii) Frequency dependence vs. 750 Hz → P.7.12

For these simulations $\Delta t = 0.01\ msec$. From the graphs, the maximum transient voltages are:

- i) Frequency-dependence model: 1.82 p.u.
- ii) 60-Hz constant-parameter model: 1.95 p.u. (+7%)
- iii) 750-Hz constant-parameter model: 1.55 p.u. (-15%)

The difference in the harmonic content is quite noticeable. The 60-Hz model exaggerates the harmonics above 60 Hz, and the 750-Hz model, while exaggerating the higher frequency harmonics, overdampens the mid-range ones.

In a second open circuit simulation, the line was energized with a unit step voltage. The voltages at the receiving end are shown in the graphs:

- i) Frequency dependence vs. 60 Hz → P.7.13
- ii) Frequency dependence vs. 750 Hz → P.7.14

($\Delta t = 0.01\ msec$). The peak voltages for this case were:

- i) Frequency dependence: 1.93 p.u.
- ii) 60-Hz parameters: 1.96 p.u. (+1.6%)
- iii) 750-Hz parameters: 1.60 p.u. (-17%)

The 60-Hz model reproduced the maximum peak voltage quite closely, but the damping of the oscillations is very low. The 750-Hz model gives an overall excessive damping, even though it exaggerates the very sharp corners (highest frequencies).

Additional examples:

As additional illustrations of the importance of the correct simulation of the different frequency components of the signal in transient simulations, the following examples are presented.

A) Line terminated in a capacitance:

In these simulations the line was terminated in a capacitive load equal to $\frac{1}{4}$ the capacitance of the line,

$$C_{\text{load}} = \frac{1}{4} C_{\text{line}} = \frac{1}{4} (0.01244 \frac{\mu F}{mi}) \times 100 \text{ mi} = 0.311 \mu F$$

With $\Delta t = 0.01 \text{ msec}$, to discriminate frequencies up to $f = \frac{1}{0.01} \times 10^3 = 10^5 \text{ Hz}$, the following simulations were run:

- a) For a unit step-voltage input and zero initial conditions, the voltage across the capacitance is shown in the following graphs:
 - i) Frequency dependence vs. 60 Hz → P.7.15
 - ii) Frequency dependence vs. 750 Hz → P.7.16
- b) For a step voltage of 100 kV, the current in the capacitance is shown in the following graphs:
 - i) Frequency dependence vs. 60 Hz → P.7.17
 - ii) Frequency dependence vs. 750 Hz → P.7.18

B) Line terminated in an L-C load:

C load = 0.311 μ F

L load = 13 mH

The value of L load was selected to give a resonant frequency in the LC combination equal to 2500 Hz.

For a step voltage of 100 kV applied at the beginning of the line, the following simulations were obtained ($\Delta t = 0.01$ msec):

a) Load voltages (in p.u.):

i) Frequency dependence vs. 60 Hz → P.7.19

ii) Frequency dependence vs. 750 Hz → P.7.20

b) Currents in the capacitance (in amps):

i) Frequency dependence vs. 60 Hz → P.7.21

ii) Frequency dependence vs. 750 Hz → P.7.22

c) Currents in the inductance (in amps):

i) Frequency dependence vs. 60 Hz → P.7.23

ii) Frequency dependence vs. 750 Hz → P.7.24

6.8 Field Test Simulation

Oscillographs and data of a field test have been made available by the Bonneville Power Administration (BPA), Portland, Oregon, U.S.A. The test consisted of a single-line-to-ground fault on an open-ended, 222 km, 500 kV, 3-phase transmission line. The short circuit was applied to phase-c. The oscillographs of the voltages at the fault location are shown in graph P.8.1(a).

The simulation of this field test using BPA's weighting functions formulation is discussed in reference [13]. In this simulation a simplified representation was used for the generators and transformers feeding the line. This representation is shown in fig. 6.2. The tower footing resistance was assumed to be 2Ω and the typical value of $100 \Omega\text{-m}$ was assumed for the earth resistivity.

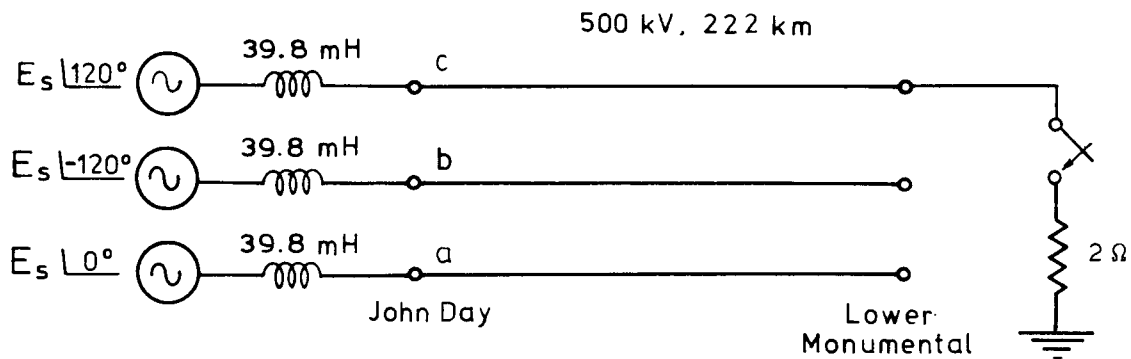


Fig. 6.2: John Day-Lower Monumental BPA's field test. Ref. [13] representation.

In BPA's simulation the zero sequence mode of the line was modelled for frequency dependence. The integration step for the EMTP was $\Delta t = 50 \mu\text{sec}$.

To compare the results obtained with the line model developed in this work with the results obtained in BPA's simulation, the same conditions as in BPA's simulation were assumed. The phase voltages obtained with the new model are shown in graph P.8.1(b). The voltages at phase-b corresponding to the field oscilloscope, BPA's simulation, and new model simulation are shown in graphs P.8.2.

As it can be seen from graph P.8.2, there is a good agreement between the simulations and the field oscilloscope. The peak voltages (in per unit of the pre-fault voltage at the site of the fault) for the different cases (including a constant-60-Hz-parameter simulation) were:

- | | |
|--------------------------------|------------------|
| i) Oscillograph: | 1.60 p.u. |
| ii) BPA's simulation: | 1.77 p.u. (+11%) |
| iii) New model simulation: | 1.71 p.u. (+7%) |
| iv) 60-Hz constant parameters: | 2.11 p.u. (+32%) |

The slightly higher value of the peak voltage given by the new model simulation as compared with the field test result may be due to a number of reasons, as for instance:

- a) A very simple source representation.
- b) Earth resistivity different from assumed value.
- c) Frequency dependence of the positive sequence mode.

These factors could also account for the slightly higher harmonic content of the frequency-dependence simulations as compared with the field test oscillograph.

An interesting factor that can be observed in graphs P.8.2 is that in the case of the field test and new model simulation, the peak voltages tend to decrease as the steady state is approached. In BPA's simulation, however, these values seem to follow a slight increase.

In BPA's frequency-dependence simulation the average time per step of the solution process was 3.13 times longer than with a constant-parameter representation. In the simulation with the new model this time was only 1.19 times longer.

(CHAPTER 6: NUMERICAL RESULTS)

LIST OF GRAPHS

LINE PARAMETERS

P.2.1: Frequency dependence of the series resistance	127
P.2.2: Frequency dependence of the series inductance	127

CHARACTERISTIC IMPEDANCE

Zero sequence:

i) Form of $Z_c(\omega)$

P.3.1: Magnitude of $Z_c(\omega)$. Zero sequence	128
P.3.2: Phase angle of $Z_c(\omega)$. Zero sequence	128
P.3.3: Real part of $Z_c(\omega)$. Zero sequence	129
P.3.4: Imaginary part of $Z_c(\omega)$. Zero sequence	129

ii) Approximation of $Z_c(\omega)$

P.3.5: Approximation of $Z_c(\omega)$, zero seq. Magnitude	130
P.3.6: Approximation of $Z_c(\omega)$, zero seq. Phase angle	130
P.3.7: Approximation of $Z_c(\omega)$, zero seq. Real part	131
P.3.8: Approximation of $Z_c(\omega)$, zero seq. Imaginary part	131
P.3.9: Approximation of $Z_c(\omega)$, zero seq. Magnitude error	132
P.3.10: Approximation of $Z_c(\omega)$, zero seq. Phase error	132

Positive Sequence:

i) Form of $Z_c(\omega)$

P.3.11: Magnitude of $Z_c(\omega)$. Positive sequence	133
P.3.12: Phase angle of $Z_c(\omega)$. Positive sequence	133
P.3.13: Real part of $Z_c(\omega)$. Positive sequence	134
P.3.14: Imaginary part of $Z_c(\omega)$. Positive sequence	134

ii) Approximation of $Z_c(\omega)$

P.3.15: Approximation of $Z_c(\omega)$, pos. seq. Magnitude	135
P.3.16: Approximation of $Z_c(\omega)$, pos. seq. Phase angle	135
P.3.17: Approximation of $Z_c(\omega)$, pos. seq. Real part	136
P.3.18: Approximation of $Z_c(\omega)$, pos. seq. Imaginary part	136
P.3.19: Approximation of $Z_c(\omega)$, pos. seq. Magnitude error	137
P.3.20: Approximation of $Z_c(\omega)$, pos. seq. Phase error	137

WEIGHTING FUNCTION

Simulation of $A_1(\omega)$ for Different Line Lengths

P.4.1: Simulation of $A_1(\omega)$. Zero sequence, 5-mi	138
P.4.2: Simulation of $A_1(\omega)$. Positive sequence, 5-mi	138
P.4.3: Simulation of $A_1(\omega)$. Zero sequence, 30-mi	139

P.4.4:	Simulation of $A_1(\omega)$.	Positive sequence, 30-mi	139
P.4.5:	Simulation of $A_1(\omega)$.	Zero sequence, 100-mi	140
P.4.6:	Simulation of $A_1(\omega)$.	Positive sequence, 100-mi	140
P.4.7:	Simulation of $A_1(\omega)$.	Zero sequence, 500-mi	141
P.4.8:	Simulation of $A_1(\omega)$.	Positive sequence, 500-mi	141
P.4.9:	Simulation of $A_1(\omega)$.	Zero sequence, 1000-mi	142
P.4.10:	Simulation of $A_1(\omega)$.	Positive sequence, 1000-mi	142

Zero Sequence, 100-mi:

i) Form of $A_1(\omega)$

P.4.11:	Magnitude of $A_1(\omega)$.	Zero sequence, 100-mi	143
P.4.12:	Phase angle of $A_1(\omega)$.	Zero sequence, 100-mi	143
P.4.13:	Real part of $A_1(\omega)$.	Zero sequence, 100-mi	144
P.4.14:	Imaginary part of $A_1(\omega)$.	Zero sequence, 100-mi	144
P.4.15:	Phase angle of $P(\omega)$.	Zero sequence, 100-mi	145

ii) Simulation of $A_1(\omega)$

P.4.16:	Simulation of $A_1(\omega)$, zero seq., 100-mi.	Magnitude	146
P.4.17:	Simulation of $A_1(\omega)$, zero seq., 100-mi.	Phase angle	146
P.4.18:	Simulation of $A_1(\omega)$, zero seq., 100-mi.	Real part	147
P.4.19:	Simulation of $A_1(\omega)$, zero seq., 100-mi.	Imaginary part	147
P.4.20:	Simulation of $A_1(\omega)$, zero seq., 100-mi.	Magnitude error	148
P.4.21:	Simulation of $A_1(\omega)$, zero seq., 100-mi.	Phase error	148

Positive Sequence, 100-mi:

i) Form of $A_1(\omega)$

P.4.22:	Magnitude of $A_1(\omega)$.	Positive sequence, 100-mi	149
P.4.23:	Phase angle of $A_1(\omega)$.	Positive sequence, 100-mi	149
P.4.24:	Real part of $A_1(\omega)$.	Positive sequence, 100-mi	150
P.4.25:	Imaginary part of $A_1(\omega)$.	Positive sequence, 100-mi	150
P.4.26:	Phase angle of $P(\omega)$.	Positive sequence, 100-mi	151

ii) Simulation of $A_1(\omega)$

P.4.27:	Simulation of $A_1(\omega)$, pos. seq., 100-mi.	Magnitude	152
P.4.28:	Simulation of $A_1(\omega)$, pos. seq., 100-mi.	Phase angle	152
P.4.29:	Simulation of $A_1(\omega)$, pos. seq., 100-mi.	Real part	153
P.4.30:	Simulation of $A_1(\omega)$, pos. seq., 100-mi.	Imaginary part	153
P.4.31:	Simulation of $A_1(\omega)$, pos. seq., 100-mi.	Magnitude error	154
P.4.32:	Simulation of $A_1(\omega)$, pos. seq., 100-mi.	Phase error	154

Time Domain Form, $a_1(t)$:

P.4.33:	Weighting function $a_1(t)$.	Zero seq., 100-mi	155
P.4.34(a):	Weighting function $a_1(t)$.	Pos. seq., 100-mi.	155
Same time scale as in graph P.4.33.			
P.4.34(b):	Weighting function $a_1(t)$.	Pos. seq., 100-mi.	155
Expanded time scale.			

FREQUENCY DOMAIN TESTS

Zero Sequence:

i) Short-circuit responses

P.5.1(a): S/C Response, zero seq.	Exact vs. approx.	Mid to high frequencies.	156
P.5.1(b): S/C Response, zero seq.	Exact vs. approx.	Low frequencies.	156
P.5.2(a): S/C Response, zero seq.	Exact vs.	60-Hz. Mid to high frequencies.	157
P.5.2(b): S/C Response, zero seq.	Exact vs.	60-Hz. Low frequencies.	157
P.5.3(a): S/C Response, zero seq.	Exact vs.	750-Hz. Mid to high frequencies.	158
P.5.3(b): S/C Response, zero seq.	Exact vs.	750-Hz. Low frequencies.	158
P.5.4(a): S/C Response, zero seq.	Magnitude error.	Approximation. Mid to high frequencies.	159
P.5.5(a): S/C Response, zero seq.	Magnitude error.	60-Hz. Mid to high frequencies.	159
P.5.6(a): S/C Response, zero seq.	Magnitude error.	750-Hz. Mid to high frequencies.	159
P.5.4(b): S/C Response, zero seq.	Magnitude error.	Approximation. Low frequencies.	160
P.5.5(b): S/C Response, zero seq.	Magnitude error.	60 Hz. Low frequencies.	160
P.5.6(b): S/C Response, zero seq.	Magnitude error.	750 Hz. Low frequencies.	160

ii) Open-circuit responses

P.5.7: O/C Response, zero seq.	Exact vs. approx.	161	
P.5.8: O/C Response, zero seq.	Exact vs. 60-Hz.	161	
P.5.9: O/C Response, zero seq.	Exact vs. 750-Hz.	162	
P.5.10: O/C Response, zero seq.	Magnitude error.	Approximation.	163
P.5.11: O/C Response, zero seq.	Magnitude error.	60-Hz.	163
P.5.12: O/C Response, zero seq.	Magnitude error.	750-Hz.	163

Positive Sequence:

i) Short-circuit responses

P.5.13(a): S/C Response, pos. seq.	Exact vs. approx.	Mid to high frequencies.	164
P.5.13(b): S/C Response, pos. seq.	Exact vs. approx.	Low frequencies.	164
P.5.14(a): S/C Response, pos. seq.	Exact vs. approx.	Mid to high frequencies.	165
P.5.14(b): S/C Response, pos. seq.	Exact vs.	60-Hz. Low frequencies.	165
P.5.15(a): S/C Response, pos. seq.	Exact vs.	750-Hz. Mid to high frequencies.	166
P.5.15(b): S/C Response, pos. seq.	Exact vs.	750-Hz. Low frequencies.	166
P.5.16(a): S/C Response, pos. seq.	Magnitude error.	Approximation. Mid to high frequencies.	167

P.5.17(a):S/C Response, pos, seq.	Magnitude error.	60-Hz.	167
	Mid to high frequencies.		
P.5.18(a):S/C Response, pos. seq.	Magnitude error.	750-Hz.	167
	Mid to high frequencies.		
P.5.16(b):S/C Response, pos. seq.	Magnitude error.	Approximation.	168
	Low frequencies.		
P.5.17(b):S/C Response, pos. seq.	Magnitude error.	60-Hz.	168
	Low frequencies.		
P.5.18(b):S/C Response, pos. seq.	Magnitude error.	750-Hz.	168
	Low frequencies.		

ii) Open-circuit responses

P.5.19:	O/C Response, pos. seq.	Exact vs. approx.	169	
P.5.20:	O/C Response, pos. seq.	Exact vs. 60-Hz.	169	
P.5.21:	O/C Response, pos. seq.	Exact vs. 750-Hz.	170	
P.5.22:	O/C Response, pos. seq.	Magnitude error.	Approximation.	171
P.5.23:	O/C Response, pos. seq.	Magnitude error.	60-Hz.	171
P.5.24:	O/C Response, pos. seq.	Magnitude error.	750-Hz.	171

TRANSIENT SIMULATIONS

Short Circuit:

P.7.1:	Short circuit simulation.	Sinusoidal source, zero at t=0. New model.	172
P.7.2:	Short circuit simulation.	Sinusoidal source, zero at t=0. 60-Hz parameters.	172
P.7.3:	Short circuit simulation.	Sinusoidal source, zero at t=0. 750-Hz parameters.	173
P.7.4:	Short circuit simulation.	Sinusoidal source, zero at t=0. New model vs. 60-Hz. First cycles.	174
P.7.5:	Short circuit simulation.	Sinusoidal source, zero at t=0. New model vs. 750-Hz. First cycles.	174
P.7.6:	Short circuit simulation.	Sinusoidal source, peak at t=0. New model vs. 60-Hz.	175
P.7.7:	Short circuit simulation.	Sinusoidal source, peak at t=0. New model vs. 750-Hz.	175
P.7.8:	Short circuit simulation.	Step excitation. New model vs. 60-Hz.	176
P.7.9:	Short circuit simulation.	Step excitation. New model vs. 750-Hz.	176
P.7.10:	Short circuit simulation.	Step excitation. New model. Extended time response.	177

Open Circuit:

P.7.11:	Open circuit simulation.	Sinusoidal source, peak at t=0. New model vs. 60-Hz.	178
P.7.12:	Open circuit simulation.	Sinusoidal source, peak at t=0. New model vs. 750 Hz.	178
P.7.13:	Open circuit simulation.	Step excitation. New model vs. 60-Hz.	179

P.7.14: Open circuit simulation. Step excitation. New model vs. 750-Hz. 179

Capacitive Loads:

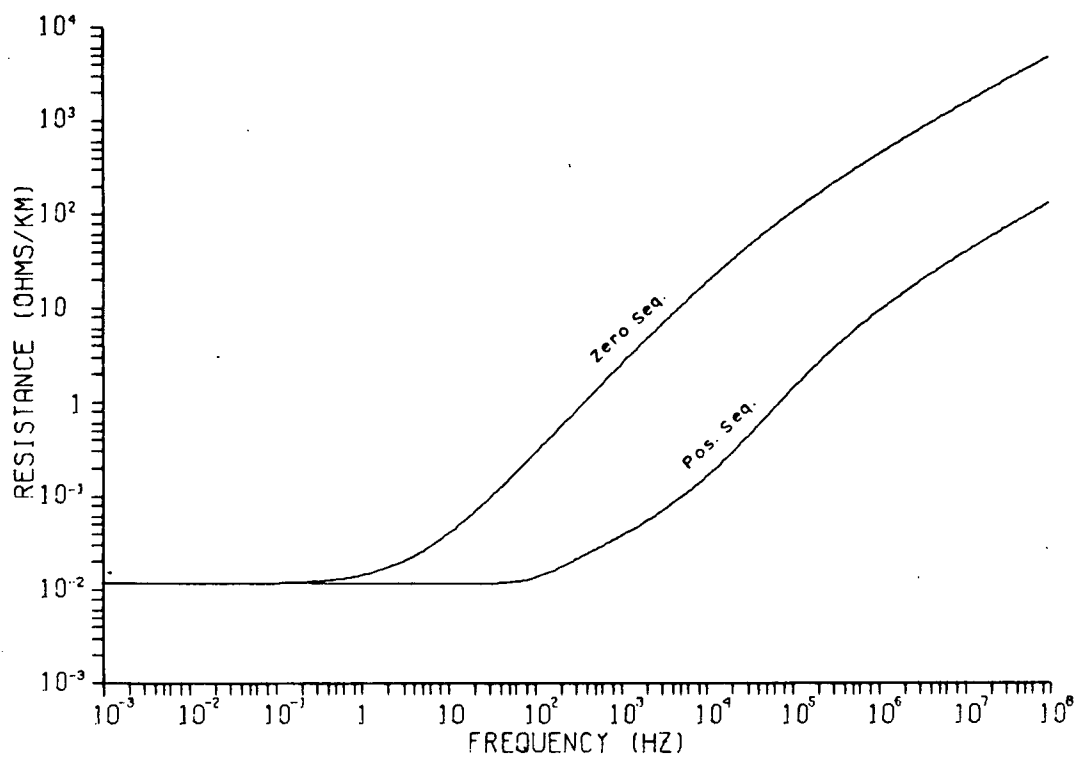
P.7.15: Capacitive load. Step excitation. Load voltage. New model vs. 60-Hz. 180
 P.7.16: Capacitive load. Step excitation. Load voltage. New model vs. 750-Hz. 180
 P.7.17: Capacitive load. Step excitation. Load current. New model vs. 60-Hz. 181
 P.7.18: Capacitive load. Step excitation. Load current. New model vs. 750-Hz. 181

L-C Load:

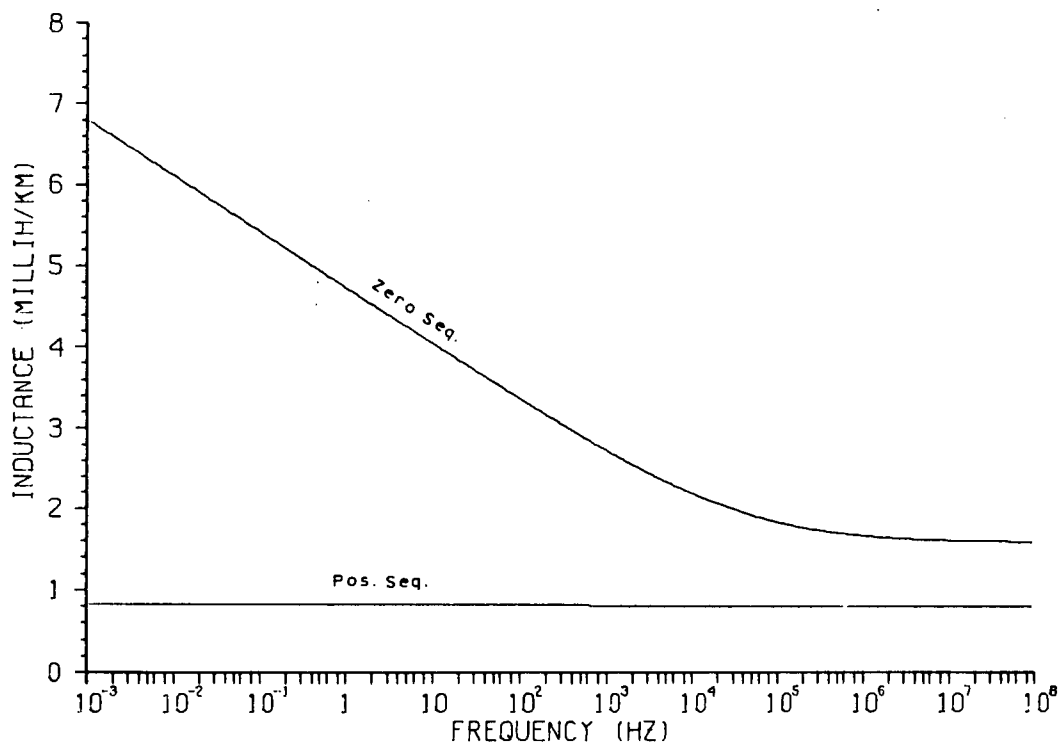
P.7.19: L-C load. Step excitation. Load voltage. New model vs. 60-Hz. 182
 P.7.20: L-C load. Step excitation. Load voltage. New model vs. 750-Hz. 182
 P.7.21: L-C load. Step excitation. Current in C. New model vs. 60-Hz. 183
 P.7.22: L-C load. Step excitation. Current in C. New model vs. 750-Hz. 183
 P.7.23: L-C load. Step excitation. Current in L. New model vs. 60-Hz. 184
 P.7.24: L-C load. Step excitation. Current in L. New model vs. 750-Hz. 184

FIELD TEST SIMULATIONS

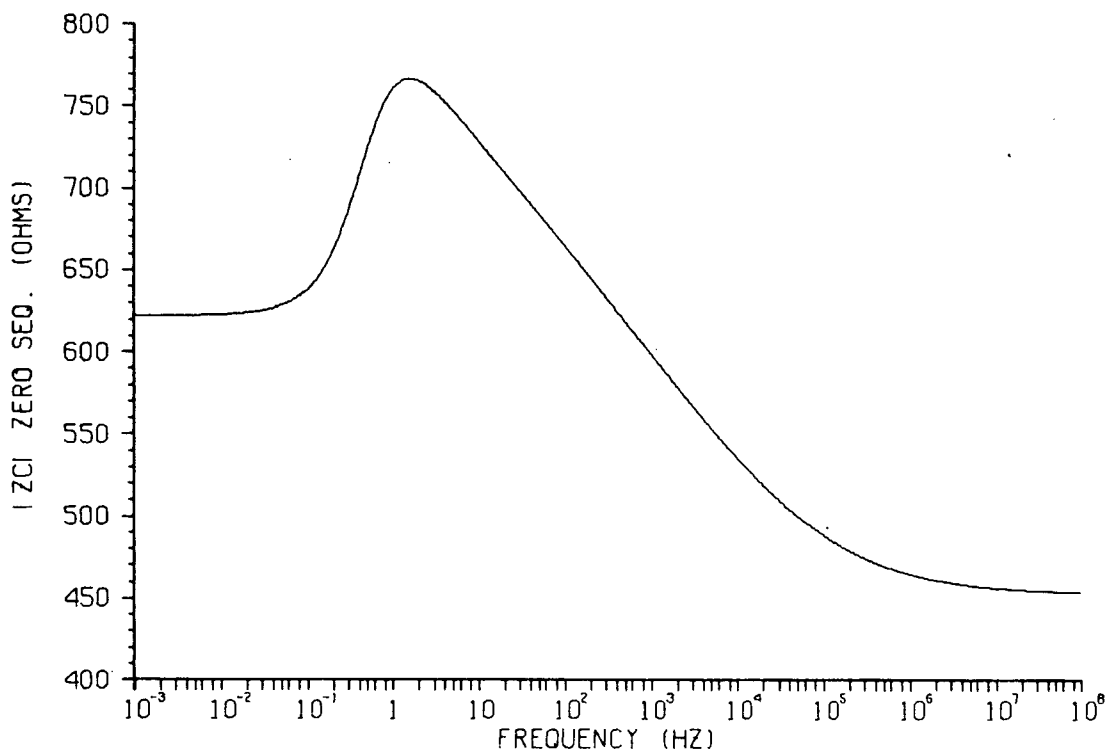
P.8.1(a): Field test oscilloscope (BPA). Single-line-to-ground fault on phase C. Receiving end voltages. 185
 P.8.1(b): Simulation of field test in P.8.1(a) with the new line model. (Only the zero sequence is modelled as frequency dependent.) 185
 P.8.2: Comparison between voltages at phase b for: a) Field test oscilloscope; b) BPA's frequency-dependence simulation; c) New model simulation. 186



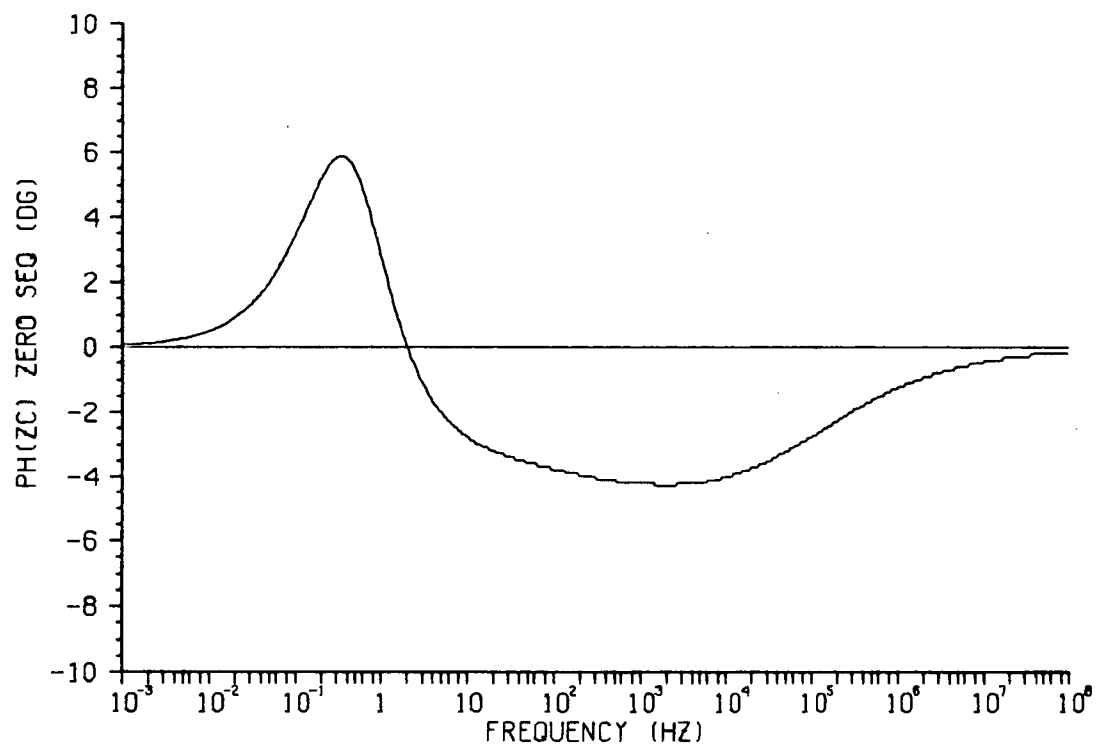
P.2.1: Frequency dependence of the series resistance.



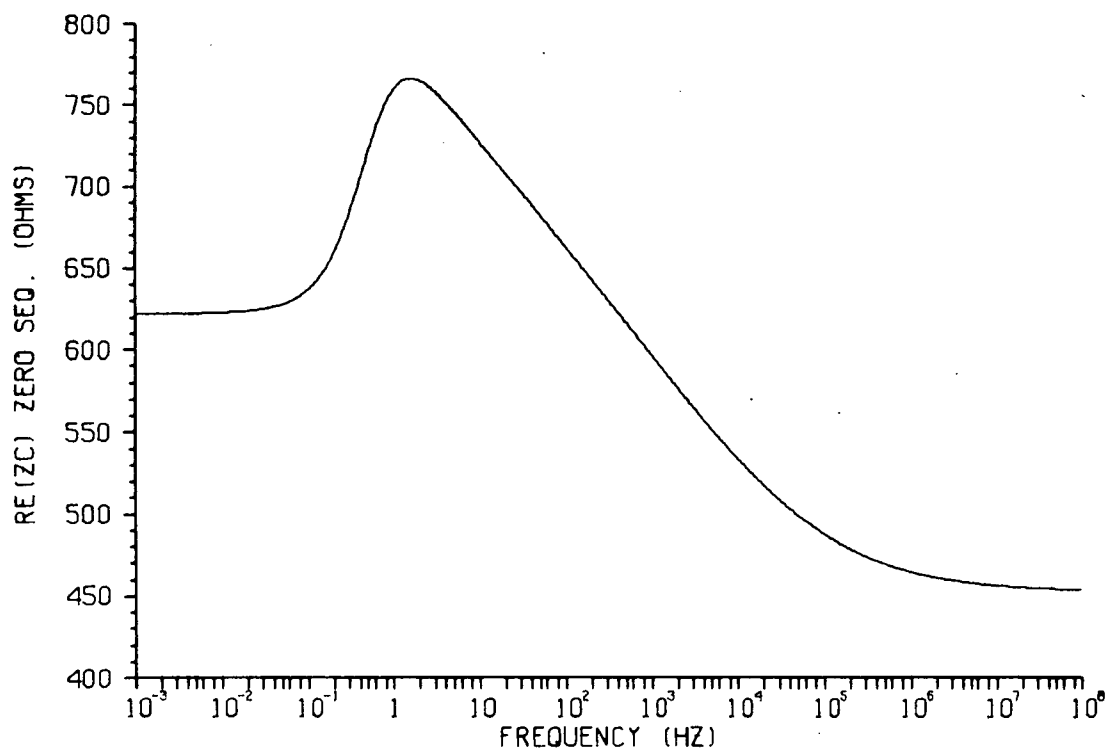
P.2.2: Frequency dependence of the series inductance.



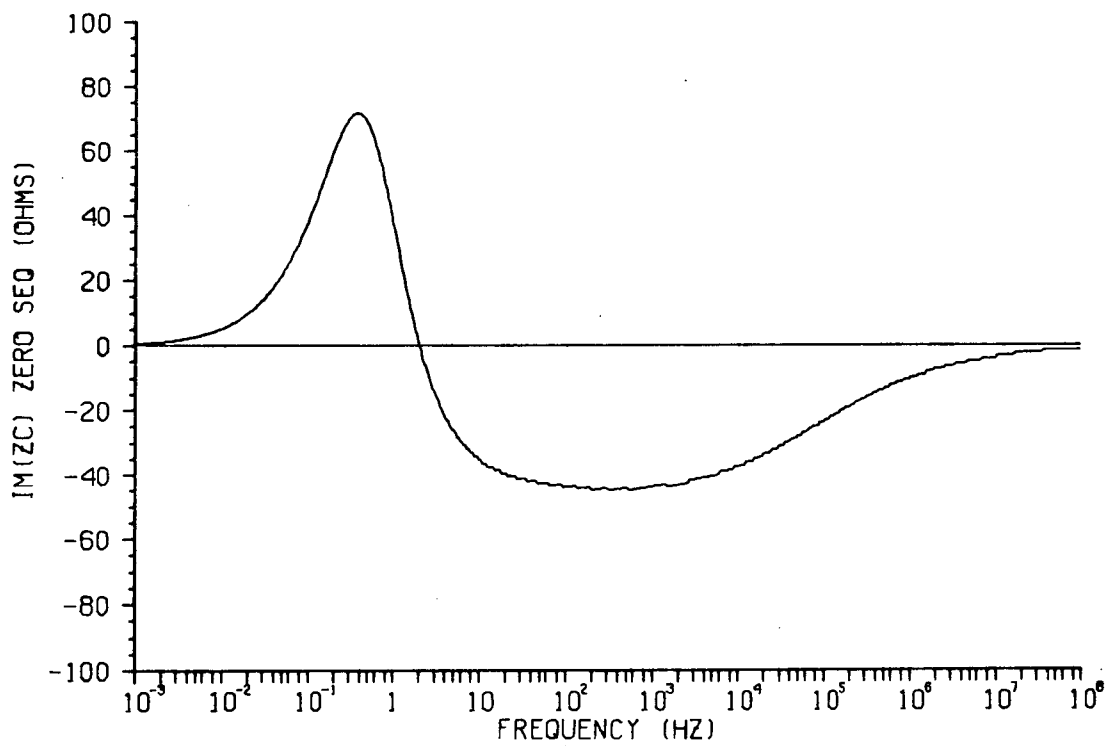
P.3.1: Magnitude of $Z_c(\omega)$. Zero sequence.



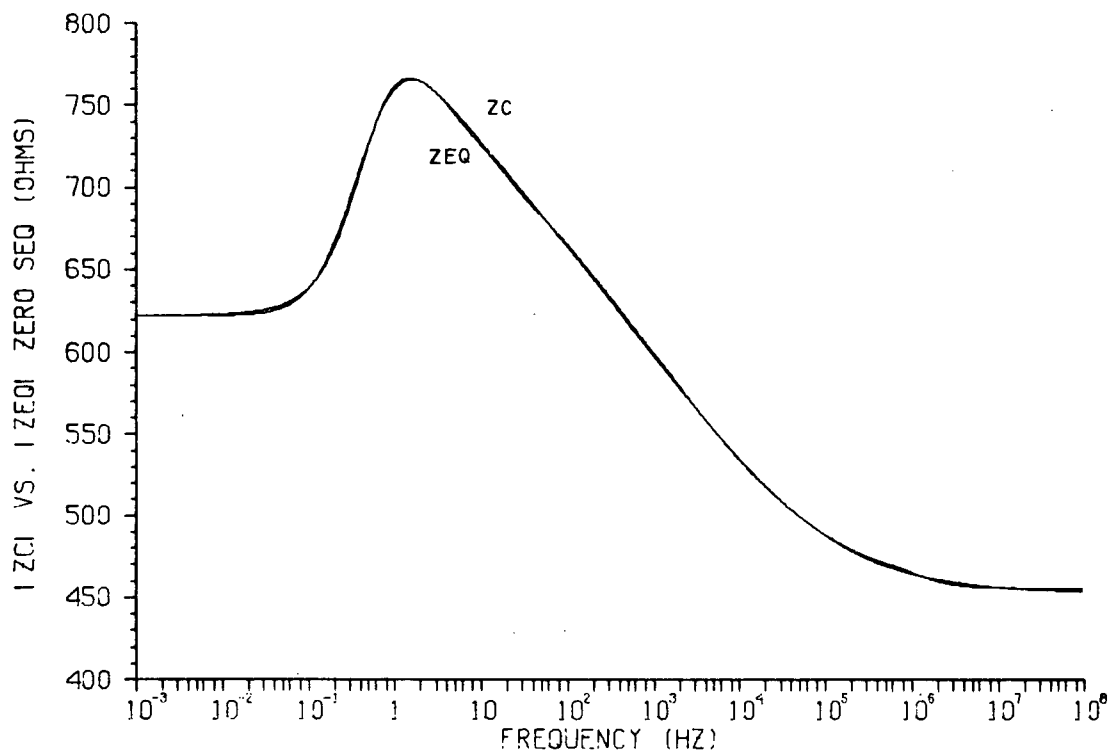
P.3.2: Phase angle of $Z_c(\omega)$. Zero sequence.



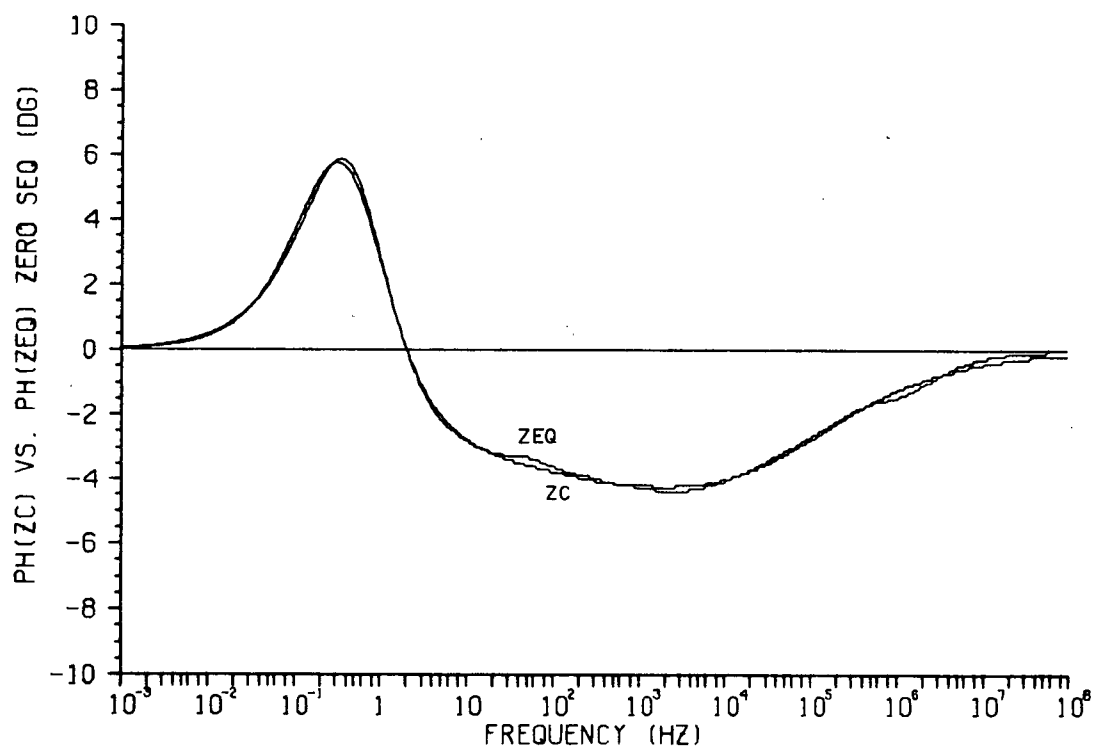
P.3.3: Real part of $Z_c(\omega)$. Zero sequence.



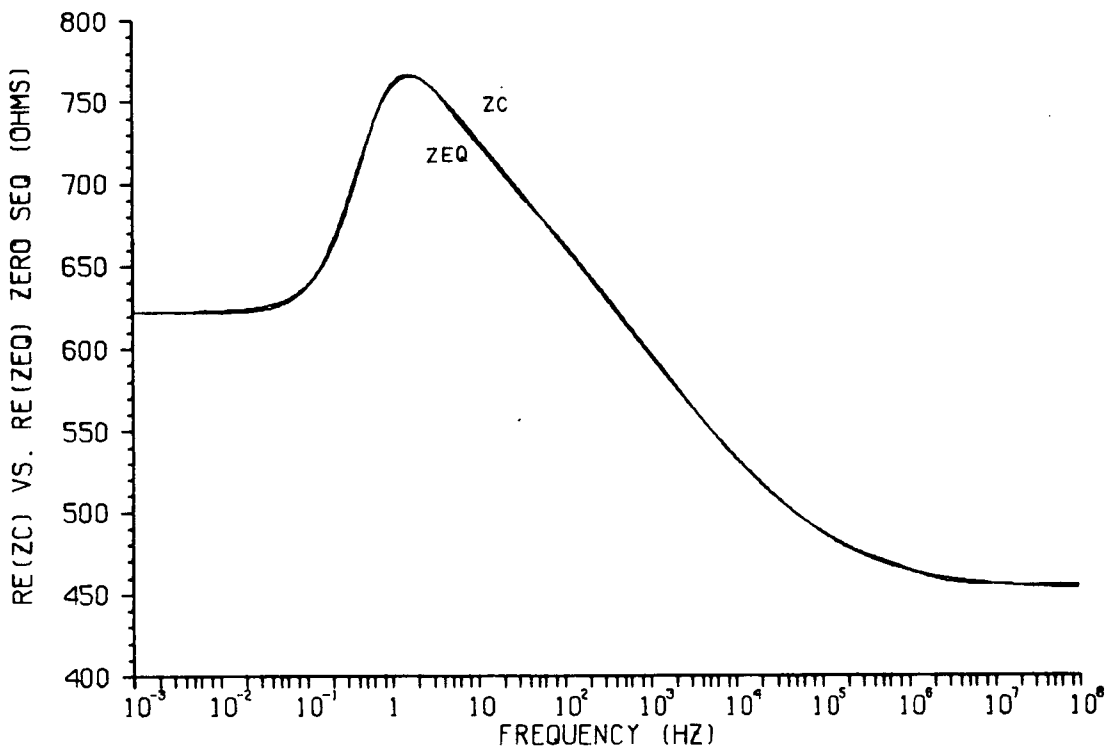
P.3.4: Imaginary part of $Z_c(\omega)$. Zero sequence.



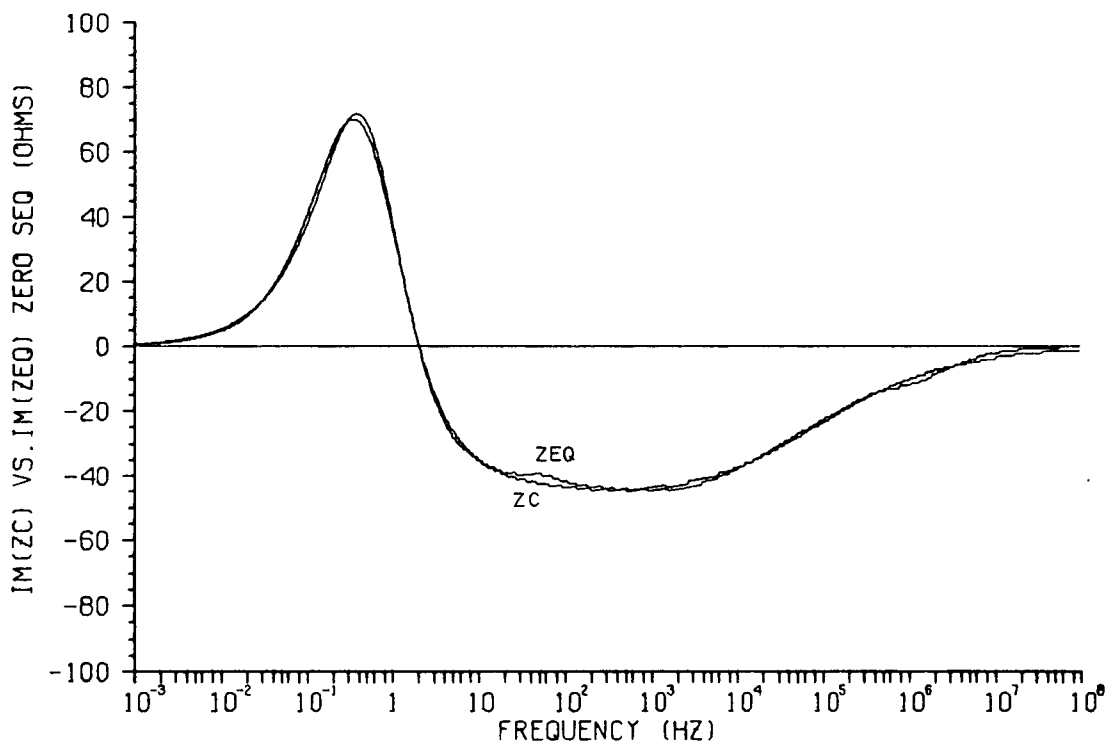
P.3.5: Approximation of $Z_c(\omega)$, zero seq. Magnitude.



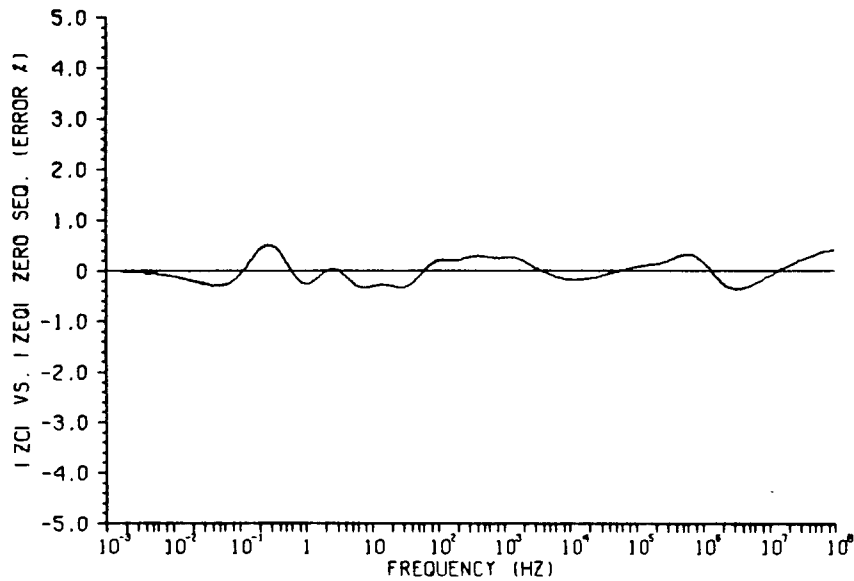
P.3.6: Approximation of $Z_c(\omega)$, zero seq. Phase angle.



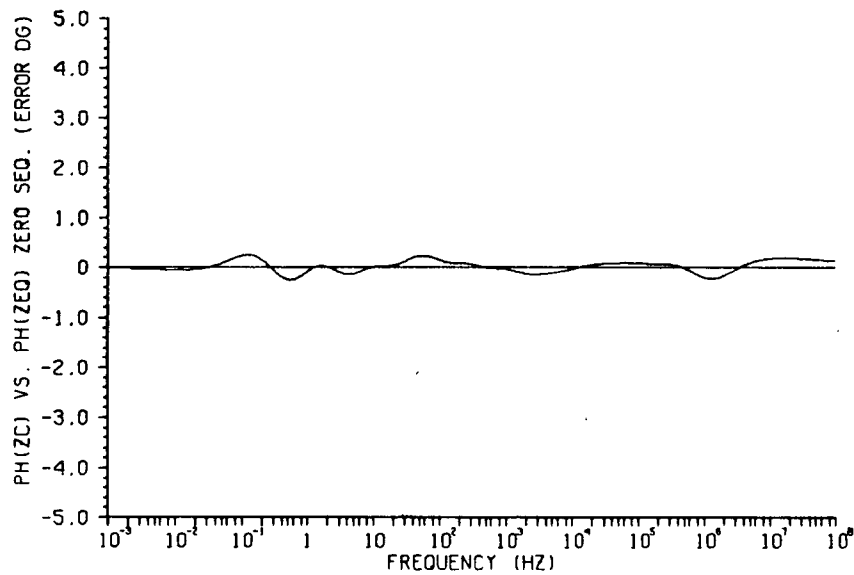
P.3.7: Approximation of $Z_c(\omega)$, zero seq. Real part.



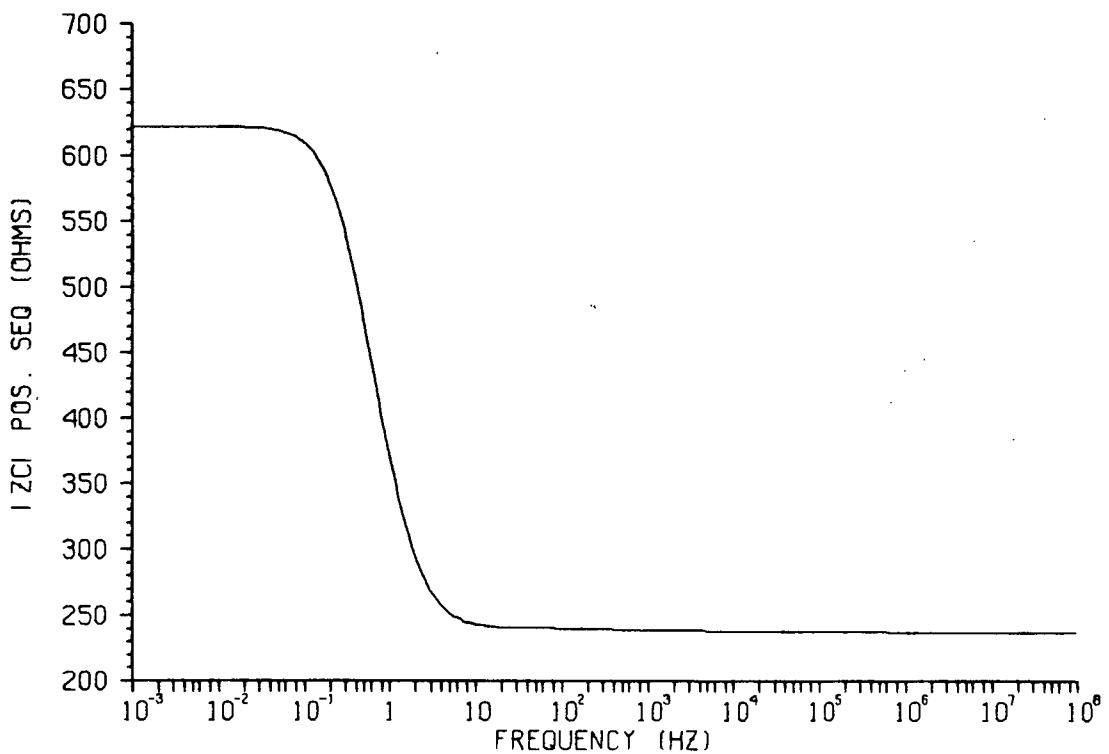
P.3.8: Approximation of $Z_c(\omega)$, zero seq. Imaginary part.



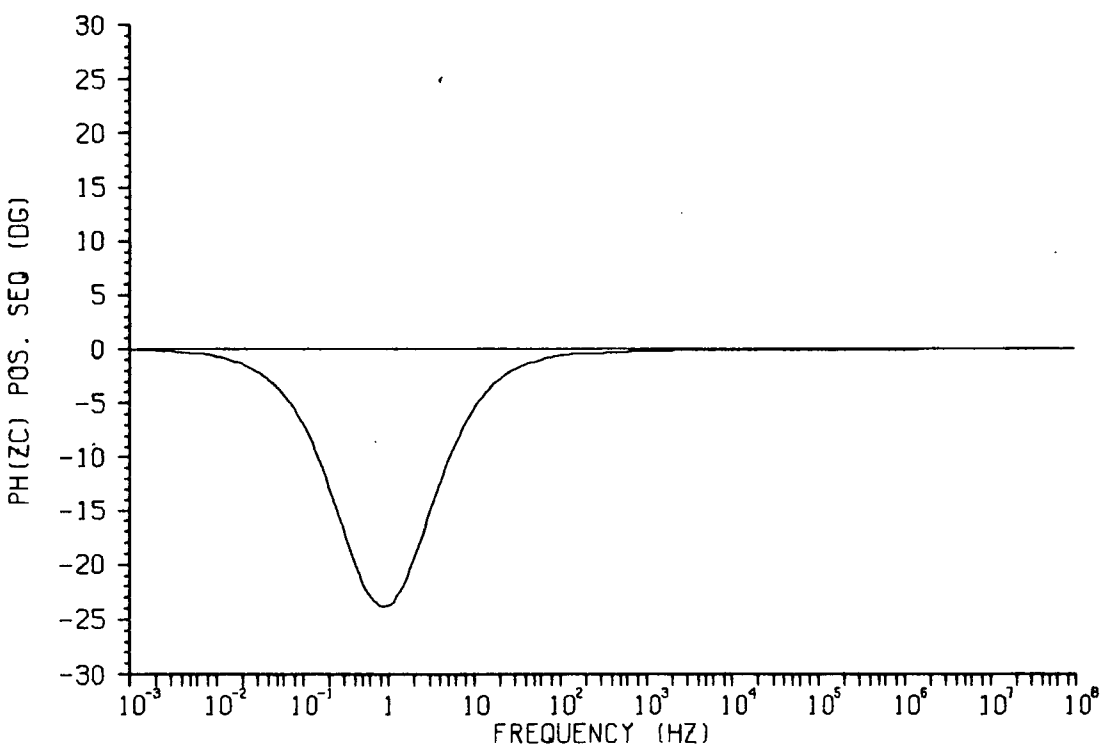
P.3.9: Approximation of $Z_c(\omega)$, zero seq. Magnitude error.



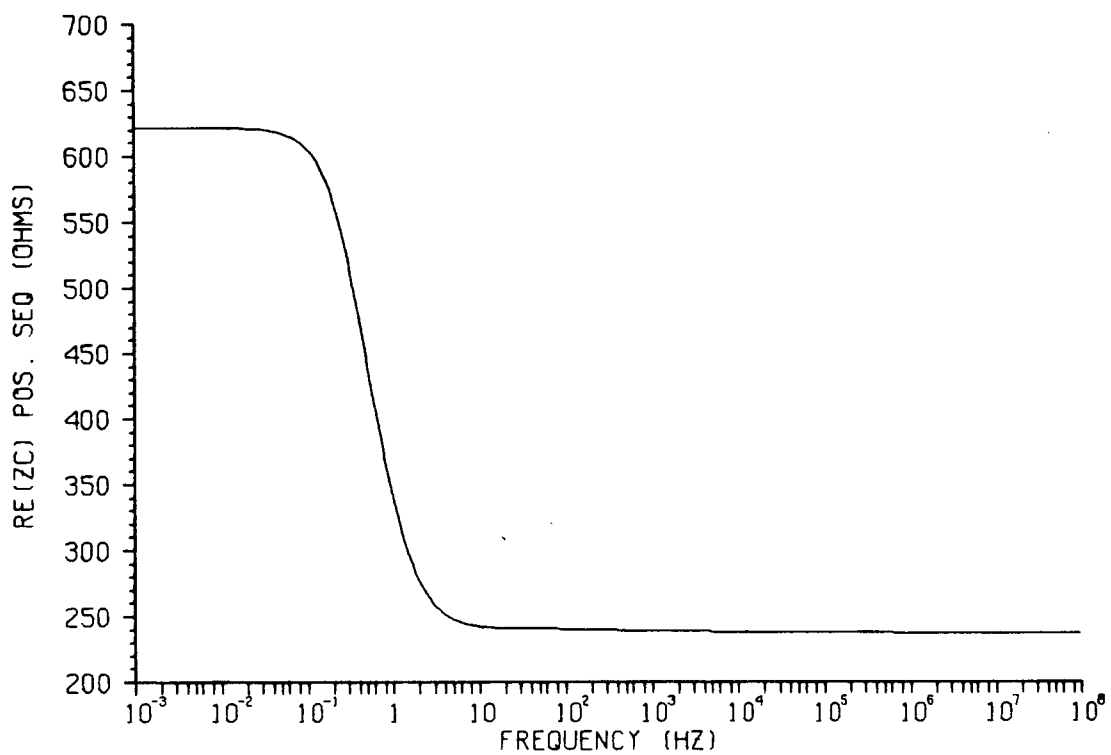
P.3.10: Approximation of $Z_c(\omega)$, zero seq. Phase error.



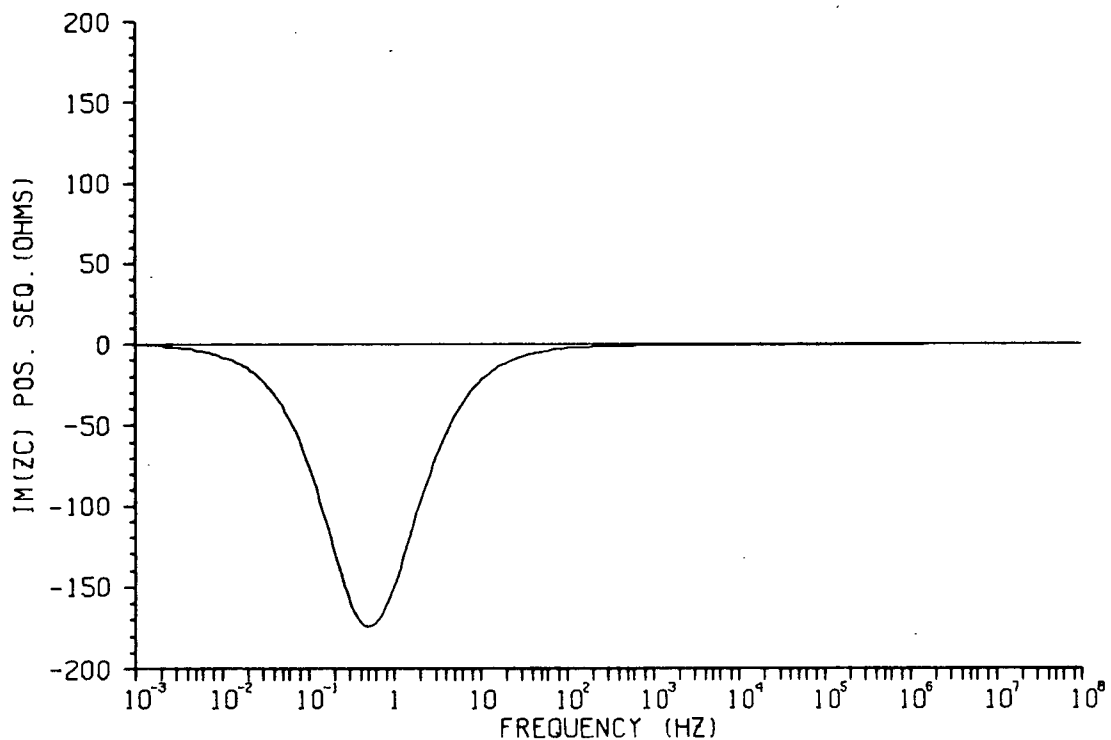
P.3.11: Magnitude of $Z_c(\omega)$. Positive sequence.



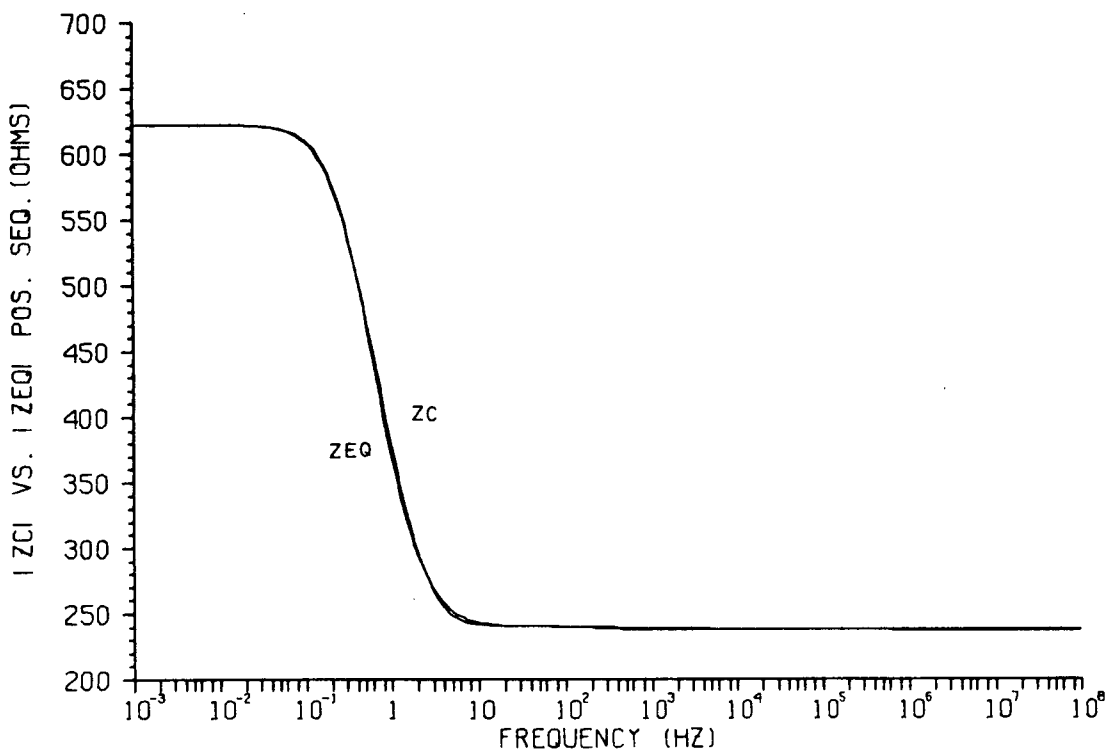
P.3.12: Phase angle of $Z_c(\omega)$. Positive sequence.



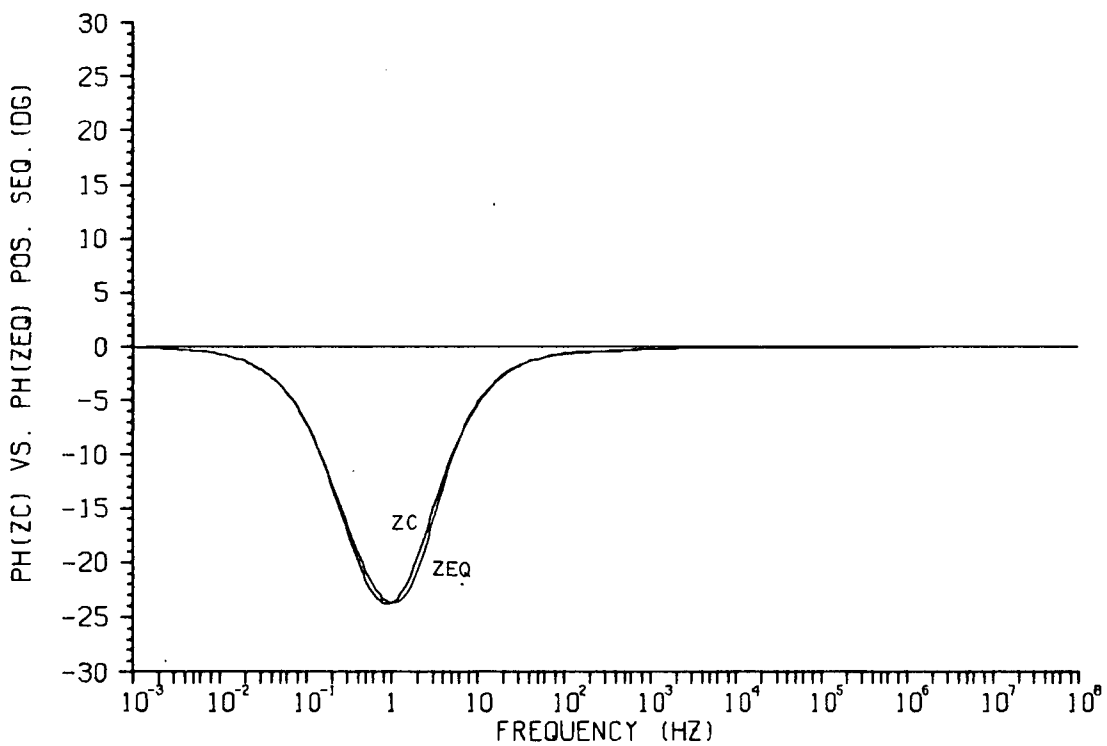
P.3.13: Real part of $Z_c(\omega)$. Positive sequence.



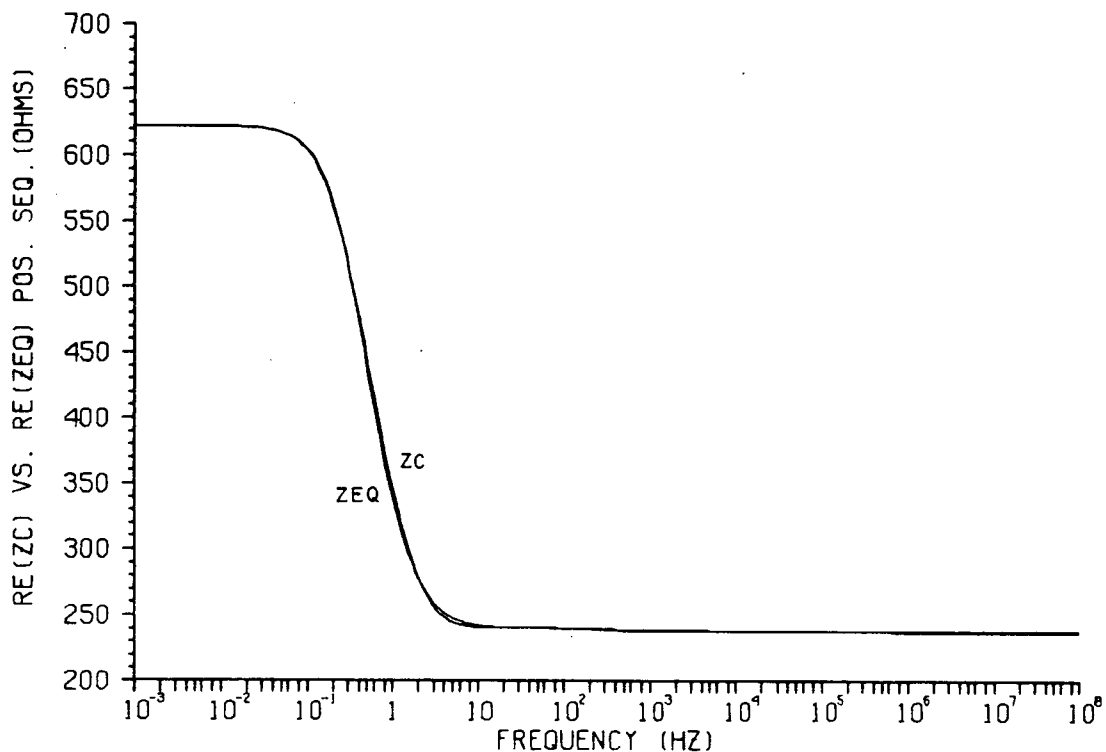
P.3.14: Imaginary part of $Z_c(\omega)$. Positive sequence.



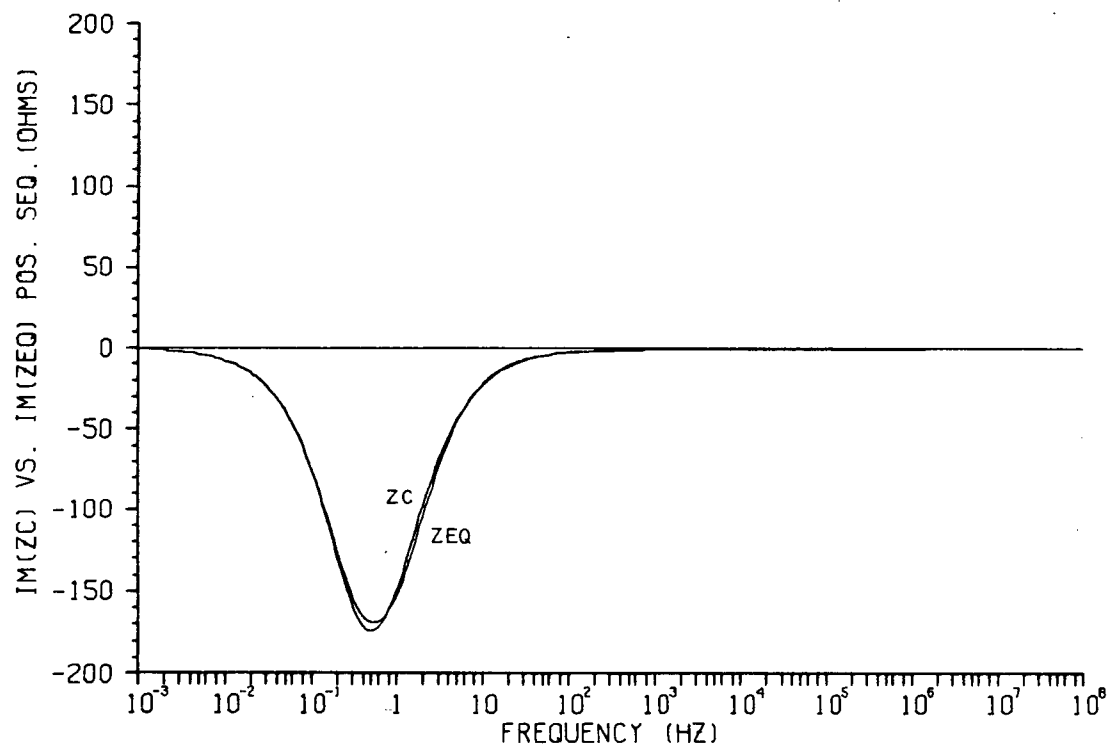
P.3.15: Approximation of $Z_c(\omega)$, pos. seq. Magnitude.



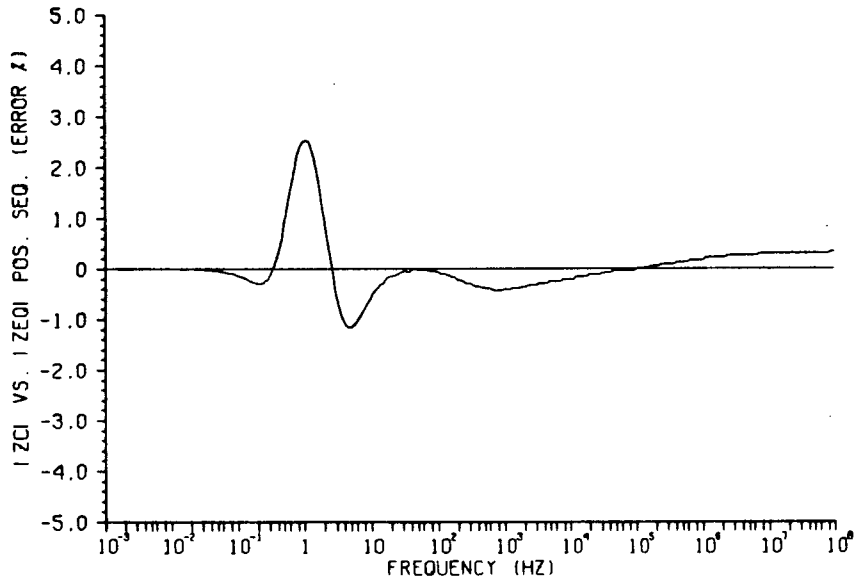
P.3.16: Approximation of $Z_c(\omega)$, pos. seq. Phase angle.



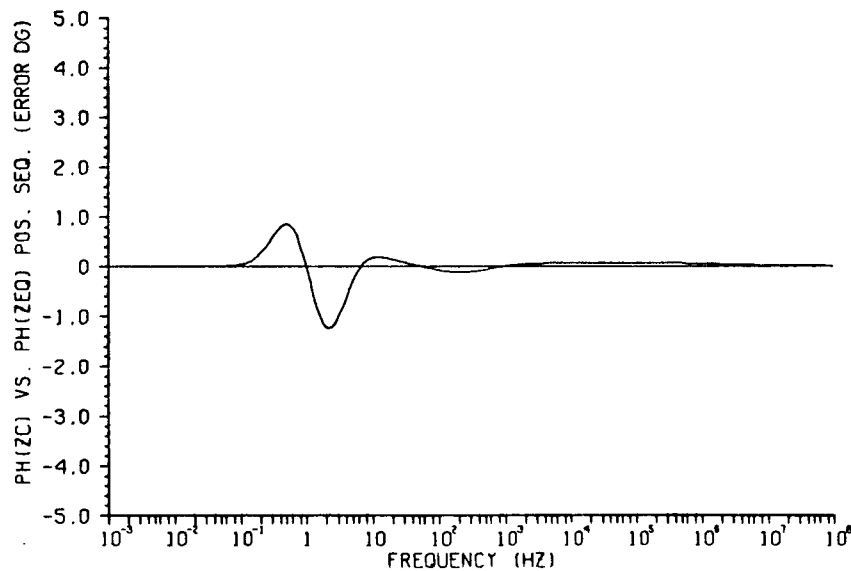
P.3.17: Approximation of $Z_c(\omega)$, pos. seq. Real part.



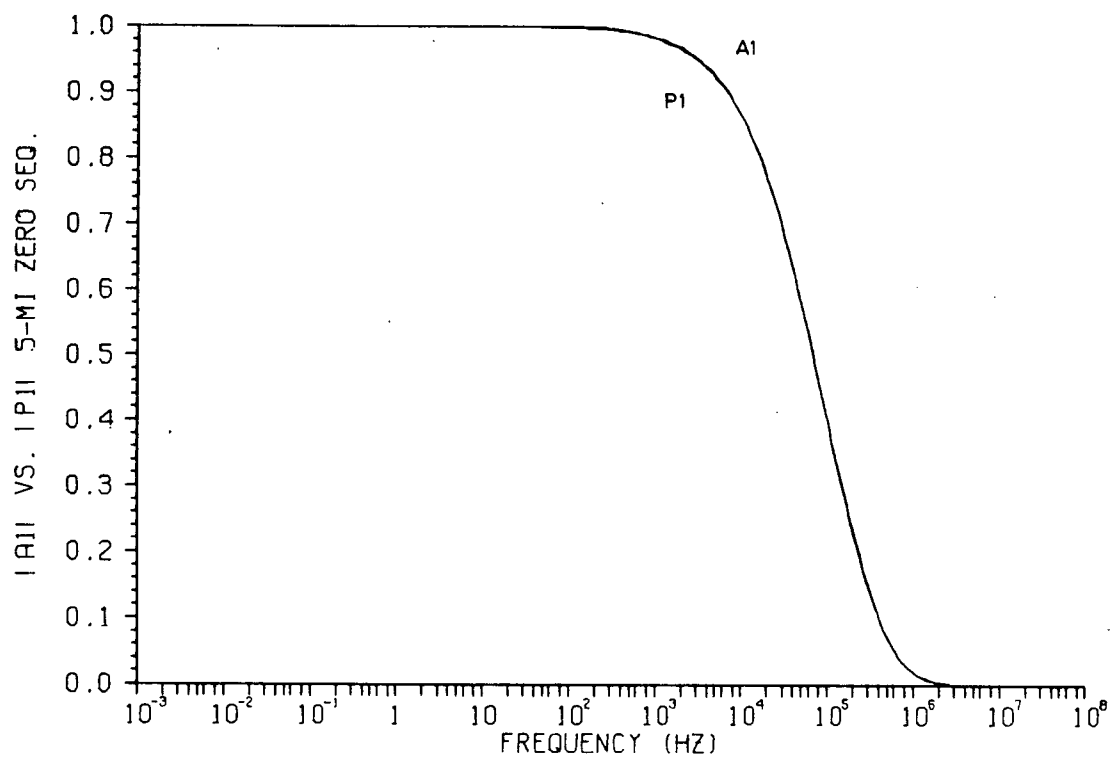
P.3.18: Approximation of $Z_c(\omega)$, pos. seq. Imaginary part.



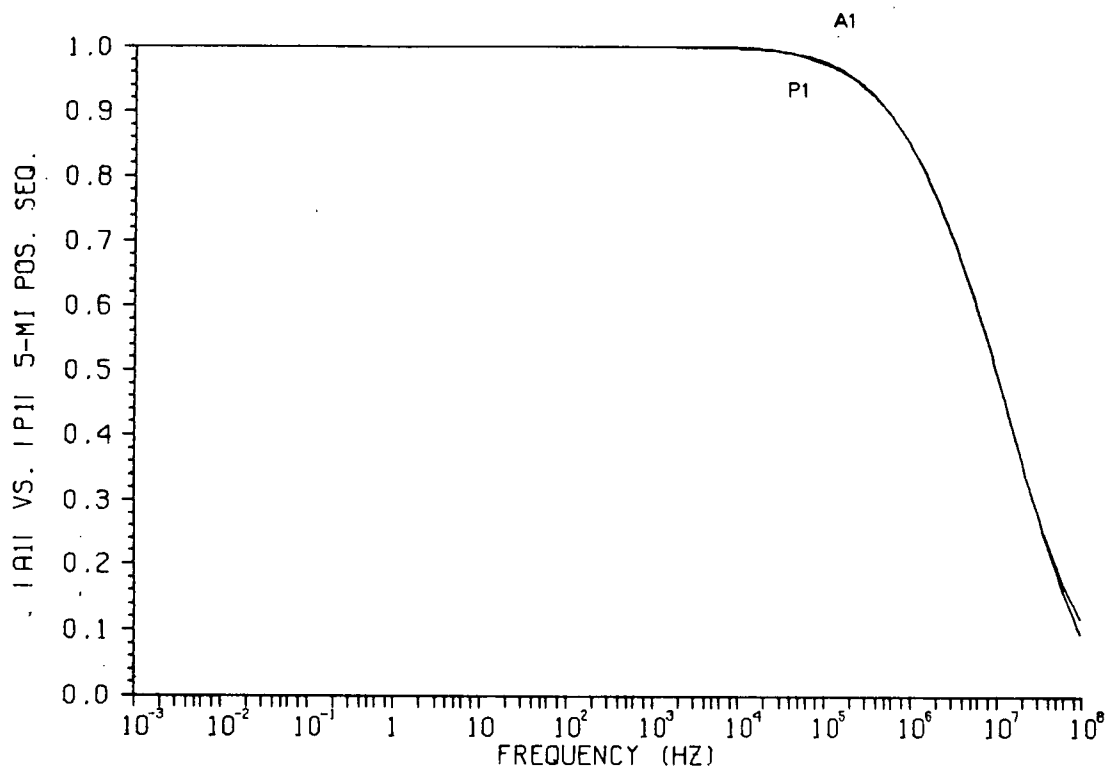
P.3.19: Approximation of $Z_c(\omega)$, pos. seq. Magnitude error.



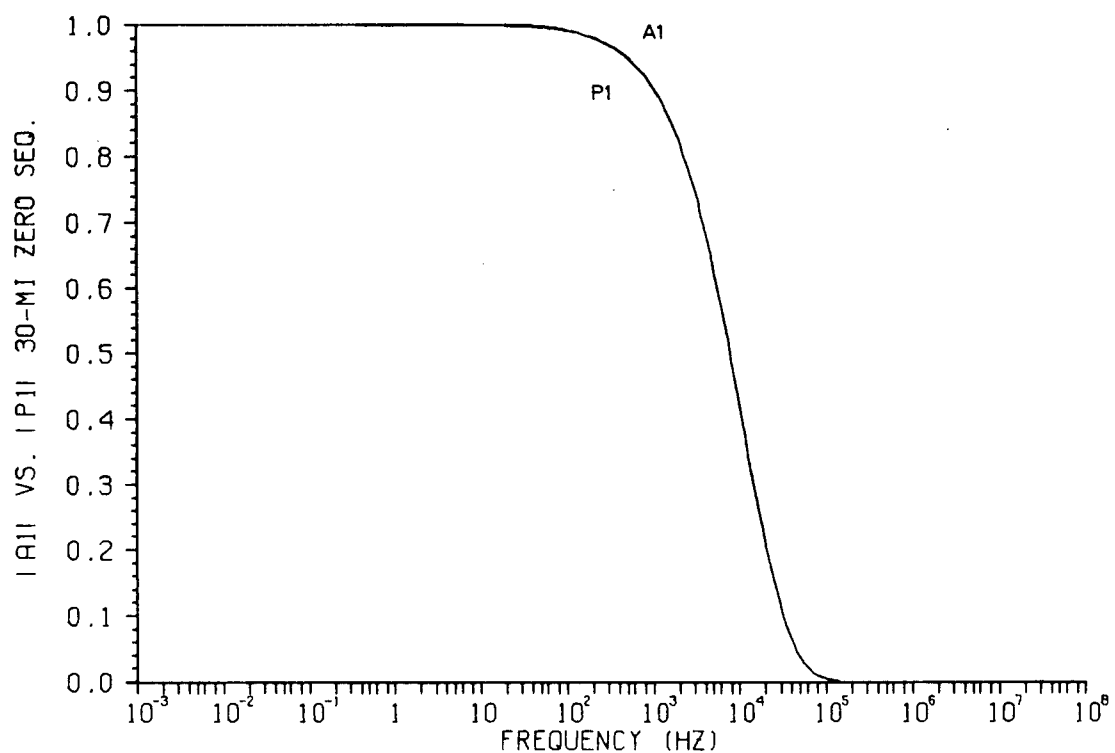
P.3.20: Approximation of $Z_c(\omega)$, pos. seq. Phase error.



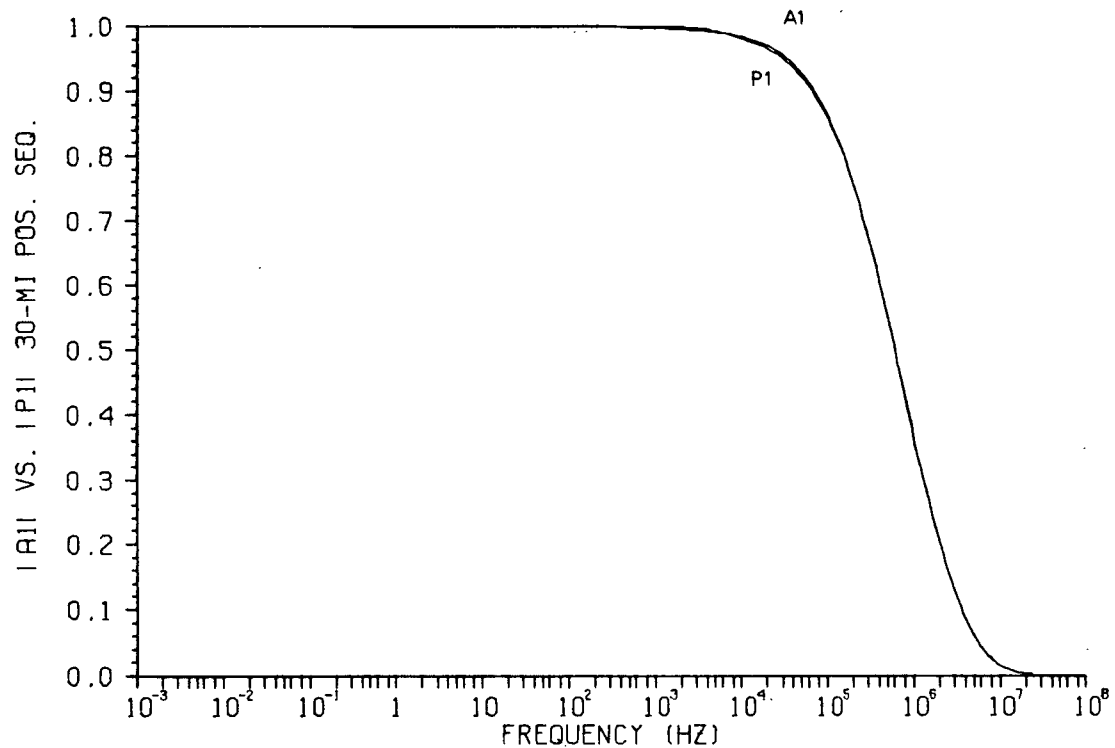
P.4.1: Simulation of $A_1(\omega)$. Zero sequence, 5-mi.



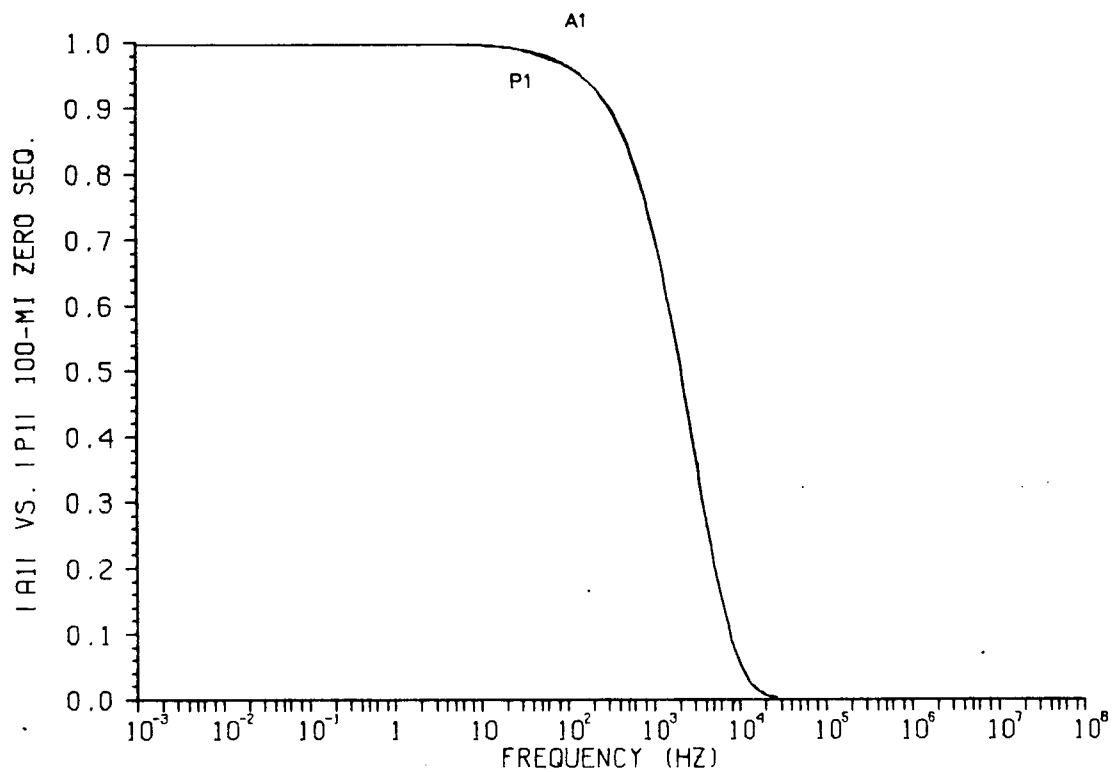
P.4.2: Simulation of $A_1(\omega)$. Positive sequence, 5-mi.



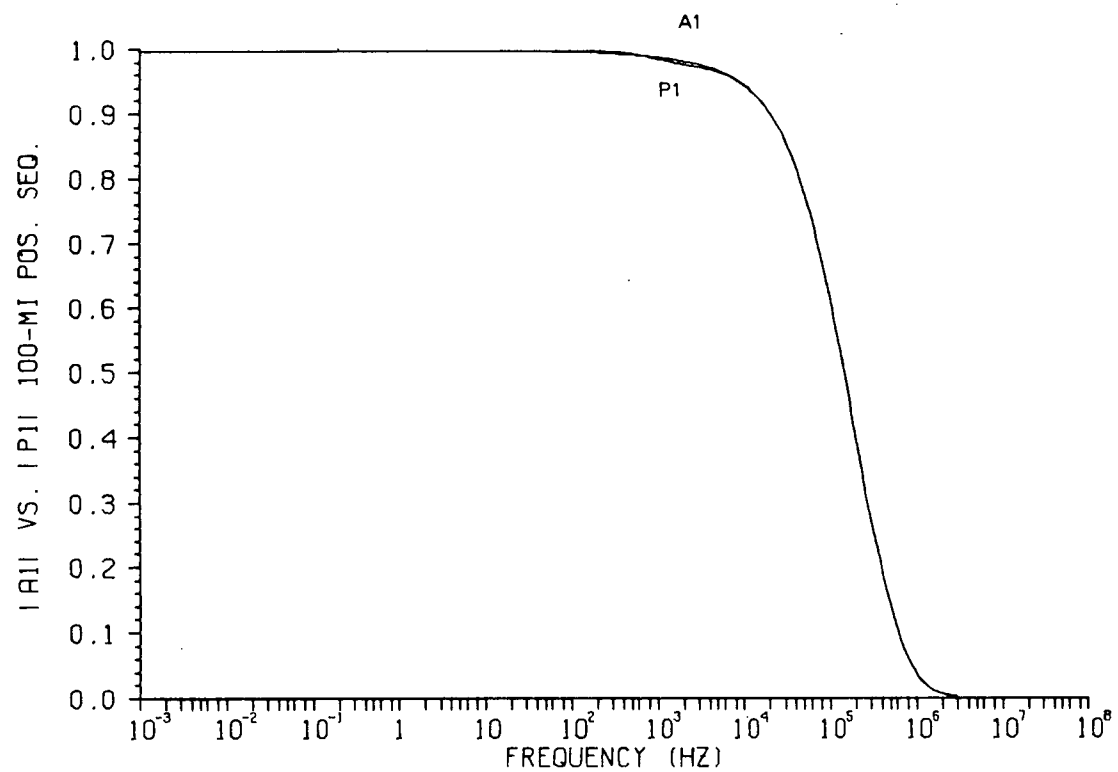
P.4.3: Simulation of $A_1(\omega)$. Zero sequence, 30-mi.



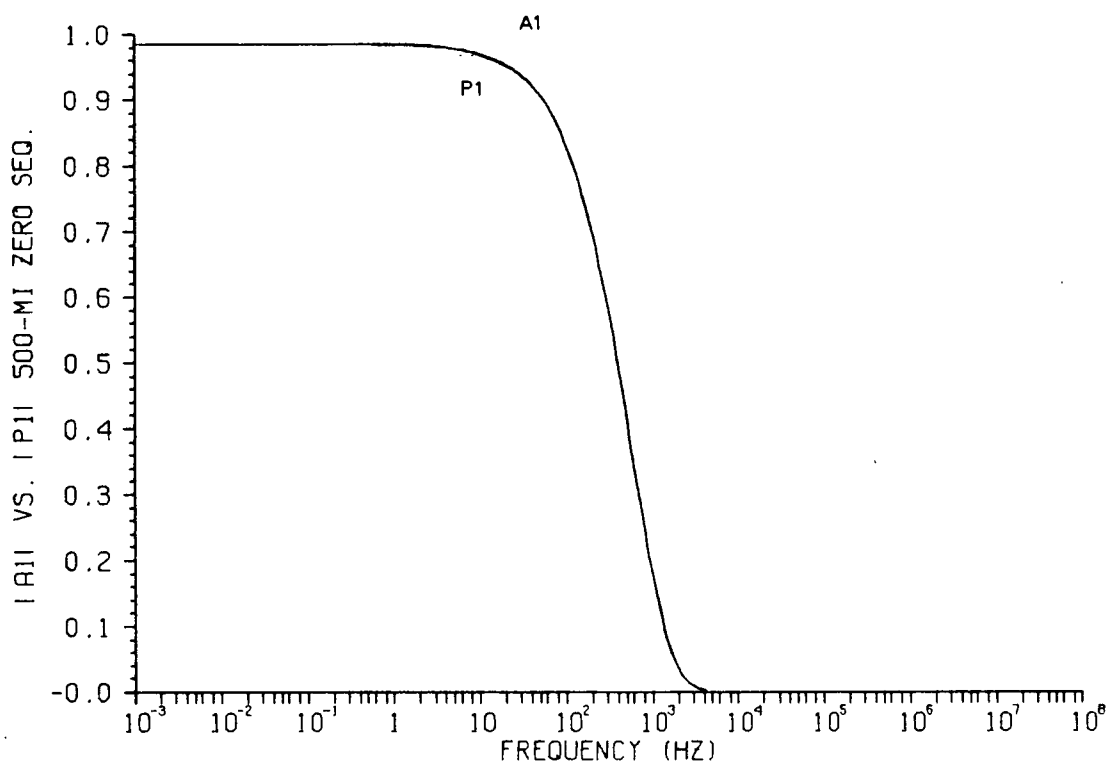
P.4.4: Simulation of $A_1(\omega)$. Positive sequence, 30-mi.



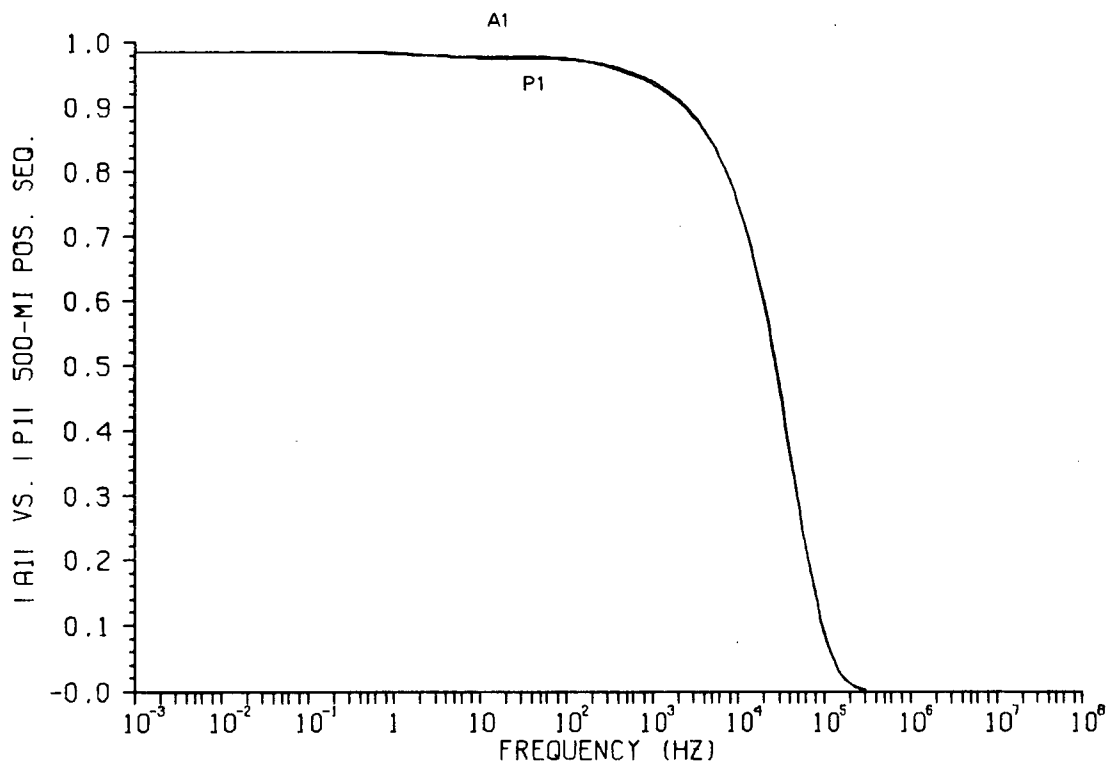
P.4.5: Simulation of $A_1(\omega)$. Zero sequence, 100-mi.



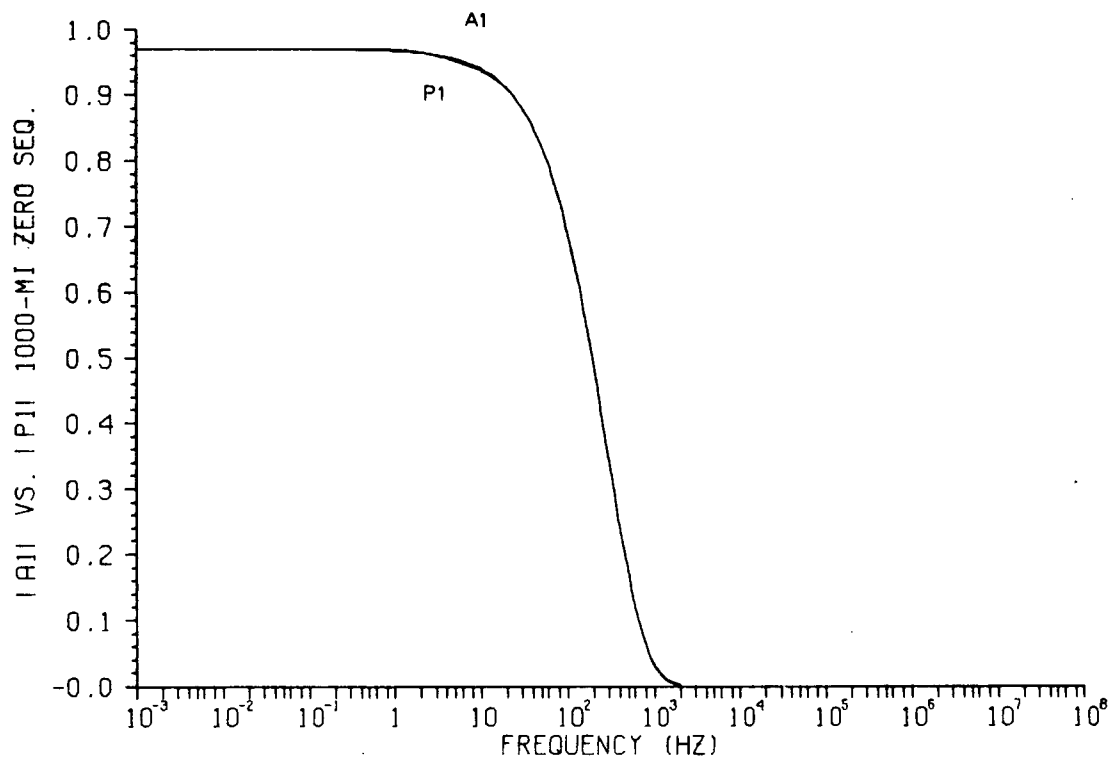
P.4.6: Simulation of $A_1(\omega)$. Positive sequence, 100-mi.



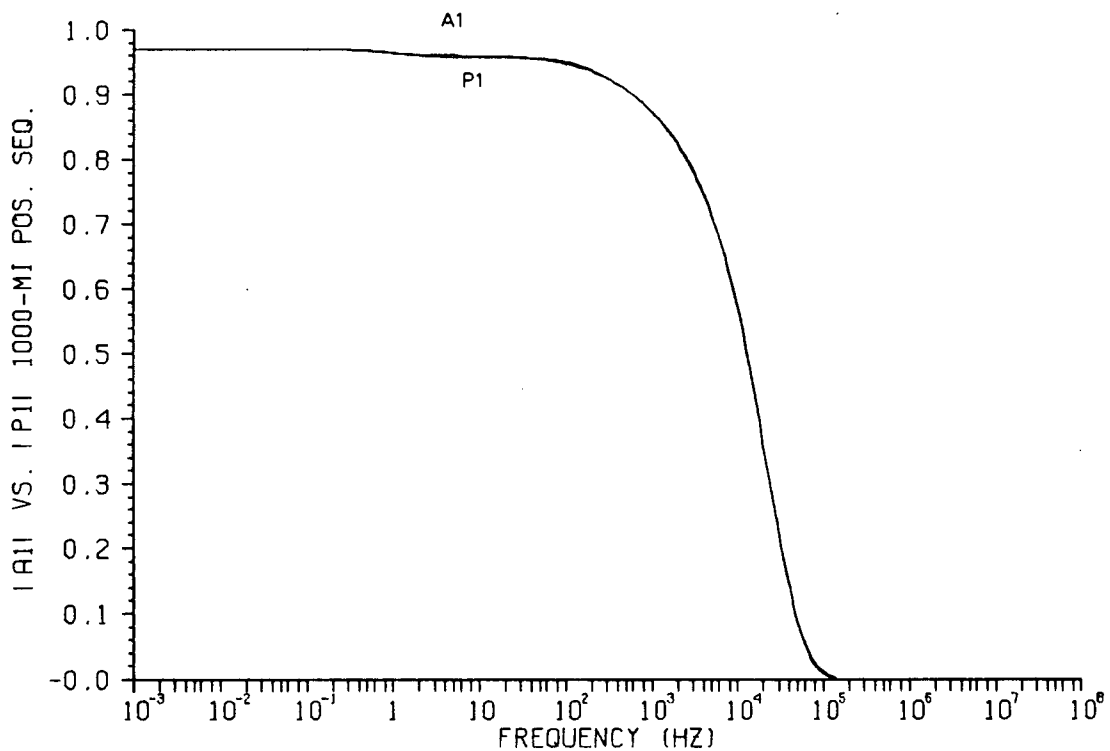
P.4.7: Simulation of $A_1(\omega)$. Zero sequence, 500-mi.



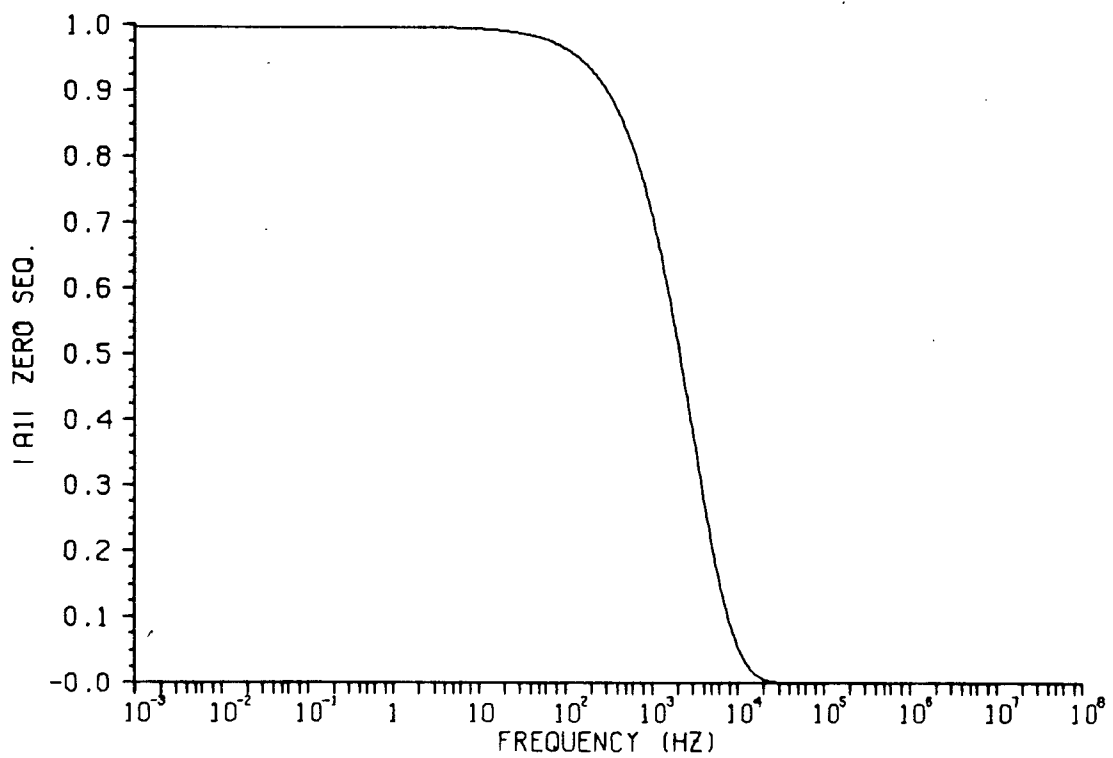
P.4.8: Simulation of $A_1(\omega)$. Positive sequence, 500-mi.



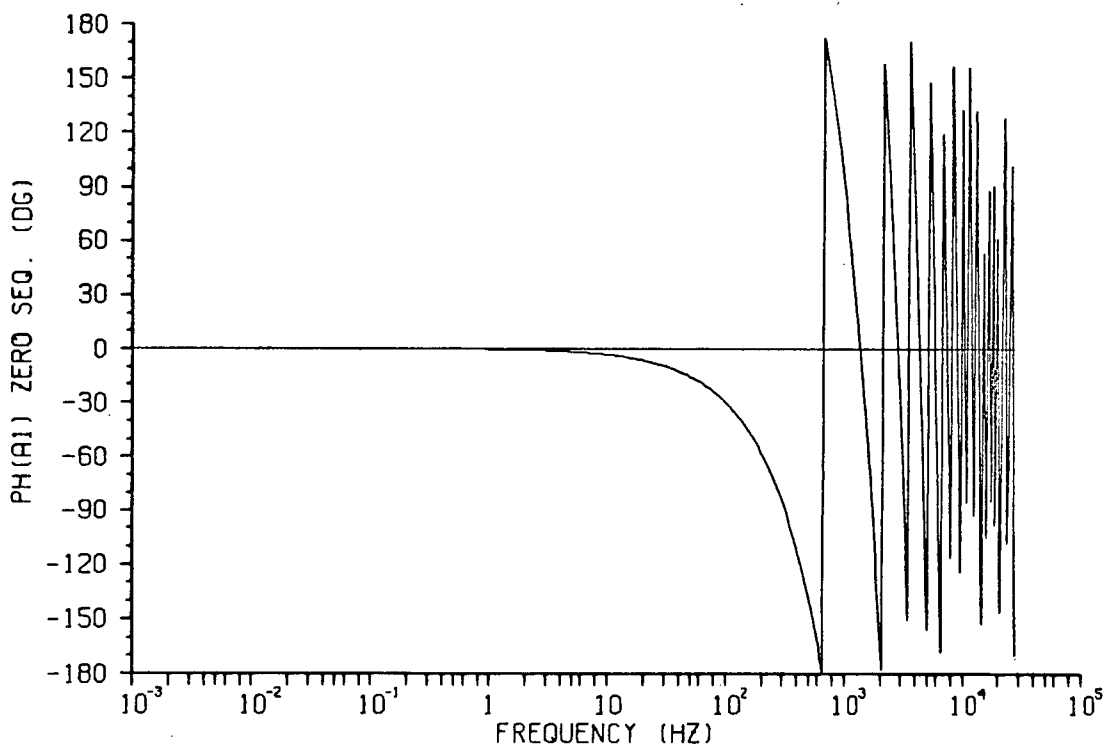
P.4.9: Simulation of $A_1(\omega)$. Zero sequence, 1000-mi.



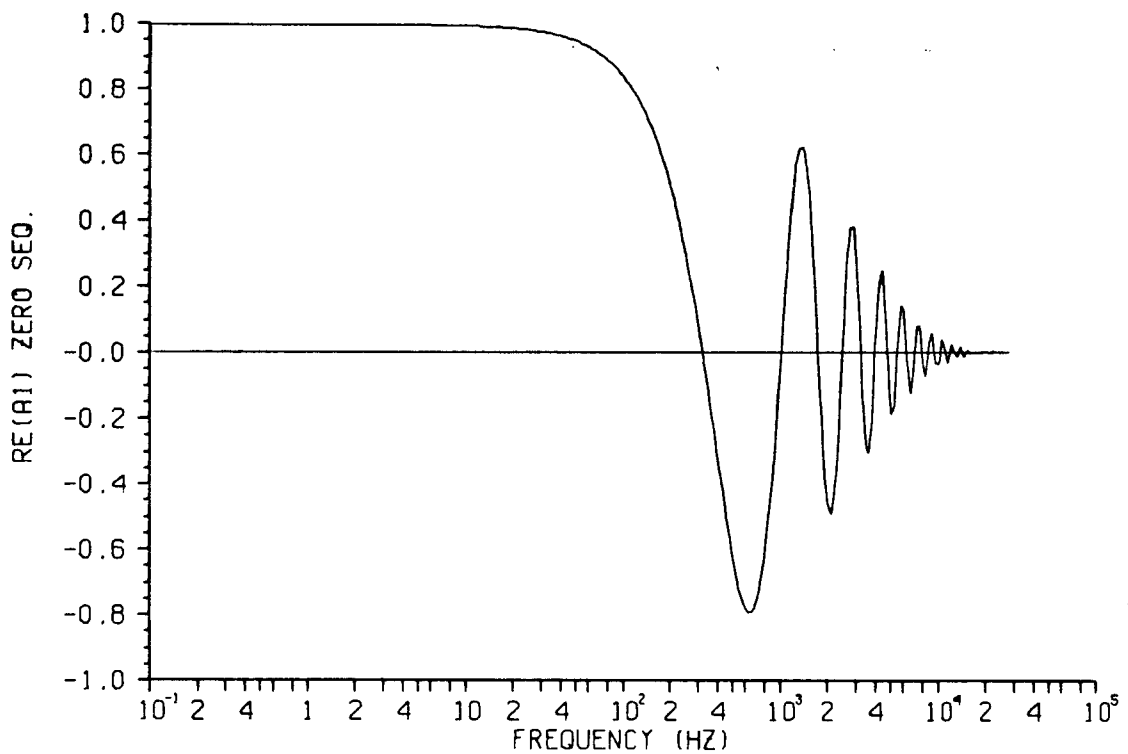
P.4.10: Simulation of $A_1(\omega)$. Positive sequence, 1000-mi.



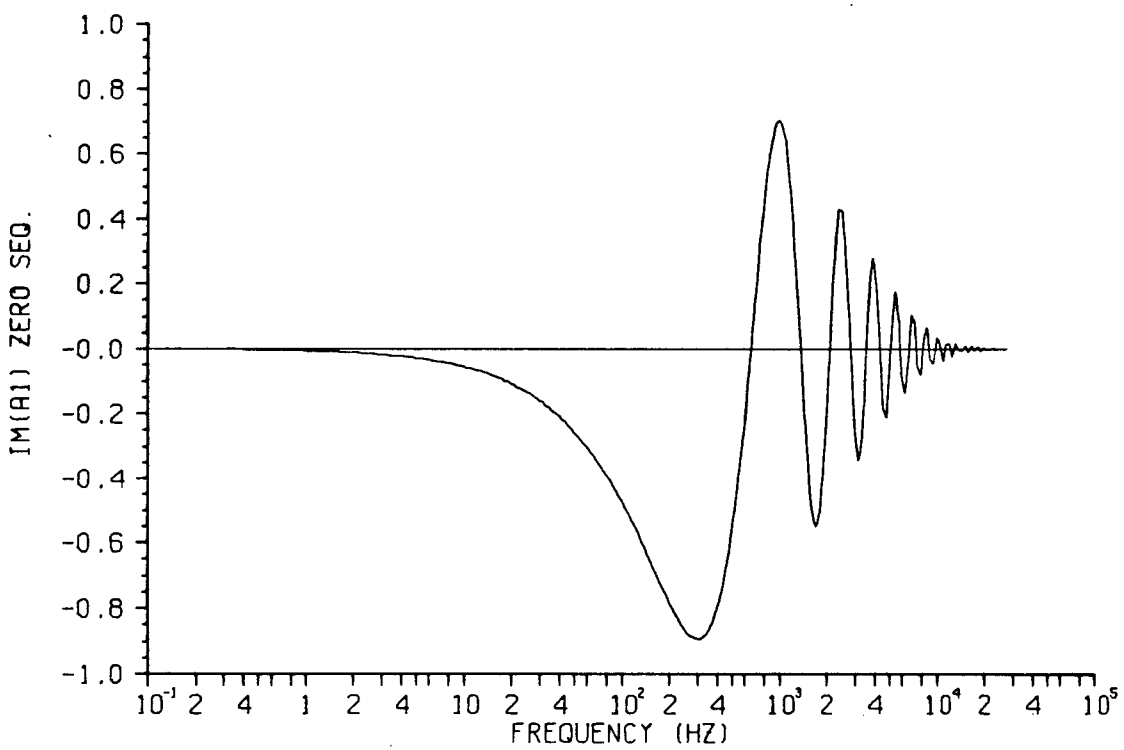
P.4.11: Magnitude of $A_1(\omega)$. Zero sequence, 100-mi.



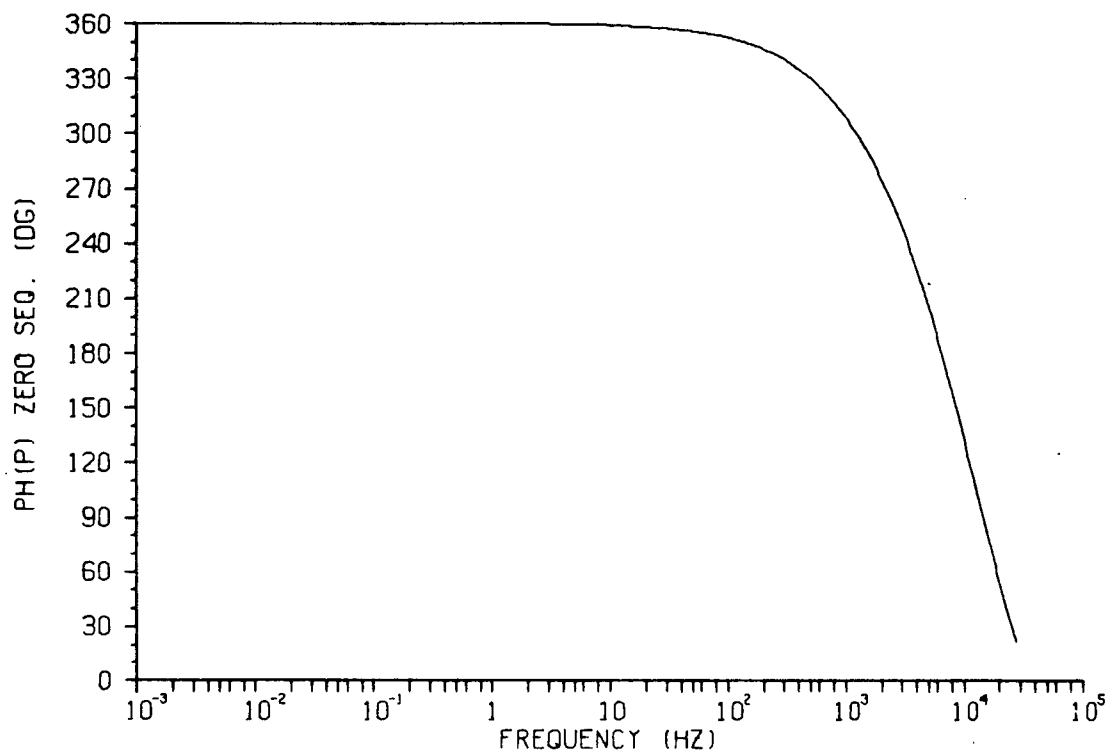
P.4.12: Phase angle of $A_1(\omega)$. Zero sequence, 100-mi.



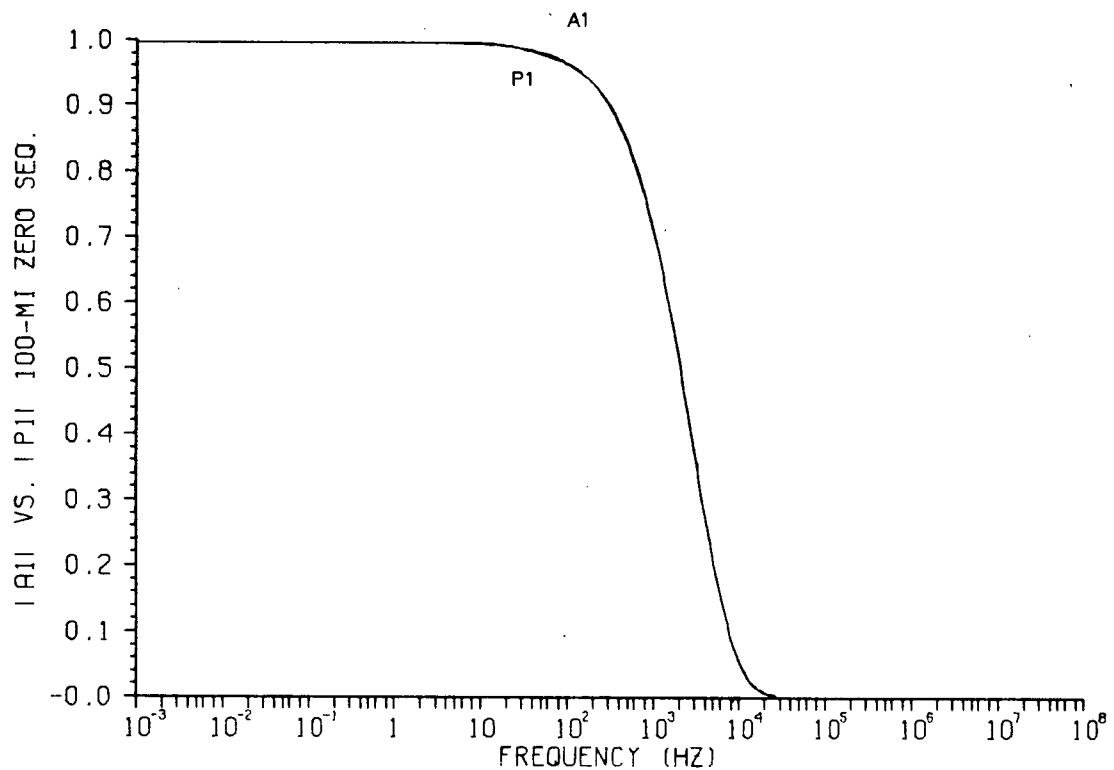
P.4.13: Real part of $A_1(\omega)$. Zero sequence, 100-mi.



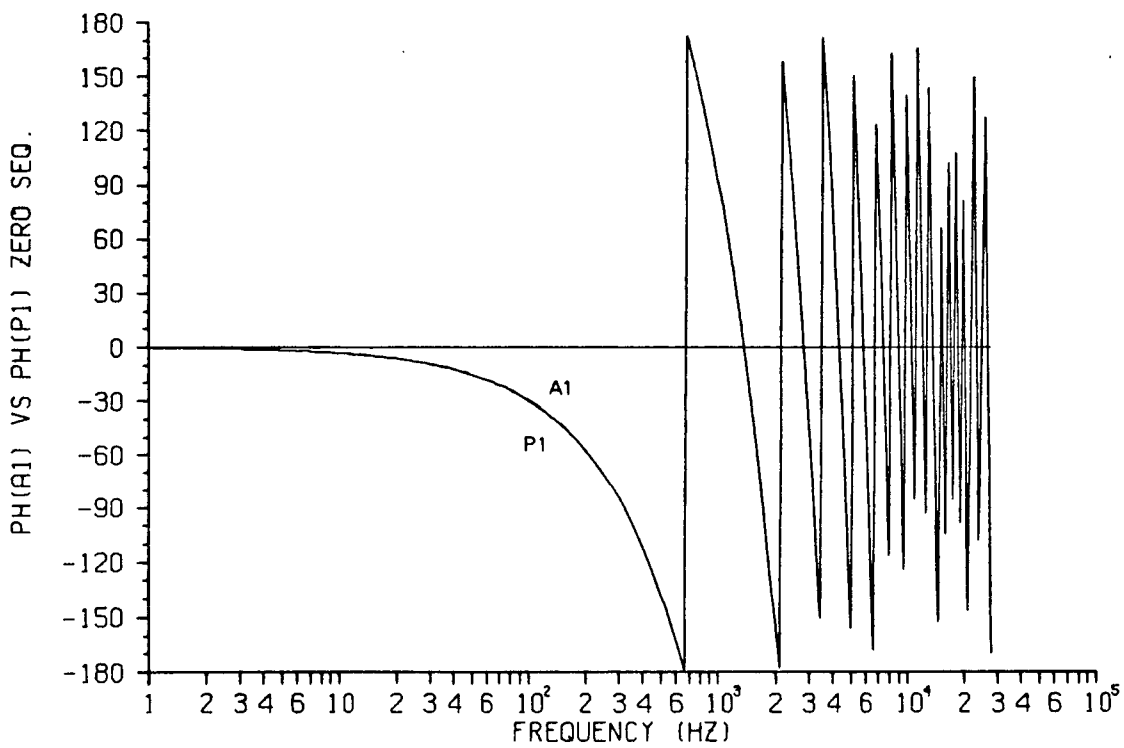
P.4.14: Imaginary part of $A_1(\omega)$. Zero sequence, 100-mi.



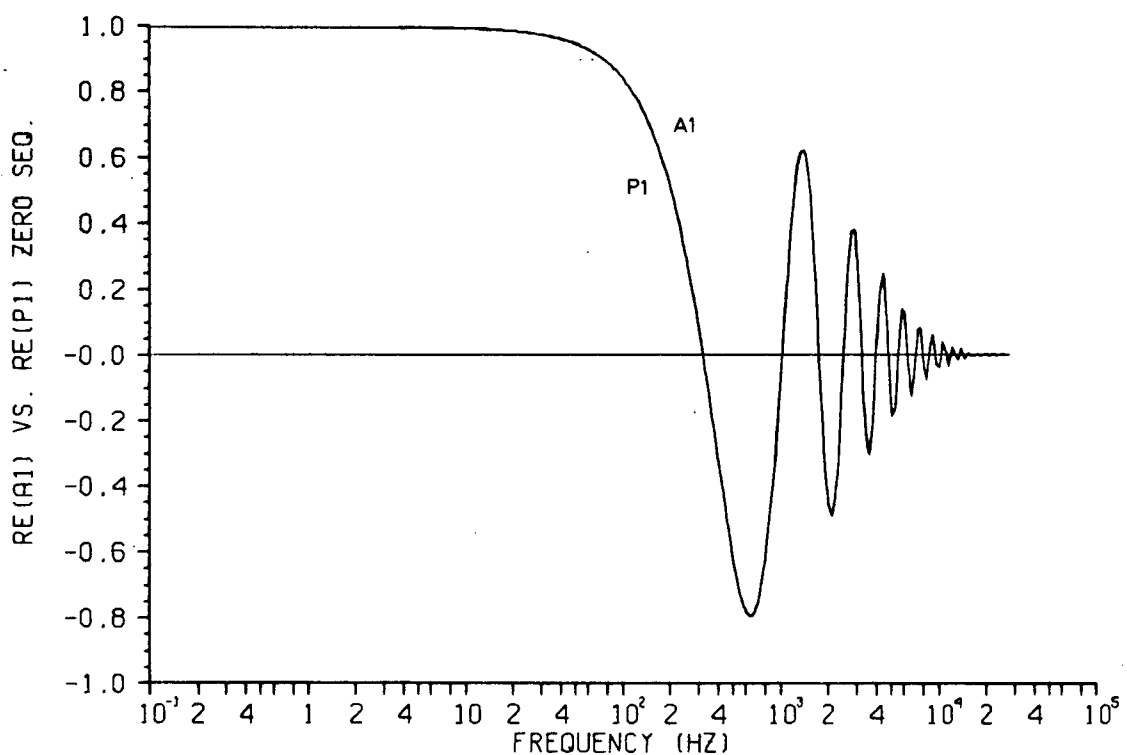
P.4.15: Phase angle of $P(\omega)$. Zero sequence, 100-mi.



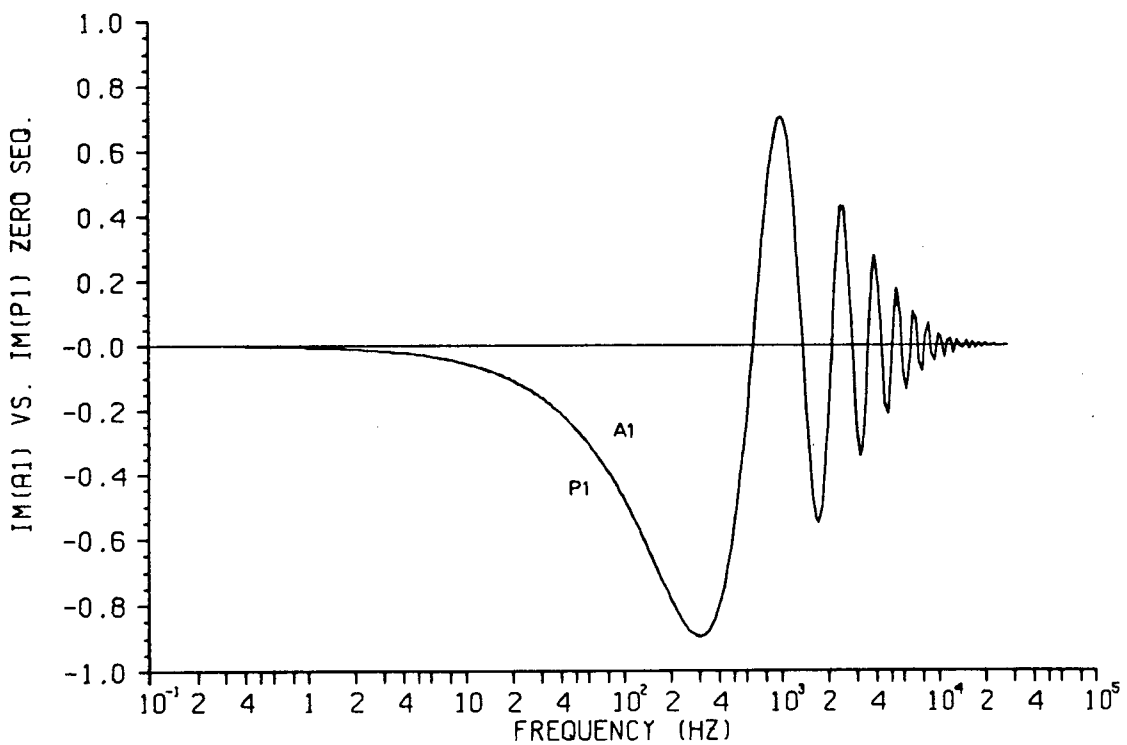
P.4.16: Simulation of $A_1(\omega)$, zero seq., 100-mi. Magnitude.



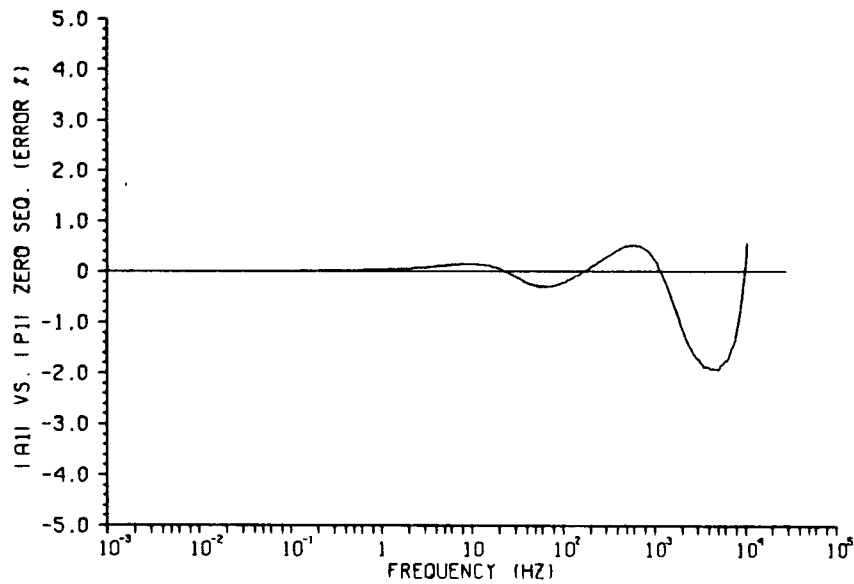
P.4.17: Simulation of $A_1(\omega)$, zero seq., 100-mi. Phase angle.



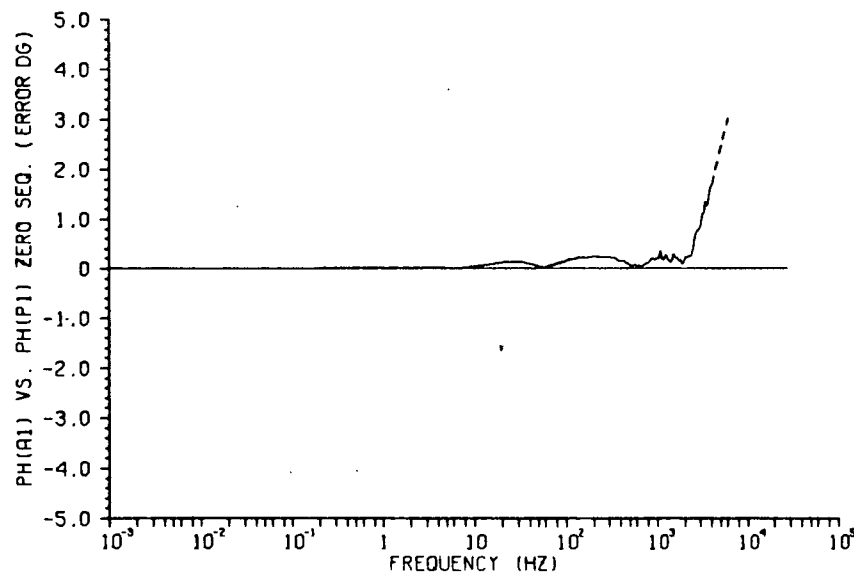
P.4.18: Simulation of $A_1(\omega)$, zero seq., 100-mi. Real part.



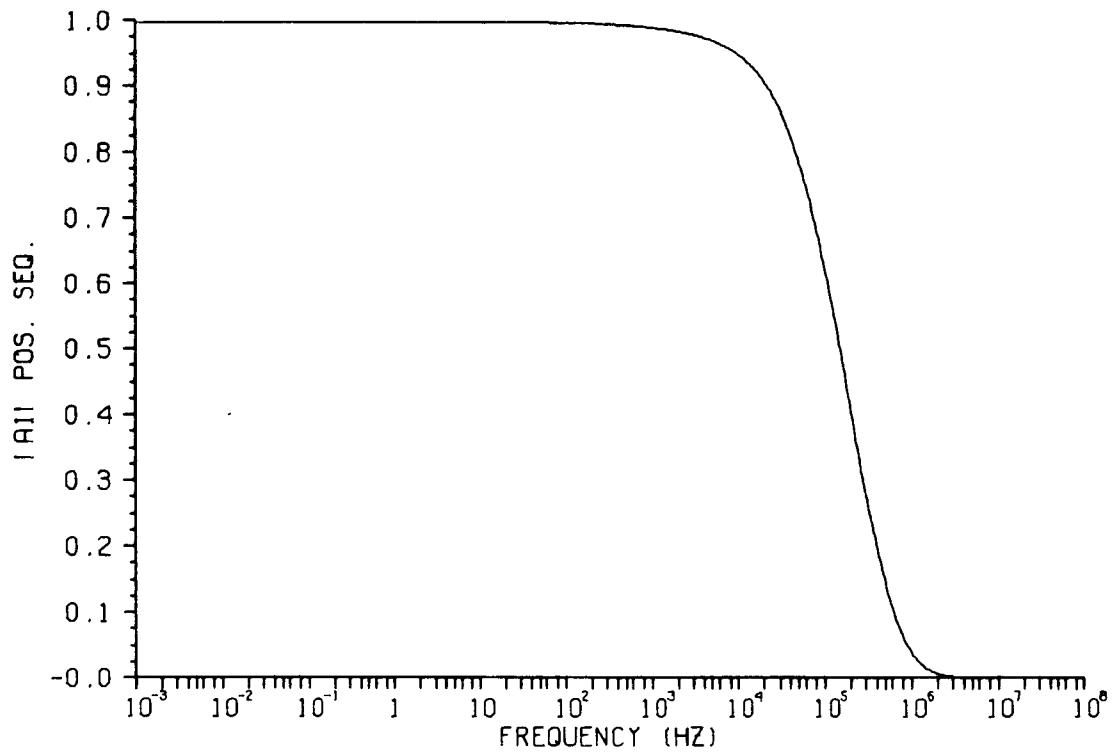
P.4.19: Simulation of $A_1(\omega)$, zero seq., 100-mi. Imaginary part.



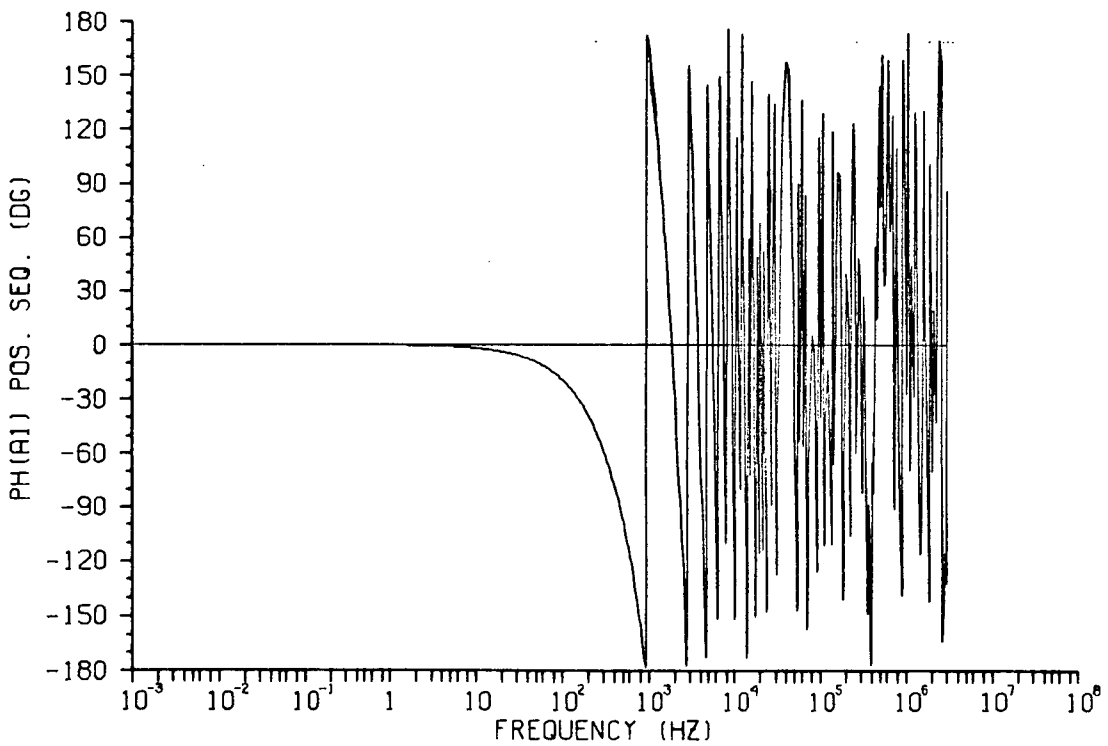
P.4.20: Simulation of $A_1(\omega)$, zero seq., 100-mi. Magnitude error.



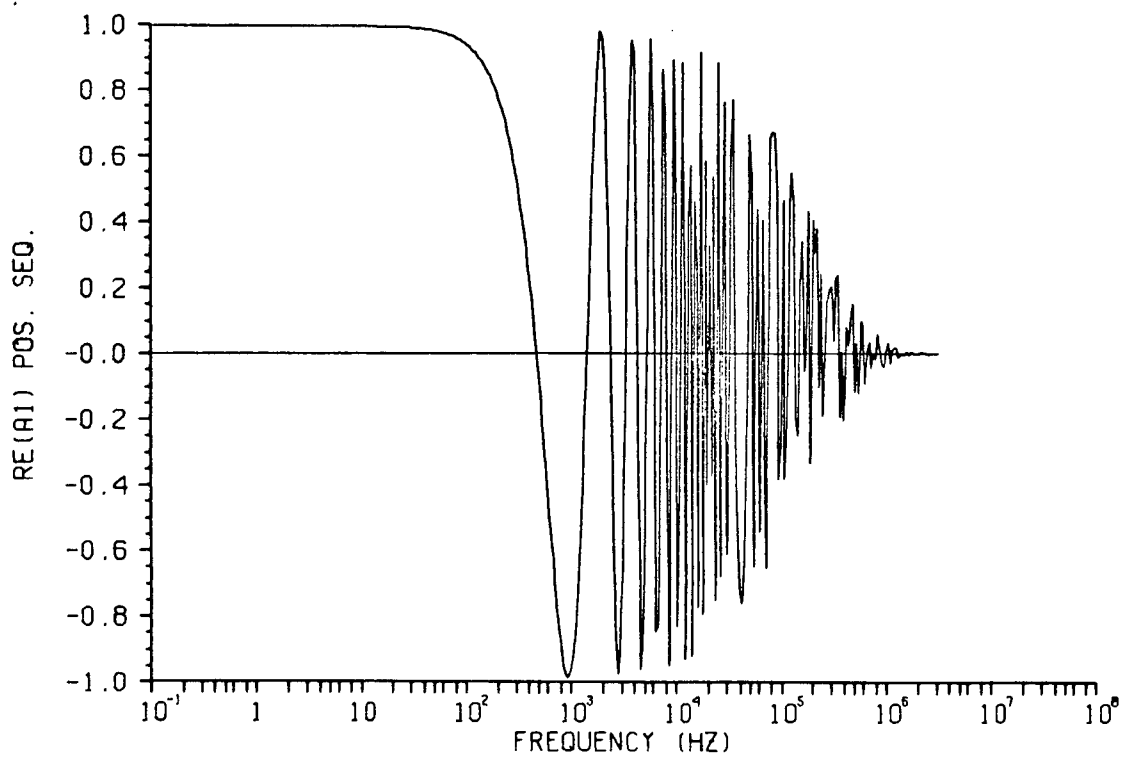
P.4.21: Simulation of $A_1(\omega)$, zero seq., 100-mi. Phase error.



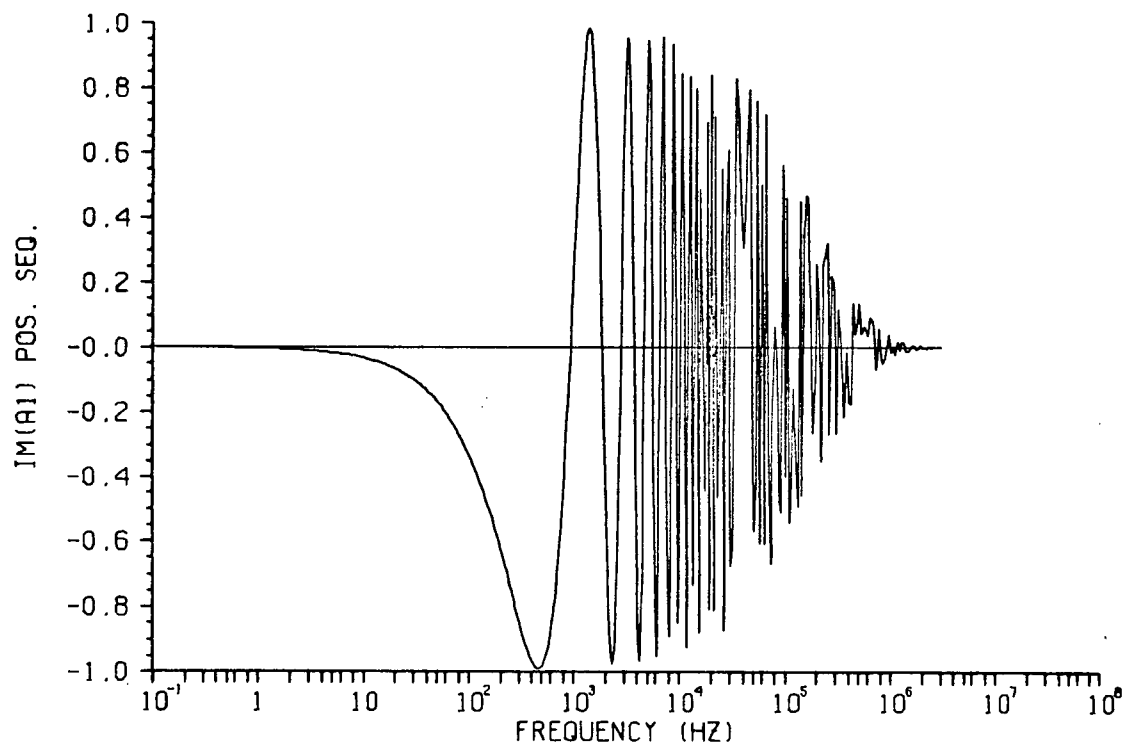
P.4.22: Magnitude of $A_1(\omega)$. Positive sequence, 100-mi.



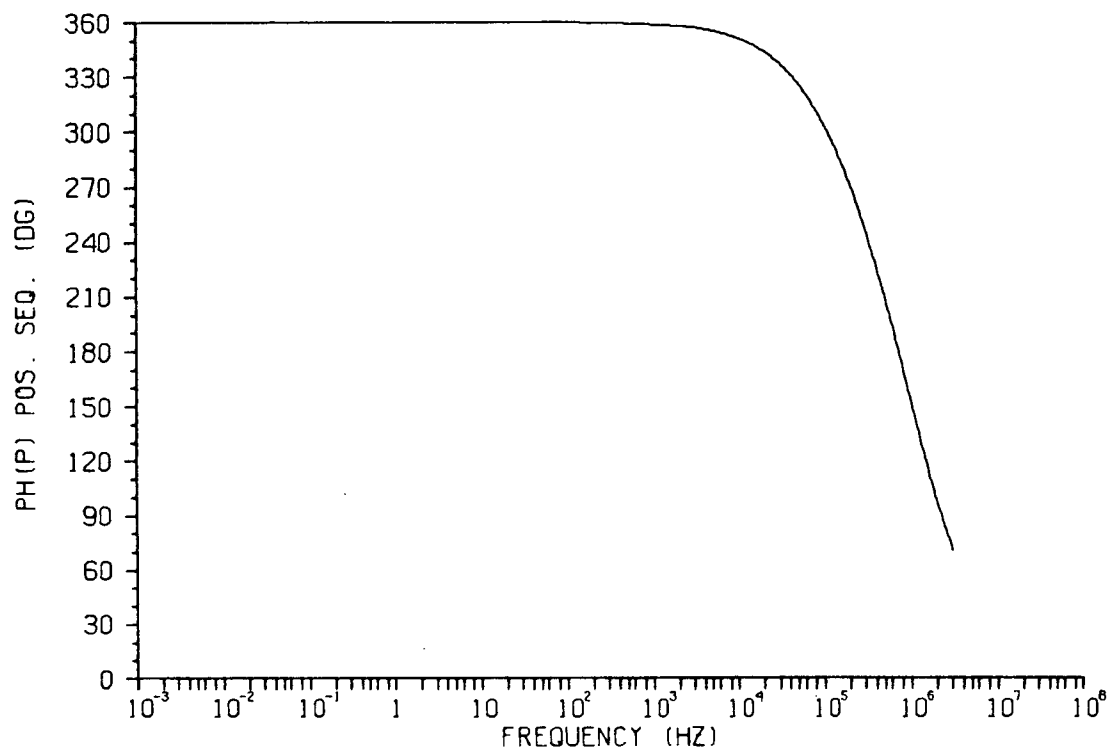
P.4.23: Phase angle of $A_1(\omega)$. Positive sequence, 100-mi.



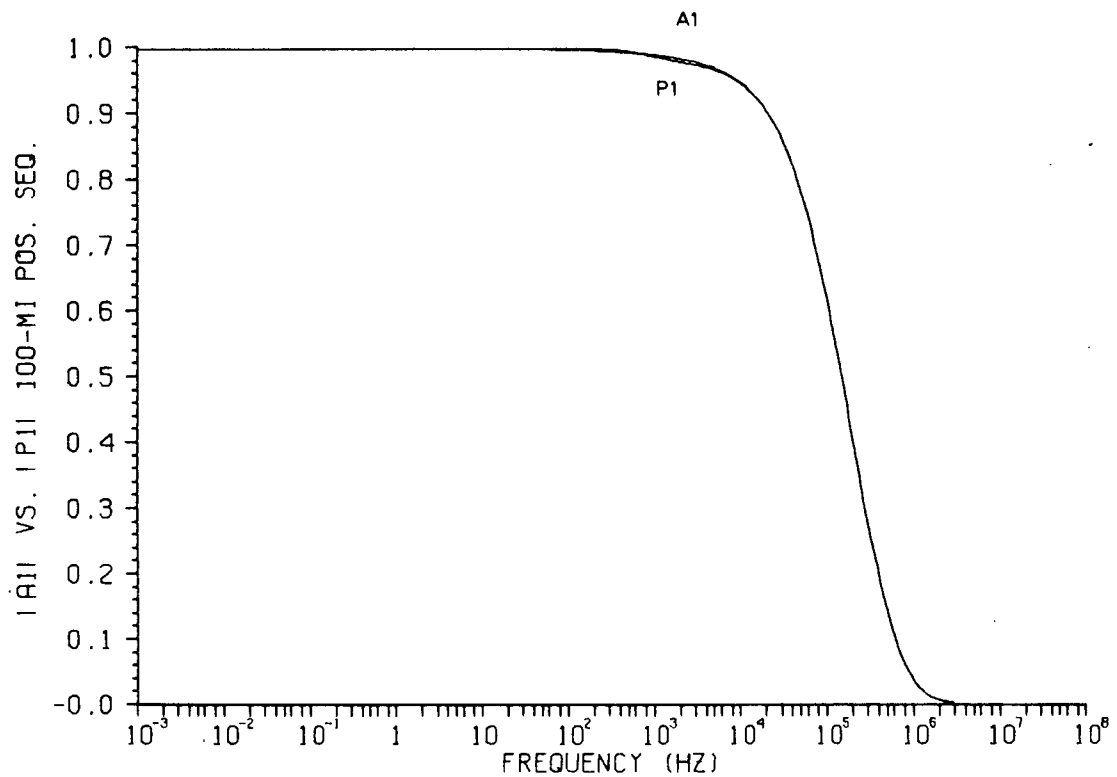
P.4.24: Real part of $A_1(\omega)$. Positive sequence, 100-mi.



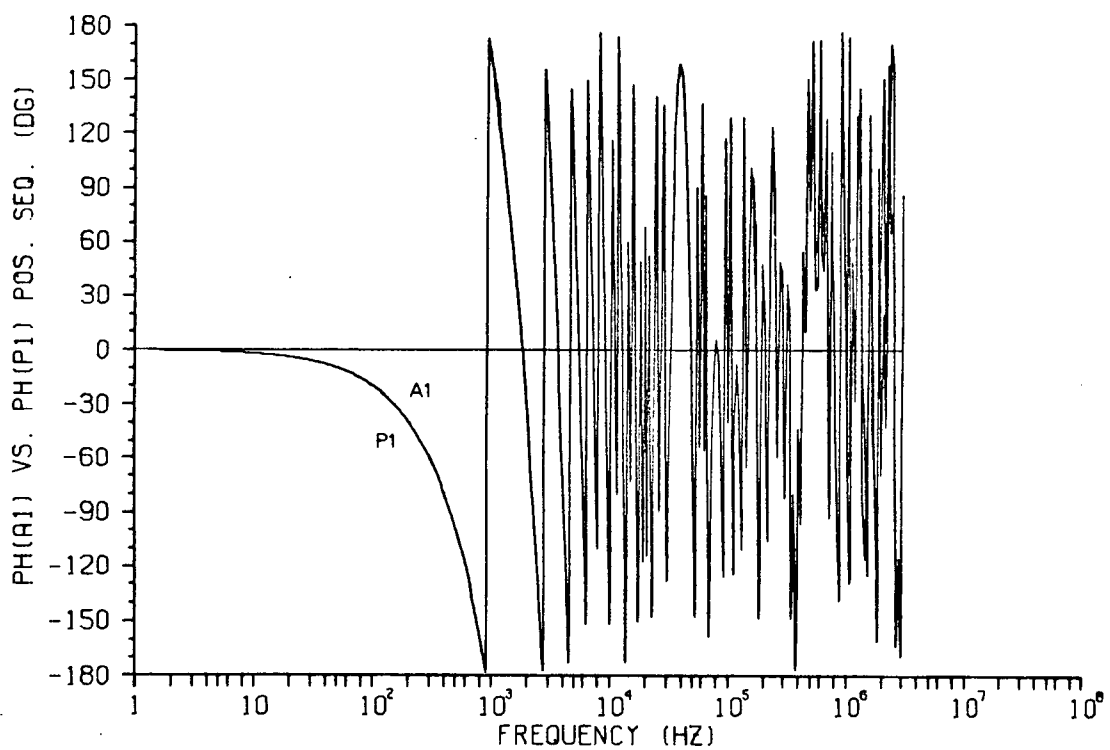
P.4.25: Imaginary part of $A_1(\omega)$. Positive sequence, 100-mi.



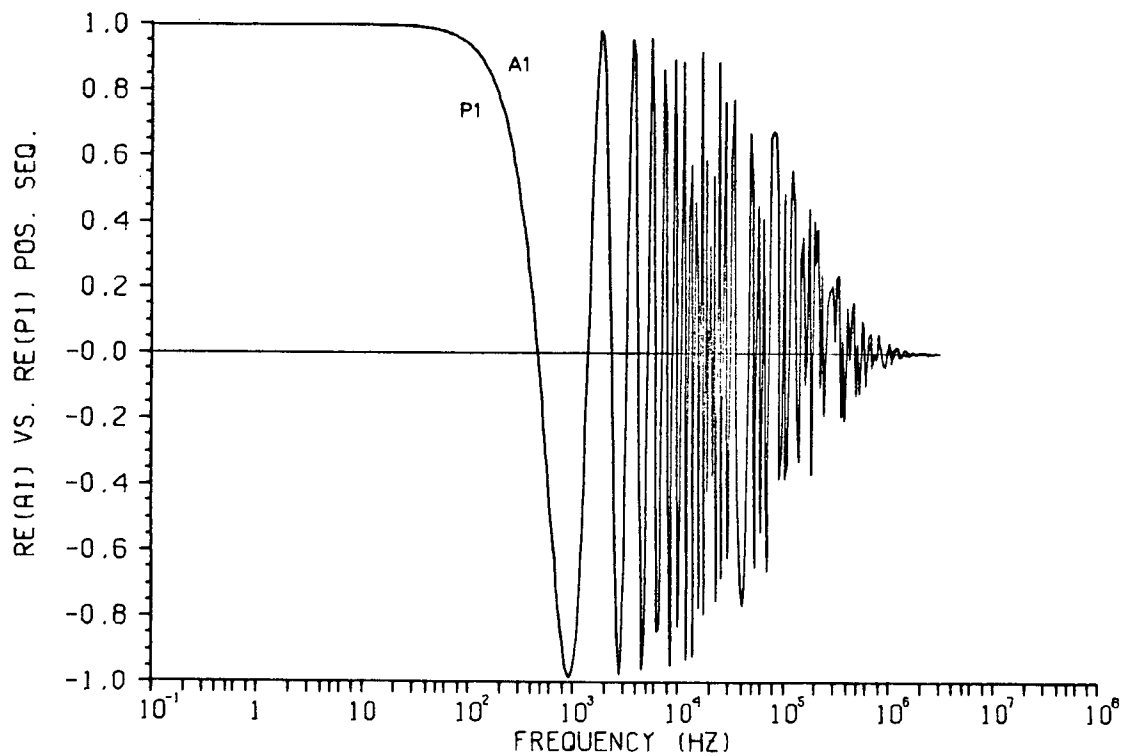
P.4.26: Phase angle of $P(\omega)$. Positive sequence, 100-mi.



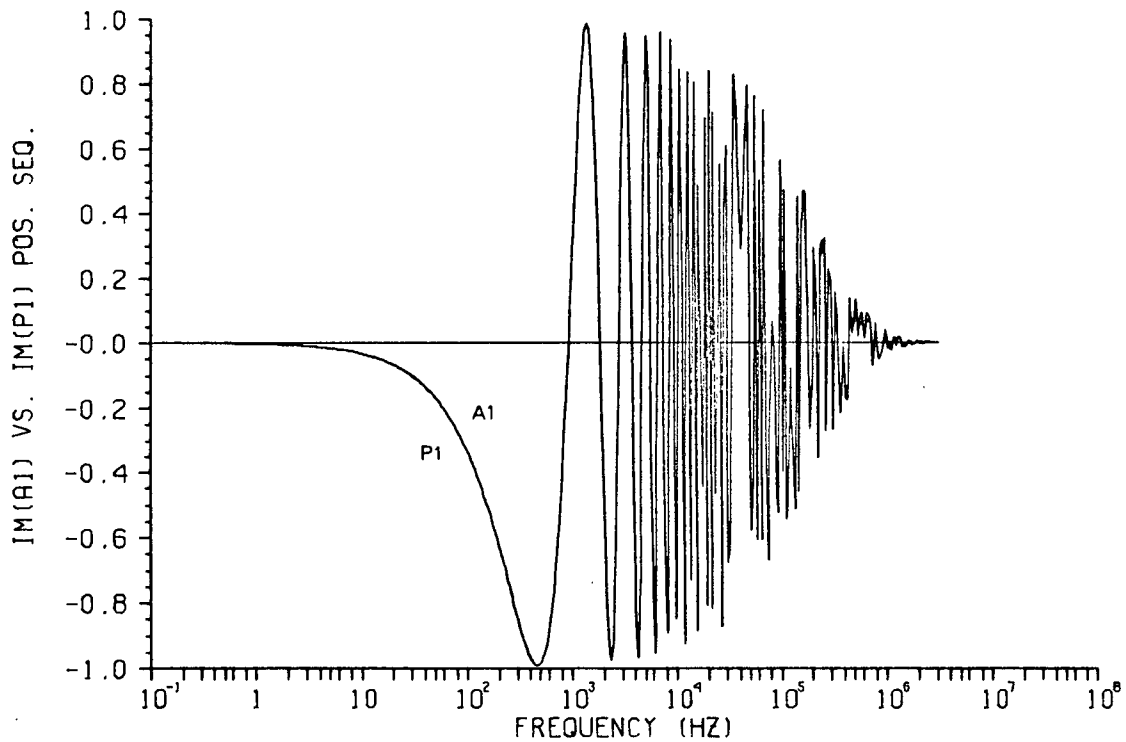
P.4.27: Simulation of $A_1(\omega)$, pos. seq., 100-mi. Magnitude.



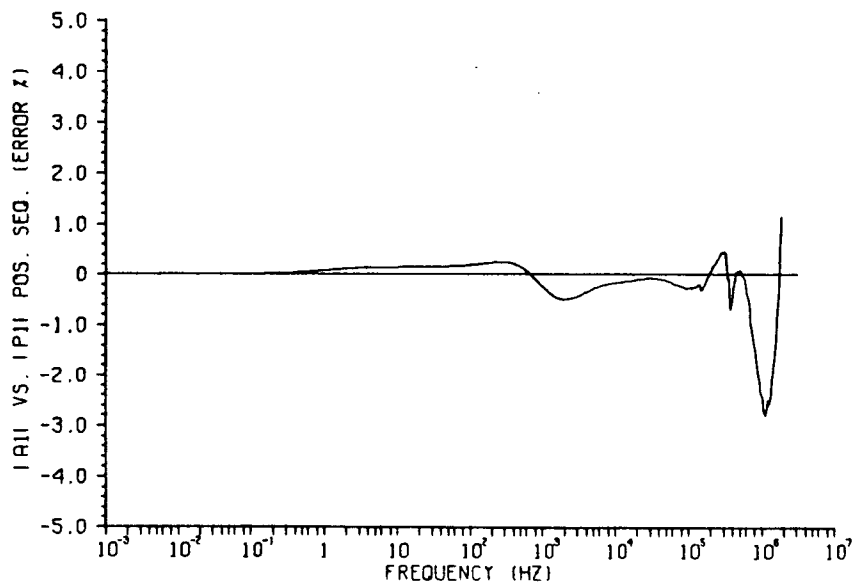
P.4.28: Simulation of $A_1(\omega)$, pos. seq., 100-mi. Phase angle.



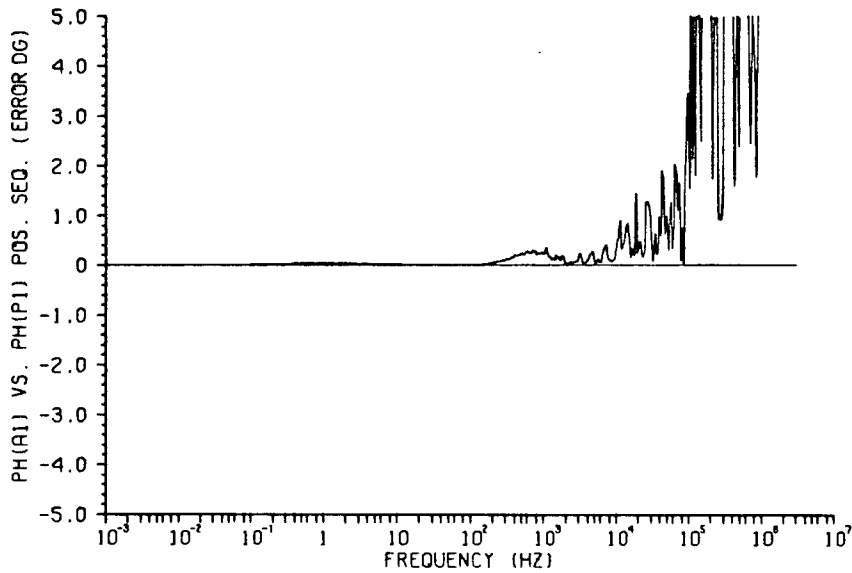
P.4.29: Simulation of $A_1(\omega)$, pos. seq., 100-mi. Real part.



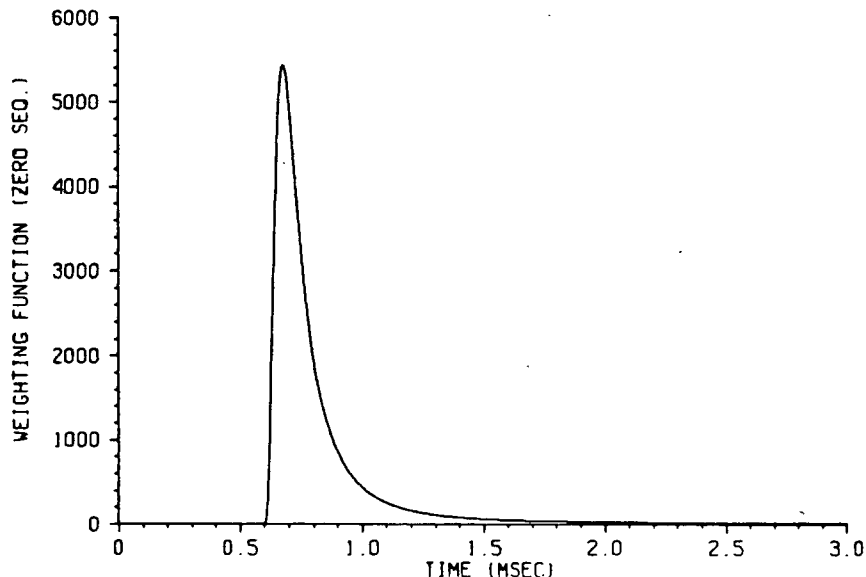
P.4.30: Simulation of $A_1(\omega)$, pos. seq., 100-mi. Imaginary part.



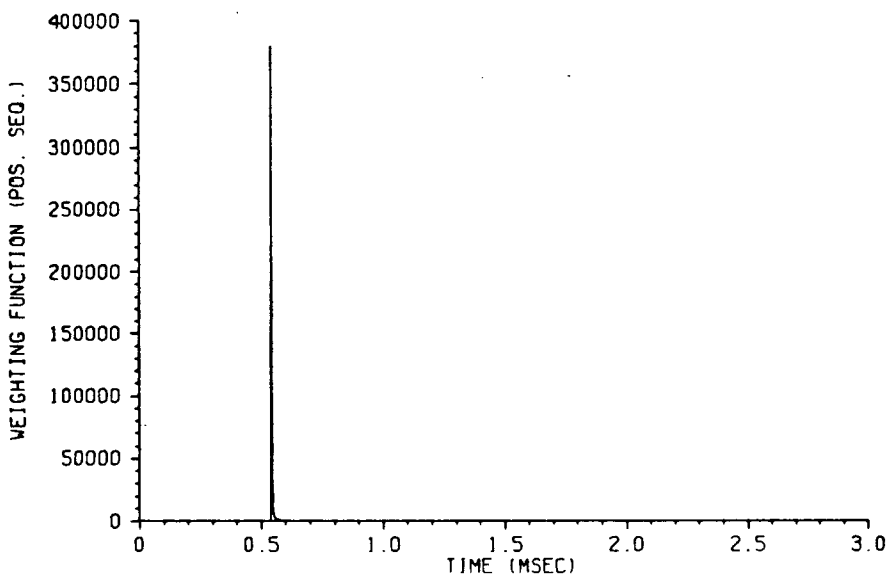
P.4.31: Simulation of $A_1(\omega)$, pos. seq., 100-mi. Magnitude error.



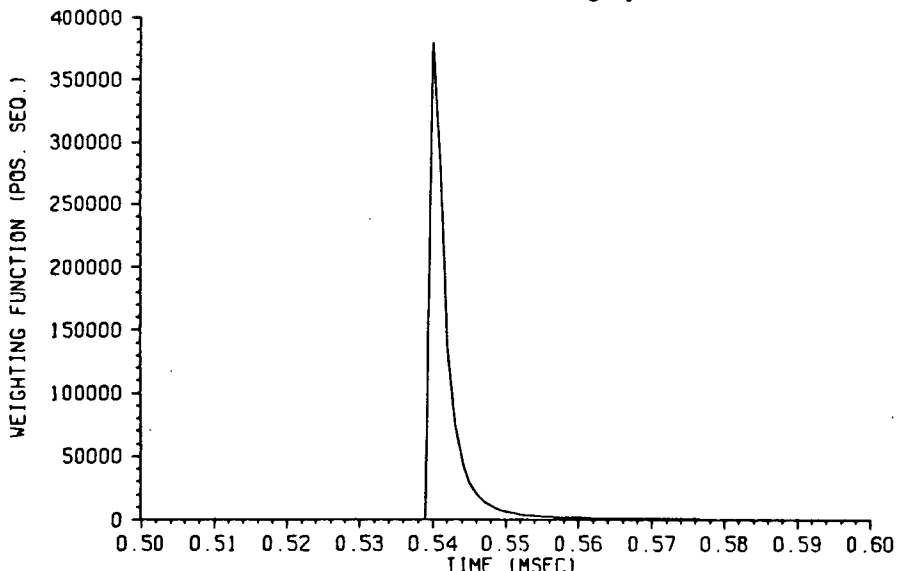
P.4.32: Simulation of $A_1(\omega)$, pos. seq., 100-mi. Phase error.



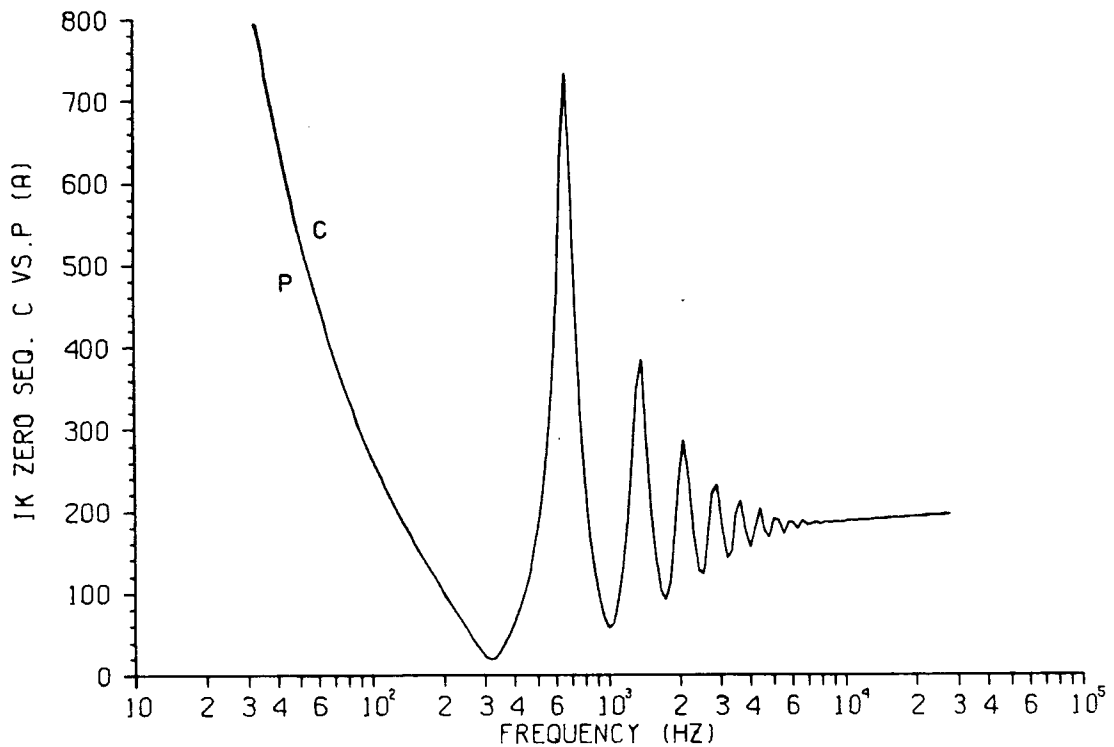
P.4.33: Weighting function $a_1(t)$. Zero seq., 100-mi.



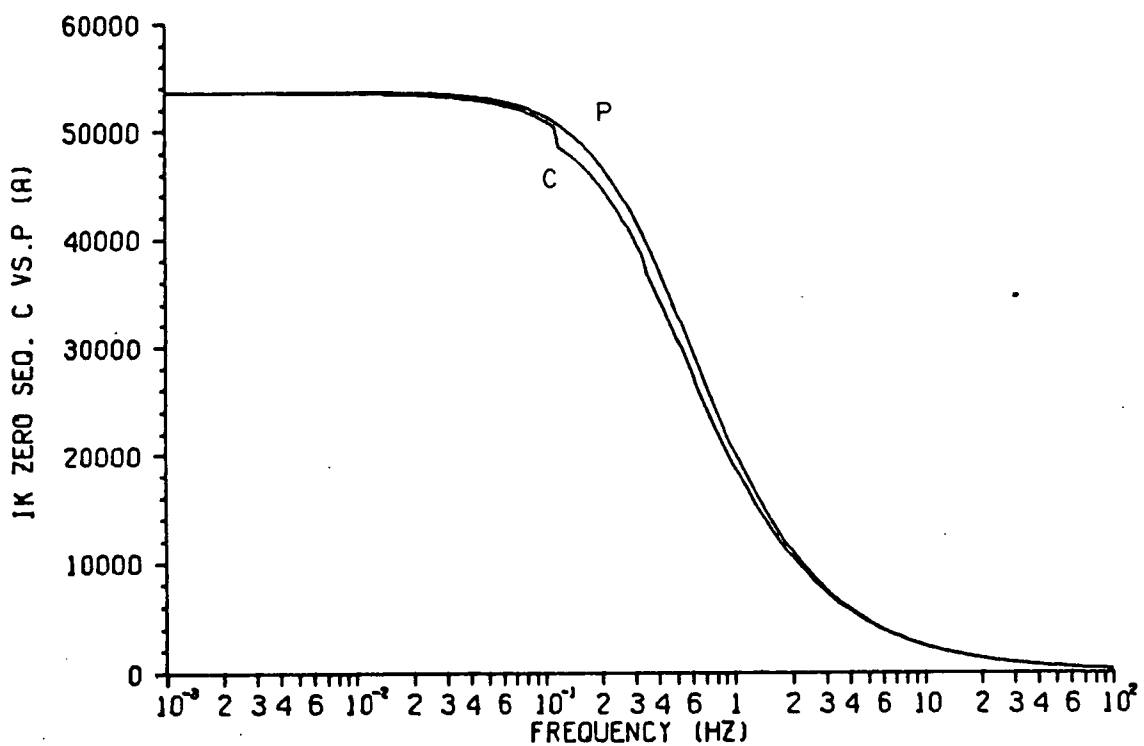
P.4.34(a): Weighting function $a_1(t)$. Pos. seq., 100-mi.
Same time scale as in graph P.4.33.



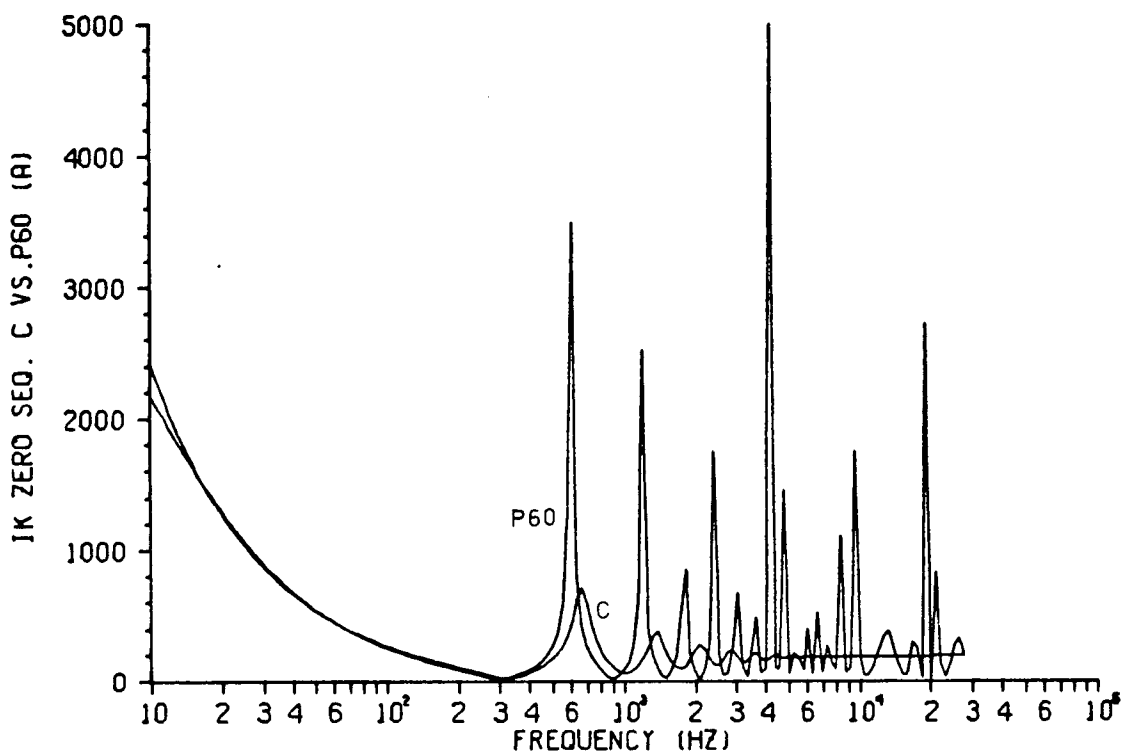
P.4.34(b): Weighting function $a_1(t)$. Pos. seq., 100-mi.
Expanded time scale.



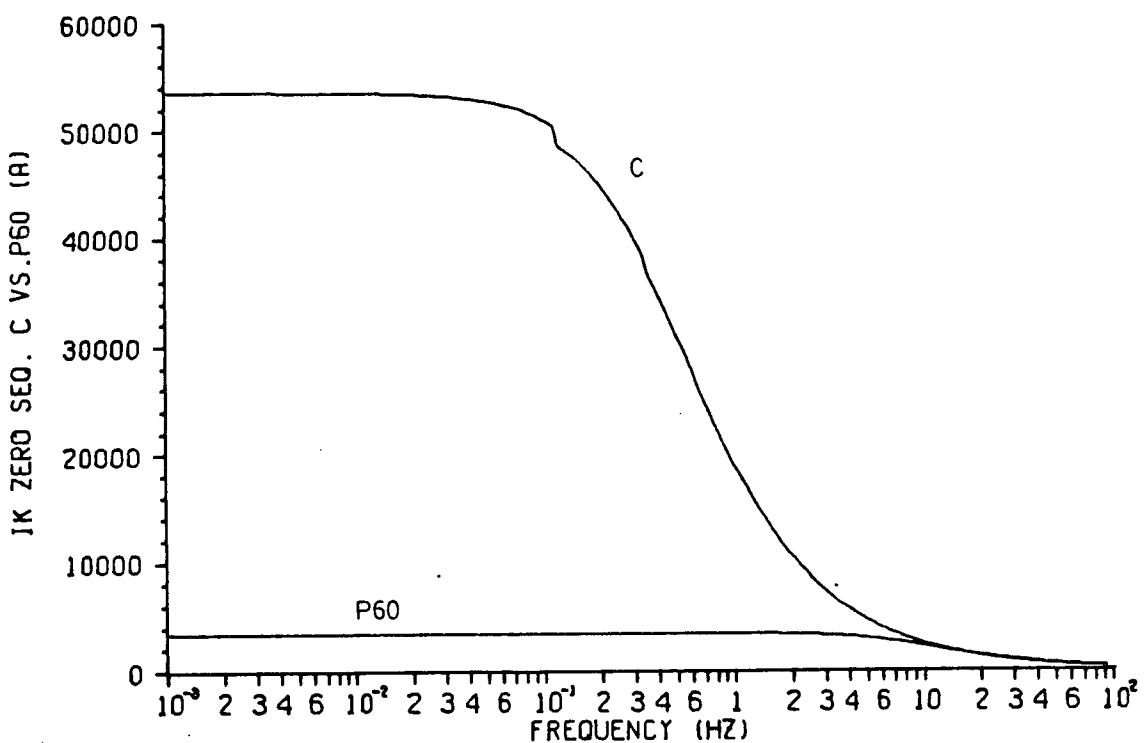
P.5.1(a): S/C Response, zero seq. Exact vs. approx.
Mid to high frequencies.



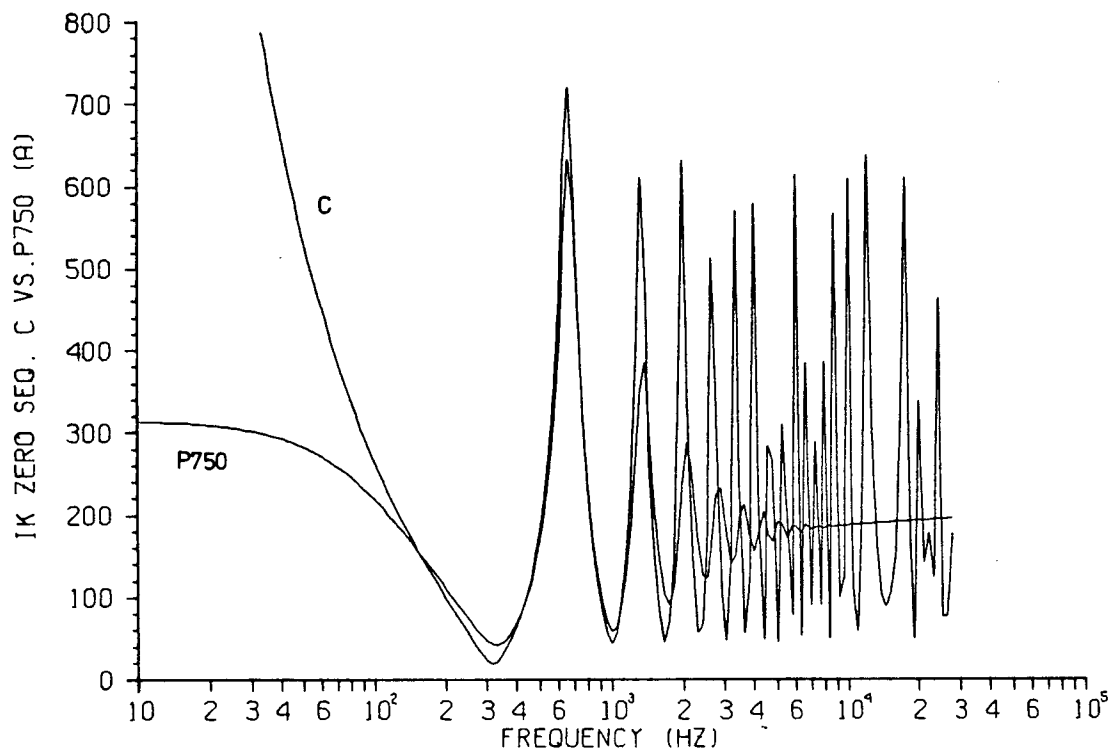
P.5.1(b): S/C Response, zero seq. Exact vs. approx.
Low frequencies.



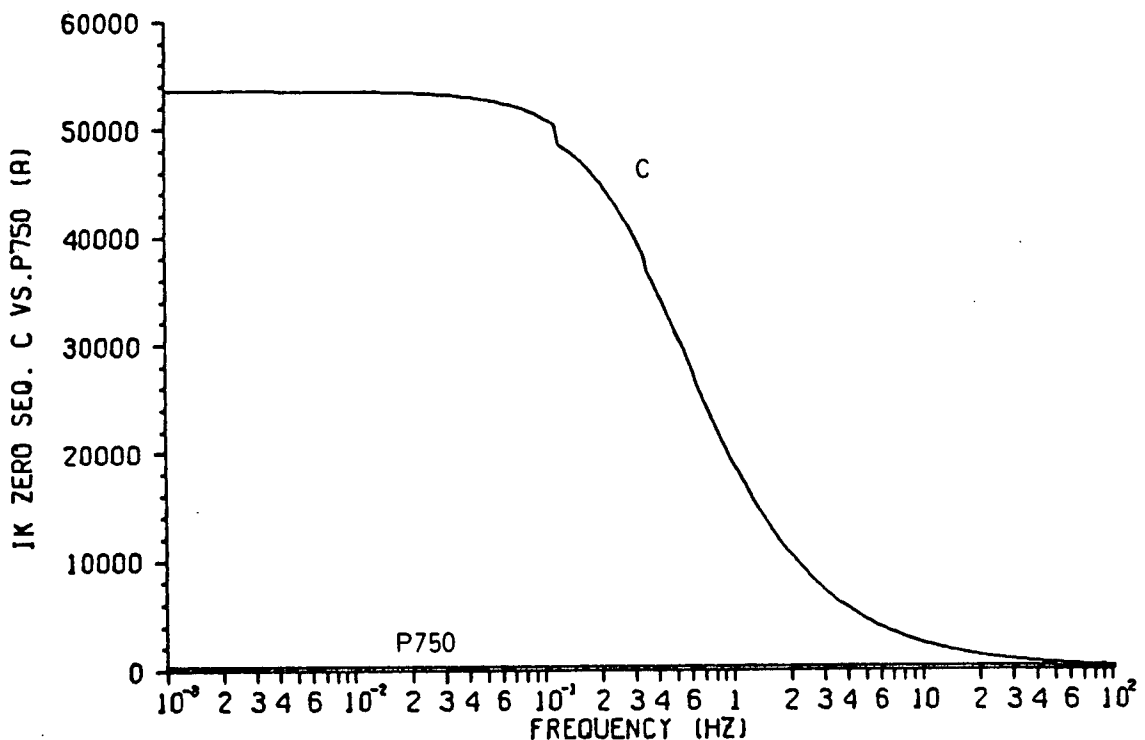
P.5.2(a): S/C Response, zero seq. Exact vs. 60-Hz.
Mid to high frequencies.



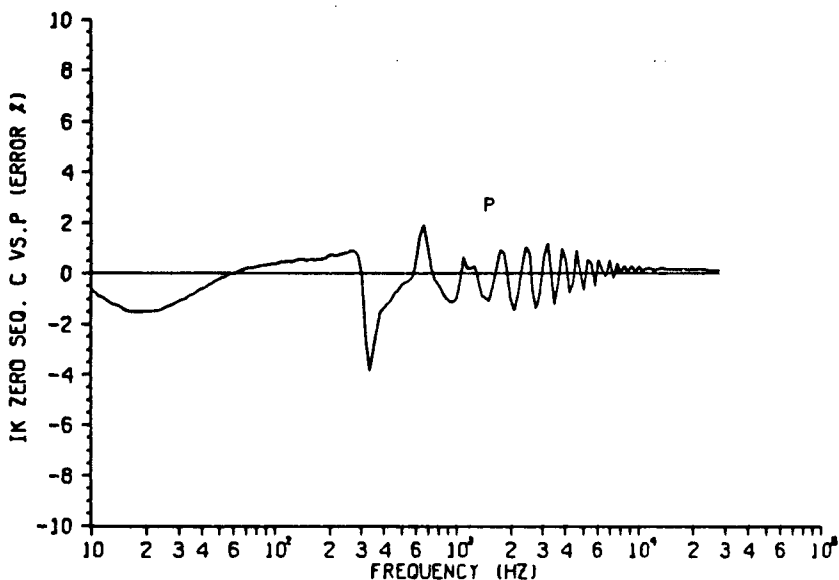
P.5.2(b): S/C Response, zero seq. Exact vs. 60-Hz.
Low frequencies.



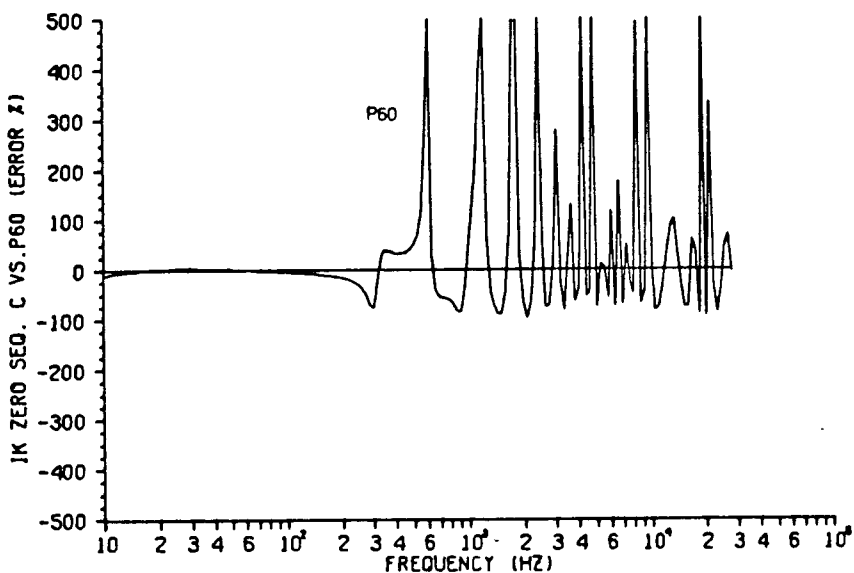
P.5.3(a): S/C Response, zero seq. Exact vs. 750-Hz.
Mid to high frequencies.



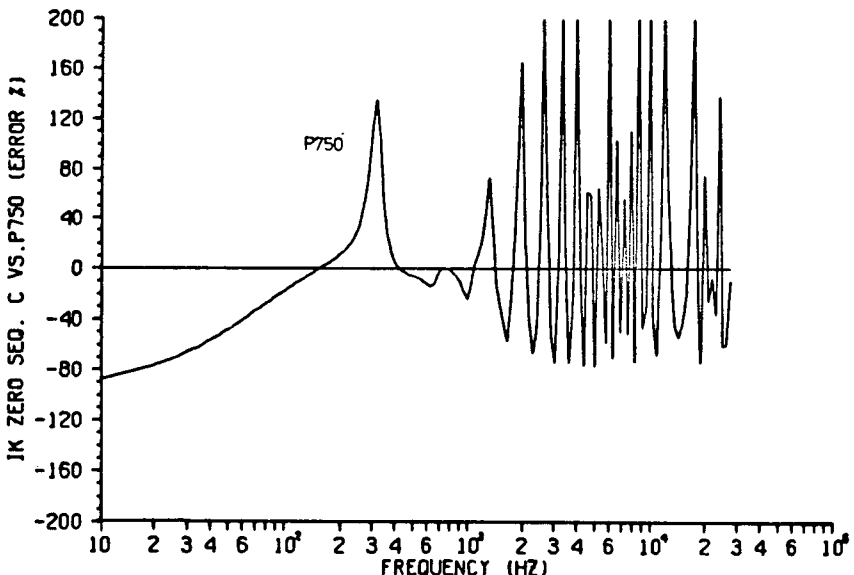
P.5.3(b): S/C Response, zero seq. Exact vs. 750-Hz.
Low frequencies.



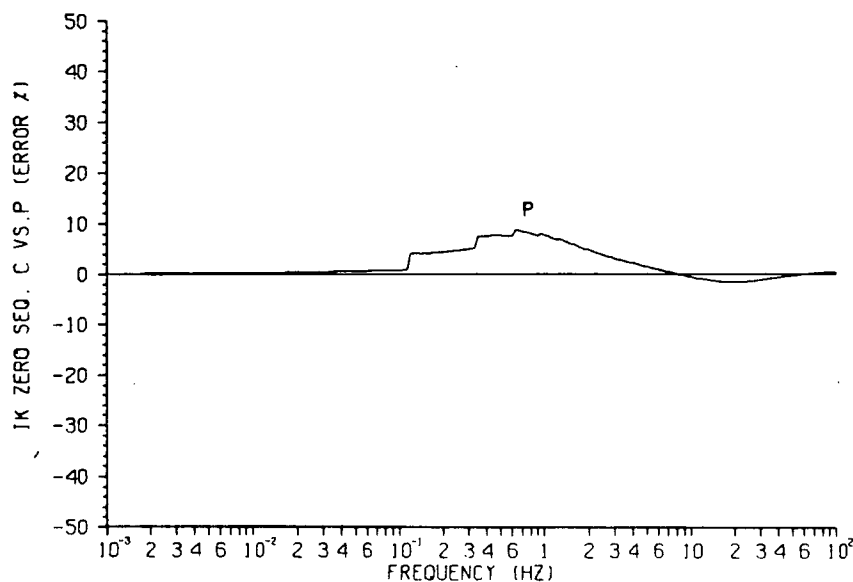
P.5.4(a): S/C Response, zero seq. Magnitude error.
Approximation. Mid to high frequencies.



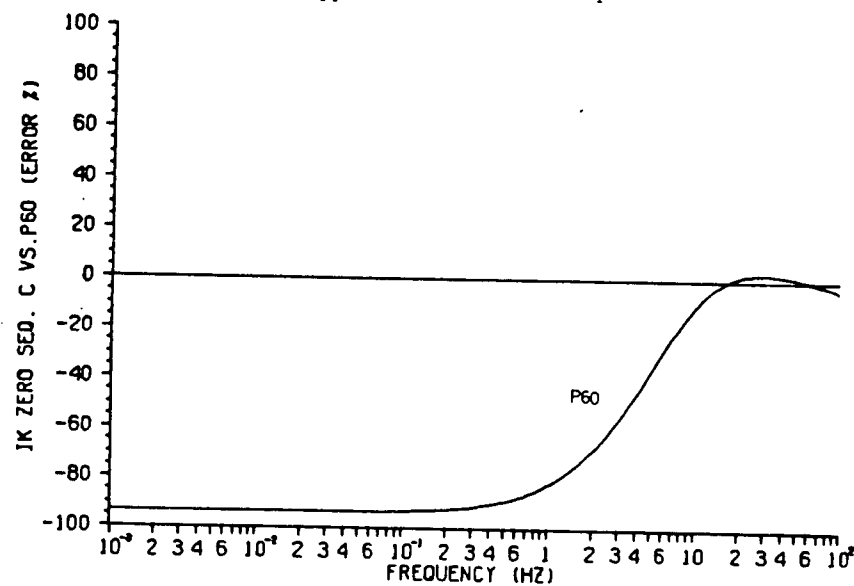
P.5.5(a): S/C Response, zero seq. Magnitude error. 60-Hz.
Mid to high frequencies.



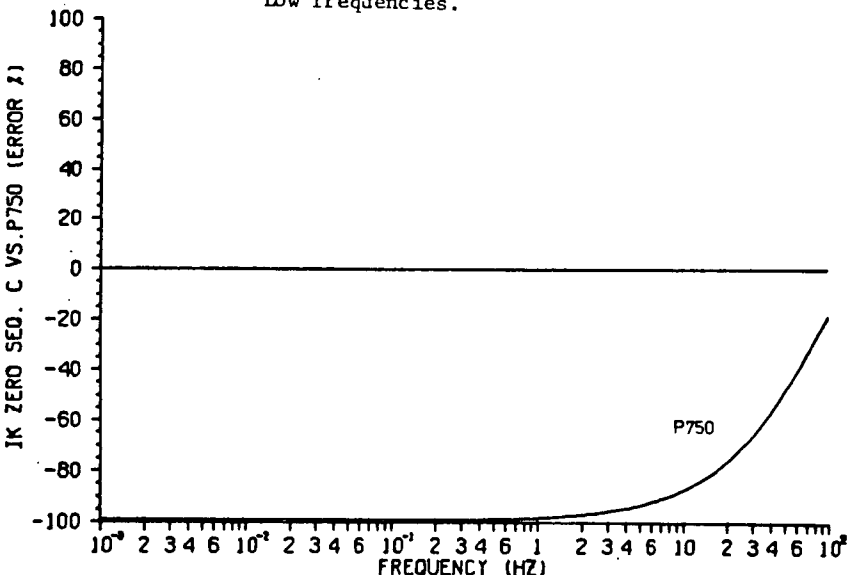
P.5.6(a): S/C Response, zero seq. Magnitude error. 750-Hz.
Mid to high frequencies.



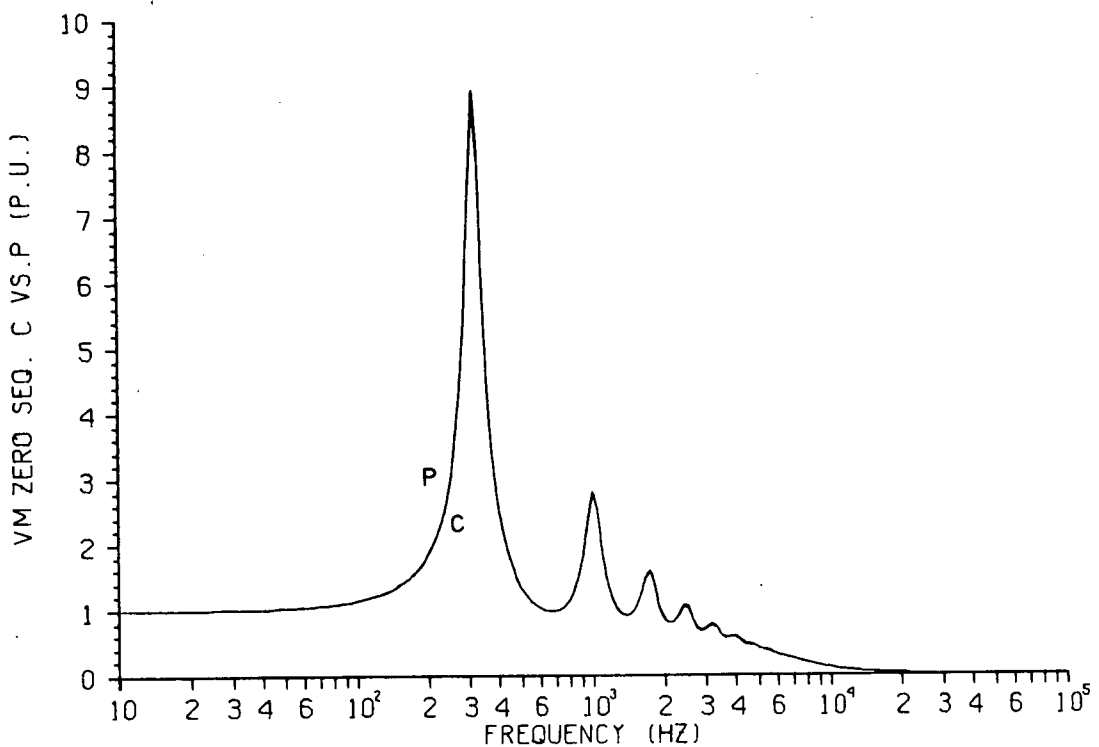
P.5.4(b): S/C Response, zero seq. Magnitude error.
Approximation. Low frequencies.



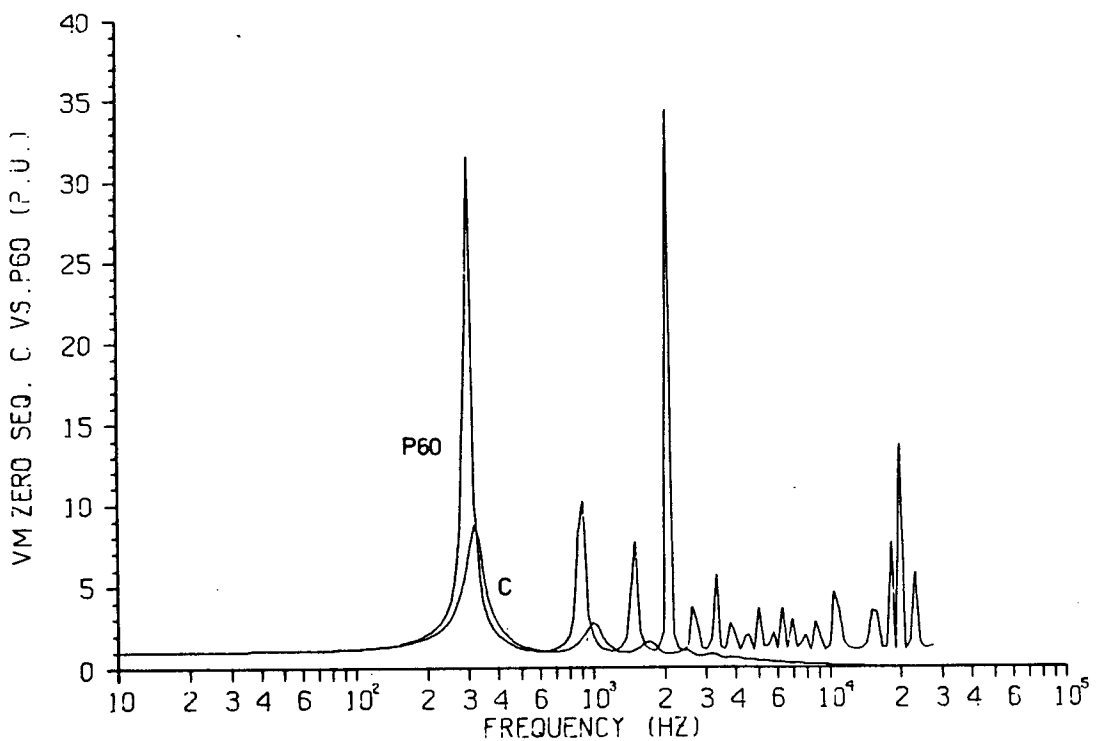
P.5.5(b): S/C Response, zero seq. Magnitude error. 60-Hz.
Low frequencies.



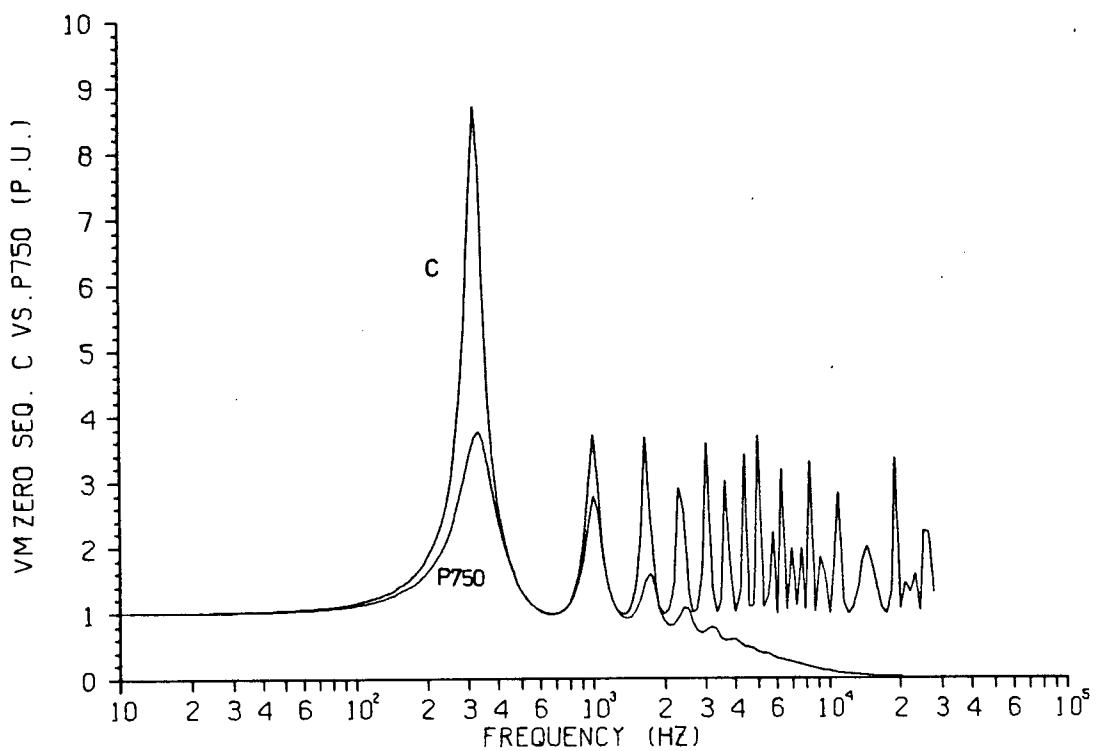
P.5.6(b): S/C Response, zero seq. Magnitude error. 750-Hz.
Low frequencies.



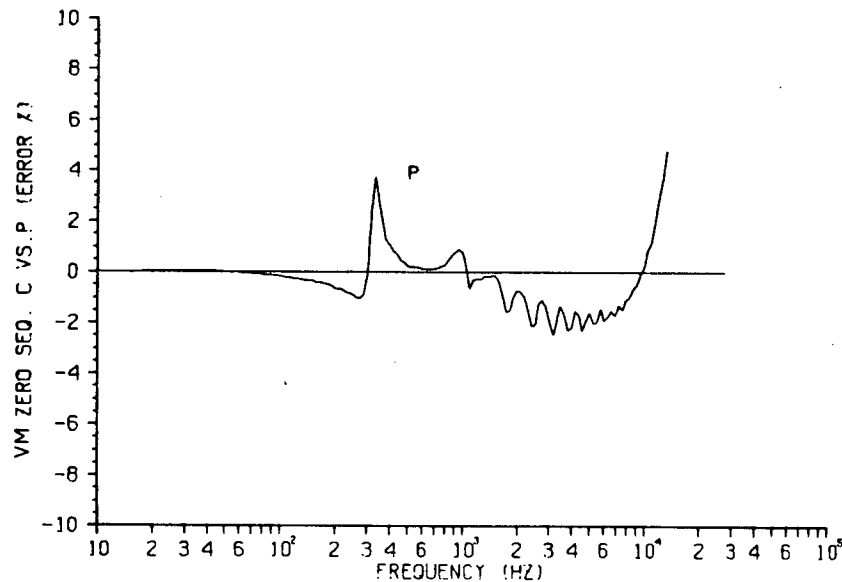
P.5.7: O/C Response, zero seq. Exact vs. approx.



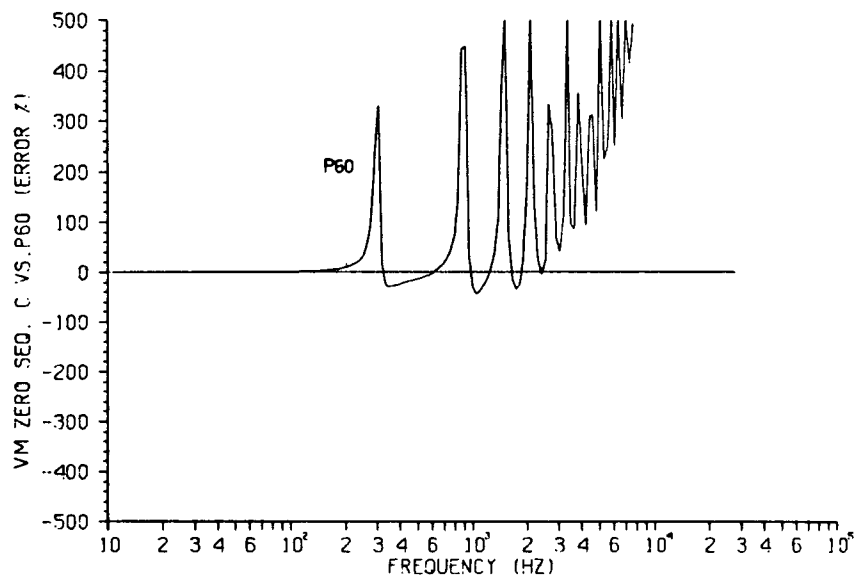
P.5.8: O/C Response, zero seq. Exact vs. 60-Hz.



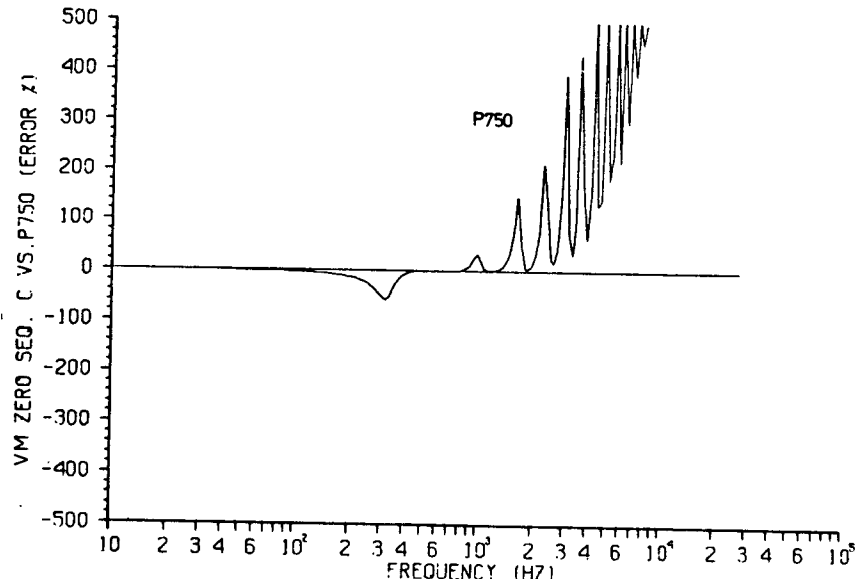
P.5.9: O/C Response, zero seq. Exact vs. 750-Hz.



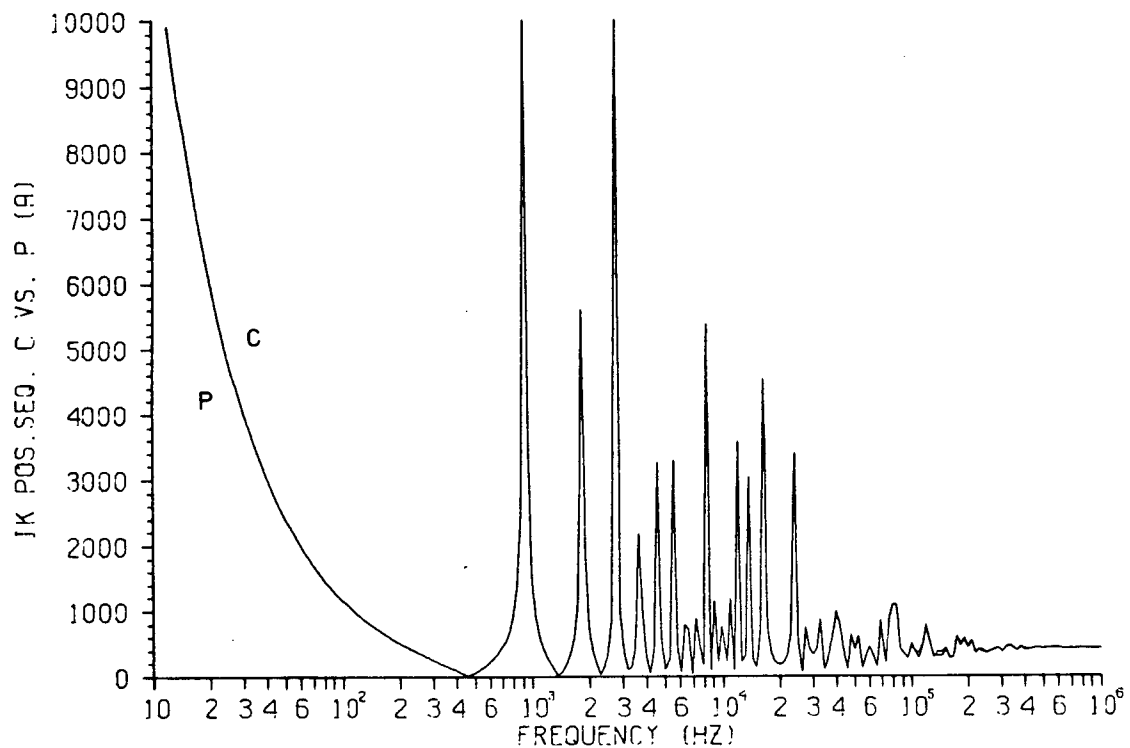
P.5.10: O/C Response, zero seq. Magnitude error. Approximation.



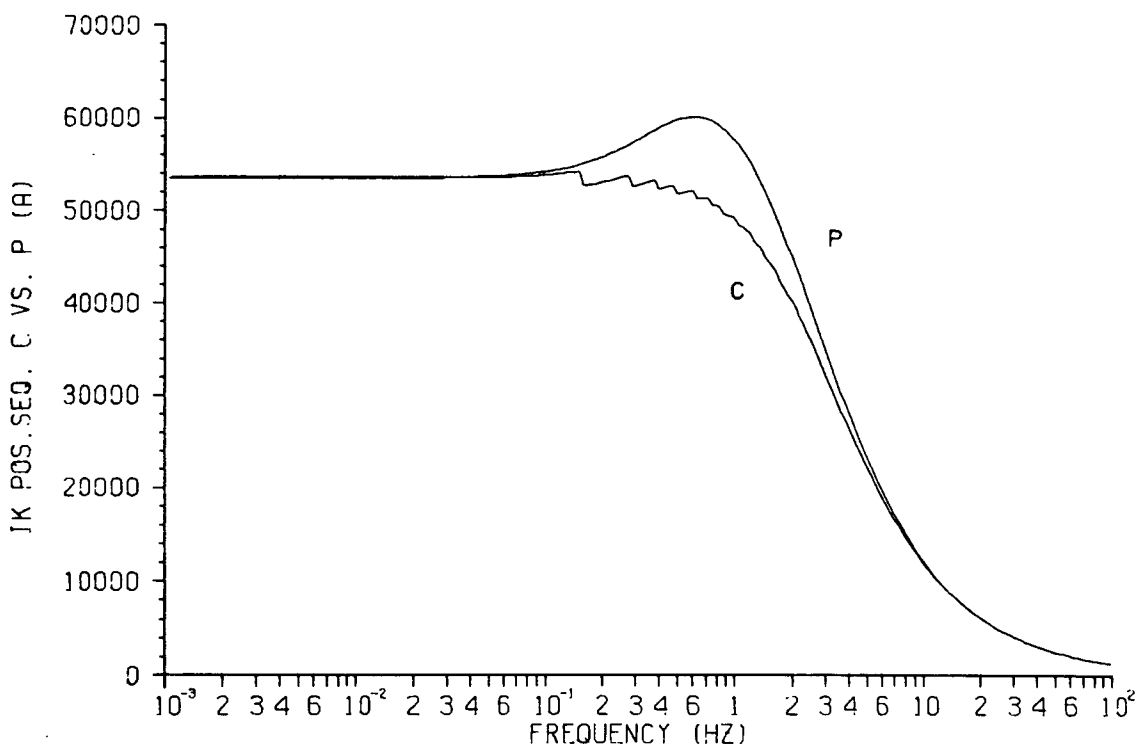
P.5.11: O/C Response, zero seq. Magnitude error. 60-Hz.



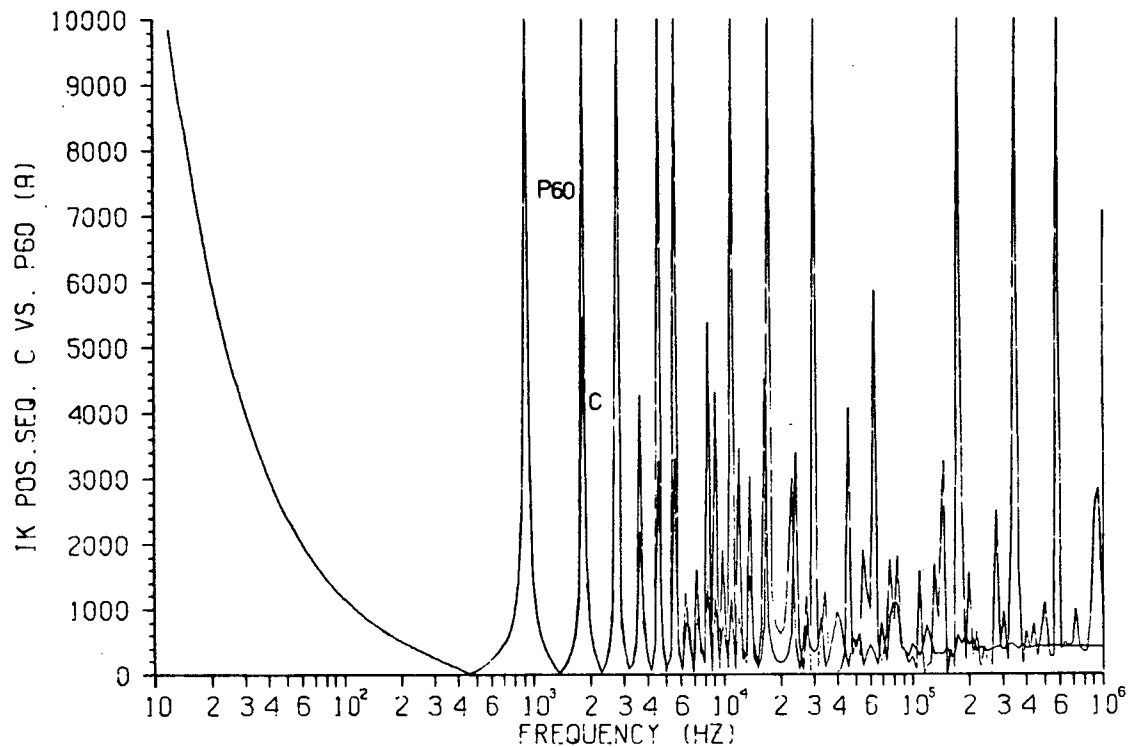
P.5.12: O/C Response, zero seq. Magnitude error. 750-Hz.



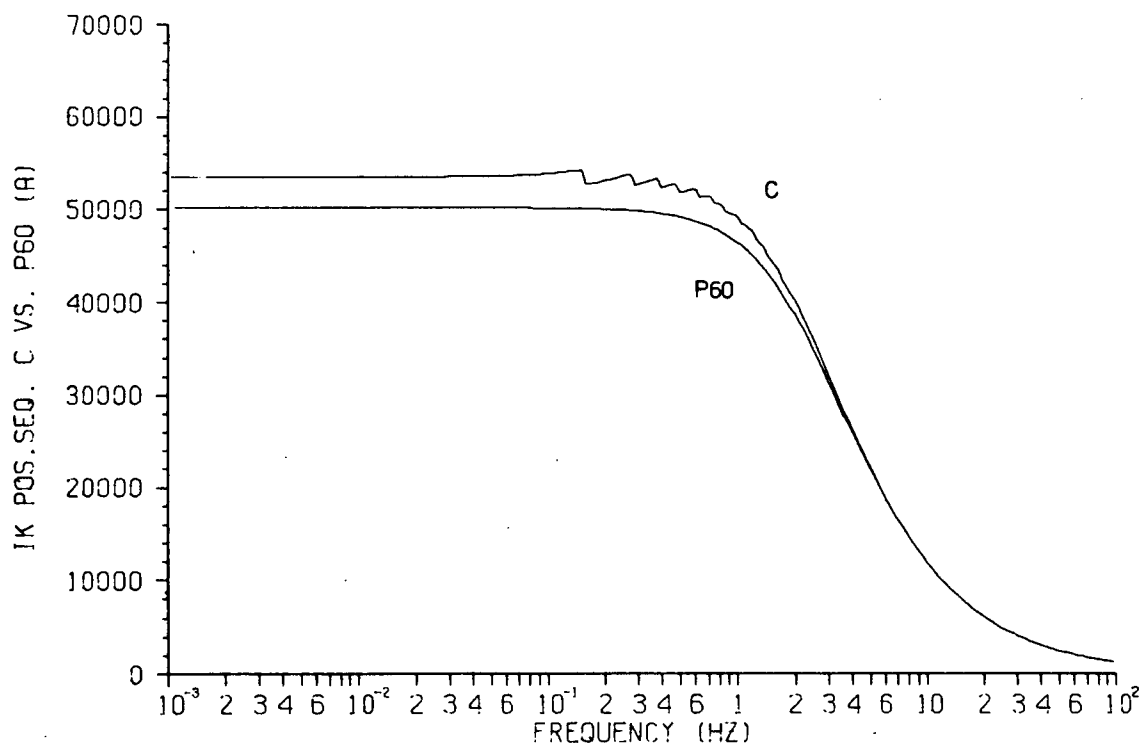
P.5.13(a): S/C Response, pos. seq. Exact vs. approx.
Mid to high frequencies.



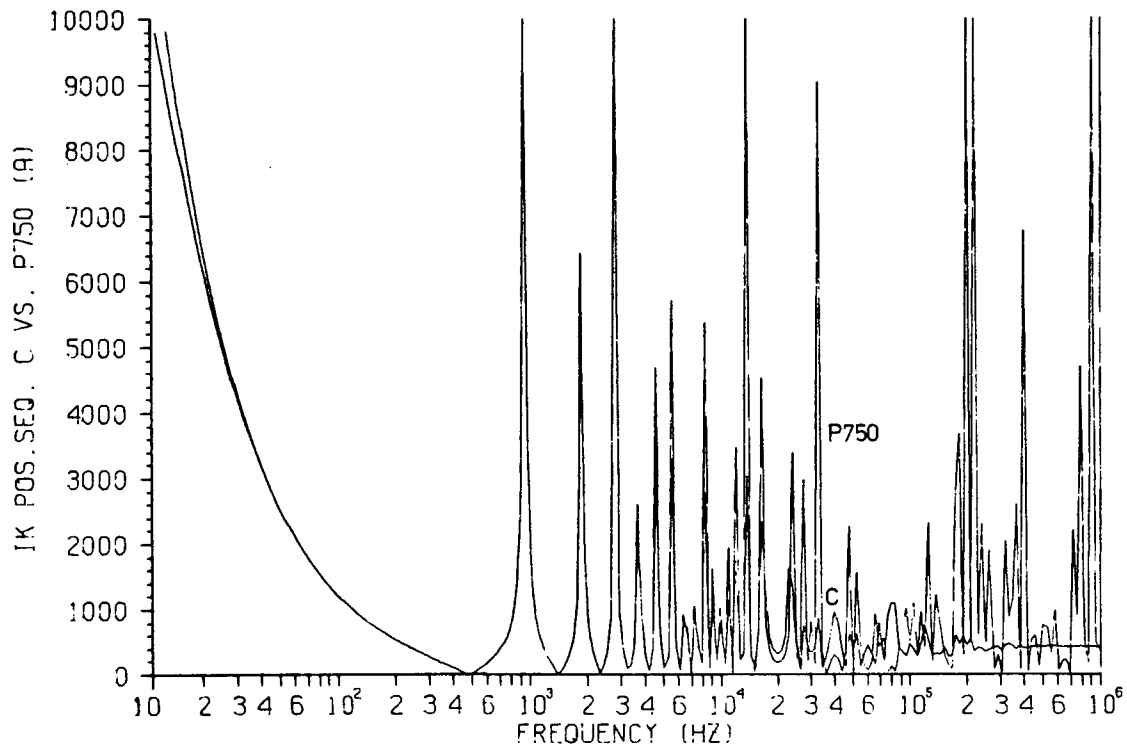
P.5.13(b): S/C Response, pos. seq. Exact vs. approx.
Low frequencies.



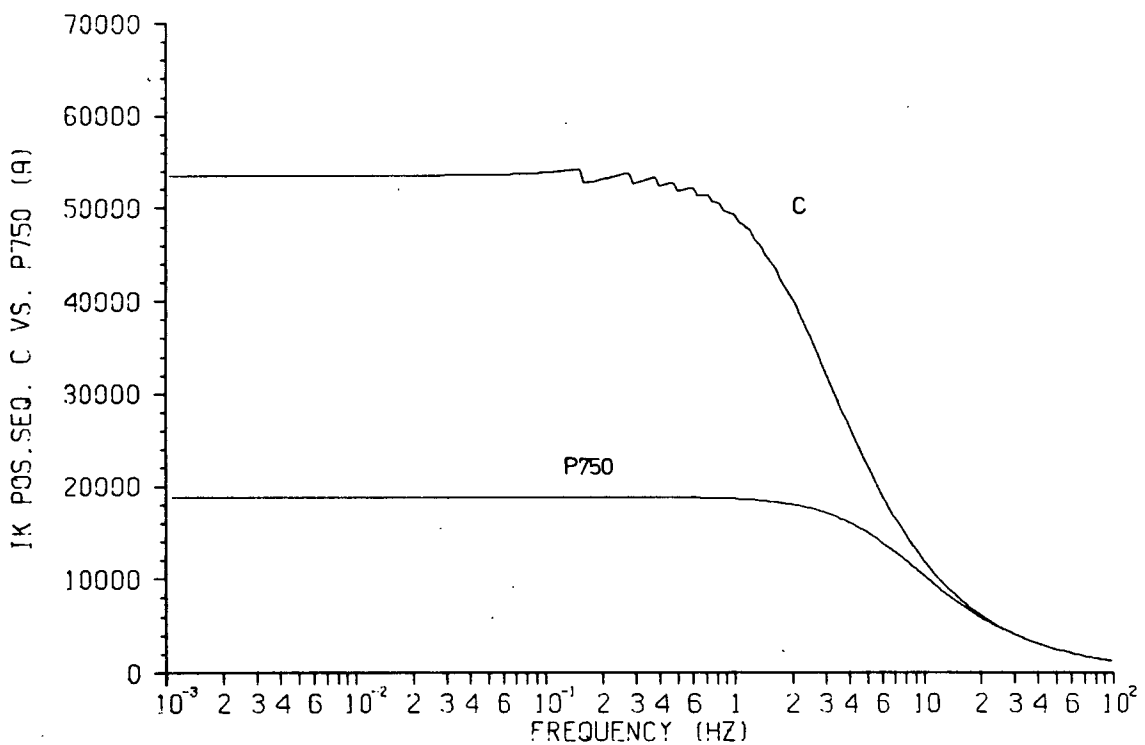
P.5.14(a): S/C Response, pos. seq. Exact vs. 60-Hz.
Mid to high frequencies.



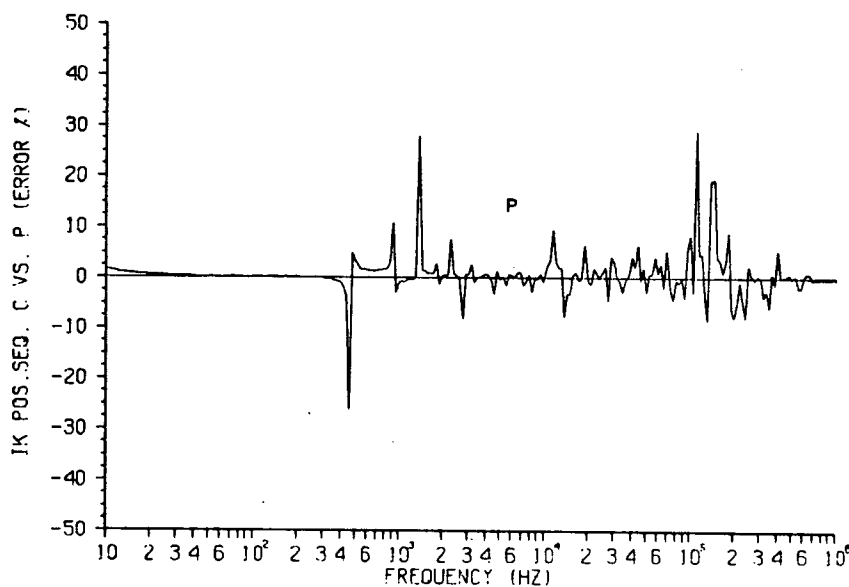
P.5.14(b): S/C Response, pos. seq. Exact vs. 60-Hz.
Low frequencies.



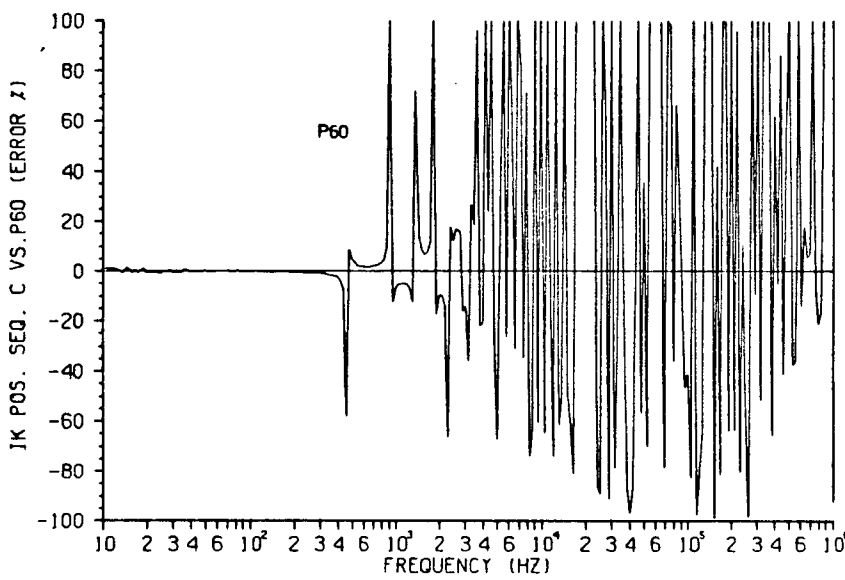
P.5.15(a): S/C Response, pos. seq. Exact vs. 750-Hz.
Mid to high frequencies.



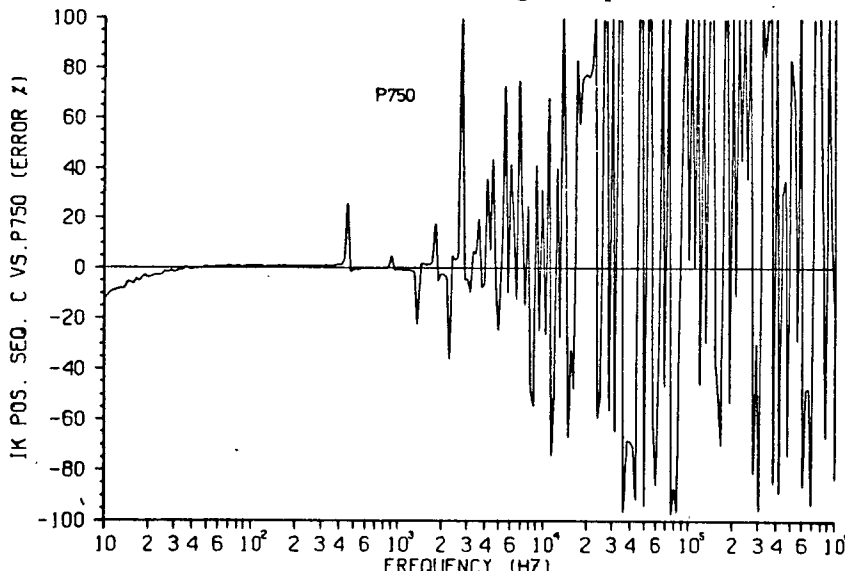
P.5.15(b): S/C Response, pos. seq. Exact vs. 750-Hz.
Low frequencies.



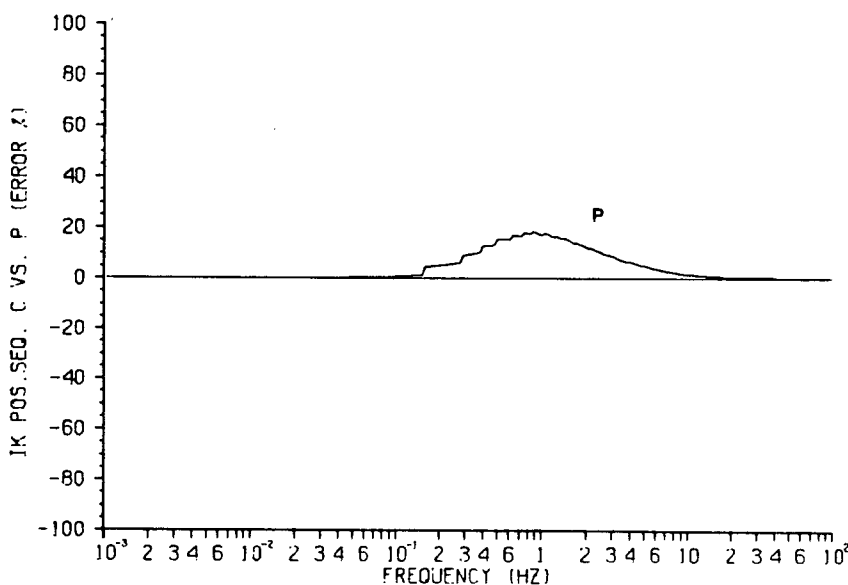
P.5.16(a): S/C Response, pos. seq. Magnitude error.
Approximation. Mid to high frequencies.



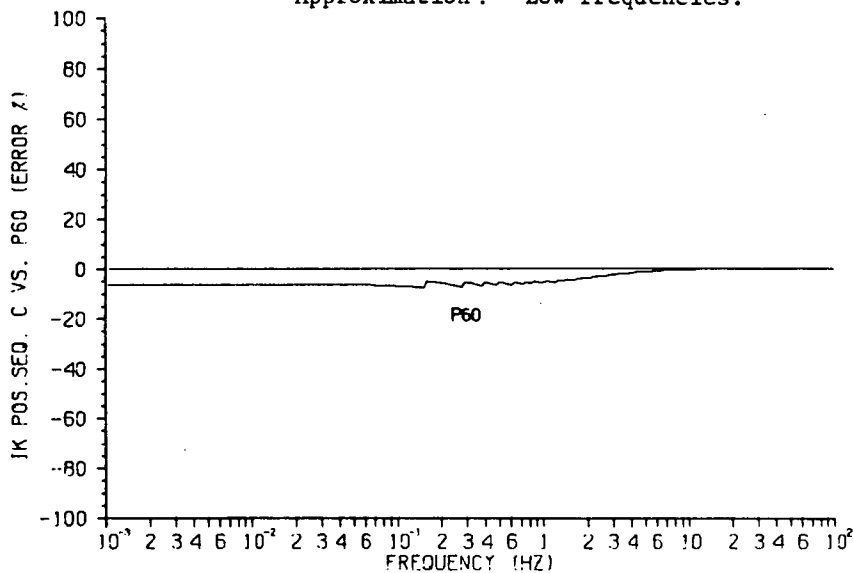
P.5.17(a): S/C Response, pos. seq. Magnitude error.
60-Hz. Mid to high frequencies.



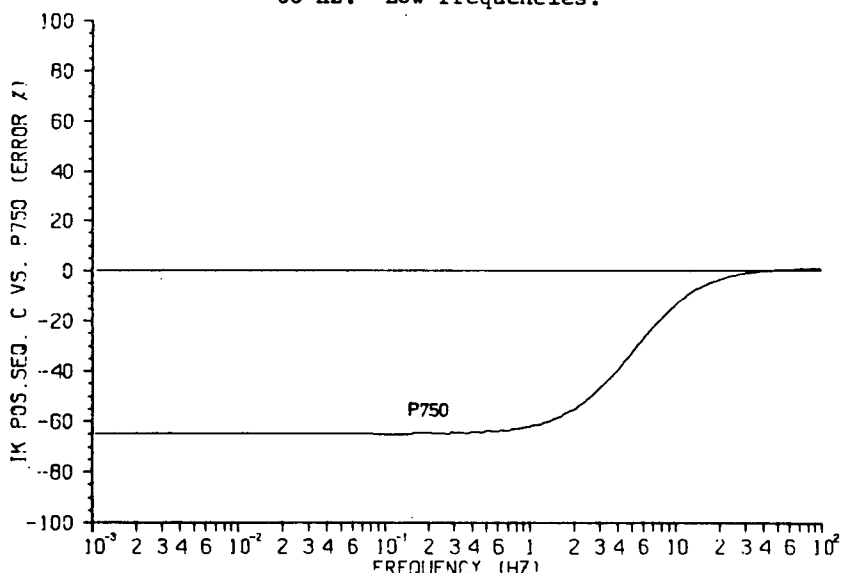
P.5.18(a): S/C Response, pos. seq. Magnitude error.
750-Hz. Mid to high frequencies.



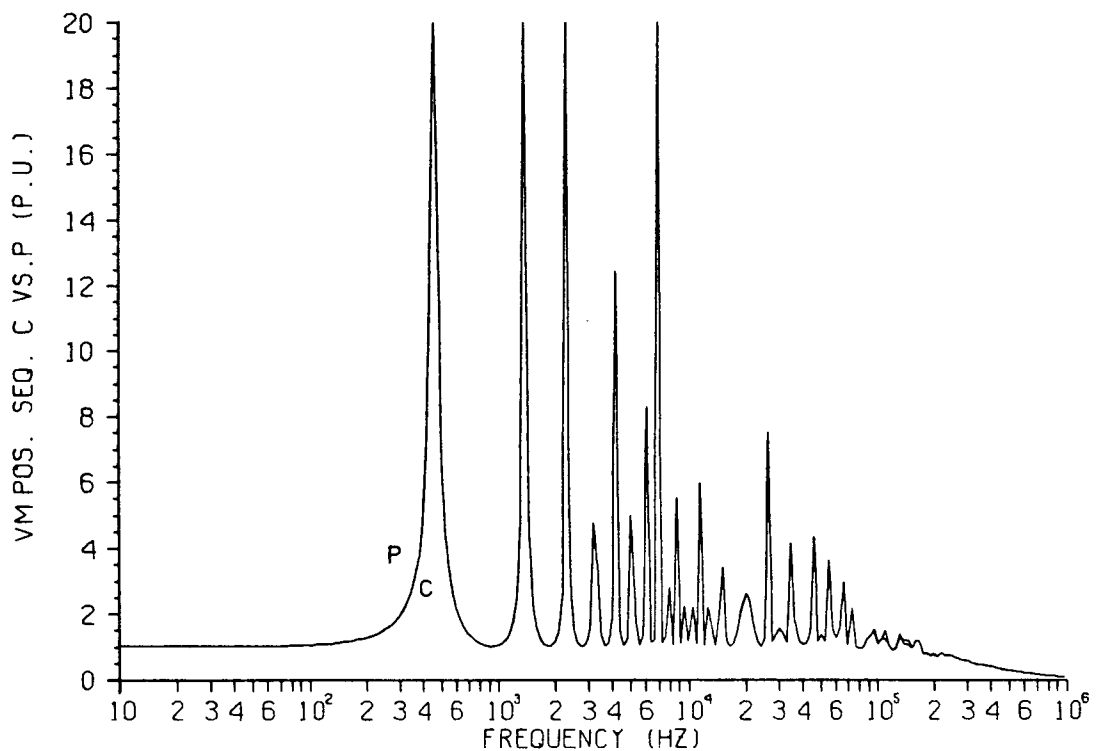
P.5.16(b): S/C Response, pos. seq. Magnitude error.
Approximation. Low frequencies.



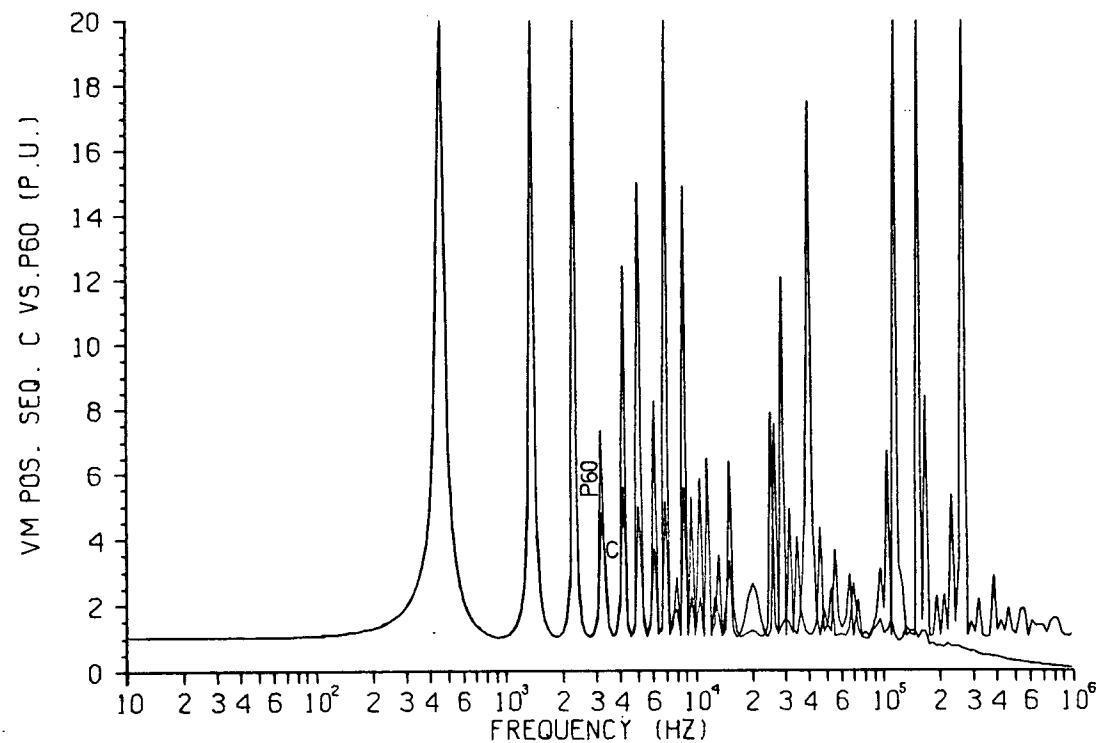
P.5.17(b): S/C Response, pos. seq. Magnitude error.
60-Hz. Low frequencies.



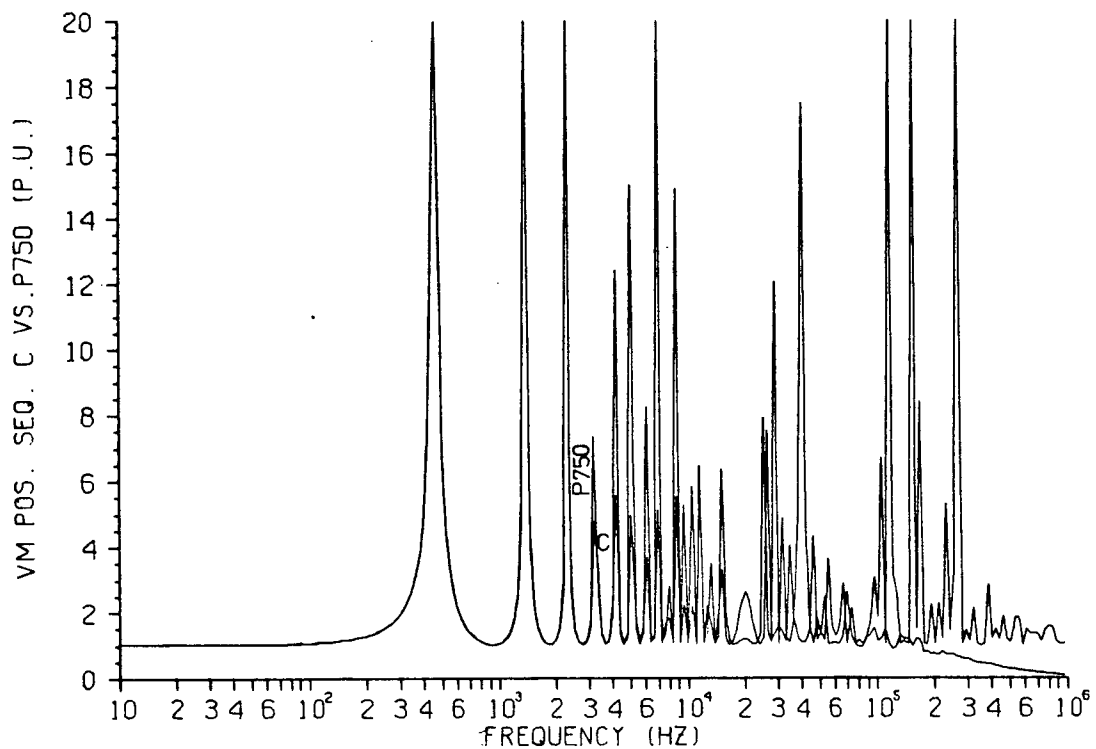
P.5.18(b): S/C Response, pos. seq. Magnitude error.
750-Hz. Low frequencies.



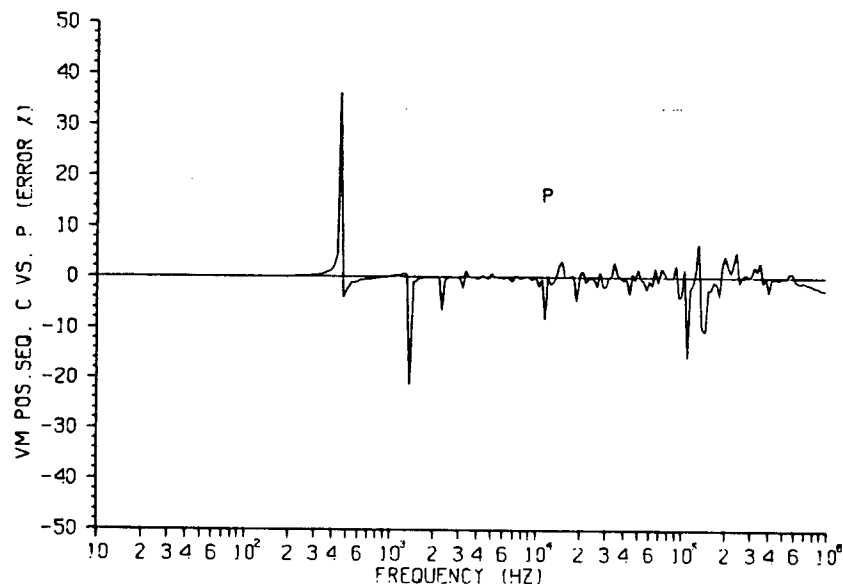
P.5.19: O/C Response, pos. seq. Exact vs. approx.



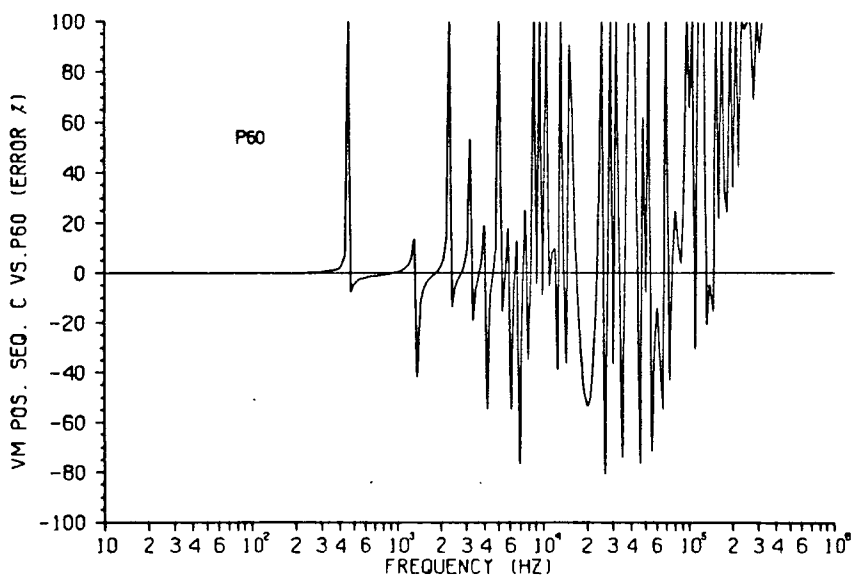
P.5.20: O/C Response, pos. seq. Exact vs. 60-Hz.



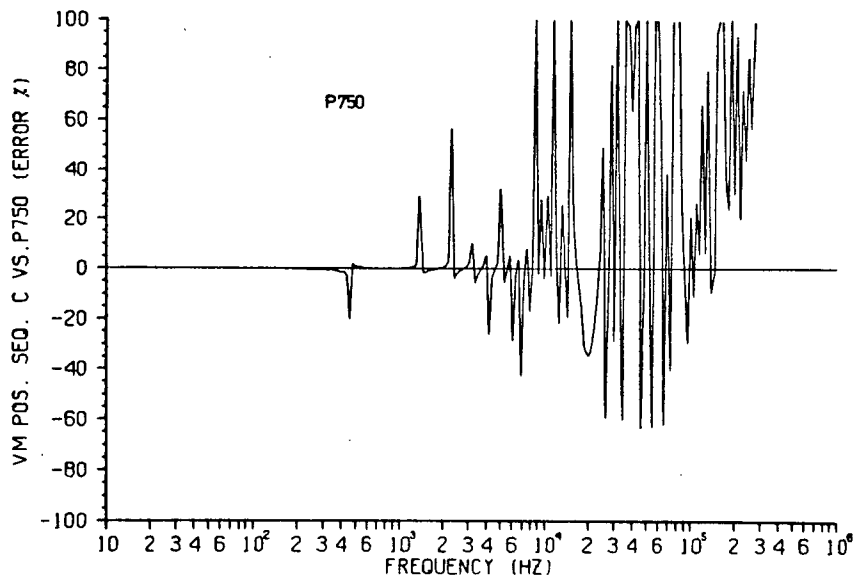
P.5.21: O/C Response, pos. seq. Exact vs. 750-Hz.



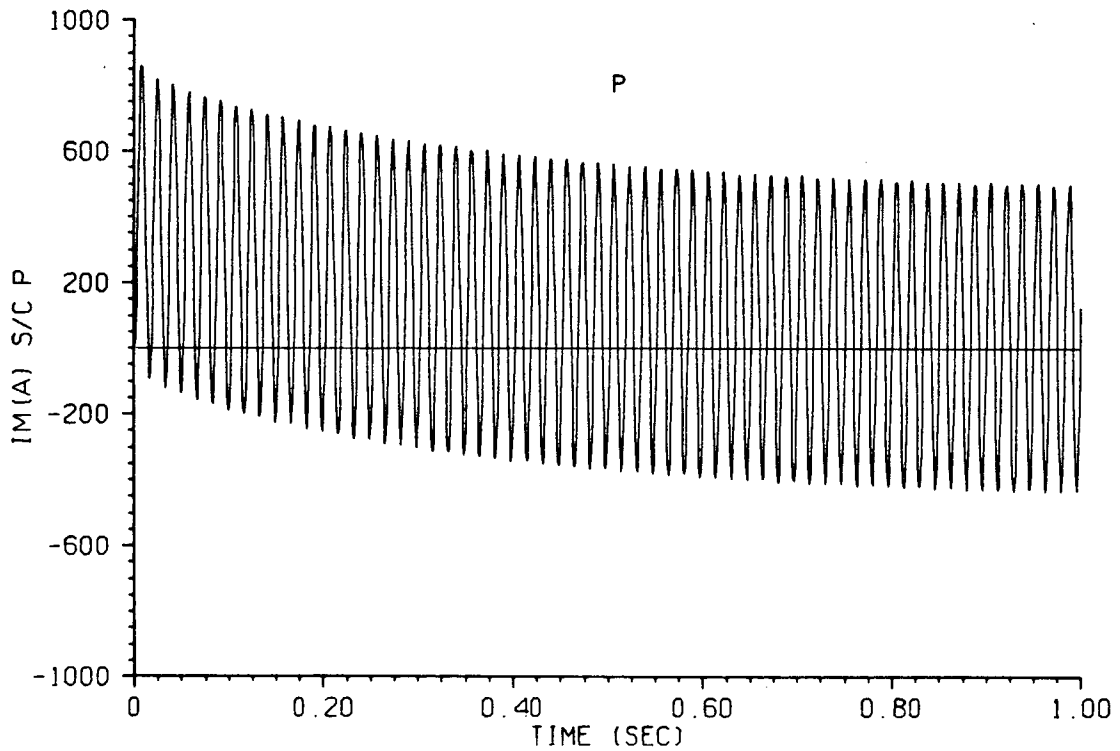
P.5.22: O/C Response, pos. seq. Magnitude error. Approximation.



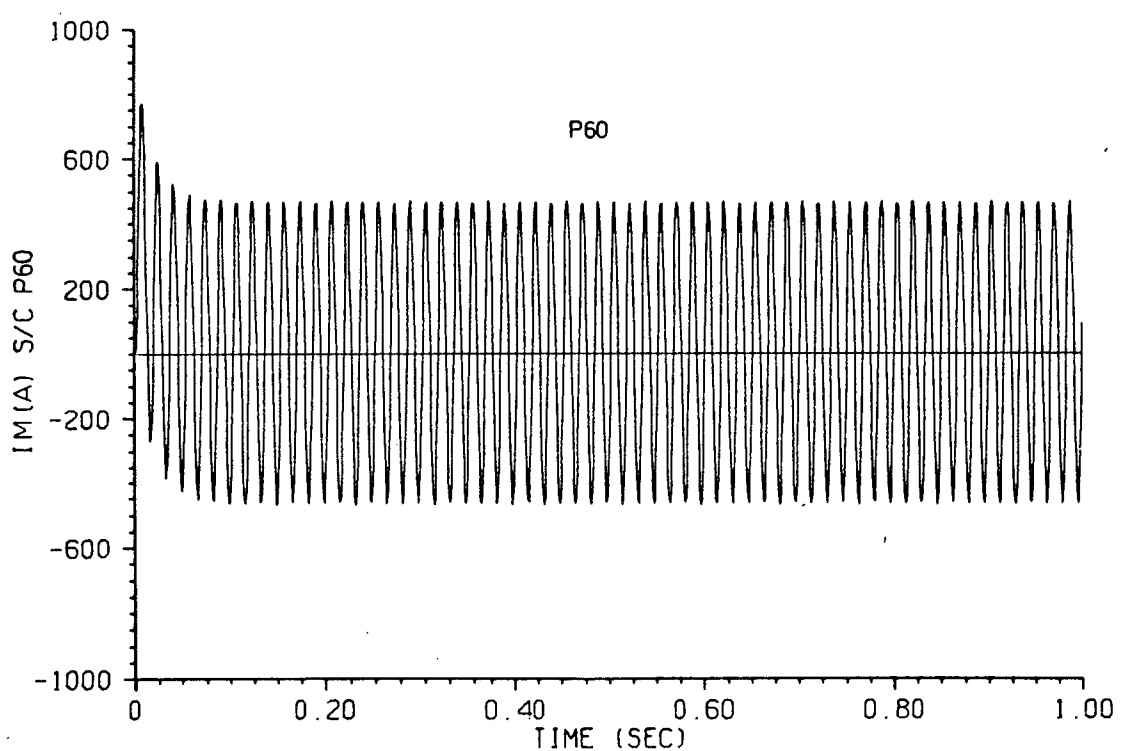
P.5.23: O/C Response, pos. seq. Magnitude error. 60-Hz.



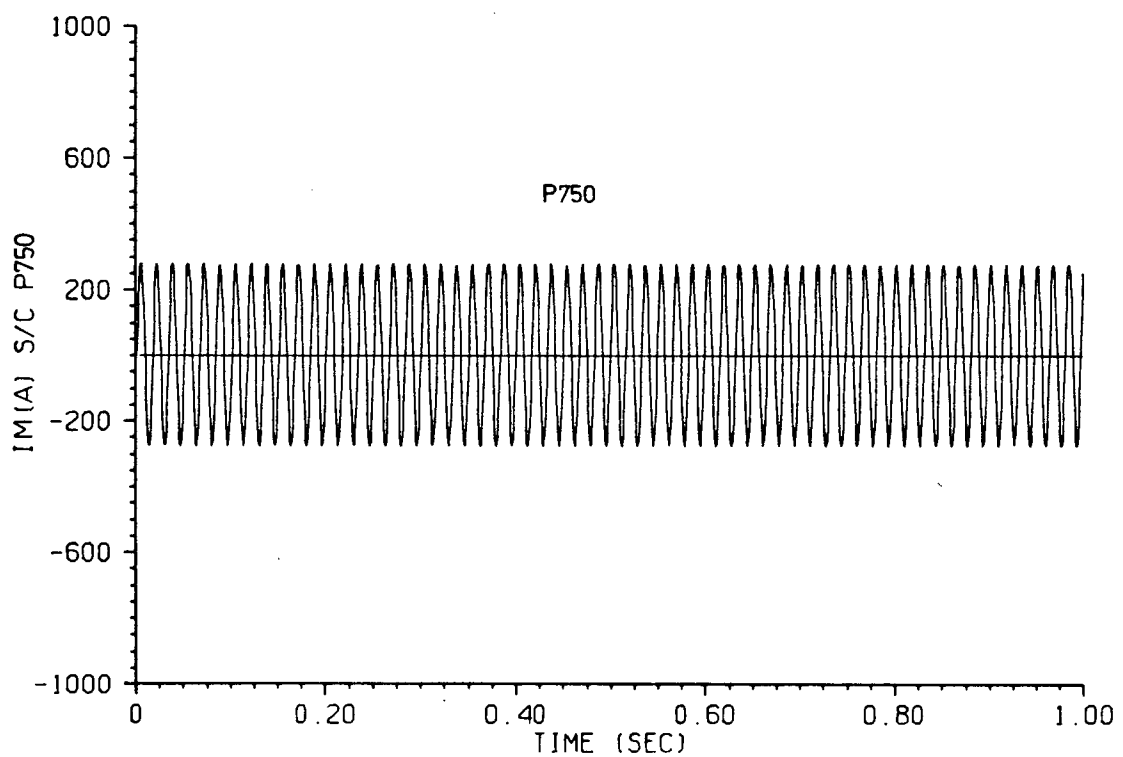
P.5.24: O/C Response, pos. seq. Magnitude error. 750-Hz.



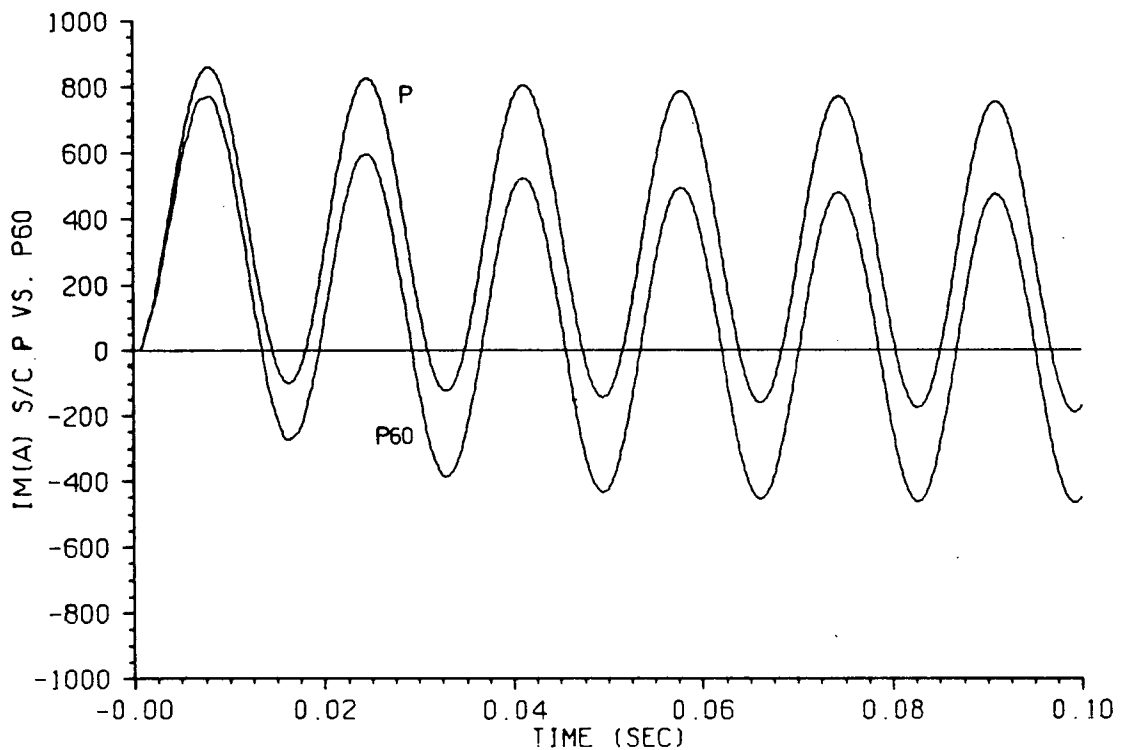
P.7.1: Short circuit simulation. Sinusoidal source, zero at $t=0$. New model.



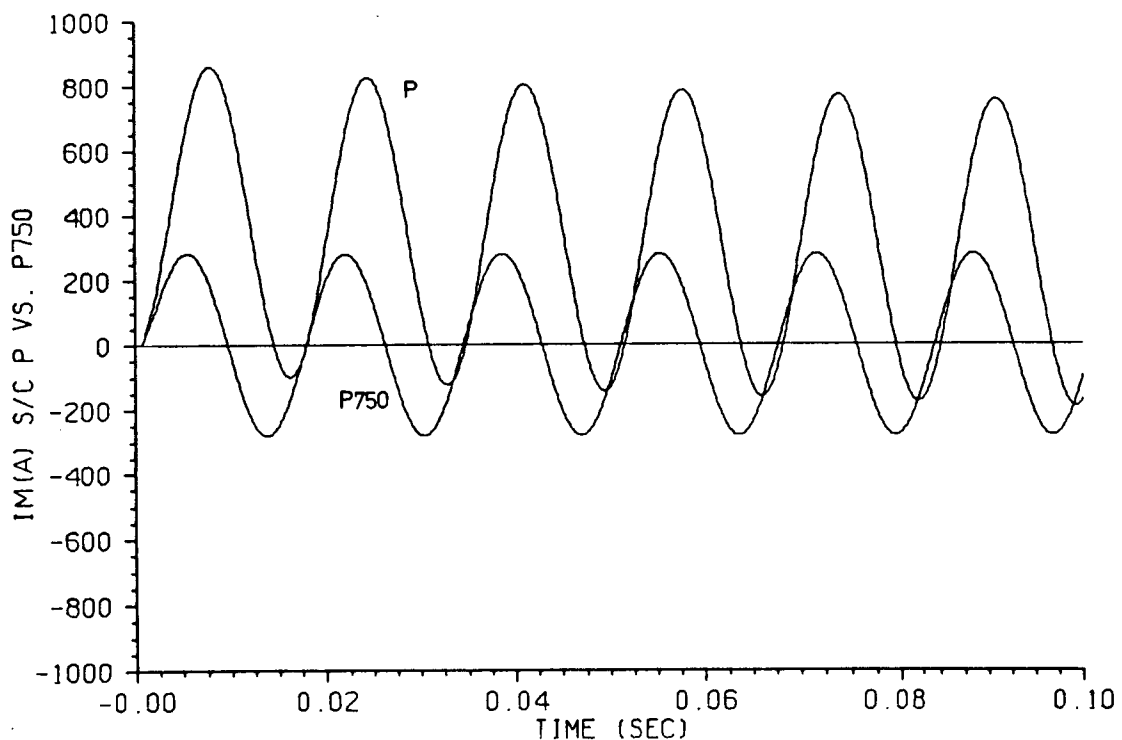
P.7.2: Short circuit simulation. Sinusoidal source, zero at $t=0$. 60-Hz parameters.



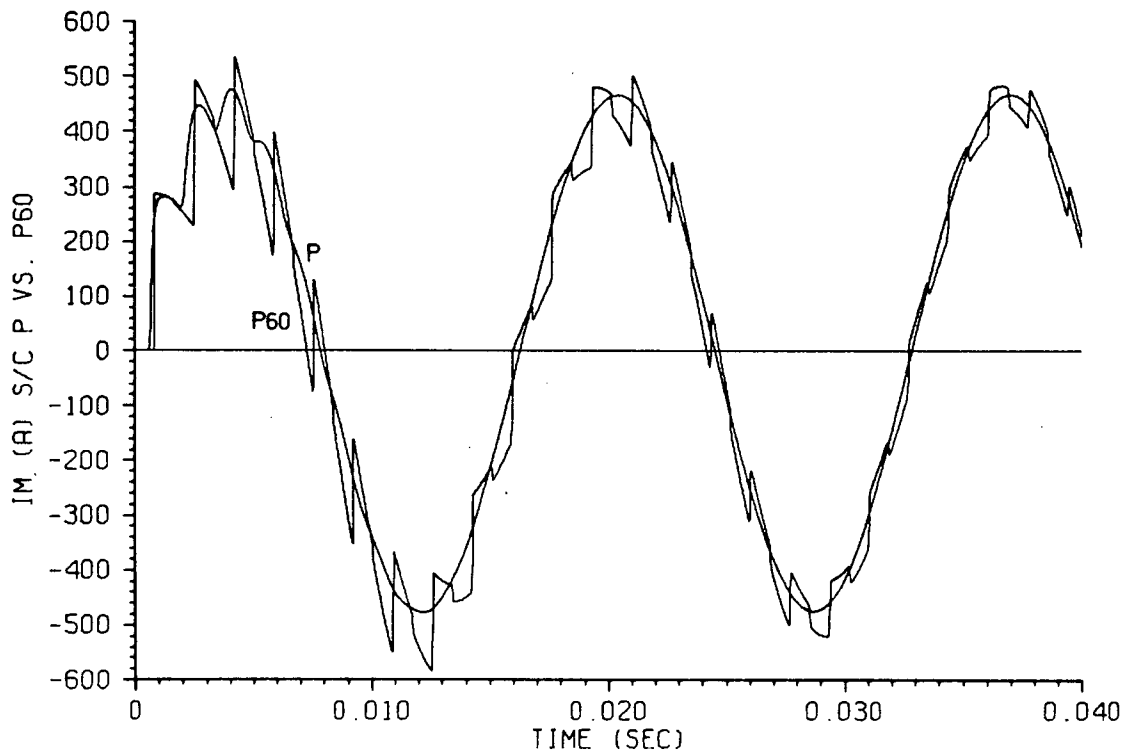
P.7.3: Short circuit simulation. Sinusoidal source, zero at $t=0$. 750-Hz parameters.



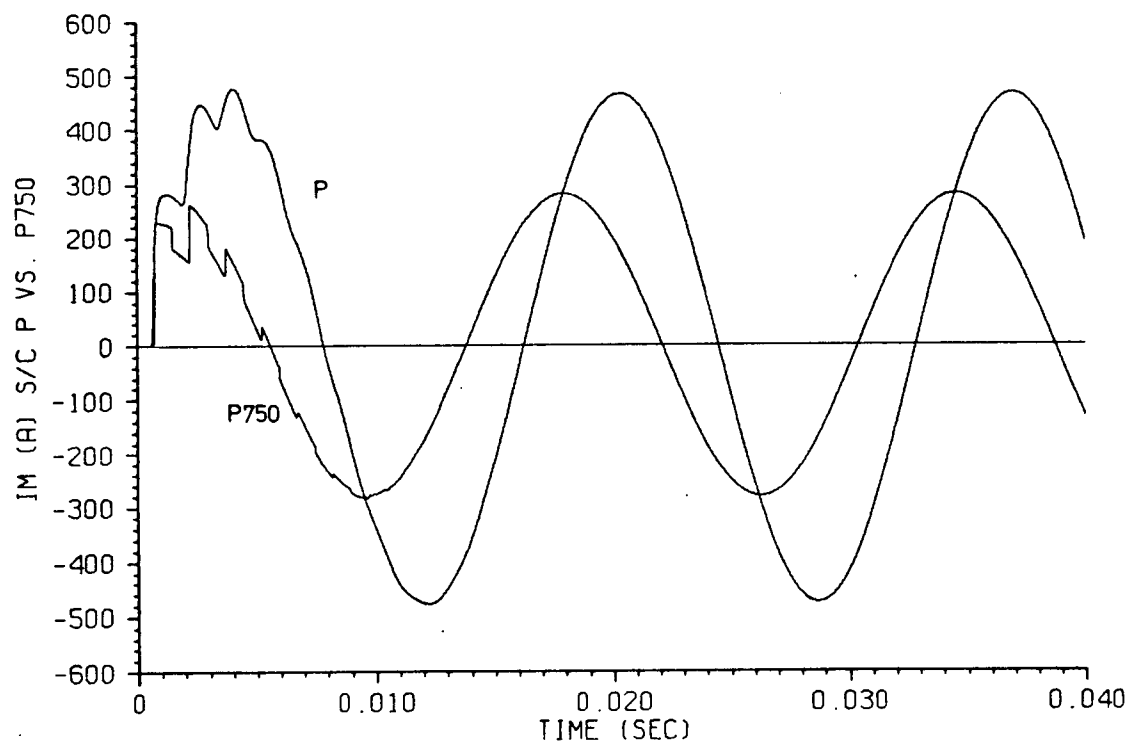
P.7.4: Short circuit simulation. Sinusoidal source, zero at $t=0$. New model vs. 60-Hz. First cycles.



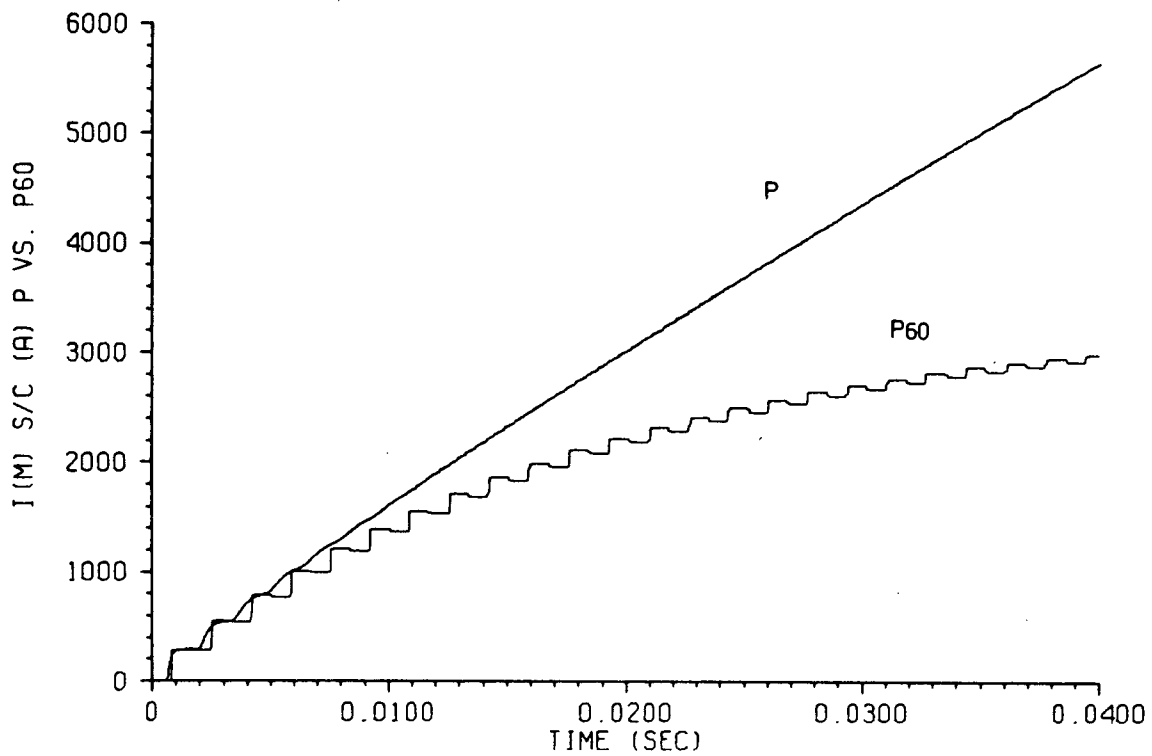
P.7.5: Short circuit simulation. Sinusoidal source, zero at $t=0$. New model vs. 750-Hz. First cycles.



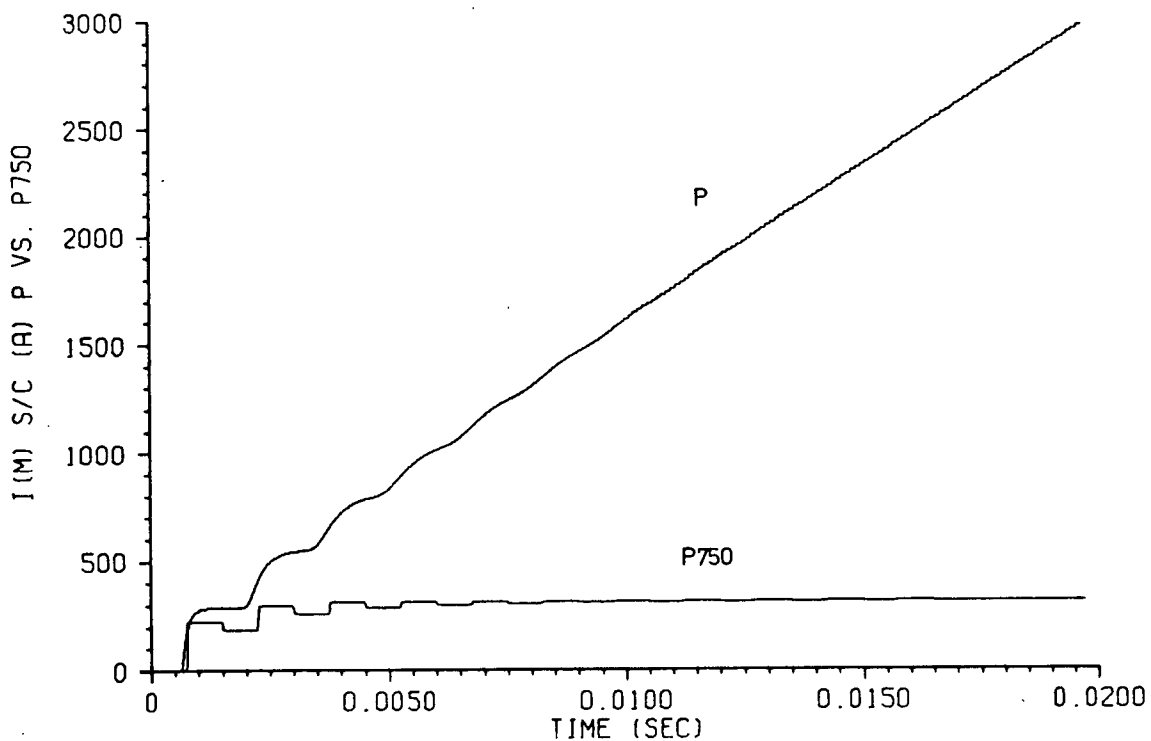
P.7.6: Short circuit simulation. Sinusoidal source, peak at $t=0$. New model vs. 60-Hz.



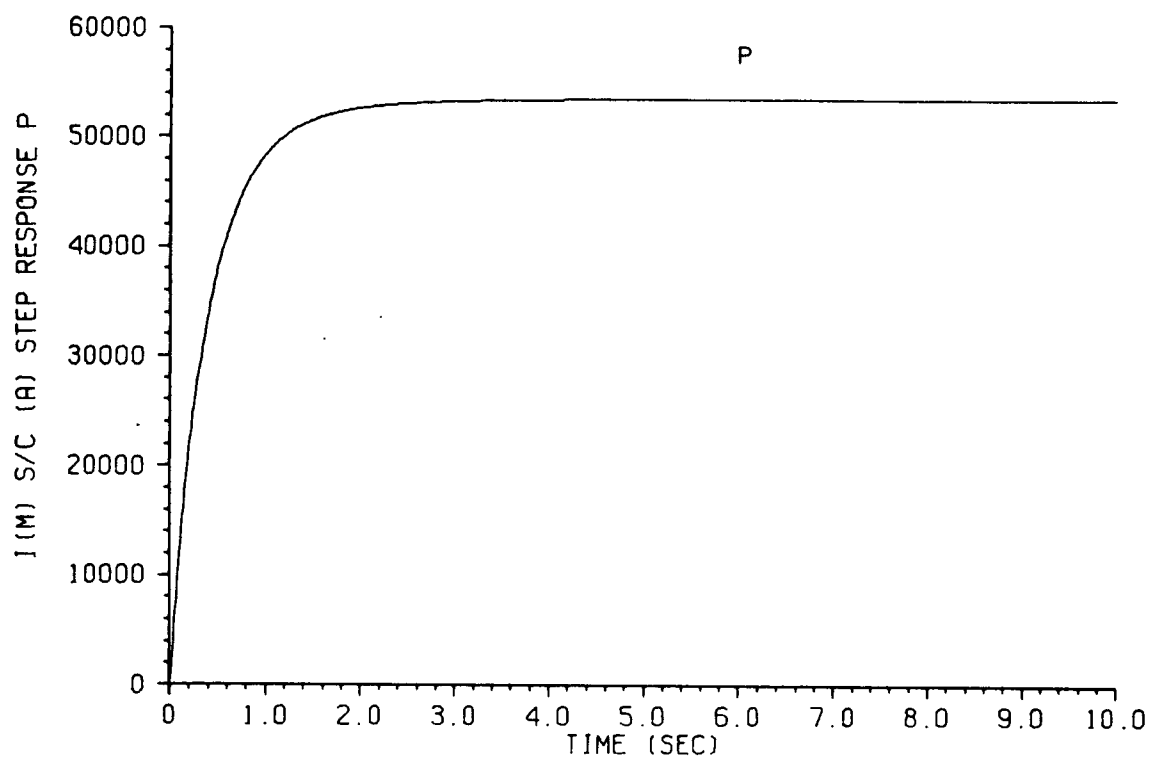
P.7.7: Short circuit simulation. Sinusoidal source, peak at $t=0$. New model vs. 750-Hz.



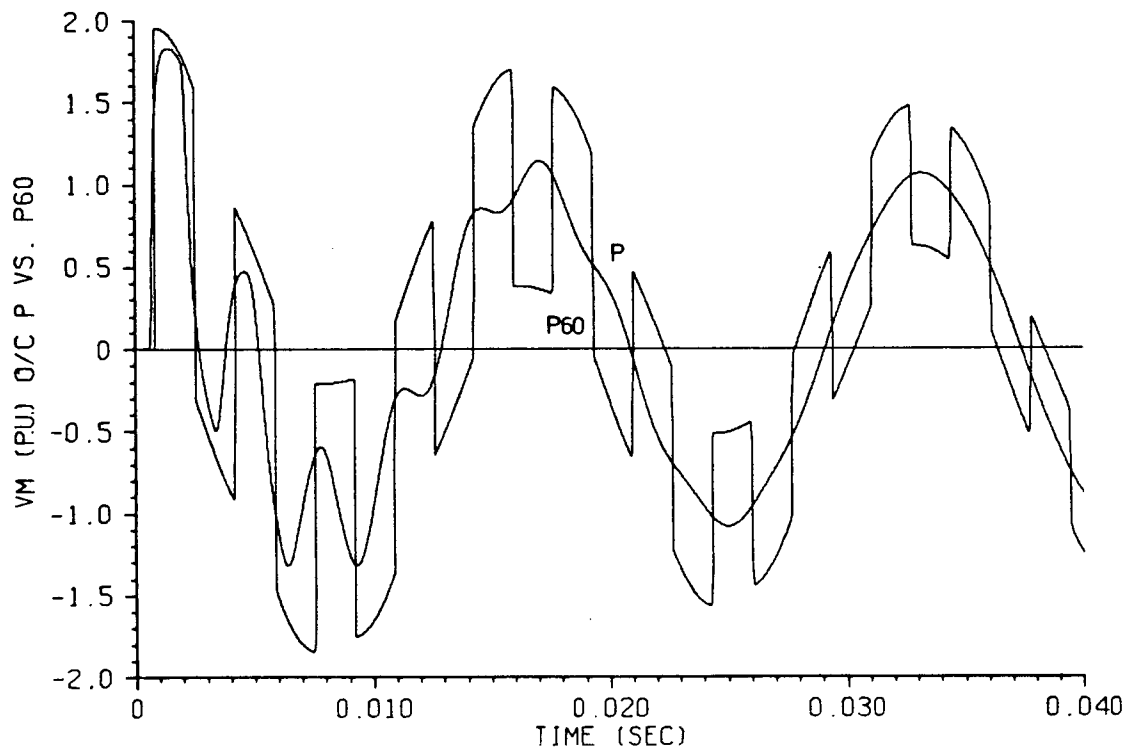
P.7.8: Short circuit simulation. Step excitation.
New model vs. 60-Hz.



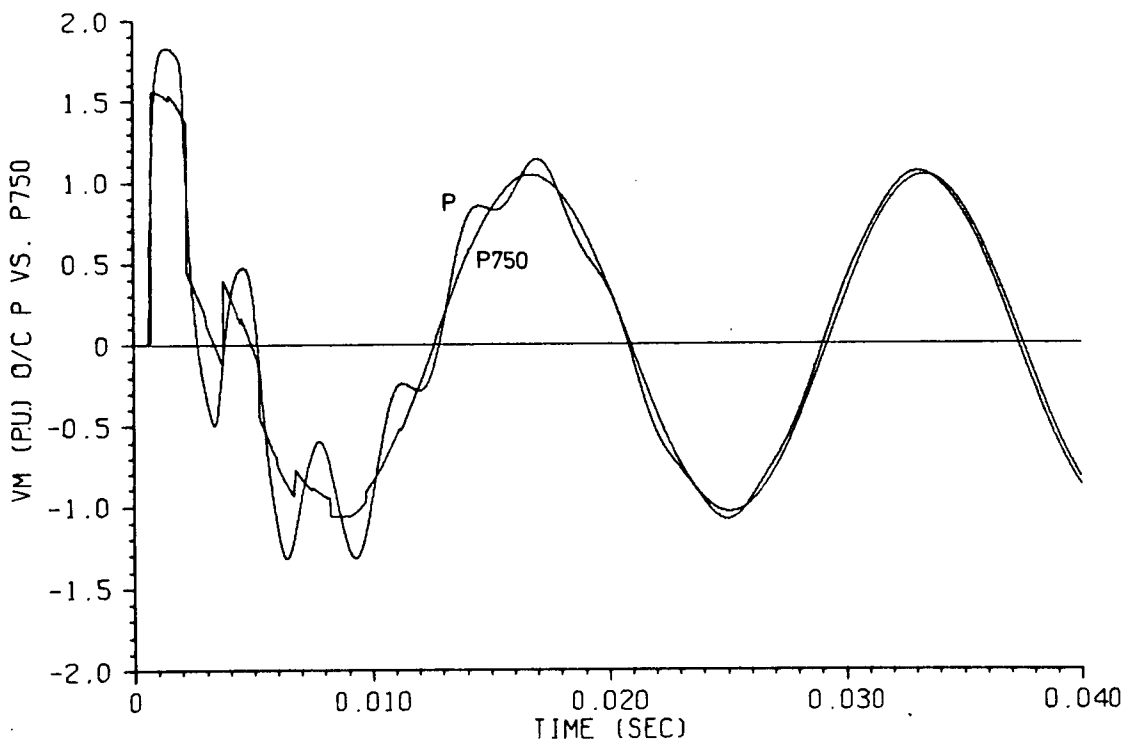
P.7.9: Short circuit simulation. Step excitation.
New model vs. 750-Hz.



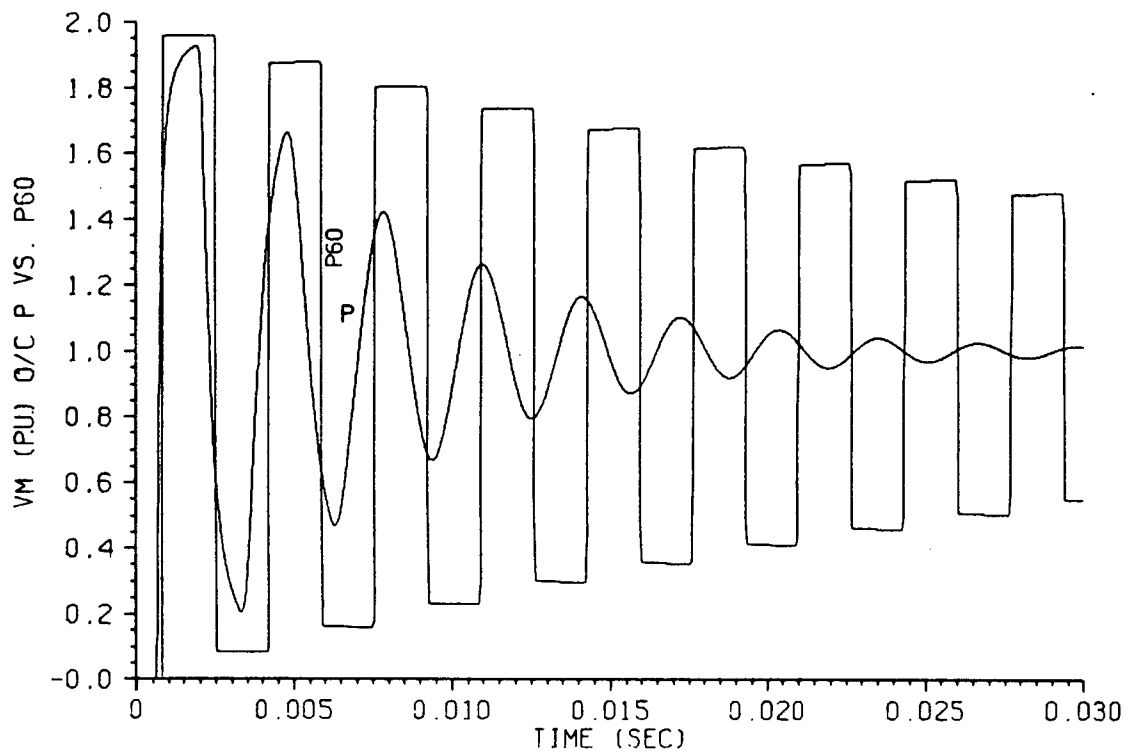
P.7.10: Short circuit simulation. Step excitation.
New model. Extended time response.



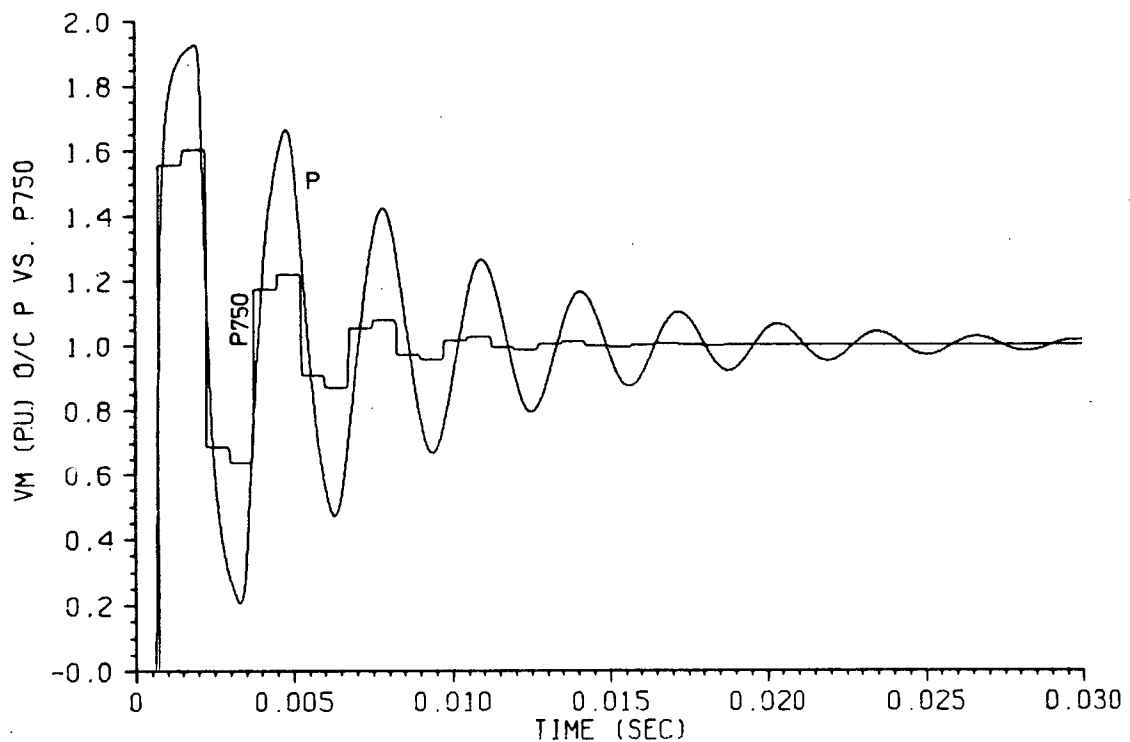
P.7.11: Open circuit simulation. Sinusoidal source, peak at $t=0$. New model vs. 60-Hz.



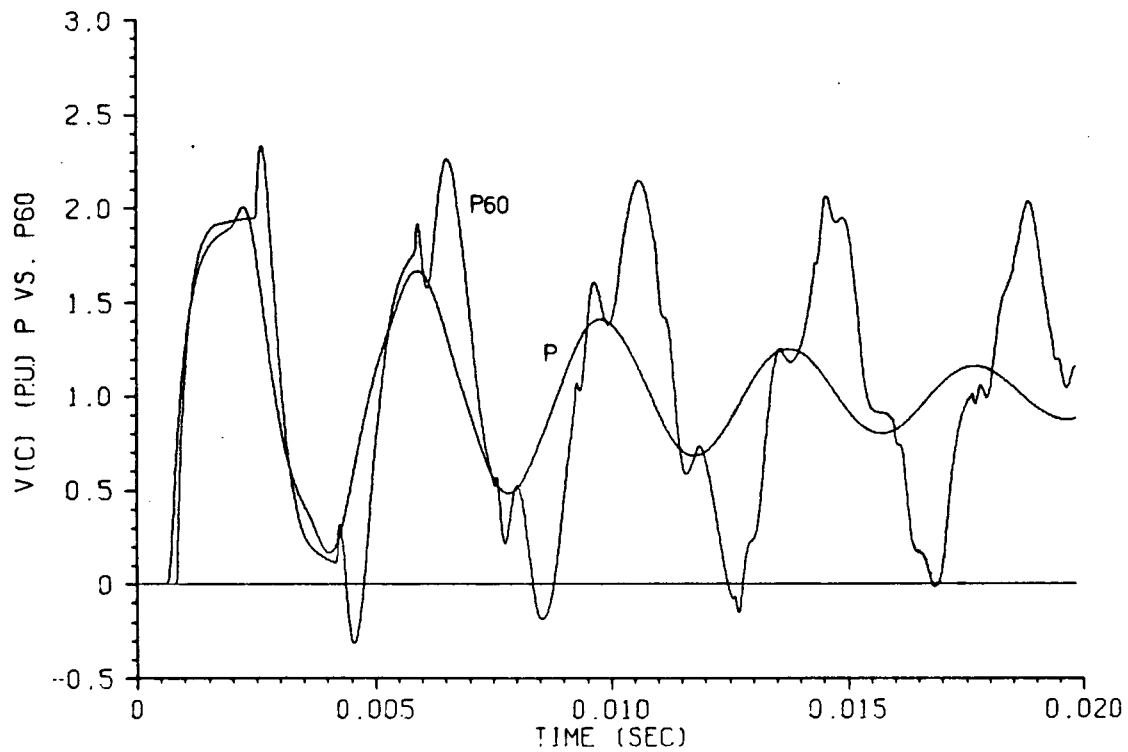
P.7.12: Open circuit simulation. Sinusoidal source, peak at $t=0$. New model vs. 750-Hz.



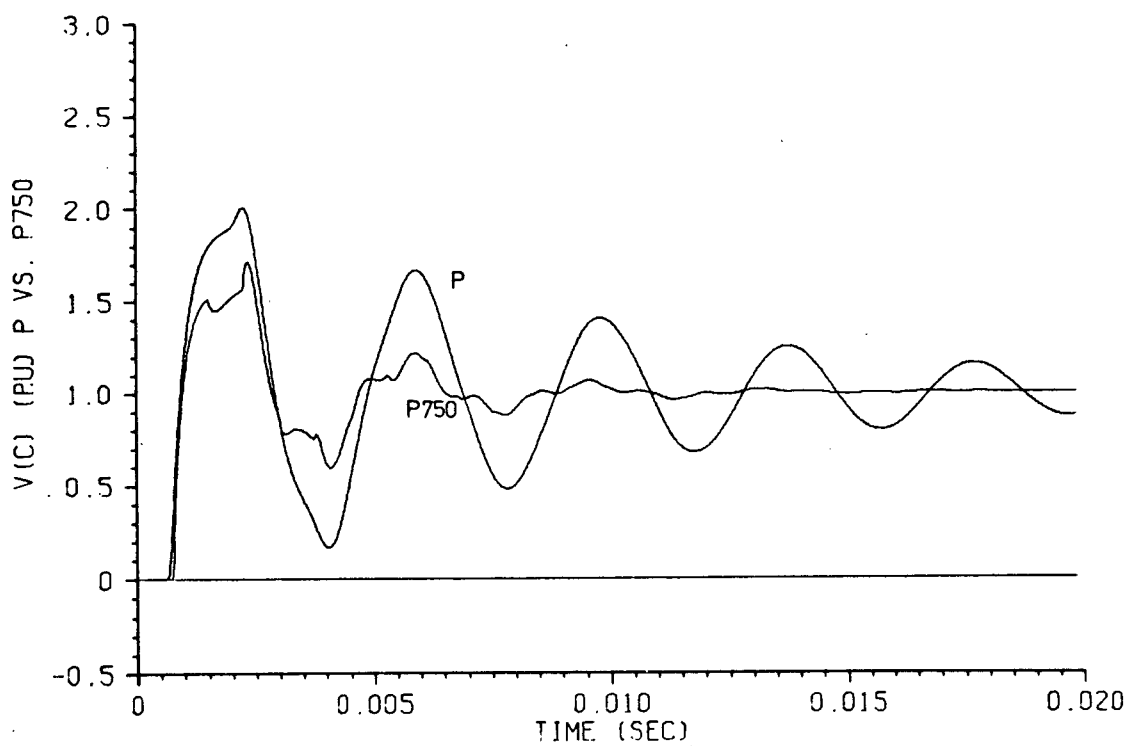
P.7.13: Open circuit simulation. Step excitation.
New model vs. 60-Hz.



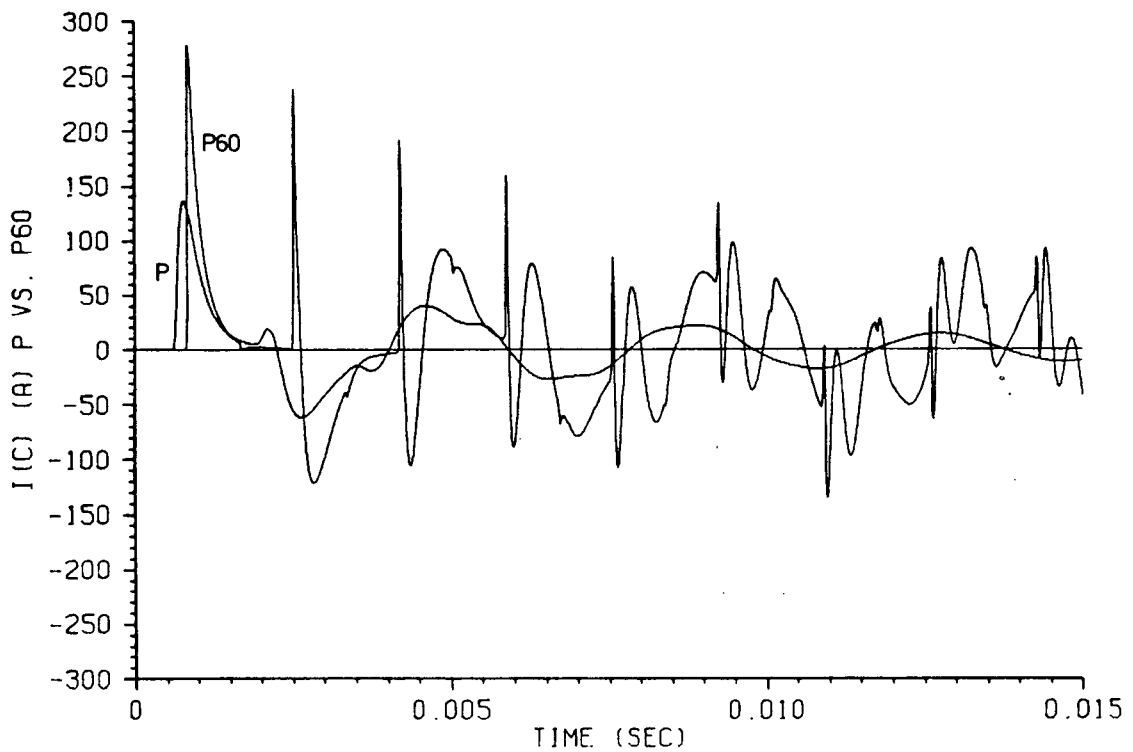
P.7.14: Open circuit simulation. Step excitation.
New model vs. 750-Hz.



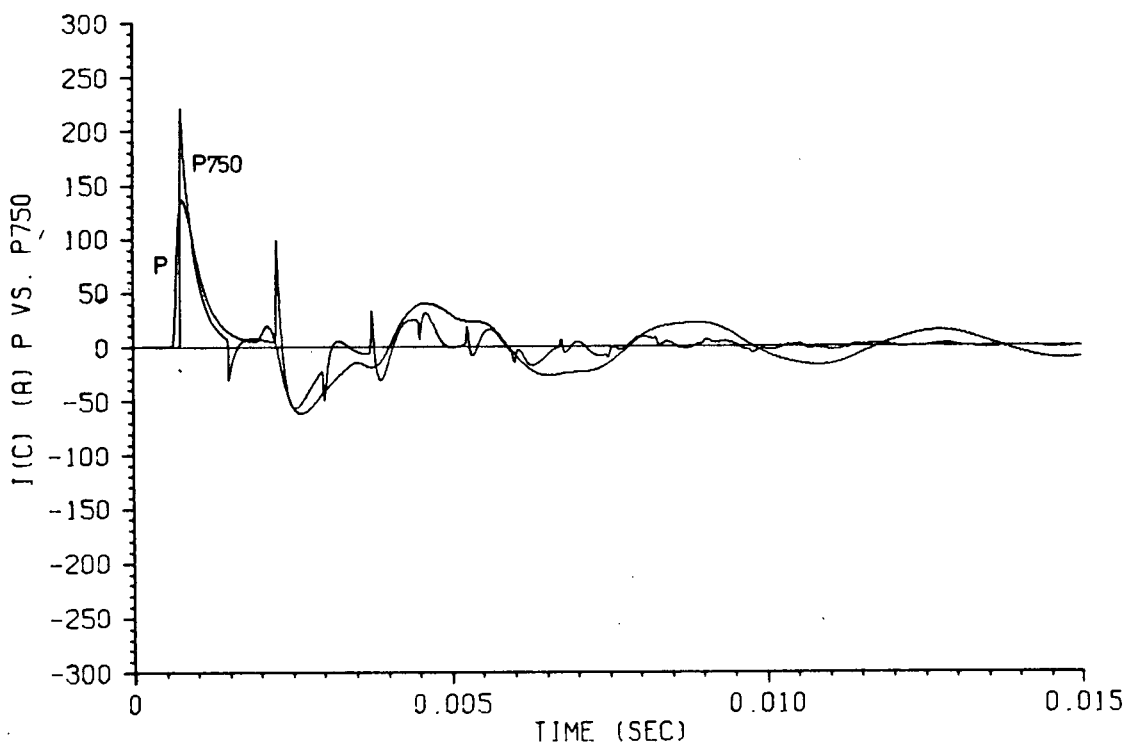
P.7.15: Capacitive load. Step excitation. Load voltage. New model vs. 60-Hz.



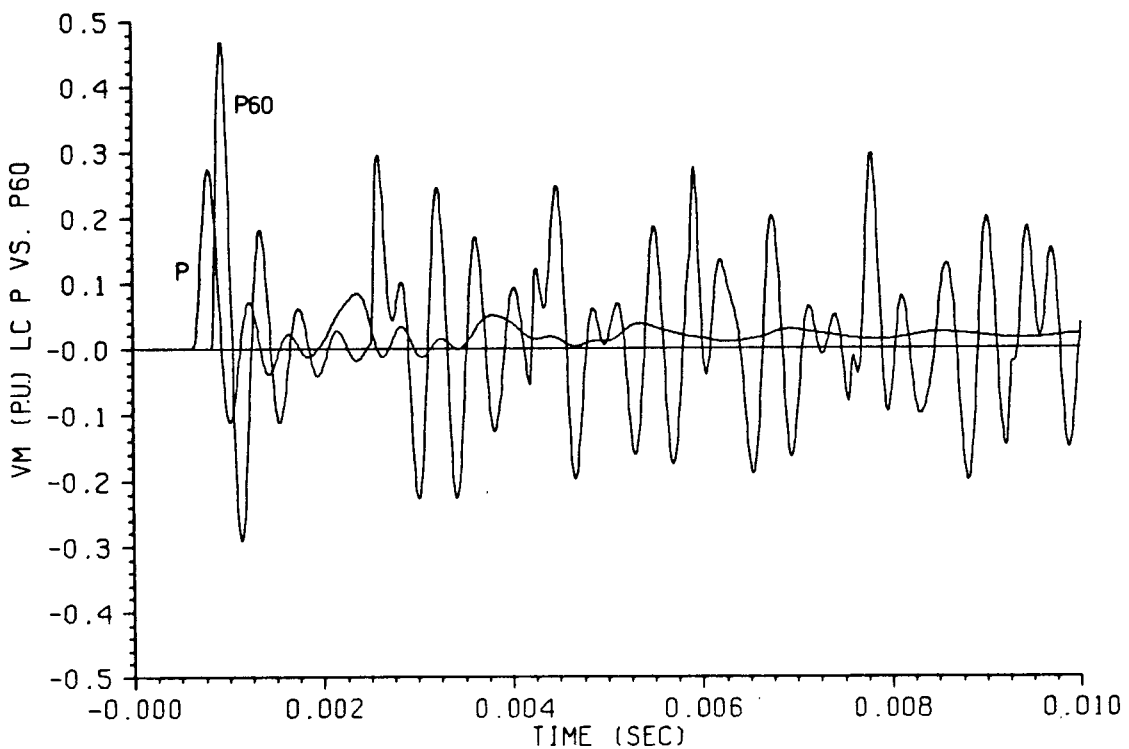
P.7.16: Capacitive load. Step excitation. Load voltage. New model vs. 750-Hz.



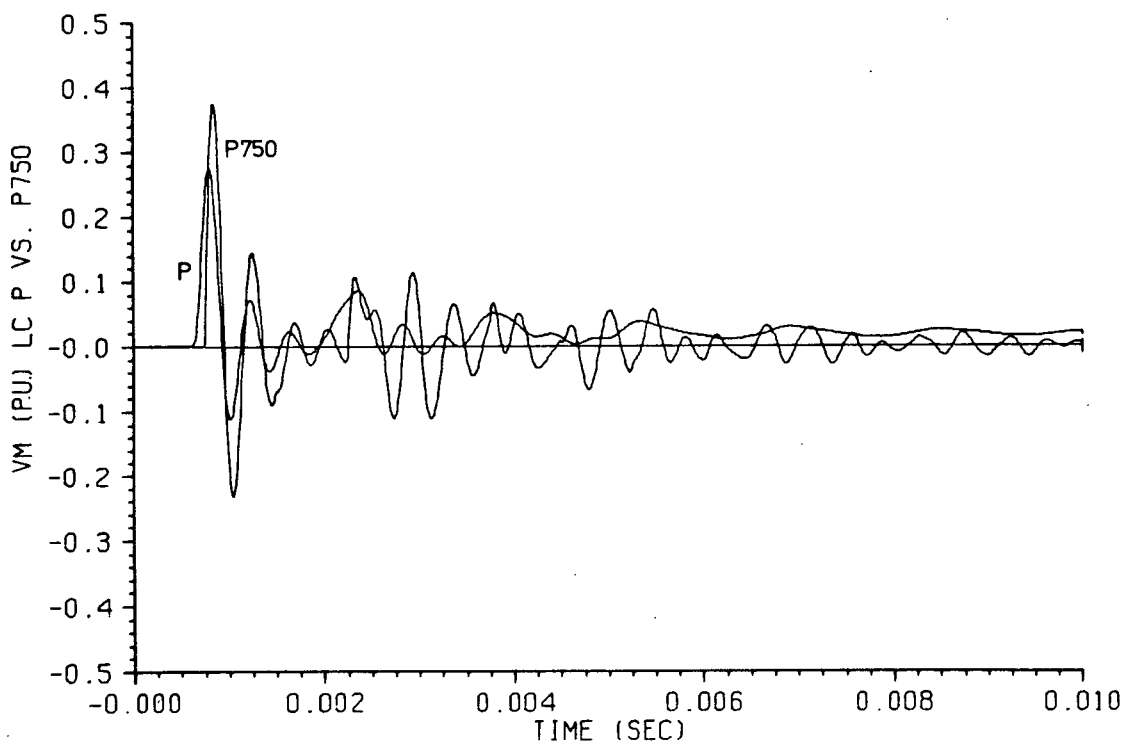
P.7.17: Capacitive load. Step excitation. Load current.
New model vs. 60-Hz.



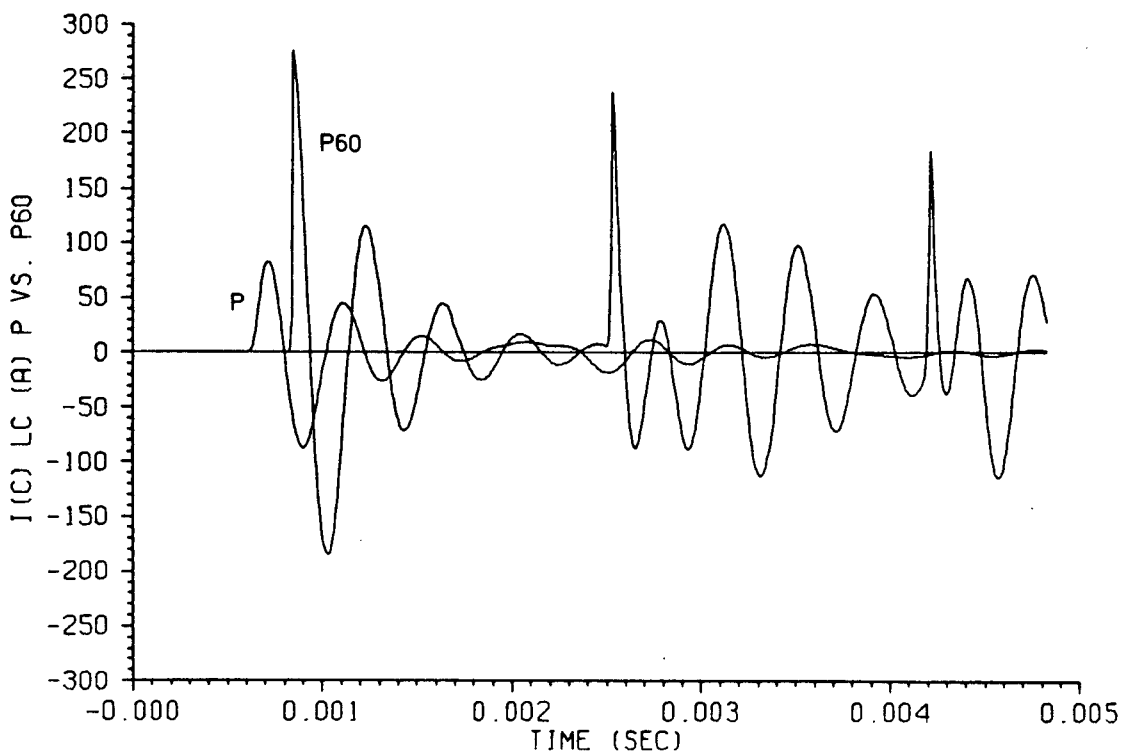
P.7.18: Capacitive load. Step excitation. Load current.
New model vs. 750-Hz.



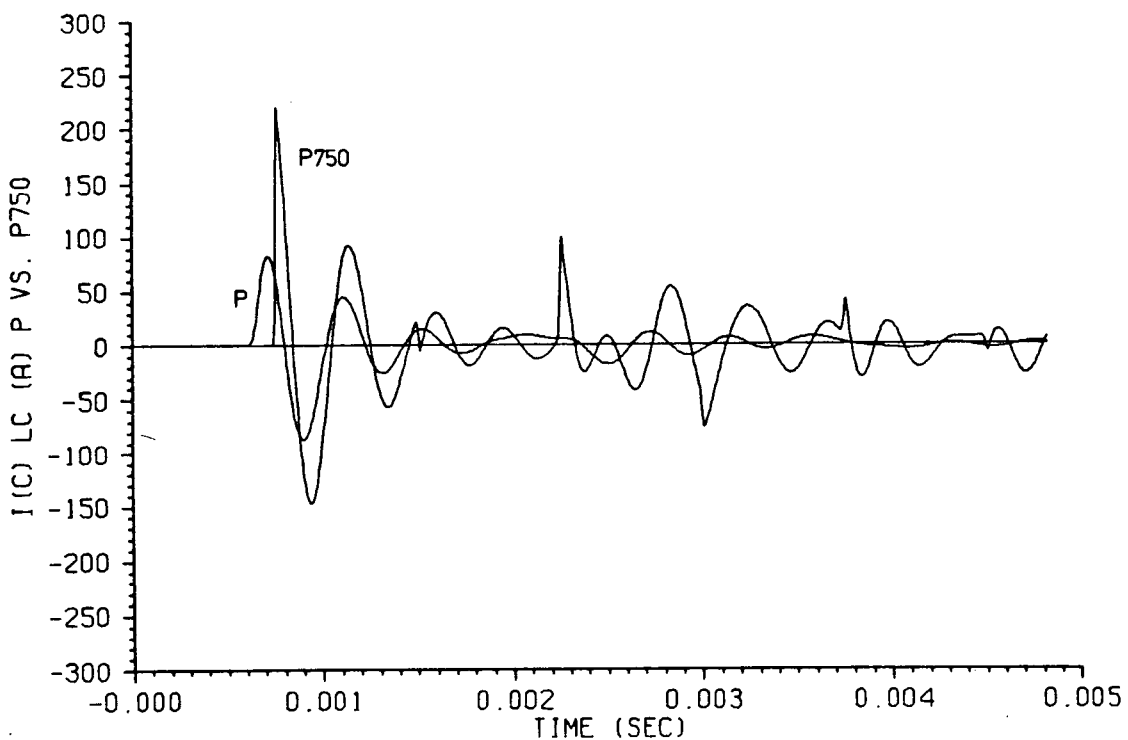
P.7.19: L-C load. Step excitation. Load voltage.
New model vs. 60-Hz.



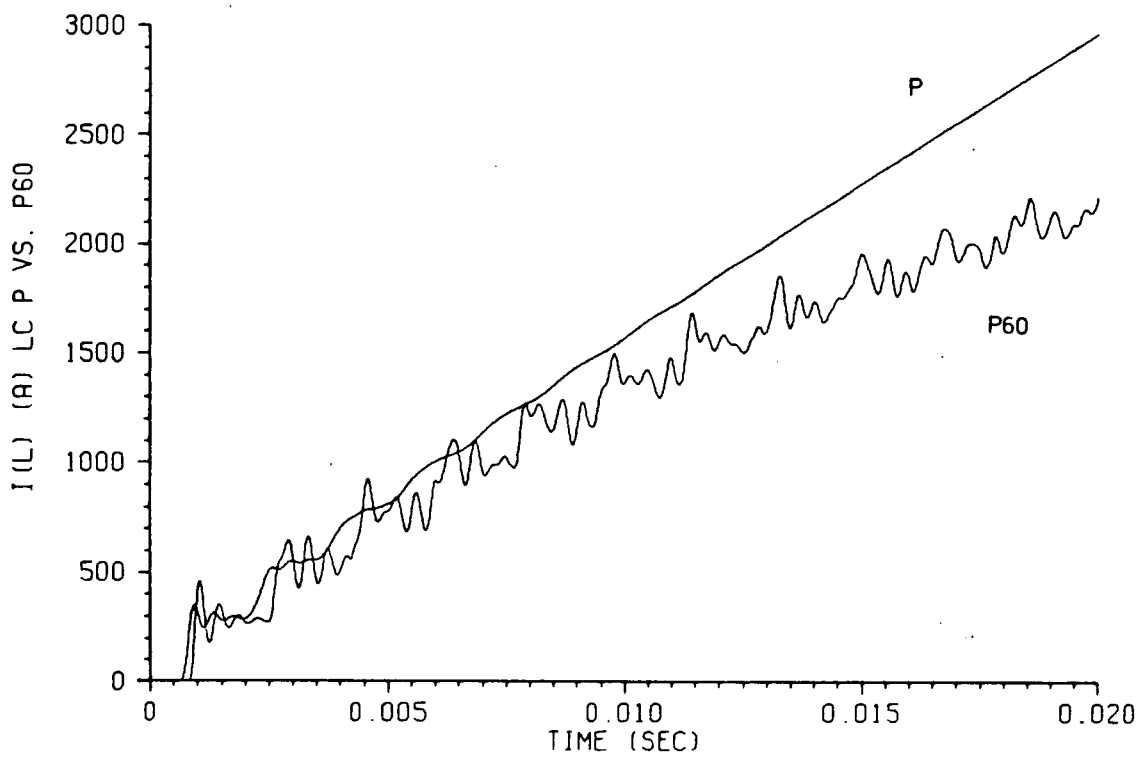
P.7.20: L-C load. Step excitation. Load voltage.
New model vs. 750-Hz.



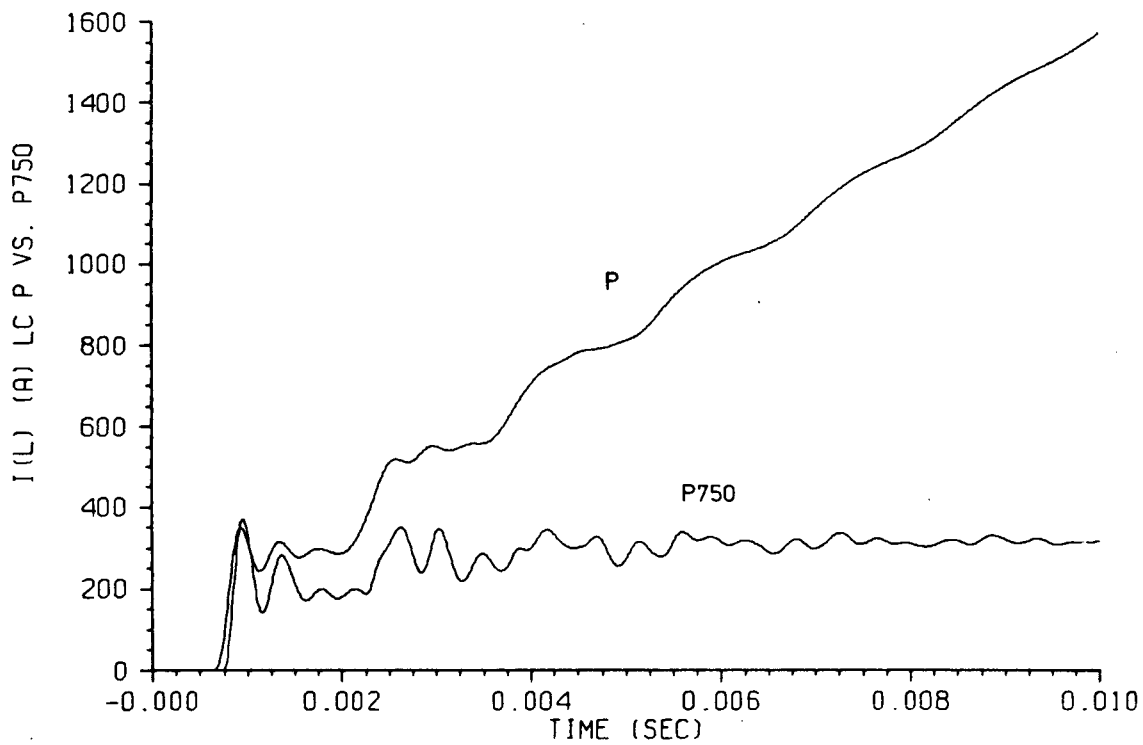
P.7.21: L-C load. Step excitation. Current in C.
New model vs. 60-Hz.



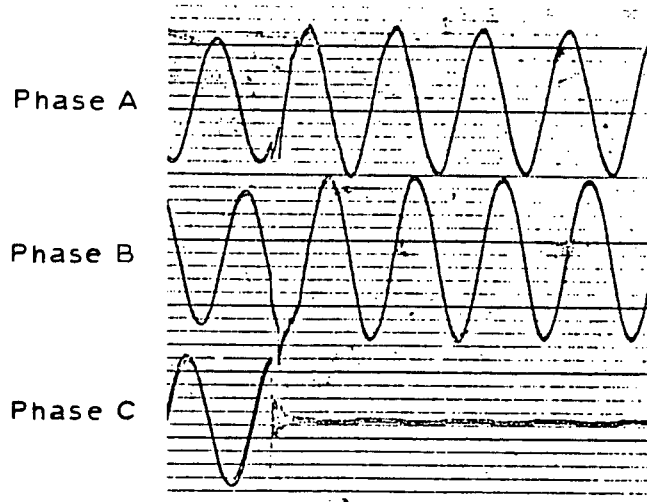
P.7.22: L-C load. Step excitation. Current in C.
New model vs. 750-Hz.



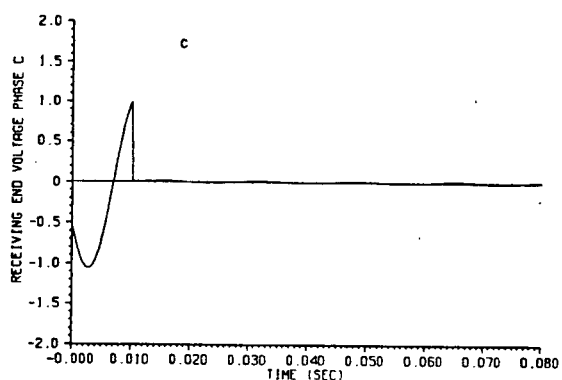
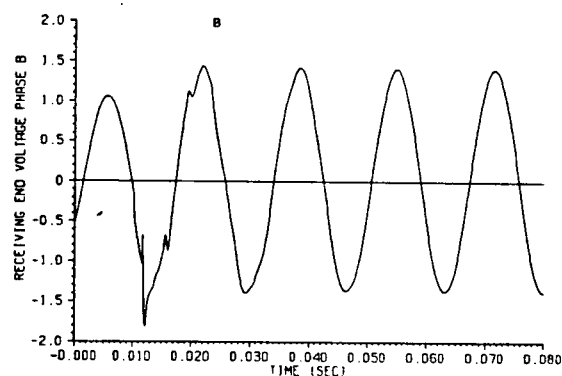
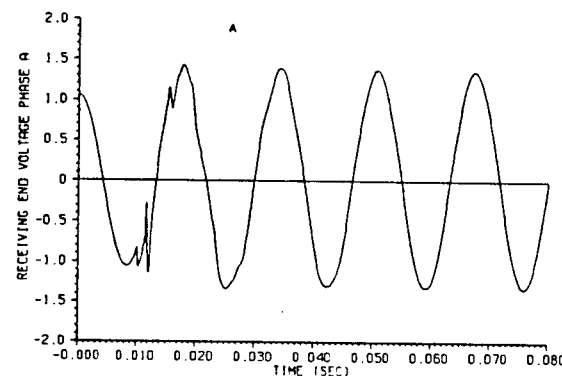
P.7.23: L-C load. Step excitation. Current in L.
New model vs. 60-Hz.



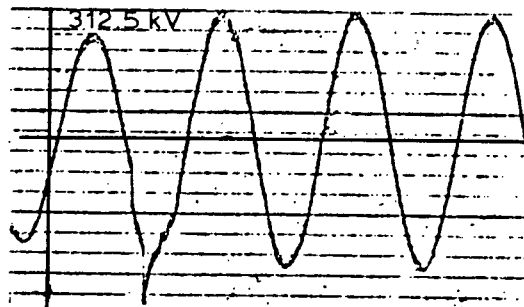
P.7.24: L-C load. Step excitation. Current in L.
New model vs. 750-Hz.



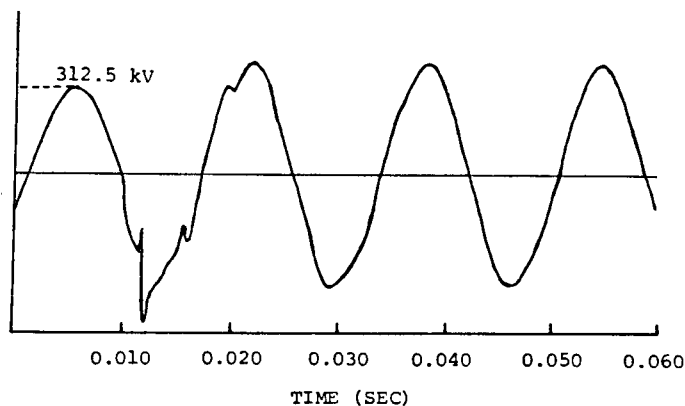
P.8.1(a): Field test oscillograph (BPA). Single-line-to-ground fault on phase C. Receiving end voltages.



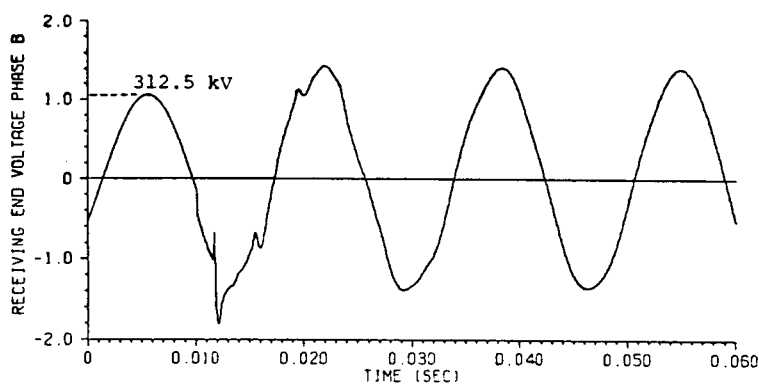
P.8.1(b): Simulation of field test in P.8.1(a) with the new line model. (Only the zero sequence is modelled as frequency dependent.)



(a)



(b)



(c)

P.8.2: Comparison between voltages at phase b for: a) Field test oscillograph; b) BPA's frequency-dependence simulation; c) New model simulation.

CONCLUSIONS

The accurate modelling of transmission lines for time-domain electromagnetic transient calculations has been considered in this work. The transmission line model that has been developed is very simple, and yet, it can very accurately represent the line behaviour over the entire frequency range of the signals. The main advantages of this new model as compared to previous frequency dependence formulations can be briefly summarized as follows:

- i) The accuracy of the model is not limited to certain specific frequencies, but includes the entire frequency range from the correct representation of dc levels to the highest frequency at which the system propagation function becomes negligible. It can, therefore, reliably model any possible system condition.
- ii) The model is very efficient and does not appreciably increase the computer time of the transient simulations over the time required by constant-parameter representations.
- iii) The numerical routines for obtaining the parameters of the model are very general, numerically stable and efficient, and do not require user-defined control parameters. The overall process can then be completely automated without the need for user intervention other than to supply the physical configuration of the line.

The generality of the principles involved in the development of the new line models presented in this work will probably allow the extension of these principles to the modelling of frequency dependence and distributed losses in other system components, as for instance, power transformers, generators, and reactors.

Another area in which it will probably be possible to extend these concepts is in the modelling of multiphase systems with frequency-dependent transformation matrices. An important example of these systems is the case of underground cables.

APPENDIX I

SOME MATRIX RELATIONS^(*)

I.1 Diagonalization of the Propagation Equations

It is first assumed that the product $(Z_{ph} Y_{ph})$ is diagonalizable by the matrix P whose columns are the eigenvectors of $(Z_{ph} Y_{ph})$, that is

$$P^{-1}(Z_{ph} Y_{ph})P = D_{zy} \text{ (diagonal).} \quad (I.1)$$

Transposing both sides of (I.1),

$$P^t(Y_{ph}^t Z_{ph}^t) (P^{-1})^t = D_{zy}^t.$$

Since Y_{ph} and Z_{ph} are symmetric and D_{zy} is diagonal, then

$$Y_{ph}^t = Y_{ph}$$

$$Z_{ph}^t = Z_{ph}$$

$$D_{zy}^t = D_{zy}$$

and

$$P^t(Y_{ph} Z_{ph}) (P^{-1})^t = D_{zy}. \quad (I.2)$$

Let $Q^{-1} = P^t$, then eqn. I.2 becomes

$$Q^{-1}(Y_{ph} Z_{ph})Q = D_{zy} = D_{yz} = D. \quad (I.3)$$

Therefore, it follows from eqns. I.1 and I.3 that if the product $(Z_{ph} Y_{ph})$ is diagonalizable by a matrix P ,

(*) The mathematical demonstrations included in this Appendix have been provided by Luis Martí (M.A.Sc. candidate at U.B.C.) in consultation with Dr. L.M. Wedepohl (Dean, Faculty of Applied Science, U.B.C.).

$$P^{-1}(Z_{ph} Y_{ph})P = D \quad (\text{diagonal}), \quad (I.4)$$

then, there exists a matrix Q such that the inverse product $(Y_{ph} Z_{ph})$ is also diagonalizable,

$$Q^{-1}(Y_{ph} Z_{ph})Q = D, \quad (I.5)$$

where

$$Q^{-1} = P^t. \quad (I.6)$$

The eigenvector matrix P can be generalized as follows:

$$P = P'D', \quad (I.7)$$

where D' is an arbitrary, constant, diagonal matrix. This is possible because the eigenvectors of a matrix conserve their properties when multiplied by an arbitrary constant. Introducing equation I.7 in equation I.6, the following general relationship between the diagonalizing matrices P and Q is obtained:

$$\begin{aligned} Q^{-1} &= (P'D')^t \\ Q &= (P'^t)^{-1}D_c, \end{aligned} \quad (I.8)$$

where D_c is again an arbitrary, constant, diagonal matrix ($D_c = (D')^{-1}$).

I.2 Diagonalization of the Drop Equations

Given any two matrices A and B with non-zero diagonal elements and two diagonal matrices D_1 and D_2 with distinct elements, if $AB = D_1$ and $BA = D_2$, then $D_1 = D_2$ and both A and B are diagonal.

Proof: $AB = D_1$

$$AD_2 = ABA,$$

then

$$AD_2 = D_1 A .$$

Let

$$A = [a_{ij}] , D_1 = [d_{kk}] , \text{ etc.}$$

The product of any two matrices is given by $[\alpha][\beta] = [\gamma]$, where

$$\gamma_{ij} = \sum_{k=1}^n \alpha_{ik} \beta_{kj} . \text{ Then,}$$

$$(AD_2)_{ij} = \sum_{k=1}^n a_{ik} d_{2kj} = (D_1 A)_{ij} = \sum_{k=1}^n d_{1ik} a_{kj} ,$$

but since $d_{kj} = 0$ for $k \neq j$, then

$$(AD_2)_{ij} = a_{ij} d_{2jj} = (D_1 A)_{ij} = d_{1ii} a_{ij} ,$$

yielding

$$a_{ij} d_{2jj} = a_{ij} d_{1ii}$$

$$a_{ij} (d_{2jj} - d_{1ii}) = 0 .$$

For $i = j$,

$$a_{ii} (d_{2ii} - d_{1ii}) = 0 ,$$

but since $a_{ii} \neq 0$, then $d_{2ii} = d_{1ii}$ and

$$D_1 = D_2 .$$

From this, and with $i \neq j$,

$$a_{ij} (d_{2jj} - d_{2ii}) = 0 ,$$

which means that if $d_{2jj} \neq d_{2ii}$, then $a_{ij} = 0$ and therefore A is diagonal.

(Note that $d_{2jj} \neq d_{2ii}$ is a sufficient, but not necessary, condition.) If A

and D_1 are diagonal, it follows directly from $AB = D_1$ that B is also diagonal.

Q.E.D.

Diagonality of the transformed matrices in the drop equations:

Recalling equations I.1 and I.3,

$$P^{-1}(Z_{ph} Y_{ph}) P = D$$

$$Q^{-1}(Y_{ph} Z_{ph}) Q = D .$$

Introducing identity matrices on the left-hand sides,

$$P^{-1} Z_{ph} (Q Q^{-1}) Y_{ph} P = D$$

$$Q^{-1} Y_{ph} (P P^{-1}) Z_{ph} Q = D ,$$

and rearranging,

$$(P^{-1} Z_{ph} Q) (Q^{-1} Y_{ph} P) = D \quad (I.9)$$

$$(Q^{-1} Y_{ph} P) (P^{-1} Z_{ph} Q) = D . \quad (I.10)$$

Let

$$A = P^{-1} Z_{ph} Q$$

$$B = Q^{-1} Y_{ph} P ,$$

substituting in I.9 and I.10,

$$AB = D$$

$$BA = D ,$$

and from the result proved first in this section, it is concluded that if D has distinct elements then A and B are diagonal; therefore,

$$P^{-1}Z_{ph}Q = D_z \text{ (diagonal)} \quad (I.11)$$

and

$$Q^{-1}Y_{ph}P = D_y \text{ (diagonal)} . \quad (I.12)$$

In the particular case in which the elements of D are not distinct, that is, the matrix $(Z_{ph} Y_{ph})$ has at least two equal eigenvalues (e.g. positive and negative sequence modes in a perfectly balanced system), it can be shown that an adequate selection of the eigenvector matrices P and Q can also diagonalize Z_{ph} and Y_{ph} , that is, satisfy eqns. I.11 and I.12^(*).

(*) Dr. Wedepohl's lecture notes for course ELEC 552, Winter Session 1979-80, U.B.C., pp. 45-57.

APPENDIX II

INTEGRATION COEFFICIENTS

II.1 Recursive Convolution Property

Consider the following convolution integral:

$$s(t) = \int_T^\infty f(t-u)e^{-\alpha(u-T)} du. \quad (\text{II.1})$$

At $t-\Delta t$,

$$s(t-\Delta t) = \int_T^\infty f(t-\Delta t-u)e^{-\alpha(u-T)} du.$$

Let $v=\Delta t+u$, then

$$s(t-\Delta t) = \int_{T+\Delta t}^\infty f(t-v)e^{-\alpha(v-T-\Delta t)} dv,$$

or, rearranging and renaming the dummy variable v as u ,

$$s(t-\Delta t) = e^{\alpha\Delta t} \int_{T+\Delta t}^\infty f(t-u)e^{-\alpha(u-T)} du. \quad (\text{II.2})$$

Separating the integral in equation II.1 into two parts,

$$s(t) = \int_T^{T+\Delta t} f(t-u)e^{-\alpha(u-T)} du + \int_{T+\Delta t}^\infty f(t-u)e^{-\alpha(u-T)} du.$$

Comparing the second integral with equation II.2 ,

$$s(t) = e^{-\alpha\Delta t} s(t-\Delta t) + \int_T^{T+\Delta t} f(t-u)e^{-\alpha(u-T)} du. \quad (\text{II.3})$$

Evaluation of the one-time-step integral:

The integral in equation II.3 can be evaluated as follows.

Let $v = u-T$ and $t_1 = t-T$, then

$$\int_T^{T+\Delta t} f(t-u) e^{-\alpha(u-T)} du = \int_0^{\Delta t} f(t_1-v) e^{-\alpha v} dv . \quad (\text{II.4})$$

In a discrete process of solution, the function f is known only at discrete points: $0, \Delta t, 2\Delta t, \dots$. To evaluate integral II.4, the intermediate values of f can be approximated by joining the known ends by a straight line, that is,

$$f(t_1-v) = f(t_1) + \frac{[f(t_1-\Delta t) - f(t_1)]}{\Delta t} v ,$$

or

$$f(t_1-v) = a + bv .$$

Integral II.4 can now be evaluated:

$$\begin{aligned} \int_0^{\Delta t} &= \int_0^{\Delta t} (a+bv) e^{-\alpha v} dv \\ \int_0^{\Delta t} ae^{-\alpha v} dv &= a \left[\frac{e^{-\alpha v}}{-\alpha} \right]_0^{\Delta t} = \frac{a}{\alpha} (1 - e^{-\alpha \Delta t}) \\ \int_0^{\Delta t} bve^{-\alpha v} dv &= b \left[\frac{e^{-\alpha v}}{\alpha^2} (-\alpha v - 1) \right]_0^{\Delta t} \\ &= \frac{b}{\alpha^2} [1 - e^{-\alpha \Delta t} (1 + \alpha \Delta t)] . \end{aligned}$$

Equation II.3 is finally given by

$$\begin{aligned} s(t) &= e^{-\alpha \Delta t} s(t-\Delta t) + \left[\frac{1}{\alpha} - \frac{1}{\Delta t \alpha^2} (1 - e^{-\alpha \Delta t}) \right] f(t-T) \\ &+ \left[-\frac{1}{\alpha} e^{-\alpha \Delta t} + \frac{1}{\Delta t \alpha^2} (1 - e^{-\alpha \Delta t}) \right] f(t-T-\Delta t) , \quad (\text{II.5}) \end{aligned}$$

or

$$s(t) = m s(t-\Delta t) + p f(t-T) + q f(t-T-\Delta t) , \quad (\text{II.6})$$

(II.5)

where m , p , and q are constants.

II.2 Dommel's Model for R-C Network

Consider Dommel's discretized representation of an R-C combination [10] shown in Fig. II.1.

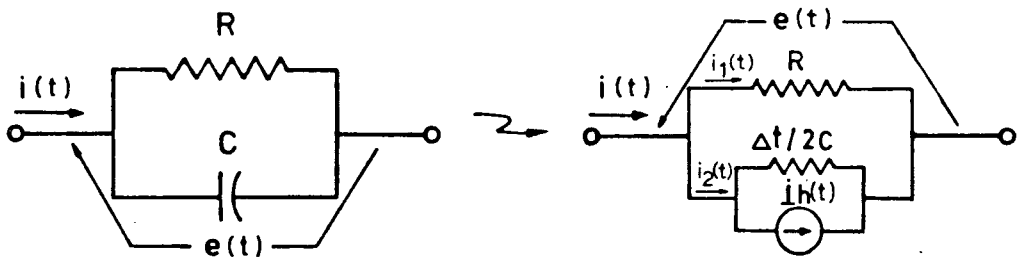


Fig. II.1

From the equations in reference [10], $i_h(t)$ is given by

$$i_h(t) = -i_2(t-\Delta t) - \frac{2C}{\Delta t} e(t-\Delta t) .$$

Solving the circuit,

$$i(t) = i_1(t) + i_2(t) , \quad i_1(t) = \frac{e(t)}{R} ,$$

$$i_2(t) = \frac{2C}{\Delta t} e(t) + i_h(t) = \frac{2C}{\Delta t} e(t) - i_2(t-\Delta t) - \frac{2C}{\Delta t} e(t-\Delta t) ,$$

but

$$i_2(t-\Delta t) = i(t-\Delta t) - i_1(t-\Delta t) = i(t-\Delta t) - \frac{1}{R} e(t-\Delta t) ,$$

then

$$i_2(t) = \frac{2C}{\Delta t} e(t) - i(t-\Delta t) + \frac{1}{R} e(t-\Delta t) - \frac{2C}{\Delta t} e(t-\Delta t) .$$

Combining terms and solving for $e(t)$,

$$\begin{aligned}
 e(t) = & \left[\frac{2RC - \Delta t}{2RC + \Delta t} \right] e(t - \Delta t) + \left[\frac{R\Delta t}{2RC + \Delta t} \right] i(t) \\
 & + \left[\frac{R\Delta t}{2RC + \Delta t} \right] i(t - \Delta t) . \quad (\text{II.7})
 \end{aligned}$$

In terms of the parameters of the partial fraction expansion of $Z_{eq}(s)$ (eqns. 4.13, 4.18, and 4.19), $R = k/\alpha$ and $C = 1/k$, it is finally obtained that

$$\begin{aligned}
 e(t) = & \left[\frac{1 - \frac{1}{2}(\alpha \Delta t)}{1 + \frac{1}{2}(\alpha \Delta t)} \right] e(t - \Delta t) + k \left[\frac{\Delta t/2}{1 + \frac{1}{2}(\alpha \Delta t)} \right] i(t) \\
 & + k \left[\frac{\Delta t/2}{1 + \frac{1}{2}(\alpha \Delta t)} \right] t(t - \Delta t) , \quad (\text{II.8})
 \end{aligned}$$

or

$$e(t) = m e(t - \Delta t) + p i(t) + q i(t - \Delta t) , \quad (\text{II.9})$$

where m , p , and q are constants.

BIBLIOGRAPHY

- [1] L.V. Bewley, Traveling Waves on Transmission Systems (book). Dover, New York, 1963 (first published in 1933).
- [2] W.W. Lewis, The Protection of Transmission Systems Against Lightning (book). Dover, New York, 1965 (first published in 1950).
- [3] E. Clarke, Circuit Analysis of A-C Power Systems (book, two volumes). Wiley, New York, 1950.
- [4] H.A. Peterson, Transients in Power Systems (book). Dover, New York, 1966 (first published in 1951).
- [5] R. Rüdenberg, Electrical Shock Waves in Power Systems (book). Harvard University Press, Cambridge, 1968 (first published in German in 1962).
- [6] H.A. Peterson, "An Electric Circuit Transient Analyser". Gen. Elec. Rev., p. 394, 1939.
- [7] J.P. Bickford, N. Mullineux, and J.R. Reed, Computation of Power-System Transients (book). Peregrinus (for the IEE), Herts (England), 1976.
- [8] L.M. Wedepohl, "Application of Matrix Methods to the Solution of Travelling-Wave Phenomena in Polyphase Systems". Proc. IEE, Vol. 110 (12), pp. 2200-2212, December 1963.
- [9] D.E. Hedman, "Propagation on Overhead Transmission Lines: I. Theory of Modal Analysis; II. Earth-Conduction Effects and Practical Results". IEEE Trans., PAS-84, pp. 200-211, March 1965.
- [10] H.W. Dommel, "Digital Computer Solution of Electromagnetic Transients in Single-and Multiphase Networks". IEEE Trans., PAS-88, pp. 388-399, April 1969.
- [11] A. Budner, "Introduction of Frequency-Dependent Line Parameters into an Electromagnetic Transients Program". IEEE Trans., PAS-89, pp. 88-97, January 1970.
- [12] J.K. Snelson, "Propagation of Travelling Waves on Transmission Lines--Frequency Dependent Parameters". IEEE Trans., PAS-91, pp. 85-91, January/February 1972.
- [13] W.S. Meyer and H.W. Dommel, "Numerical Modelling of Frequency-Dependent Transmission-Line Parameters in an Electromagnetic Transients Program". IEEE Trans., PAS-93, pp. 1401-1409, September/October 1974.
- [14] A. Semlyen and A. Dabuleanu, "Fast and Accurate Switching Transient Calculations on Transmission Lines with Ground Return using Recursive Convolutions". IEEE Trans., PAS-94, pp. 561-571, March/April 1975.

- [15] A. Ametani, "A Highly Efficient Method for Calculating Transmission Line Transients". IEEE Trans., PAS-95, pp. 1545-1551, September/October 1976.
- [16] A. Semlyen and R.A. Roth, "Calculation of Exponential Step Responses - Accurately for Three Base Frequencies". IEEE Trans., PAS-96, pp. 667-672, March/April 1977.
- [17] A. Morched and A. Semlyen, "Transmission Line Step Response Calculation by Least Square Frequency Domain Fitting". IEEE PES Summer Meeting, Portland, OR, July 1976.
- [18] L.F. Woodruff, Principles of Electric Power Transmission (book). Wiley, New York, 1938.
- [19] J.R. Carson, "Wave Propagation in Overhead Wires with Ground Return". Bell Syst. Tech. J., vol. 5, pp. 539-554, 1926.
- [20] F. Pollaczek, "Über das Feld einer unendlich langen wechselstromdurchflossenen Einfachleitung" ("About the field of an infinite ac excited single-phase line") Elek. Nachrichtentech, vol. 3, pp. 339-359, 1926. Translation by J.B. Pomey into French, "Sur le champ produit par un conducteur simple infiniment long parcouru par un courant alternatif". Gen. Elec. Rev., vol. 29, pp. 851-867, 1931.
- [21] H. Karrenbauer, "Ausbreitung von Wanderwellen bei verschiedenen Anordnungen von Freileitungen im Hinblick auf die Form der Einschwingspannung bei Abstandskurzschlüssen". ("Propagation of travelling waves for various overhead line tower configurations, with respect to the shape of the transient recovery voltage for short line faults".) Ph.D. dissertation, Technical University Munich, Germany, 1967.
- [22] P.C. Magnusson, "Travelling Waves on Multi-Conductor Open-Wire Lines - A Numerical Survey of the Effects of Frequency Dependence of Modal Composition". IEEE Trans., PAS-92, pp. 999-1008, May/June 1973.
- [23] R.G. Wasley and S. Selvarinayagamoorthy, "Approximate Frequency-Response Values for Transmission-Line Transient Analysis". IEE Proc., vol. 131 (4), pp. 281-286, April 1974.
- [24] H.W. Dommel and W.S. Meyer, "Computation of Electromagnetic Transients". IEEE Proc., vol. 62(7), pp. 983-993, July 1974.
- [25] E. Groschupf, "Simulation transienter Vorgänge auf Leitungssystemen der Hochspannungs-Gleichstrom-und-Drehstrom-Übertragung". ("Simulation of transient phenomena in systems with HVDC and ac transmission lines".) Ph.D. dissertation, Technical University Darmstadt, Germany, 1976.
- [26] UBC - Overhead Line Parameters Program. Originally written by H.W. Dommel at the Bonneville Power Administration, Portland, Oregon. Modified at the University of British Columbia (UBC), Canada, by I.I. Dommel, K.C. Lee, and T. Hung. User's manual, UBC, August 1980.

- [27] H.W. Dommel, Notes on Power Systems Analysis. University of British Columbia, Department of Electrical Engineering, 1975.
- [28] E.A. Guillemin, Synthesis of Passive Networks (book). Wiley, New York. 1957.
- [29] S. Karni, Network Theory: Analysis and Synthesis (book). Allyn and Bacon, Boston, 1966.
- [30] A. Semlyen, "Contributions to the Theory of Calculation of Electromagnetic Transients on Transmission Lines with Frequency Dependent Parameters". IEEE Trans., PAS-100, pp. 848-856, February 1981.
- [31] S.W. Director, "Survey of Circuit-Oriented Optimization Techniques". IEEE Trans., CT-18, pp. 3-10, January 1971.
- [32] G. Szentirmai, "Computer Aids in Filter Design: A Review". IEEE Trans., CT-18, pp. 35-40, January 1971.
- [33] H.W. Bode, Network Analysis and Feedback Amplifier Design (book). Van Nostrand, New York, 1945.
- [34] A. Papoulis, The Fourier Integral and its Applications (book). McGraw-Hill, New York, 1962.
- [35] B.W. Arden (editor), What Can Be Automated? The Computer Science and Engineering Research Study (COSERS) (book). The MIT Press, Cambridge, Massachusetts, 1980.
- [36] R.W. Hornbeck, Numerical Methods (book). Quantum, New York, 1975.
- [37] H.W. Dommel and N. Sato, "Fast Transient Stability Solutions". IEEE Trans., PAS-72, pp. 1643-1650, July/August 1972.
- [38] UBC - Electromagnetic Transients Program (EMTP). Originally written by H.W. Dommel at the Bonneville Power Administration, Portland, Oregon. Modified at the University of British Columbia (UBC), Canada, by H.W. Dommel. User's manual, UBC, August 1978 (first published in 1976).
- [39] J. Umoto and T. Hara, "A New Digital Analysis of Surge Performances in Electric Power Networks Utilizing the Convolution Integral". (Translated from Denki Gakkai Zasshi, vol. 91(5), pp. 907-916, May 1971.) Electrical Engineering in Japan, vol. 91(3), pp. 48-57, 1971.